

Atrium Models for the Analysis of Thermal Comfort and Energy Use

A Report of Task 12
Building Energy Analysis and
Design Tools for Solar Applications

Project A.3 Atrium Model Development

Edited by
Ida Bryn and
Per Arne Schiefloe

T.12.A.3-1

Published by SINTEF Energy, Indoor Environmental Technology

Additional copies of this report can be ordered from :
SINTEF Energy, Indoor Environmental Technology
N-7034 Trondheim
NORWAY

Phone +47 73 59 39 00, Fax +47 73 59 31 86

March 1996

PREFACE

INTRODUCTION TO THE INTERNATIONAL ENERGY AGENCY

BACKGROUND

The International Energy Agency was founded in November 1974 as a cooperation among industrialized nations to address energy policy issues. It is an autonomous body within the framework of the Organization for Economic Cooperation and Development (OECD). Twenty-one countries are presently members, with the Commission of the European Communities also participating in the work of the IEA under a special agreement.

One element of the IEA's program involves cooperation in the research and development of alternative energy resources in order to reduce excessive dependence on oil. A number of new and improved energy technologies which have the potential of making significant contribution to global energy needs were identified for collaborate efforts. The IEA Committee on Energy Research and Development (CRD), comprising representatives from each member country, supported by a small Secretariat staff, is the focus of IEA R & D activities. Four Working Parties (Conservation, Fossil Fuels, Renewable Energy, and Fusion) are charged with identifying new areas for cooperation and advising the CRD on policy matters in their respective technology areas.

SOLAR HEATING AND COOLING PROGRAM

Solar Heating and Cooling was one of the technologies selected for joint activities. During 1976 - 1977, specific projects were identified in key areas of this field and a formal implementing Agreement drawn up. The Agreement covers the obligations and rights of the Participants and outlines the scope of each project or "Task" in annexes to the document. There are now twenty signatories to the Agreement:

Australia	France	Spain
Austria	Germany	Sweden
Belgium	Italy	Switzerland
Canada	Japan	Turkey
Denmark	Netherlands	United Kingdom
European Commission	New Zealand	United States
Finland	Norway	

The overall program is managed by an Executive Committee, while the management of the individual Tasks is the responsibility of Operating Agents. The tasks of the IEA Solar Heating and Cooling Programme, their

respective Operating Agents, and current status (ongoing or completed) are as follows:

- | | |
|---------|--|
| Task 1 | Investigation of the Performance of Solar Heating and Cooling Systems, Technical University of Denmark (Completed) |
| Task 2 | Coordination of Research and Development of Solar Heating and Cooling-Solar Research Laboratory-GIRN, Japan (Completed) |
| Task 3 | Performance Testing of Solar Collectors - University College, Cardiff, UK (Completed) |
| Task 4 | Development of an Isolation Handbook and Instrument Package - U.S. Department of Energy (Completed) |
| Task 5 | Use of Existing Meteorological Information for Solar Energy Application, Swedish Meteorological and Hydrological Institute (Completed) |
| Task 6 | Performance of Solar Heating, Cooling, and Hot Water Systems Using Evacuated Collectors - U.S. Department of Energy (Completed) |
| Task 7 | Central Solar Heating Plants with Seasonal Storage - Swedish Council for Building Research (Completed) |
| Task 8 | Passive and Hybrid Solar Low Energy Building - U.S. Department of Energy (Completed) |
| Task 9 | Solar Radiation and Pyranometry Studies - KFA Jülich, Germany (Completed) |
| Task 10 | Solar Materials R&D-AIST, Ministry of International Trade and Industry, Japan (Completed) |
| Task 11 | Passive and Hybrid Solar Commercial Building-Swiss Federal Office of Energy (Completed) |
| Task 12 | Building Energy Analysis and Design Tools for Solar Applications - U.S. Department of Energy (Ongoing) |
| Task 13 | Advanced Solar Low Energy Buildings - Norwegian Institute of Technology (Ongoing) |
| Task 14 | Advanced Active Solar Energy Systems - Canadian Department of Energy, Mines and Resources (Ongoing) |

- Task 15 Advanced Central Solar Heating Plants with Seasonal Storage
(In Planning Stage)
- Task 16 Photovoltaics in Buildings - KFA, Jülich, Germany (Ongoing)
- Task 17 Measuring and Modelling Spectral Radiation Affecting Solar
Systems and Buildings - KFA, Jülich, Germany (Ongoing)
- Task 18 Advanced Glazing Material - U.K. Department of Energy
(Ongoing)
- Task 19 Solar Air Systems in Buildings - Swiss Federal Office of En-
ergy (Ongoing)
- Task 20 Solar Energy in Building Renovation - Swedish Council for
Building Research (Ongoing)
- Task 21 Daylighting - Danish Building Research Institute (Ongoing)

**TASK 12: BUILDING ENERGY ANALYSIS AND DESIGN TOOLS FOR
SOLAR APPLICATIONS**

The scope of Task 12 includes: (1) Selection and development of appropriate algorithms for modelling of solar energy related materials, components and systems within the building in which these solar elements are integrated, (2) Selection of analysis and design tools and evaluation of the algorithms as to their ability to model the dynamic performance of the solar elements in respect to accuracy and ease of use, and (3) Improvement of the usability of the analysis and design tools, through preparation of common formats and procedures, and by standardization for input/output, default values and other user-related factors.

The subtasks of this project are:

- A: Model Development
- B: Model Evaluation
- C: Model Use

The participants in this Task are: Denmark, Finland, Germany, Norway, Spain, Sweden, Switzerland and the United States. The United States serves as Operating Agent for this Task, Michael Holtz of Architectural Energy Corporation serves as the Operating Agent on behalf of the U.S. Department of Energy.

This report documents work carried out under Subtask A.3 of this Task entitled Atrium Model Development.

Project A.3 Atrium Model Development

Project leader: Norway

Participants:

Denmark

Mr. Kjeld Johnsen
Danish Building Research Institute
P.O. Box 119
2970
Phone +45-42-865533, Fax +45-42-867535

Norway

Dr. Ida Bryn
Erichsen & Horgen A/S
P.O.Box 4464 Torshov,
N-0403 OSLO
Phone +47-22 02 63 00 Fax +47-22 02 63 90

Sweden

Dr. Maria Wall
Dr. Bertil Fredlund
Lund Institute of Technology
Department of Building Science,
P.O.Box 118, S-22100 Lund
Phone +46-46-2220000, Fax +46-46-2224719

Switzerland

Mr. Dominique Chuard
Mr. Pierre Jaboyedoff
Sorane SA
Route de Châtelard 52
CH-1018 Lausanne
Phone +41-21-6471175, Fax +41-21-6468876

NOTICE

This report was prepared as an account of work sponsored by the Norwegian Research Council for the International Energy Agency. Neither Norway, nor the Norwegian Research Council, nor the International Energy Agency, nor any of their employees, nor any of their contractors, subcontractors, or their employees makes any warranty, express or implied, or assumes any legal liability or responsibility for the accuracy, completeness or usefulness of any information, apparatus, product or process disclosed, or represents that its use would not infringe privately owned rights.

List of Authors/Editors

- BF Bertil Fredlund**, Lund Institute of Technology, Department of Building Science,
P.O.Box 118, S-22100 Lund
Phone +46-46-2220000, Fax +46-46-2224719
- DA Dario Aiulfi**, Sorane SA, rte de Châtelard 52, CH-1018 Lausanne
Phone +41-21-6471175, Fax +41-21-6468876
- DC Dominique Chuard**, Sorane SA, rte de Châtelard 52, CH-1018 Lausanne
Phone +41-21-371-175, Fax +41-21-6468876
- HK Hasse Kvist**, Lund Institute of Technology, Department of Building Science,
P.O.Box 118, S-22100 Lund
Phone +46-46-2220000, Fax +46-46-2224719
- IB Ida Bryn**, Erichsen & Horgen A/S, P.O.Box 4464 Torshov, N-0403 OSLO
Phone +47-22 02 63 00 Fax +47-22 02 63 90
- JR Johann Reiß**, Fraunhofer Institut für Bauphysik, Nobelstraße 12,
P.O.Box 80 04 69, D-70569 Stuttgart 80
Phone +49 71 1-970 3337 (0000), Fax +49-711-970 3399
- KJ Kjeld Johnsen**, Danish Building Research Institute, DK-2970
Phone +45-42-865533, Fax +45-42-867535
- KK Kurt Källblad**, Lund Institute of Technology, Department of Building Science,
P.O.Box 118, S-22100 Lund
Phone +46-46-2220000, Fax +46-46-2224719
- KKo Kjell Kolsaker**, Norwegian University of Science and Technology,
Department of Refrigeration and Air Conditioning, N-7034 Trondheim
Phone +47 73 59 38 60, Fax +47 73 59 38 59
- KTA Karl Terpøger Andersen**, Danish Building Research Institute,
DK-2970 Hørsholm
Phone +45-42-865533, Fax +45-42-867535
- MJH Michael J. Holtz**, Architectural Energy Corporation
2540 Frontier Avenue, Suite 201, Boulder, Colorado 80301 USA
Phone +1-303 444-4149, Fax +1-303 444-4304
- MW Maria Wall**, Lund Institute of Technology, Department of Building Science,
P.O.Box 118, S-22100 Lund
Phone +46-46-2220000, (direct line 2229662) Fax +46-46-2224719
- PAS Per Arne Schiefloe**, SINTEF Energy, N-7034 Trondheim
Phone +47 73 59 16 34, Fax +47 73 59 39 26
- POT Per Olaf Tjelflaat**, Norwegian University of Science and Technology,
Department of Refrigeration and Air Conditioning, N-7034 Trondheim
Phone +47 73 59 38 60, Fax +47 73 59 38 59
- PS Peter Schild**, Norwegian University of Science and Technology,
Department of Refrigeration and Air Conditioning, N-7034 Trondheim
Phone +47 73 59 38 60, Fax +47 73 59 38 59

Abstract

This report describes models for thermal comfort and energy consumption in atria. These are models which have not been included in many of the commonly used building energy simulation tools today, and improvements of these programs constitute the main result of this work. The models include infiltration and natural ventilation, stratification, air flow patterns, surface film coefficients and solar radiation. Some of the models have been tested against monitored performance data. In cases where data have been unavailable, they have been obtained by use of computational fluid dynamics (CFD) models. CFD models have also been used in order to validate the simplified models developed here.

The models have been integrated in different computer programs. These are generally simplified tools, often used in the design phase of atria and other, more conventional buildings. As a result of this, these programs have become more reliable and accurate as they include new and better models.

Contents

Preface [MJH]	I
List of Task XII project A.3 members	IV
List of authors/editors	VI
Abstract [PAS]	WI
Contents	IX
Background [IB]	XIII
1 Executive summary-problem definition [IB]	1:1
1.1 Introduction	1:1
1.2 Thermal comfort	1:1
1.3 Stratification	1:2
1.4 Natural ventilation	1:4
1.5 Surface heat transfer coefficient	1:4
1.6 Solar radiation	1:5
1.7 Test studies	1:6
1.8 Computational fluid dynamics studies	1:6
1.9 Building energy simulation programs	1:7
2 Thermal comfort [IB]	2:1
2.1 Introduction	2:1
2.2 The ISO 7730 Standard	2:3
2.3 Local thermal discomfort	2:5
2.4 Draught due to cooled air falling down along cold surfaces	2:7
2.5 The PPD comfort models incorporated in FRES	2:7
2.6 Summary and conclusions	2:14
2.7 Symbol list	2:15
2.8 References	2:16
3 Stratification of the temperature in atria [DA]	3:1
3.1 Introduction	3:1
3.2 Physical theory	3:2
3.3 When is stratification important?	3:3

3.4	Examples of existing atria	3:5
3.5	Influence of the temperature stratification on thermal comfort and energy consumption	3:10
3.6	Simplified models	3:13
3.7	Linear model	3:13
3.8	Use of standard building dynamic simulation program	3:21
3.9	Glazed courtyard at Taman simulated with DEROB-LTH	3:22
3.10	Attached atrium of the University of Neuchâtel simulated with the type 56 of TRNSYS	3:29
3.11	ELA atrium of the University of Trondheim simulated with type 56 of TRNSYS	3:39
3.12	Single volume model with different air nodes and wall temperatures in the vertical direction	3:56
3.13	Summary and conclusion	3:66
3.14	List of symbols	3:68
3.15	References	3:69
4	Natural ventilation [KTA]	4:1
4.1	Introduction	4:1
4.2	Ventilation by thermal buoyancy	4:1
4.3	Wind ventilation	4:26
4.4	Infiltration	4:33
4.5	Use of formula. Implementation	4:35
4.6	Summary	4:39
4.7	List of symbols	4:40
4.8	References	4:42
5	Surface heat transfer coefficients [KTA]	5:1
5.1	Introduction	5:1
5.2	Radiation heat transfer coefficient	5:2
5.3	Convective heat transfer coefficients	5:15
5.4	Interior building surfaces	5:29
5.5	Exterior building surfaces	5:36
5.6	Summary	5:49
5.7	List of symbols	5:50
5.8	References	5:51
6	Solar radiation [MW, BF]	6:1
6.1	Incident solar radiation [BF]	6:1
6.2	Long wave radiation [BF]	6:14
6.3	Solar radiation through windows [KK]	6:18
6.4	Distribution of solar radiation within and between rooms [KK]	6:28

6.5	Solar processor in DEROB-LTH [HK]	6:31
6.6	Solar processor in FRES [KKo]	6:37
6.7	Solar processor in SUNREP (TRNSYS) [DC]	6:41
6.8	Solar processor in TSBI3 [KJ]	6:47
6.9	Shading module Xsun [KJ]	6:54
6.10	The shoebox study [MW]	6:61
6.11	A simplified method to estimate solar energy utilisation in glazed spaces [MW]	6:88
6.12	Summary and conclusion [MW]	6:96
6.13	List of symbols	6:98
6.14	References	6:104
7	Test studies [IB]	7:1
7.1	Neuchatel University - NUNI [DA]	7:1
7.2	Residential buildings - Taman [MW]	7:1
7.3	Bertolt Brecht Secondary School, Dresden [JR]	7:15
7.4	Technical University - ELA [IB]	7:22
7.5	Summary and conclusions [IB]	7:28
7.6	References	7:28
8	The use of computational fluid dynamics in Task XII [DA]	8:1
8.1	Introduction [DA]	8:1
8.2	What are CFD programs? [DA]	8:4
8.3	Guidelines boundary conditions used in atria [POT, PS]	8:16
8.4	Example of CFD applications in atria [DA]	8:37
8.5	Conclusion [DA]	8:52
8.6	Summary [DA]	8:55
8.7	List of symbols	8:56
8.8	References	8:58
9	Building energy simulation programs [IB]	9:1
9.1	Introduction [IB]	9:1
9.2	DEROB-LTH [MW]	9:3
9.3	FRES [IB, KKo]	9:6
9.4	TRNSYS Type 56 (version 1.3) : Multi zone building [DA]	9:11
9.5	tsbi3 [KJ]	9:19
9.6	Summary and conclusions [IB]	9:23
9.7	List of symbols	9:23
9.8	References	9:25

Background

An atrium has become a fashionable feature to use in commercial and institutional building design. It provides a dramatic visual and spatial experience and brings light and view to the interior of the building. Saving energy is not the primary reason why atria are incorporated into the design of buildings. Nevertheless, energy has become a concern because these atrium spaces typically incorporate large areas of glazed surfaces, and the resultant solar heat gains and thermal losses may play a significant role in the overall energy performance of the building. An atrium reduces the daylight level, but due to the buffer effect, the glazing in the walls between the atrium and adjacent spaces may be increased, and the need for electric lighting reduced.

Improper design of an atrium may result in significantly higher energy costs than if the atrium was excluded from the design. However, given that atria will be incorporated into the design for non-energy reasons, it is essential that it is designed to be at a minimum energy neutral; that is, it does not adversely impact the total building energy costs. A better approach is to design the atrium to provide a net energy benefit, actually reducing the total energy costs of the building.

An atrium represents a complex thermal and luminous environment. Numerous interactions exist between the atrium, the outdoor environment and the spaces adjacent to the atrium. These interactions are dynamic and vary by time of day and season, and by the operation of the building's HVAC and lighting systems. The effective design of an atrium requires an understanding of these various thermal and luminous interactions, and an ability to assess the influence of various design configurations on them.

Apart from measuring a physical model, calculations and simulations are the only means for a designer to determine the performance variables of the building. The results of the calculations form the basis for the evaluation of the design.

Simplified design tools are to be used in an early design phase when basic parameters are set and indication of where problems may occur is important. Detailed simulation tools are used as the design evolves and more details are available to solve problems that remain. The following example shows how tools at different levels can be used when developing ideas. An architect plans a shopping centre with a glass-covered street that connects the shops. The street is to be unheated. An "outdoor" cafe is planned in connection with a restaurant. In the early design phase the designer uses a simplified design tool that calculates the monthly energy consumption in the main building, monthly average, maximum and minimum temperatures in the atrium and the main building. The results indicate that the energy consumption, minimum and average temperatures are acceptable, but that over-heating may occur in the south facade of the main building. A more detailed model is used to simulate the south facade as a temperature zone hour by hour, and a satisfactory solution is found by applying shading and night ventilation. A whole year simulation for the building is also performed as more detailed data are available. The comfort analysis in the program indicates that draught may be a problem in parts of the atrium. A Computational Fluid Dynamics model is used to study the air movements and temperatures in the atrium. A one metre high shelter is put up around the cafe increasing comfort for people sitting within this shelter.

Experience shows that simplified design tools for calculation of the thermal and energy conditions on a monthly basis are not very accurate, but they are quick and simple to understand. They provide means to give a good overview of the thermal and energy performance at an early phase of the design, but they should not be used for anything more than that. When detailed solutions are to be studied, building energy simulation programs should be used. As the building energy simulation programs can handle several temperature zones, they have been most commonly used when studying atria. Research findings show that these tools also have several limitations. The following limitations of existing tools are reported in "IEA Task XI, Passive and Hybrid Solar Commercial Buildings" (Hastings, 1994. *Passive Solar Commercial and Institutional Buildings*. Wiley, England):

"In attempting to simulate energy performance and comfort conditions in atria, several limitations in existing analysis tools are encountered. The key problems are identified below:

INFILTRATION AND NATURAL VENTILATION: The algorithms used in most existing simulation programs to calculate infiltration and natural ventilation rates do not account for the interaction of temperature and wind pressure dependent air flow between a particular space and its surrounding spaces and environ-

ment, or the dependence of either component of air flow on the geometric configuration of the space, mode of operation (e.g., presence of ventilation openings), or interaction with mechanical ventilation. In order to properly represent buoyancy and cross venting effects, simulation programs must be capable of predicting air flow rates in multi-zone configurations, accounting for both natural and mechanical ventilation, and including the dependence on height and temperature gradients in the space.

STRATIFICATION: Existing simulation programs calculate a single indoor air temperature in each thermal zone being analyzed. The real temperature distributions in the space are important in determining transmission heat losses; air change rate between the atrium and ambient, and between the atrium and adjacent spaces; air motion within the atrium; and comfort conditions. In order to provide a more faithful representation of thermal conditions in an atrium, the spatial distribution of air and surface temperatures must be determined.

AIR FLOW PATTERNS: None of the existing simulations account for air movements within individual zones. Air movements influence transient thermal conditions, temperature distributions, comfort conditions and energy performance. For example, none of the programs explicitly estimate the impact of "drafts" caused by downward air flow at cold surfaces on comfort conditions, or the impact of free upward convection from heating devices on heat losses through surfaces above the heater. Algorithms are needed which enable local air flow distribution to be calculated.

SURFACE FILM COEFFICIENTS: Most calculation programs provide fixed, global values for surface film coefficients, and many do not even account separately for the convective and radiant components of heat transfer at the surface. Because there are often substantial local differences of air flow and temperature conditions within atria, the magnitudes of each component can vary significantly from surface to surface, affecting heat transfer and comfort conditions.

SOLAR RADIATION: Few simulation programs use geometric models to calculate the distribution of solar radiation on surfaces internal to a zone, or solar radiation transmission through glazed partition walls to adjacent spaces. Failure to accurately account for the distribution of solar gains between the atrium and its adjacent spaces negatively impacts the reliability of daylighting and thermal calculations. Furthermore, proper accounting for the distribution of solar gains among surfaces is necessary in order to properly calculate surface temperature, and therefore air flow profiles,

convection coefficients at surfaces, interior air temperature distributions, and radiative exchange between surfaces.

All of the problems identified above are interconnected, and, to some extent, result from the basis of existing programs in heat transfer, rather than mass transfer. Various "tricks" can be used to circumvent some of the problems - at least in part. For example, temperature stratification and air flow patterns in large spaces such as atria can be approximated by sub-zoning the space into two or more adjacent zones which can be at different temperatures and between which air exchange can be modelled; this allows the spatially continuous variation in temperatures within the larger space to be approximated as discrete changes in temperature across sub-zone partitions. While this may improve the representation of the atrium in the simulation, it requires considerable engineering judgement that is typically not based on well defined facts: in the example cited above, a sub-zoning configuration must be postulated and an air flow path (typically with constant heat transfer coefficients representing a certain air velocity) must be defined. These "tricks" may improve the model, but they are not entirely satisfactory.

Other ways of dealing with mass transfer in atria should be considered. Complex simulation programs have been developed for calculating heat and mass transfer, considering turbulence effects and transient temperature dependent physical properties of the medium. A fundamental shortcoming of many of these programs in application to atria is that while they provide technically sound analyses at high air speeds, the solution of the Navier Stokes equation becomes unstable with decreasing velocities in non-constant local fields. In addition, because of the complexity of the programs, unacceptably long computation time is required to deal with the time (e.g., annual) and spatial (e.g., tens of meters) scales of interest in atrium analysis. Furthermore, most of these programs were developed for aerospace applications where fixed boundary conditions commonly can be assumed; as a result, these programs do not account for the effect on temperature distribution and energy balances of user scheduled parameters (e.g., shading), for complex building heating, cooling, and ventilation systems and controls. In short, these more detailed methods too are seriously limited in analysis of atria."

As seen in the contents of this report, it is the limitations listed above we have concentrated on in this project.

Another problem that arise when choosing a simplified simulation program is how to identify the critical factors for the problem in question. Which principles must be studied in detail and which can be omitted? For example, is the solar energy distribution in the atrium critical for the calculation of the energy consumption in the building? and is it necessary to study the whole building or will a part of it suffice? When choosing the level of detail, it is also necessary to be aware of the availability or the accuracy of the input data. An example is the availability and accuracy of infiltration data for an atrium. Thus the problems with choosing and using models as discussed above, can be generalized in the following questions:

Model:

Does the program have the algorithms for the principles to be studied?

If it has the algorithms, do they "work" for the problem in question?

- Does the program offer the right time-steps to study the problems?

Data:

- Do the data exist that the program requires?
- How accurate are these data?

The correctness of the simulation results depends heavily on how positive these questions may be answered. Information to answer these questions should therefore be developed for the simulation programs and their algorithms. It is our wish that this report can answer some of these questions for researchers and designers that study atrium buildings.

1 Executive summary -problem definition

1.1 Introduction

The goal of this project was to define, describe and develop better building energy simulation models for infiltration and natural ventilation, stratification, air flow patterns, surface area film coefficients and solar radiation in atria. As these simplified models will not cover all situations, Computational Fluid Dynamics, (CFD), models were used and compared to monitored results. The CFD models are used to cover the lack of measurements and in connection to zonal models to provide input data for these. Methodology on how to use these models to study thermal comfort in atria and how to combine them with zonal models was also developed.

1.2 Thermal comfort

Extreme thermal situations (hot, cold, draught, direct sun) often occur in atria. A thermal comfort model is useful to predict the usability of the atrium. A thermal comfort model that considers air and surface temperatures and cold draughts is developed and integrated into the Norwegian program FRES.

Thermal comfort is the state when the human is satisfied with his or her thermal environment, the person's body feels thermally neutral—not too warm or too cold. Thermal comfort is a widely used criterion when designing the HVAC system in a building.

This chapter contains a description of the ISO 7730 standard, "Moderate Thermal Environments - Determination of the PMV and PPD Indices and Specification of the Conditions for Thermal Comfort", that gives a method to evaluate the thermal comfort for the body as a whole.

In addition, limits for the following local thermal comfort parameters are given in the appendix of the ISO 7730 standard :

- Vertical temperature difference
- Warm and cold floors
- Asymmetric radiation.

The parameters that define thermal comfort are:

For the users: Activity level and clothing
For the room/area: Room air temperature, surface temperatures, solar radiation, air velocity and vapour pressure.

Room air temperature, surface temperatures, vapour pressure and solar radiation are reported from building energy simulation programs. Air velocity can be defined by a minimum value, calculated manually or by CFD programs

These values are suggested as input to ISO 7730 standard to determine the thermal comfort in the area under study.

An example is shown by using the building energy simulation program FRES. It calculates thermal comfort for five situations:

- Air temperature.
- Air and surface temperatures.
- With window surface temperature as dominant surface temperature.
- In direct sun.
- With window surface temperature as dominant surface temperature and with draught from the window.

Operative temperature is also calculated and presented.

1.3 Stratification

Stratification occurs in atria in periods of high solar gains. The stratification is important for calculation of thermal comfort, and it is also critical for heat recovery systems that utilize the surplus heat under the ceiling. Norway and Switzerland have developed algorithms for stratification that are included in simplified calculation programs. Sweden has tested a method in DEROB.

The temperature stratification is an important characteristic of large glazed spaces such as an atrium. The stratification depends on the thermal condition, and particularly on the distribution of the solar and internal heat gains. The air movement in the atrium and between the outside or adjacent zones also have a significant influence on stratification.

The three atria presented in this chapter illustrate different situations where temperature stratification occurs, and when a homogenous temperature assumption is not far from reality. Temperature can be seen as positive for the comfort of the occupied zone at the ground level, but can also lead to overheating problems if the upper part is occupied or in adjacent offices. In winter, temperature stratification is a disadvantage because the atrium will require more heat in order to obtain comfortable conditions on the ground level. In summer, natural ventilation is often used to obtain thermal comfort. The stratification is then reduced, and a simulation tool that assumes well mixed air will give reasonable results.

For energy consumption prediction, it is probably not important to take into account the temperature stratification. Very often, heated spaces are not stratified, as for example, in the ELA building. The reason is that convectors (heat sources) and cold surfaces (glazing of the gable and the roof) are creating a strong air movement which will mix the air.

The studies conclude that the linear temperature stratification model works well in the ELA building case. This temperature profile is, however, not valid in cases where there are air vents at different levels.

When no temperature profile is assumed, but the volume is simply divided horizontally, the correct distribution of the solar gains in the vertical partitioning is the most important parameter for the correct temperature calculation. Simulation tools that are able in their standard form to predict this distribution, such as DEROB, give reasonable results. Other programs, such as TRNSYS, must be corrected as shown in chapter 3.11.3.

A simple flow field assumption also gives reasonable results, particularly when vents are opened and the atrium is naturally vented. Down draught problems cannot be identified with these simple flow field models.

The effect of the temperature stratification on building energy consumption seems not to be very important in most atria. But more sensitivity studies must be completed before a final conclusion can be drawn.

1.4 Natural Ventilation.

Natural ventilation is a widely used technique for cooling in atria, but problems with thermal comfort often occur in spring and autumn.

Natural ventilation can be used as a means to cool atria and the adjacent building, based on both buoyancy and wind induced natural ventilation effects. This chapter provides formulas to study natural ventilation by buoyancy and wind, separate and together. It also gives data on infiltration in existing and new atria.

A method is presented on how to calculate thermal buoyancy for two separate openings, a single vertical and a single horizontal. For two separate openings, natural axis, air velocities and ventilation capacity as a function of opening area can be studied. Required and optimum opening area can be calculated.

The influence of thermal stratification on natural ventilation is also shown. Resistance and contraction values for the openings are suggested.

Calculation of natural ventilation can be performed by hand, as a part of a CFD simulation or by a building energy simulation program.

The infiltration rate in buildings and especially in atria is hard to determine. It varies depending on climate, building shape, site and location. The infiltration rate strongly influences the thermal climate and the energy consumption in the atrium. This chapter presents monitoring results on infiltration for old and new atrium buildings in Sweden. The monitoring shows a wide variation in the infiltration rate.

1.5 Surface heat transfer coefficients

The heat loss through the glazing in an atrium varies depending on convection and long wave radiation towards the sky. The surface heat transfer is composed of radiation and convection. This chapter contains a description of the theoretical and practical interior and exterior surface heat transfer coefficients.

The principle of radiative heat transfer between surfaces is described. For interior surfaces emissivity values are suggested. For exterior surfaces sky temperature studies are presented and values suggested. The influence of surface slope is also shown.

The theory of free convection on vertical, inclined and horizontal surfaces is presented. The location of the heat source or warm surface is also discussed. Formulas are presented for both forced and combined free and forced convection.

For interior surfaces a method to combine radiation and convection coefficients into a simple coefficient is presented. Results of laboratory

and full scale measurements are shown. Recommendations are given on values for radiation and convective coefficients for warm and cold ceilings, floors and walls.

For exterior surfaces, it is suggested not to combine radiation and convection. Monitoring results are presented on wind tunnel and full scale measurements, and recommended values are given for walls and roofs.

1.6 Solar Radiation

The solar radiation into and through an atrium influences both thermal comfort and energy consumption in a building. It is hard to make estimates of the solar gains due to the building's and solar movement's geometrical complexity.

In order to take solar radiation into account, different levels of detail could be used in building energy simulation programs. The incident solar radiation should be calculated and so must the radiation transmitted through windows. The transmitted radiation has to be distributed to the different surfaces in the room and to adjacent rooms. The part of the transmitted radiation that will be absorbed should also be calculated. Each of these parts could be calculated by methods providing different levels of accuracy or treated as input data. The level of accuracy is of course dependent on the application. For example, in an atrium building, a simple calculation method for solar radiation will give less accuracy than for an ordinary building.

The long wave sky radiation also should be calculated when studying atrium buildings. The long wave sky radiation will, especially when having glazed roofs, influence the temperature in the atrium, the level of comfort and the energy need.

The differences in the calculation methods and levels of detail concerning short wave radiation were exemplified in a study of a room with two windows, and which in some cases was connected to a sunspace. Three different sunspaces were used. The first had all the outer walls and the roof glazed. The second had only the south facade glazed. And the third had only the roof glazed. The influence of the short wave absorptivity of the inner surfaces was also studied. The four different programs evaluated, showed very large differences in calculation results. The conclusion is that if atrium buildings or other types of glazed spaces are to be studied, it is essential to base the calculations on a geometrical description of the buildings, taking into account transmission through windows, reflections, absorptivity and retransmissions through windows. It is important

to take into account the retransmission of solar radiation to the outside or into adjacent rooms as only the radiation staying in the sunspace will be a part of the energy balance used for calculation of temperatures and energy needs. Building energy simulation programs used for ordinary buildings are not automatically suitable for atrium buildings.

A simplified method to calculate how much of the transmitted solar radiation will be absorbed in a sunspace is presented. Four types of glazed spaces are studied and the influence of different parameters is evaluated. The method is based on calculations with DEROB-LTH, which is a building energy simulation program using a geometrical description of the building to calculate the solar radiation.

An example of a method calculating shadows is also presented. The method has been implemented in a PC software application, called Xsun, which can function as a stand-alone design tool or may be integrated with programs for thermal simulation of buildings or solar systems. An example is given where Xsun is integrated with the thermal simulation tool TSBI3.

1.7 Test Studies

When developing and testing models in building energy simulation programs and CFD tools, a few cases were used as example buildings. These buildings are Neuchatel University in Switzerland, Taman in Sweden, Bertholt Brecht Secondary School in Germany and the Technical University in Trondheim, Norway. Neuchatel, Taman and Technical University are existing atrium buildings where solar radiation, temperatures, air infiltration and energy consumption have been monitored. These measurements are used for comparison when simulating temperatures and energy consumption and when studying temperatures and air movements with CFD models.

Bertholt Brecht school has an open courtyard that will be covered with glazing to make an atrium. Different strategies for renovation are studied with the building energy simulation tool SUNCODE. After the renovation is performed the atrium will be monitored.

1.8 CFD models

CFD models are useful to make detailed studies of natural ventilation, stratification, air flow patterns and thermal comfort. They are also useful

when there is a lack of monitoring results. There is little experience with using such models for atrium buildings.

The principal recommendations for the CFD users are: CFD can play an important role in the HVAC design of atria, though its use demands sound engineering judgement. To keep design costs down, CFD should be used sparingly, and always together with simpler design tools. CFD should therefore generally be limited to the last stage of the design process in order to verify the proposed ventilation design. The required computational accuracy is dictated by the requirement for thermal comfort.

The k-c turbulence model is satisfactory for most ventilation design applications, though it is recommended that the k and ϵ equations include damping functions and buoyancy terms to more accurately model low-Reynolds number flow present in atria, including damping effect of stable thermal stratification.

It is important to calculate net solar gain accurately and to distribute it realistically among the atrium surfaces. This requires a geometric model of the building. It is not necessary to account for internal reflections (specular or diffuse) between surfaces; doing so marginally improves the correctness of the CFD analysis. The best surface boundary condition for absorbed solar radiation is to superimpose it as a plane heat source as described in the chapter.

Care should be taken to refine the computational grid in regions of locally steep gradients. Automatic grid generation (adaptive grid methods) makes this easier. Steady-state supply jets should be modelled using either the box method or the prescribed velocity method. This reduces the number of grid points needed to model the atrium.

It is vital to account for heat transfer by surface-to-surface radiation exchange and it is important to model the thermal capacity of an atrium's building structure. This is most simply done by carrying out a steady state CFD simulation of the worst case condition, using quasi steady-state boundary conditions taken from a dynamic model.

A more exact method is to carry out a transient CFD analysis with boundary conditions taken from coupled dynamic thermal mode. However, the computing time/costs may be prohibitive for detailed transient analysis.

1.9 Building Energy Simulation Programs

This chapter contains a short description of the Building Energy Simulation Programs used in this study. The simulation programs are DEROB-

LTH (Sweden), Fres (Norway), TRNSYS (developed in USA, used by Switzerland) and *tsbi3* (Denmark).

A building energy simulation model is a simplified description of the building. The simplification has in this case been carried out from an energy and indoor climate point of view, so that the model only describes the aspects which are relevant in this connection.

A standard list is used to describe each program to make it possible to compare the programs. For each program the following are described: Energy transmission (numerical method, heat transmission), solar radiation and distribution, shading devices and shadow, infiltration, stratification and air movements, ventilation and air conditioning, internal gains, heating and cooling, other systems (heat storage, heat pump), daylight, moisture, thermal comfort, limitations, input/output.

The building energy simulation programs can be used to study thermal comfort and energy consumption in atrium buildings to different levels of detail. If air velocities are to be studied, a CFD tool must be used.

2 Thermal comfort

2.1 Introduction

2.1.1 Thermal comfort

Thermal comfort is a prerequisite for good indoor climate. Thermal comfort is perceived when a human is satisfied with his or her thermal environment, that is when the person's body feels thermally neutral- not too warm and too cold. The person should neither feel any disturbing local cooling nor heating on the body (Fanger (1970)).

It is necessary, but not satisfactory, that the body is in thermal balance with the environment. In addition, the skin temperature and sweat should be at a level that feel neutral at a given metabolism (Fanger (1970)).

The ISO 7730 standard "Moderate Thermal Environments - Determination of the *PMV* and *PPD* Indices and Specification of the Conditions for Thermal Comfort" gives a method to evaluate the thermal comfort for the body as a whole.

In addition the appendix of the standard gives limits for the following local thermal comfort parameters:

- Vertical temperature difference
- Warm and cold floors
- Asymmetric radiation.

A method to calculate draught risk will also be included in the next edition of ISO 7730. The parameters that define thermal comfort are:

For the building users:

Activity level and clothing

For the room/area:

Room air temperature, surface temperatures, solar radiation, air velocity and vapour pressure.

This chapter describes problems connected to thermal comfort in atria, and defines comfort relations and simplified models to estimate draught. Finally an example shows how the thermal comfort post processor is included in a building energy simulation program.

2.1.2 Studying thermal comfort using building energy simulation programs

Thermal comfort can be calculated in a post processing unit to building energy simulation programs. Most building energy simulation programs produce data about solar gain, room air temperature and surface temperatures. Air velocity can be defined or calculated in a post processor. Together with user input on activity and clothing, this gives a basis to calculate thermal comfort as shown in figure 2.1.

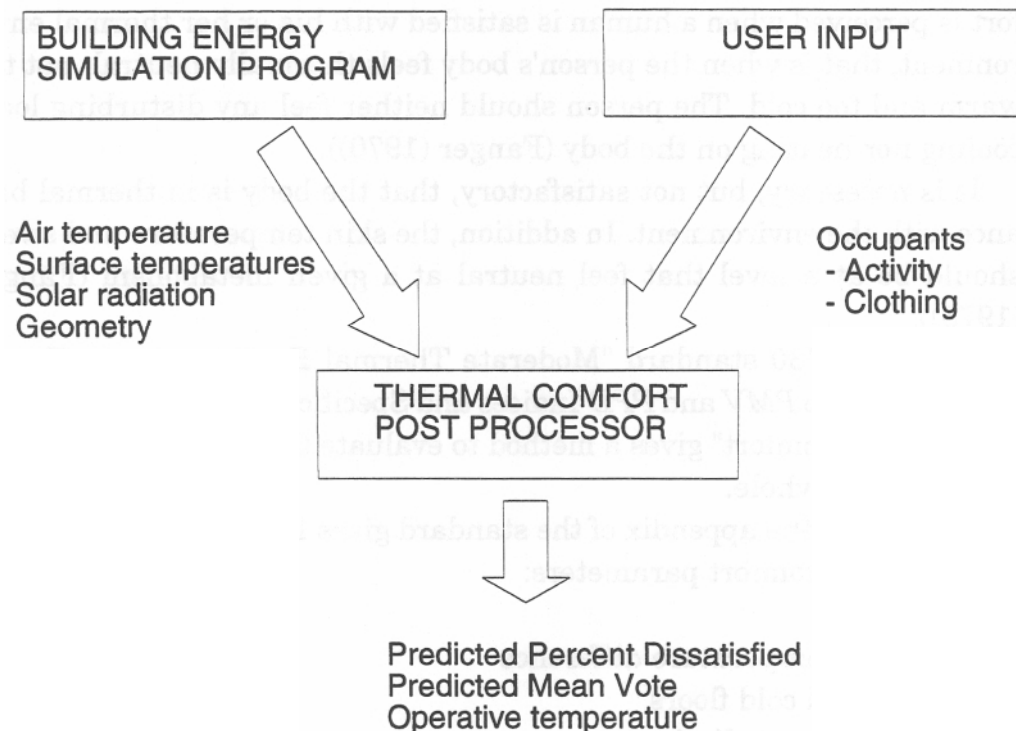


Figure 2.1 A thermal comfort post processor connected to a building energy simulation program.

2.1.3 Thermal comfort in atria

Atria are often large rooms with cold surfaces where stratification and air movements readily occur due to strong thermal forces.

When designing the atrium, it is important to clearly define its use. An atrium designed for sedentary work must be designed for narrow limits of operative temperature, while a shopping street could have a climate like a mild outdoor climate.

If narrow limits of operative temperature are required for some activities, such as in a cafe, local climatization could be a solution instead of heating the whole space.

Local climatization can include heating of floor or furnitures in the occupied area and shelters towards radiation to cold surfaces and cold down draught. Both the air movement and the temperatures in the air and at the surfaces must then be calculated to predict the thermal comfort of different architectural solutions.

Zonal models can be used to study the overall thermal comfort in an atrium. However, in order to study detailed local phenomena and local climatization, a computational fluid dynamics (CFD) model is necessary.

In most cases the thermal comfort model works as a postprocessor on the results of the zonal or CFD model. In a few cases the zonal models include possibilities to use a thermal comfort parameter like operative temperature as a control parameter.

2.2 The ISO 7730 Standard

The ISO 7730 Standard - "Moderate Thermal Environment- Determination of the *PMV* and *PPD* Indices and Specification of the Conditions for Thermal Comfort Standard" (1988) gives a method to estimate expected sensation of thermal comfort for humans as a function of physical activity, clothing, air temperature, mean radiant temperature, air velocity and air humidity. A short description of the content of the standard is given in the following.

2.2.1 The *PMV* Index

To quantify the degree of discomfort, a *PMV* (Predicted Mean Vote) index has been introduced. The *PMV* index is based on a seven point scale as a result of large scale tests on a group of subjects:

- +3 hot
- +2 warm
- +1 slightly warm
- 0 neutral
- 1 slightly cool
- 2 cool
- 3 cold

The *PMV* is based on a heat balance of the human body. It is calculated with the following main parameters that should be within the below listed ranges:

- Metabolism: $M = 46$ to 232 [W/m²], (0.8 to 4 met)
- Clothing: $I_{cl} = 0$ to 0.31 [m²K/W], (0 to 2 clo)
- Air temperature: $t_a = 10$ to 30 [°C]
- Mean radiant temperature: $\bar{t}_r = 10$ to 40 [°C]
- Air velocity : $v_{ar} = 0$ to 1 [m/s]
- Vapour pressure: $p_{da} = 0$ to 2700 [Pa]

The *PMV* value is determined from the following equation:

$$\begin{aligned}
 PMV = & (0.303 \cdot e^{-0.036 \cdot M} + 0.028) \cdot [(M - W) - 3.05 \cdot 10^{-3} \\
 & [5733 - 6.99(M - W) - p_{da}] - 0.42[(M - W) - 58.15] \\
 & - 17 \cdot 10^{-6} \cdot M (5867 - p_{da}) - 1.4 \cdot 10^{-3} \cdot M (34 - t_a) - 39.6 \cdot 10^{-9} \cdot f_{cl} \\
 & [(t_{cl} + 273)^4 - (\bar{t}_r + 273)^4] - f_{cl} \cdot \alpha_c(t_{cl} - t_a)] \quad (2.1)
 \end{aligned}$$

where: (estimated by iteration)

$$\begin{aligned}
 t_{cl} = & 35.7 - 0.028(M - W) - 0.155 \cdot I_{cl} \\
 & [39.6 \cdot 10^{-9} \cdot f_{cl} [(t_{cl} + 273)^4 - (\bar{t}_r + 273)^4] + f_{cl} \cdot \alpha_c(t_{cl} - t_a)]
 \end{aligned}$$

2.2.2 The PPD index

The *PPD* (Predicted Percentage of Dissatisfied) index gives a quantitative predicted number of people who will not be satisfied with the thermal environment. The *PPD* value is therefore an appropriate and easily understandable expression for the quality of the thermal comfort. When the *PMV* index is estimated, the *PPD* index can be found from Figure 2.2, eventually it can be calculated from the Eq. 2.2:

$$PPD = 100 - 95 \cdot e^{-0.03353 \cdot PMV^4 - 0.2179 \cdot PMV^2} \quad (2.2)$$

It is important to note that the lowest value of *PPD* is 5 %, which corresponds to *PMV* = 0. So even if the *PMV* value predicts thermal neutrality, a person may feel local thermal discomfort.

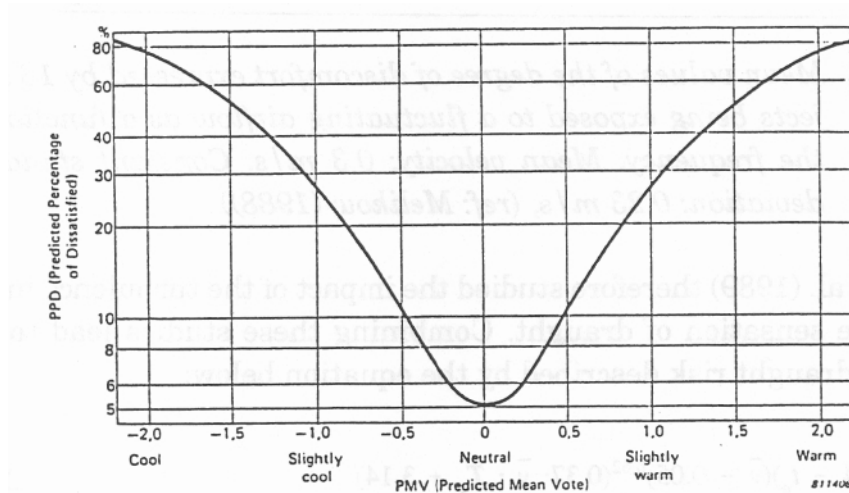


Figure 2.2 The relationship between *PPD* (Predicted Percentage of Dissatisfied) and *PMV* (Predicted Mean Vote), (ref Olesen (1982))

2.3 Local thermal discomfort

Local discomfort may be caused by several conditions, in this report we deal with local convective cooling or down draught caused by cold surfaces, mainly window surfaces. Draught is defined as an undesired cooling of the human body caused by fluctuating air flows. It has been shown that a fluctuating air flow is more uncomfortable than a constant flow.

Figure 2.3 from Melikow (1988), shows the sensation of comfort as a function of the frequency of the fluctuating air velocity. P.O. Fanger and N.K. Christensen studied air velocities with fluctuations for ventilated spaces and derived an equation with the predicted percentage of dissatisfied occupants as a function of mean velocity and air temperature. Comparable studies have been done but the results varies significantly.

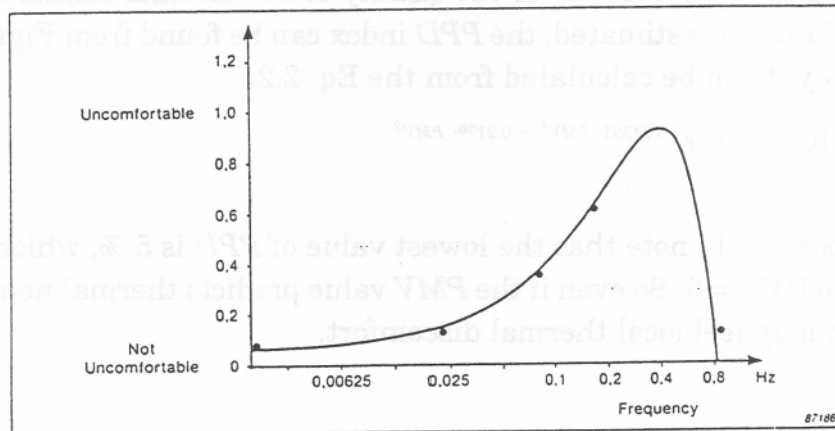


Figure 2.3 Mean values of the degree of discomfort expressed by 16 subjects being exposed to a fluctuating airflow as a function of the frequency. Mean velocity: 0.3 m/s. Constant standard deviation: 0.23 m/s, (ref Melikow (1988))

Fanger et. al. (1989) therefore studied the impact of the turbulence intensity on the sensation of draught. Combining these studies lead to the model for draught risk described by the equation below:

$$PPD = (34 - t_u)(\bar{v} - 0.05)^{0.62}(0.37 \cdot \bar{v} \cdot T_u + 3.14) \quad (2.3)$$

for $\bar{v} < 0.05$ m/s use $\bar{v} = 0.05$ m/s
 for $PPD > 100$ % use $PPD = 100$ %

$$T_u = \frac{SD_v}{\bar{v}} \cdot 100 \quad (2.4)$$

T_u = turbulence intensity, [%]
 SD_v = standard deviation, [m/s]
 \bar{v} = mean air velocity, [m/s]

Figure 2.7 shows the relationship between the mean air velocity and the turbulence intensity.



2.4 Draught due to cooled air falling down along cold surfaces

Draught is usually caused by convective air currents along windows. Especially during the winter, natural downward convective air currents along windows may create considerable velocities in the occupied zone. Skåret (1986), shows that no great errors are made, estimating the maximum velocity, U_{\max} , by using the same equation on both steady state and turbulent convective air flow. Given that the flow is self-conserving and independent of width, and that there is a constant window surface temperature and the pressure is equal to the surrounding air pressure, using Reynolds analogy for turbulent flow over a flat plate (Kreith and Black (1980)), and Blassius theory, yields:

$$U_{\max} = 0.54 \cdot (g \cdot \beta_T \cdot \Delta T_f)^{0.5} \cdot x^{0.5} \quad (2.5)$$

g	=	Acceleration of gravity, [m/s ²]
β_T	=	Volumetric thermal expansion coefficient, [°C ⁻¹]
ΔT_f	=	Temperature difference between the window surface and the ambient air, [K]
x	=	Height of window, [m]
U_{\max}	=	Velocity at the lower edge of the window [m/s]

This formula gives the air velocity of draught from windows and can be used as input to calculate draught risk in formula 2.3.

2.5 The PPD comfort models incorporated in FRES

FRES, version 2.0, a building energy simulation program described in chapter 9, contains 5 different models for estimating the PPD value. This description of the five models is based on Frydenlund and Rømen (1992).

In each case the *PPD* value is estimated from the correlation equation between the *PMV* and the *PPD* index (Eq.2.2) and the formula for the *PMV* value (Eq. 2.1). Seven parameters are used to calculate the *PPD* values.

$$M, W, I_{cl}, t_w, \bar{t}_r, v_{ar}, p_{da}$$

Metabolism, *M*, external work, *W*, thermal resistance of clothing, *I_{cl}*, and the ambient air vapour pressure, *p_{ar}*, are inputs selected by the user depending on expected activity level, clothing level and indoor climate of the building.

The air temperature, *t_a*, obtains the instantaneous air temperature value estimated by the FRES simulations. However, there is one exception. If the stratification model in FRES, shown in figure 2.4, is used, the temperature *Y* metres above the floor is calculated and used in the *PPD* estimation. This stratification model has been experimentally verified by Mathisen (Kolsaker and Mathisen (1991)), and it shows that the profile in many cases becomes more or less linear. For most *PPD* models in FRES, the relative air velocity, *v_{ar}*, is set equal to zero. However, the exception is when calculating the down draught using Eq. 2.5.

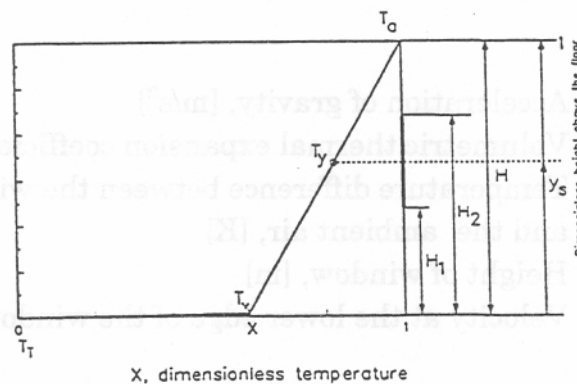


Figure 2.4 The stratification model implemented in FRES, (ref Kolsaker and Mathisen (1991))

2.5.1 Calculation of mean radiant temperature

"The mean radiant temperature related to a person in a given body posture and clothing placed at a given point in a room, is defined as that uniform temperature of black surroundings which will give the same radiant heat loss from the person as the actual case under study", Fanger (1970). The mean radiant temperature in relation to a human being

depends on the person's location and orientation in the room. This must be known to calculate exact values. To evaluate the mean radiant temperature, it is therefore necessary to calculate the angle factors between the body and the surrounding surfaces, as shown in figure 2.5. To estimate the angle factors, it is further necessary to know the right geometrical form, size and distances. In FRES, there are no defined geometrical relationship or geometrical connection between the different surfaces, so the computer program does not have any geometrical "picture" of the rooms or the building. The way the mean radiant temperature is calculated, is therefore simply by using the mean surface area temperature, \bar{t}_r^* , according to the equation below.

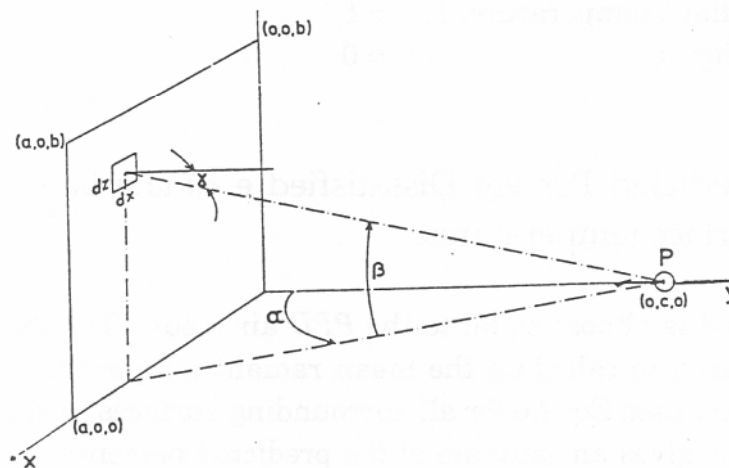


Figure 2.5 Diagram for the development of the evaluation of the angle factor between a person (center in P and facing towards the center of the coordinate system) and a rectangle (a x b) in the x-z plane, ref. Fanger (1970)

$$\bar{t}_r^* = \frac{\sum_{i=1}^{\infty} A_i \cdot t_i}{\sum_{i=1}^{\infty} A_i} \tag{2.6}$$

- \bar{t}_r^* = mean surface area temperature, [°C]
- A_i = ith surface area, [m²]
- t_i = ith surface temperature, [°C]

2.5.2 Predicted Percent Dissatisfied estimate based on air temperature

This model calculates the *PPD* value with regard to the air temperature, t_a , either directly or estimated from the simple linear stratification model. Relative air velocity, v_{ar} , is equal to zero, and the mean radiant temperature, \bar{t}_r , is set to be equal to the air temperature. This identifies the quantity of dissatisfied people for the simulated building with a given metabolism, external work and clothing, just influenced by the air temperature.

Parameters:

Air temperature, t_a	= estimated by FRES
Mean radiant temperature, \bar{t}_r	= t_a
Air velocity, v_{ar}	= 0

2.5.3 Predicted Percent Dissatisfied estimate based on air and surface temperatures.

This model is almost equal to the *PPD* air model. The difference is the method used to calculate the mean radiant temperature, \bar{t}_r . The *PPD* room model uses Eq. 2.6 for all surrounding surfaces, including the windows. This gives an estimate of the predicted percentage dissatisfied of the people seated in the middle of the room, influenced by the air temperature and the temperature of the surrounding surfaces.

Parameters:

Air temperature, t_a	= estimated by FRES
Mean radiant temperature, \bar{t}_r	= \bar{t}_r^* , derived from temperatures calculated by FRES.
Air velocity, v_{ar}	= 0

2.5.4 Predicted Percent Dissatisfied close to a window without considering draught.

This model is a more extreme variant of the *PPD* room model. Instead of estimating a mean surface temperature, the mean radiant temperature is said to be equal to the window temperature, t_w , calculated by FRES. This will give an indication of the thermal comfort influenced by the asymmetric radiation for people seated close to the window.

Parameters:

- Air temperature, t_a = estimated by FRES
- Mean radiant temperature, \bar{t}_r = \bar{t}_w , window surface temperature estimated by FRES.
- Air velocity, v_{ar} = 0

2.5.5 Predicted Percent Dissatisfied when exposed to sun

This model estimates the PPD value for people seated in the middle of the room exposed by direct solar radiation. Using Eq. 2.7 from Fanger (1970), the mean radiant temperature is calculated.

$$(T_r + 273)^4 = (\bar{t}_r^* + 273)^4 + (const \cdot f_p \cdot \alpha \cdot Q_{sun}) \tag{2.7}$$

- T_r = total mean radiant temperature incl. solar radiation, [K]
- const = $1/0.97\sigma$
- σ = $5.77 \cdot 10^{-8}$, Stephan Boltzman's constant, [W/m²K⁴]
- f_p = projected area factor
- α = 0.6, absorption factor

$$Q_{sun} = \frac{I_{tot}}{\sin(\beta)} \cdot \alpha_k \tag{2.8}$$

- I_{tot} = horizontal total radiation per unit area, [W/m²]
- β = altitude, [°]
- α_k = shading factor

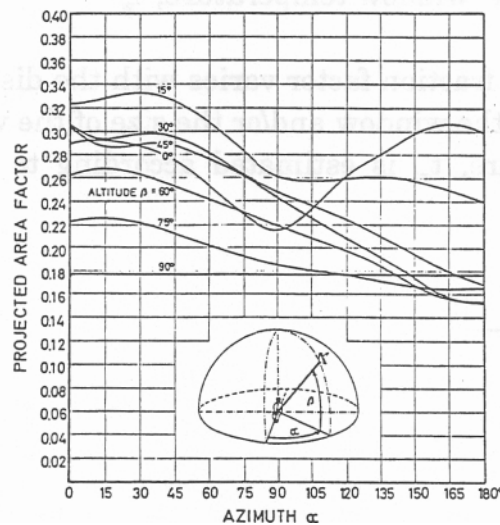


Figure 2.6 Projected area factor for seated persons, nude and clothed, Fanger (1970)

It should be noted that reflected solar radiation has a considerable effect. Figure 2.6 shows the projected area factor as a function of azimuth and altitude angle used to estimate f_p in Eq. 2.7. The graph in figure 2.6 is tabulated in FRES for $\alpha = 0$.

Parameters

- Air temperature: t_a , = estimated by FRES
- Mean radiant temperature, \bar{t}_r = estimated by FRES, Eq. 2.7
- Air velocity, v_{ar} = 0

2.5.6 Predicted Percent Dissatisfied when draught from the window is considered.

This model calculates the *PPD* value in two ways. In both cases the relative air velocity is equal to the maximum air velocity estimated from Eq. 2.5, caused by cold window surfaces. The mean values of the three curves between the air velocity and the turbulence intensity in figure 2.7 is tabulated in FRES. Using Eq. 2.3 alone and Eq. 2.1 and 2.2 together, the two *PPD* values are estimated. FRES always displays the most critical value of the two. The critical area for local discomfort caused by down draught, is the ankles. The air temperature, t_a , used in the equations is therefore replaced by an ankle temperature, t_{ank} , described by Eq. 2.9.

$$t_{ank} = \alpha_f \cdot t_w + (1 - \alpha_f) \cdot t_a \tag{2.9}$$

- α_f = the down draught fraction factor
- $\alpha_f = 0$, gives the air temperature, t_a
- $\alpha_f = 1$, gives the window temperature, t_w

The down draught fraction factor varies with the distance between the seated person and the window and/or the size of the window. The mean radiant temperature, \bar{t}_r , is estimated according to the two following equations.

$$\bar{t}_r^{**} = \frac{\sum_{i=1}^{\infty} A_i \cdot t_i - A_w \cdot t_w}{\sum_{i=1}^{\infty} A_i - A_w} \tag{2.10}$$

$$\bar{t}_r = \frac{\bar{t}_r^{**} + t_w}{2} \tag{2.11}$$

\bar{t}_r^{**} = mean surface area temperature, not including window; [°C]

A_w = total window area, [m²]

t_w = window temperature, [°C]

The window temperature constantly count the same as the rest of the surrounding surfaces.

Parameters:

Air temperature, t_a = estimated by FRES

Mean radiant temperature, \bar{t}_r = $(\bar{t}_r^{**} + t_w)/2$

Air velocity, $v_{ar} = \bar{v}$ = U_{max}

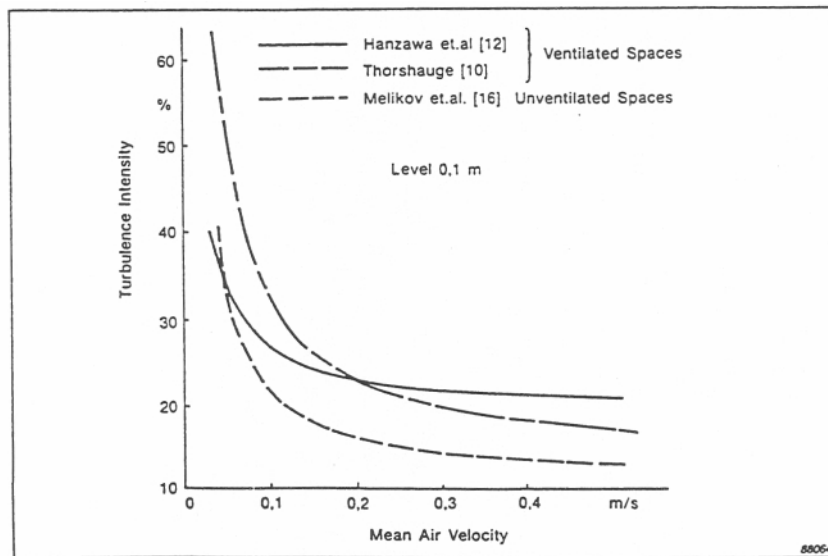


Figure 2.7 Relationship between turbulence intensity (Tu) and mean velocity (v) in ventilated spaces and heated rooms without mechanical ventilation (unventilated spaces), (ref Melikow (1988))

2.5.7 Operative temperature

The operative temperature, t_o , is often used as a measurement of the thermal comfort in a building. The operative temperature in relation to

a person in a given body posture and clothing placed at a given point in a room, is defined as the mean value of a uniform temperature of black surroundings and the air temperature, which will give the same radiant and convective heat loss from the person as the actual case under study. The operative temperature is described by the Eq. 2.12 for thermal comfort mainly at low activity level.

$$t_o = \frac{t_r + t_a}{2} \quad (2.12)$$

\bar{t}_r (mean radiant temperature) and t_a (air temperature) are derived from the simulation results with the level of detail corresponding to the simulation model.

The air- and the operative temperature are graphically presented together with the PPD values for the room or building.

2.6 Summary and conclusions

Thermal comfort is the state when the human is satisfied with his or her thermal environment, that the person's body feel thermally neutral- not too warm and too cold. Thermal comfort is a widely used criterion when designing the HVAC system in a building.

This chapter contains a description of the ISO 7730 standard "Moderate Thermal Environments - Determination of the PMV and PPD Indices and Specification of the Conditions for Thermal Comfort" that gives a method to evaluate the thermal comfort for the body as a whole.

In addition, the appendix of the standard gives limits for the following local thermal comfort parameters:

- Vertical temperature difference
- Warm and cold floors
- Asymmetric radiation.

The parameters that define thermal comfort are:

For the users: Activity level and clothing

For the room/area: Room air temperature, surface temperatures, solar radiation, air velocity and vapor pressure.

Room air temperature, surface temperatures, vapor pressure and solar radiation are output from building energy simulation programs. Air velocity can be defined by a minimum value, calculated manually or by computational fluid dynamics programs

These values are suggested as input to ISO 7730 standard to determine the thermal comfort in the area being studied.

An example using the building energy simulation program FRES is given. Thermal comfort for five situations are calculated:

- Air temperature.
- Air and surface temperatures.
- With window surface temperature as dominant surface temperature.
- In direct sun.
- With window surface temperature as dominant surface temperature and with draught from the window.

Operative temperature is also calculated and presented.

2.7 Symbol list

M	=	Metabolism
W	=	External work
I_{cl}	=	Thermal resistance of clothing
t_a	=	Air temperature
\bar{t}_r	=	Mean radiant temperature
\bar{t}_w	=	Window surface temperature
v_{ar}	=	Air velocity
p_{da}	=	Vapour pressure
T_u	=	turbulence intensity, [%]
SD_v	=	standard deviation, [m/s]
v	=	mean air velocity, [m/s]
g	=	Acceleration of gravity, [m/s ²]
β_T	=	Volumetric thermal expansion coefficient, [°C ⁻¹]
ΔT_f	=	Difference in temperature between the window surface and the ambient air, [K]
x	=	Height of window, [m]
U_{max}	=	Velocity at the lower edge of the window
\bar{t}_r	=	mean surface area temperature, [°C]
A_i	=	i th surface area, [m ²]
t_i	=	i th surface temperature, [°C]
t_{rad}	=	total mean radiant temperature including solar radiation [°C]
σ	=	$5.77 \cdot 10^{-8}$, Stephan Boltzman's constant, [W/m ² °K ⁴]
f_p	=	projected area factor
α	=	0.6, absorption factor
$E_{tot}\beta$	=	horizontal total radiation per unit area, [W/m ²]
	=	altitude, [°]
α_k	=	shading factor
α_f	=	the down draught fraction factor
α_f	=	0, gives the air temperature, t_a
α_f	=	1, gives det window temperature, t_w
\bar{t}_r^{**}	=	mean surface area temperature, not including windows, [°C]
A_w	=	total window area, [m ²]

2.8 References

- Fanger, P.O. (1970). *Thermal comfort. (Analysis and Applications in Environmental Engineering)*. Danish Technical Press. Copenhagen. Denmark.
- Fanger, P.O. et.al. (1989) *Turbulens og trekk. (Eng: Air turbulence and sensation of draught)*. (Norsk VVS No 2). Oslo. Norway.
- Frydenlund, F., Rømen, B.H. (1992). *Thermal Comfort Simulation using FRES*. (SINTEF Report no STF A92014). Trondheim. Norway.
- ISO 7730 Standard (1988) *Moderate thermal environment- Determination of the PMV and PPD indices and specification of the conditions for thermal comfort*.
- Kolsaker, K. and Mathisen, H.M. (1991) *Computer simulation of energy use and thermal climate in glazed spaces*. (STF 15 A92056). SINTEF Applied Thermodynamics. Trondheim. Norway.
- Kreith, F. , Black, W.Z. (1980) *Basic Heat Transfer*. Harper & Row Publishers. New York. USA.
- Melikow, A.K. (1988) *Quantifying draught risk. (Brüel & Kjær Technical Review No.2)*. Nærum. Denmark.
- Olesen, B.W. (1982). *Thermal comfort. (Brüel & Kjær Technical Review No. 2)*. Nærum. Denmark.
- Skåret, E. (1986). *Ventilasjonsteknikk*. NTH. Trondheim. Norway.

3. Stratification of the Temperature in Atria

3.1 Introduction

One important characteristic of large glazed spaces such as atrium is that the air temperature is not always homogeneous but can increase with the height of the atria. This phenomena is called temperature stratification. Depending on the thermal situation, we can define four main temperature distributions in large enclosures.

1. Constant in the height
2. Increasing linearly
3. No linear profile, increasing rapidly in the lower part
4. No linear profile, increasing rapidly in the upper part

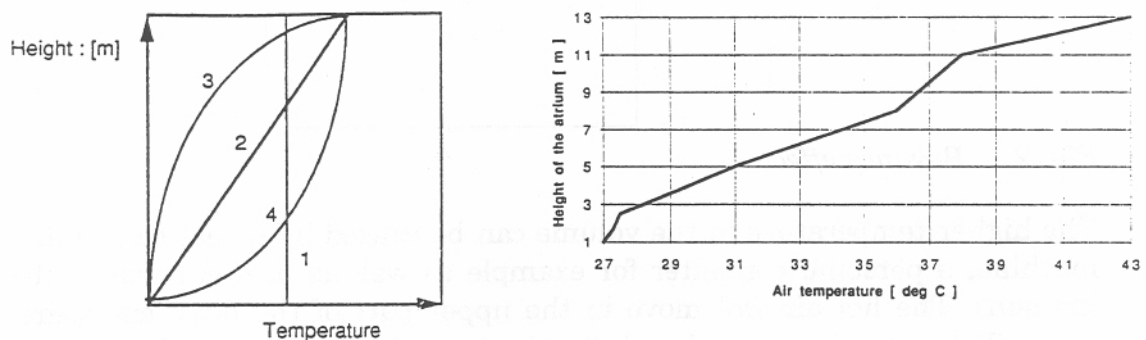


Fig. 1 Typical vertical temperature profiles

Real Case : ELA

Profile 1 is typical for complete mixed situation

Profile 2 is typical in atria where the heat sources are uniformly distributed in the space and its surfaces.

Profile 3 represents the common case where either central heat source or sources generates a column of heated air which rises rapidly to the roof prior to mixing and tends to pool at the upper level, or heat sources are distributed only in the upper part (internal shading under the roof for example).

Profile 4 represents the case where heat sources are close to the floor level.

These temperature distributions are caused by different thermal effects which will be explained later. It is important to notice that on the horizontal direction the temperature of the air is always quite homogeneous.

3.2 Physical theory

The temperature stratification in large enclosures is due to the following effects :

A volume of air which is heated and then reaches a higher temperature than its surrounding will be affected by a driving force, due to density differences between the warm air and the cold air (the warm air is lighter than the cold one), which will tend to displace it in the vertical direction.

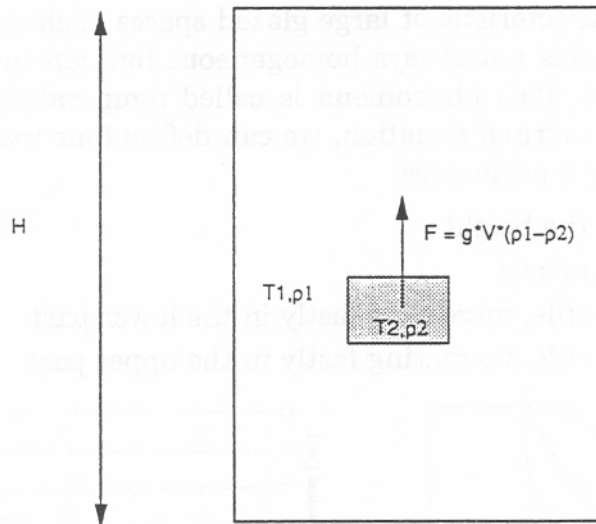


Fig. 2 Buoyancy effect

The higher temperature in the volume can be caused by a heat source of a machine, a personal computer for example as well as heated surfaces (by the sun). The hot air will move in the upper part of the large enclosure, this will tend to increase the air temperature in that region. But as the warm air going up must be replaced by surrounding air, a back flow will take place which will create some mixing.

If the heat source is placed at the floor level there will be no relevant stratification (see fig. 3). In the other hand if the heat source is placed in the middle of the space some temperature stratification will occur.

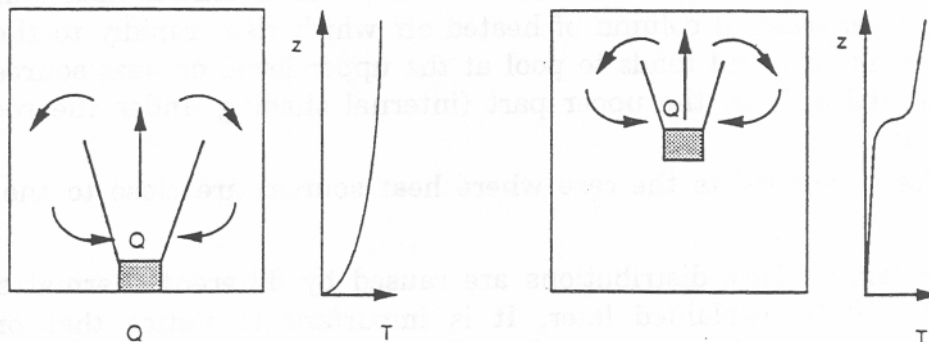


Fig. 3 Position of the heat source and effect on the stratification

3.3 When is stratification important ?

The stratification of the temperature is relevant when the following conditions are fulfilled:

- Height of the volume is important
- Heat transfer to the air from the heat source in the upper part or linearly distributed through the height of the volume.
- Hatches (vents) not opened (or only partially)
- Volume with small air movements
- The internal shading devices will tend to create some stratification.

In order to illustrate the problem, different typical atria situation are shown in the following figures.

a)

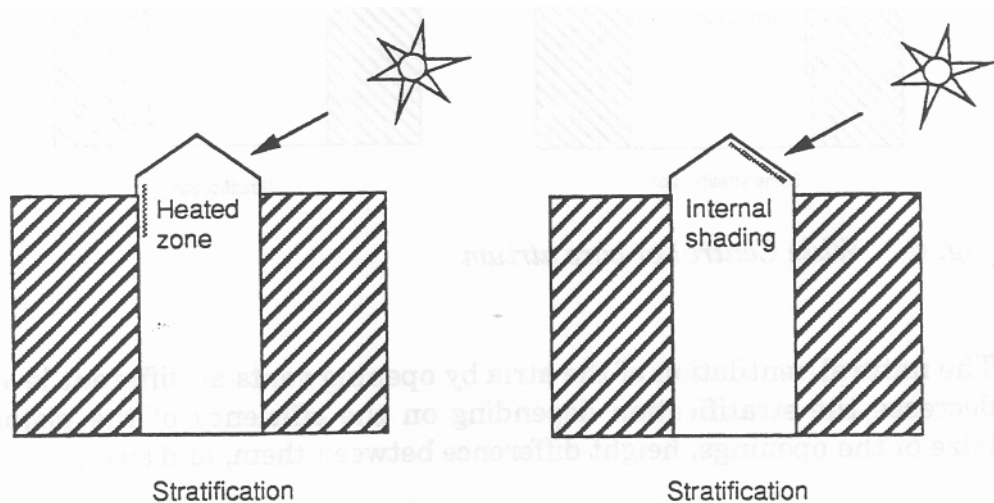


Fig. 4 Central or core atrium

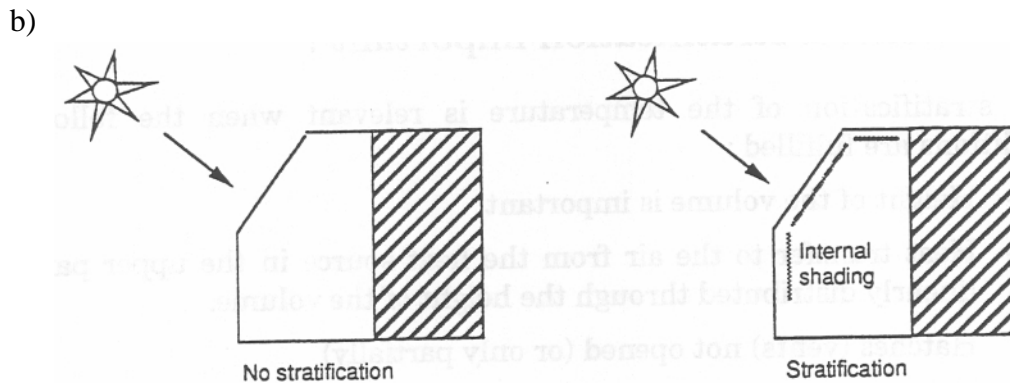


Fig 5 Attached atrium

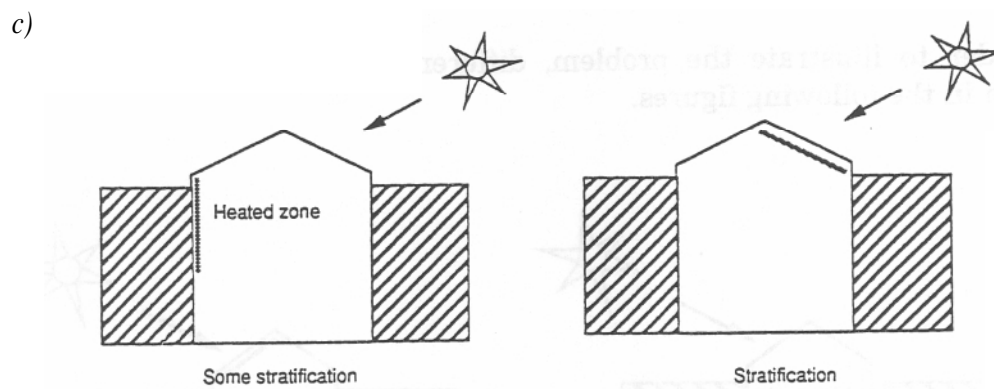


Fig. 6 Wide Central or core atrium

The natural ventilation of the atria by opening vents at different levels will decrease the stratification depending on the efficiency of the piston flow (size of the openings, height difference between them, and so on).

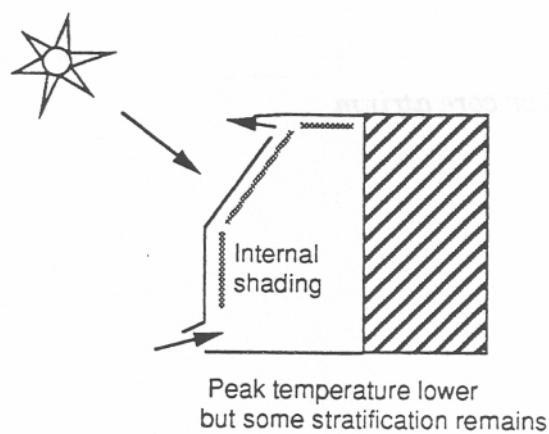


Fig. 7 Attached atrium naturally ventilated

3.4 Examples of existing atria

To illustrate the temperature profiles of existing atria three examples are shown:

- Atrium of the university of Neuchâtel (CH) type b of p.3.4
- Atrium of the university of Trondheim (N) type a of p. 3.3
- Glazed courtyard at Tärnan (S) type c of p. 3.4

In the first two examples, the temperature profile was stratified, in the last one no relevant stratification has been measured. All the three atria are naturally ventilated in the summer.

3.4.1 Atrium of the University of Neuchâtel (Nuni)

The new building of the faculty of literature of the University of Neuchâtel has an attached sunspace. A detailed description of this atrium can be found into chapter 7.1.

The temperature profile that can be encountered in such an attached atrium are summarized by the three typical days represented in figure 8.

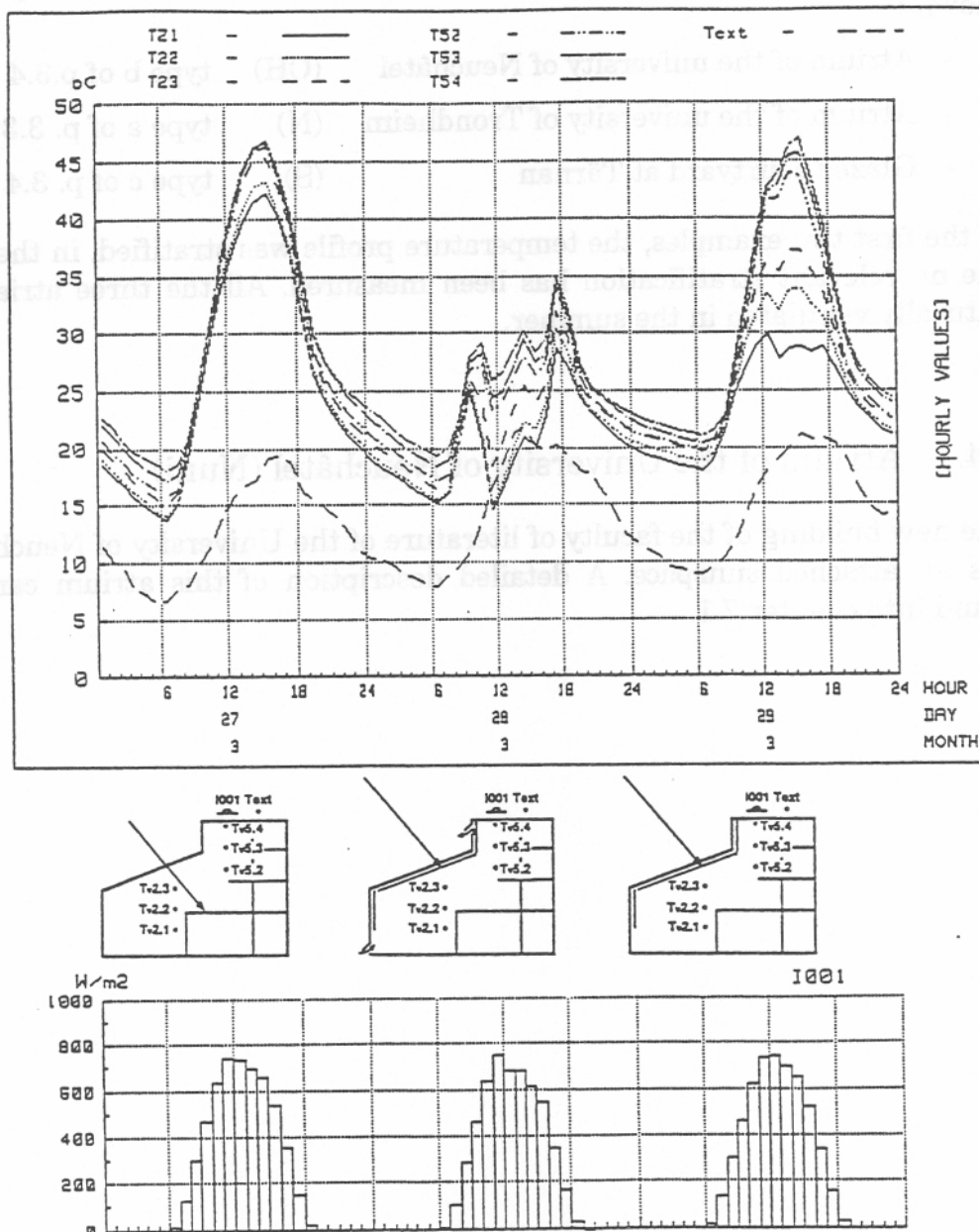


Fig. 8 Measured temperature profiles for three typical days

First day

- No internal shading is used
- The hatches are closed

The air stratification is not relevant (only 4°C), because the solar gains are heating also the lower part of the atrium (ground, walls), and create in this way a mixed temperature condition.

Second day

- The hatches are opened
- The internal shading devices are used

The air stratification is reduced in comparison of the third day (8-10°C), the average temperature in the atrium is also reduced and the occupied zone becomes comfortable.

Third day

- The hatches are closed
- The internal shading devices are used

The air stratification is important (15°C) ! The upper shading devices are intercepting the main part of the solar gains and do not allow them to reach the lower part of the atrium (or at least only small amounts). In the lower part of the atrium the vents are opened briefly (point 7) and a wide mobile wall is opened. The lower part of the atrium is exchanging air with the building which is 20°C.

3.4.2 Atrium of the University of Trondheim (ELA)

A field study has been conducted in Trondheim on a glazed atrium of the university. The dimensions of this large enclosure are 46 m x 10 m x 17 m (high).

A detailed description can be found in chapter 7.4.

Figure 9 shows the effect on the internal air temperature when opening the ventilation hatches at two heights inside the atrium in the summer.

The first 3 days represent opened hatches during which the maximum temperature difference at 13 m and 1,7 m above the floor was only 3 degrees. In the last 2 days during which the hatches are closed a temperature difference as high as 16°C (max. temperature at roof level : 46°C) was recorded.

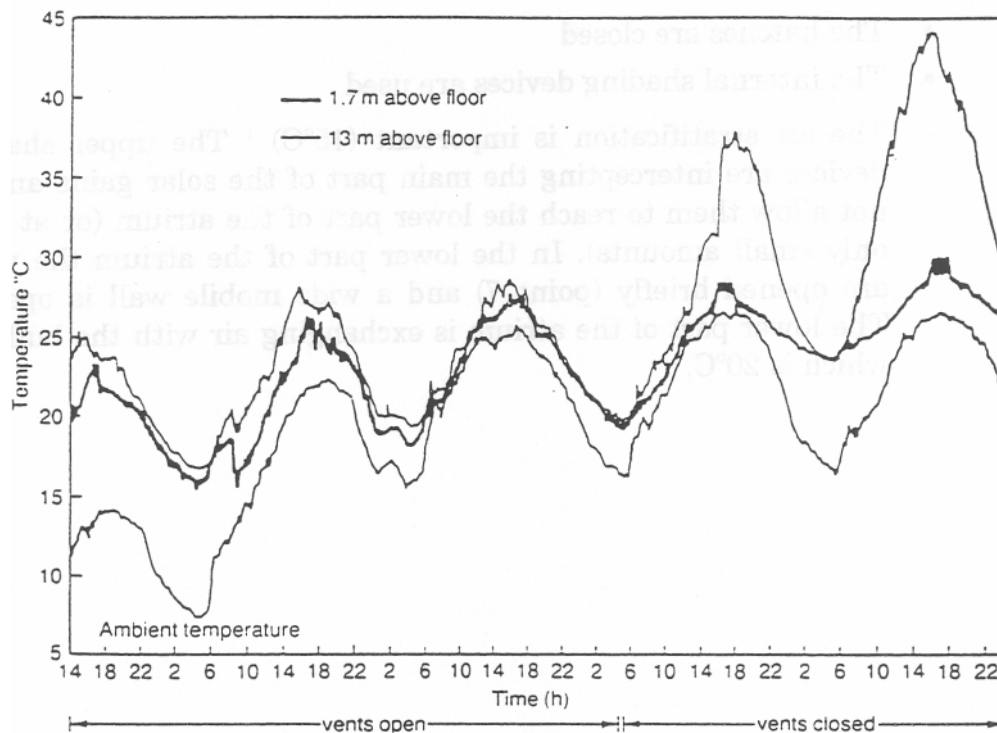


Fig. 9 Measured air temperature at two levels in a glazed atrium with and without passive ventilation

3.4.3 Glazed courtyard at Taman

Also here a detailed description of this atrium can be found in chapter 7.2.

The temperature measurement at different level during a sunny week in May are presented in the next figure.

This week, the curtains were used as insulation during the nights and as sun shades during parts of the days. The vents were open parts of the day during all days except the last one which was cold and cloudy and no curtains were used during daytime.

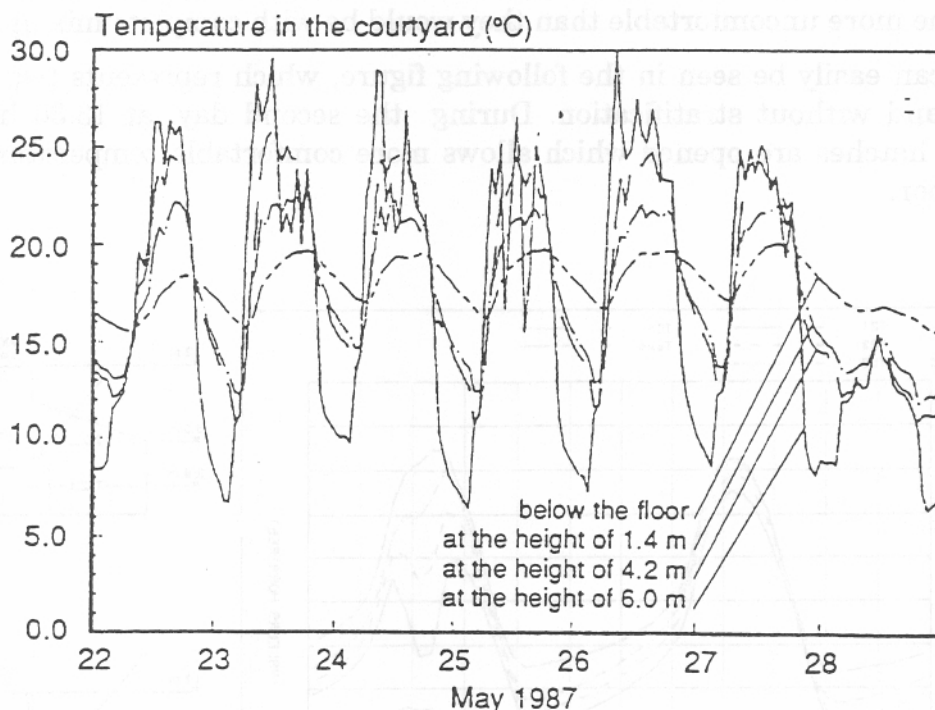


Fig. 10 The temperature at different levels in the glazed courtyard during a week in May 1987

As can be seen, there is not a big stratification between 1,4 m and 6 m height. The irregular shape of the temperature is due to the changes in the shading devices and opened hatches.

In such an atrium configuration (type c p.4) with a small height (~ 6 m) no important stratification is taking place, especially when the vents are opened and the space naturally ventilated.

3.5 Influence of the temperature stratification on thermal comfort and energy consumption

3.5.1 Thermal comfort

During the summer, temperature stratification can be seen as positive for the comfort of the occupied zone at the ground level.

If the peak temperature of the upper part of the atrium is not increased by the internal shading devices which tend to create stratification, the upper occupied zone or the rooms at that level of the adjacent building will not become more uncomfortable than they would be with complete mixing.

This can easily be seen in the following figure, which represents two days with and without stratification. During the second day, at 13.30 h; the lower hatches are opened which allows more comfortable temperature on the floor.

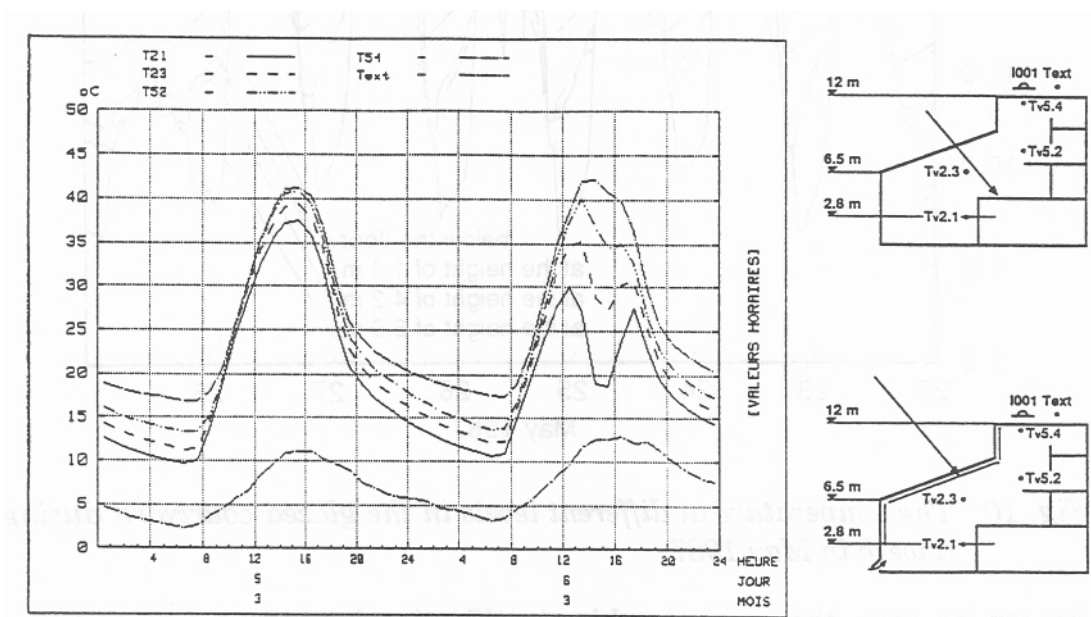


Fig. 11 Temperature profiles with and without stratification for the March 5 or 6 1989 in Neuchâtel

In fact, stratification of the temperature in the summer is not very often sufficient to provide comfortable conditions at the ground level and natural ventilation must be used. It is also important to notice that the atrium configuration which tend to produce a temperature profile of the type 3 (fig .1) will be better for the comfort if there is some occupied zones at different levels. The same remark is valid for the adjacent buildings room especially if they have openable windows to the atrium.

Winter time

In winter time, especially in heated atria, temperature stratification is a disadvantage, because it will require the heating system to overheat the upper part of the atrium to obtain comfortable conditions in the occupied zone (lower part of the atrium).

3.5.2 Energy consumption

For the comfort point of view it is important for the designer to be able to predict the temperature stratification in the atrium. On the other hand : it is not quite clear if it is very important to take into account the temperature stratification in the annual energy consumption of the atrium and the adjacent building.

In order to illustrate the problem three type of calculations have been done with the atrium of the University of Neuchâtel (Nuni).

1. The first calculation assumes that the air temperature of the atrium is fully mixed, and that the use of the shading devices and of the vents are controlled using this mixed air temperature. When the air temperature is greater than 26°C the shading devices are used and the vents opened.
2. The second calculation takes into account the temperature stratification using the model presented in chapter 6.5. The use of the shading devices and of the vents (opening for natural ventilation) is controlled using the temperature of the first zone (ground level). The shading devices and the vents are used when this temperature is greater than 26°C.
3. The third calculation is the same case as number two except for the control value which is not the first zone any more but the last one (top of the atrium).

In the three calculations the control temperature for heating is 16°C. The outside glasses of the atrium have a U value of 1.5 W/m²,K

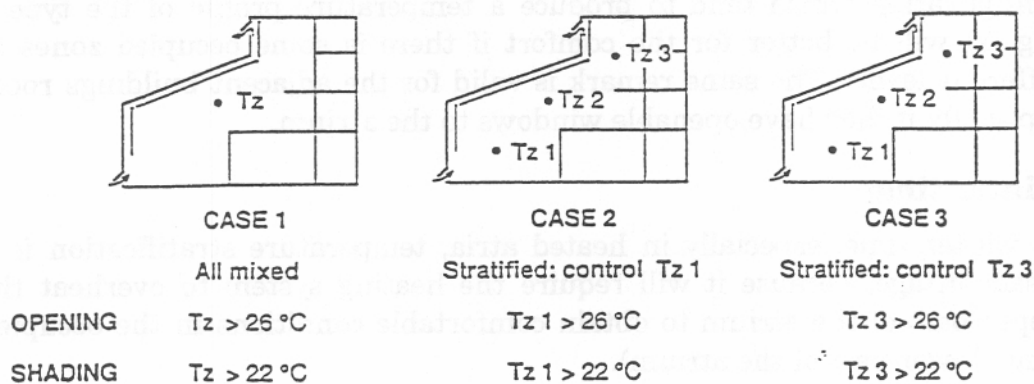


Fig. 12 Energy consumption calculation *with three different control strategies for the opening of the vents*

For a cold day without the stratification there will be no difference between the three calculations. For a sunny day with reasonable outside temperatures the calculation number 3 will open the vents more rapidly if stratification occurs. The number 2 is the one which will open the vents latest, the number 1 being in between.

The results of the heat consumption of the atrium and of the adjacent building for the three calculations are given in the next table. The simulation have been done for a year.

	1. Mixing		2. Stratification : Control based on lower zone temp.		3. Stratification : Control based on upper zone temp.	
	Total	Atrium	Total	Atrium	Total	Atrium
kWh	324608	9979	323398	9467	325968	10565
%	100	100	100	95	100	106

The differences are not very important if we are interested in the total energy consumption of the building. So that in the case of Nuni, we can conclude that for the energy calculation it is not important to be able to model the temperature stratification. The mixed assumption give already a good result. Of course if one is interested only in the atrium consumption we have a difference of 6 % between the case 1 and 3.

In other atrium types (higher thermal mass, core or central atrium) the differences could be more significant.

3.6 Simplified models

3.6.1 Definition of the simplified models

Existing simulation programs calculate a single indoor air temperature in each thermal zone being analyzed. The real temperature distributions in the space are important in determining transmission heat losses, air change rate between the atrium and ambient, between the atrium and adjacent spaces, air motion within the atrium and comfort conditions. In order to provide a more faithful representation of thermal conditions in an atrium, the spatial distribution of air and surface temperatures must be determined.

The simplified model (S.M.) should be able to be incorporated in a dynamic building energy simulation program in order to overcome the lack of information of the single indoor air temperature model.

3.6.2 Modeling approaches

During this IEA task, different approaches have been used by the participants. They will be briefly presented :

1. Linear model (Norway)
2. Superposition of standard single zone model of a building simulation program (Sweden + Switzerland)
3. Single volume with different air nodes and wall temperatures in the vertical direction (Switzerland)

Each approach will be briefly presented, and some comparison with measurements in atrium will be shown.

3.7 Linear model

All the information from this chapter is coming from the paper of K. Kolsaker and H.M. Mathisen presented in Roomvent 92.

3.7.1 Background

The use of glazed atria has become more common during the last years. One typical characteristic of these type of premises is that the air stratifies with a temperature increasing with the height. The displacement ventilation system, which has the same quality has also become common in use. It is therefore a demand for simulation programs for calculation of the annual energy use and peak loads in such situations.

In glazed atria the ventilation airflow rate is often zero. Consequently, if we have the infiltrations the temperature stratification is maintained only by the convection flows, i.e. flows from heat sources like windows and other surfaces heated by the sun and flows directed downwards due to surfaces with a temperature lower than the room air temperature.

If the atrium is ventilated by air blown in with an impulse strong enough to cause mixing of the air, a uniform temperature will be the result.

The dominant heat losses in an atrium is due to transmission losses through glazing and infiltration losses.

Accordingly :

Under conditions with complete mixing (heating in the lower part and/or significant down draft, no solar radiation) simulations with programs using one node to represent the air temperature, should give adequate results for air temperature and energy demand for potential heating. During the hours of the year when there is some solar radiation and a heating demand, (i.e. some stratification), these simulations will underestimate the heating demand. Heat of the lower part of the atrium will be necessary in spite of that the upper part is thermally comfortable.

Under conditions with poor mixing, the simulated air temperature will represent the temperature in the upper part of the atrium (more so in a linear and a core atrium than in an attached and envelope atrium). The calculated thermal climate gives us little information about the climate at floor level.

3.7.2 Linear temperature stratification model

As mentioned, simple algebraic calculation of convection flows in rooms with a changing vertical gradient is difficult. Experiments and field measurements have shown that the profile in many cases becomes more or less linear, as shown in principle in figure 13.

The reason is that the heat sources are distributed by radiation to the surfaces in the room. Thermal transmission through walls and windows may also influence on the thermal stratification.

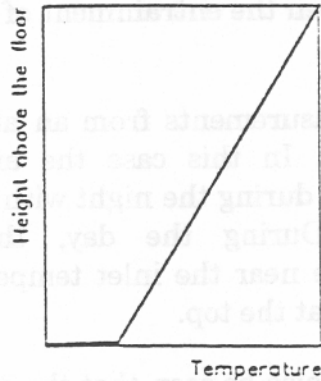


Fig. 13 Temperature profile in rooms with weak and distributed heat sources and little mixing of the air

An air temperature distribution dependent on the level above floor level and some characteristics about the room is also an interesting alternative, and may be more simple to implement than a two or multi-zone model.

In figure 14 examples from measurements in a test room with displacement ventilation are shown. The dimensionless temperature $\frac{T_{actual} - T_{supply}}{T_{exhaust} - T_{supply}}$ is plotted against the height above the floor. The temperatures were measured from the surface of the floor to a point close to ceiling.

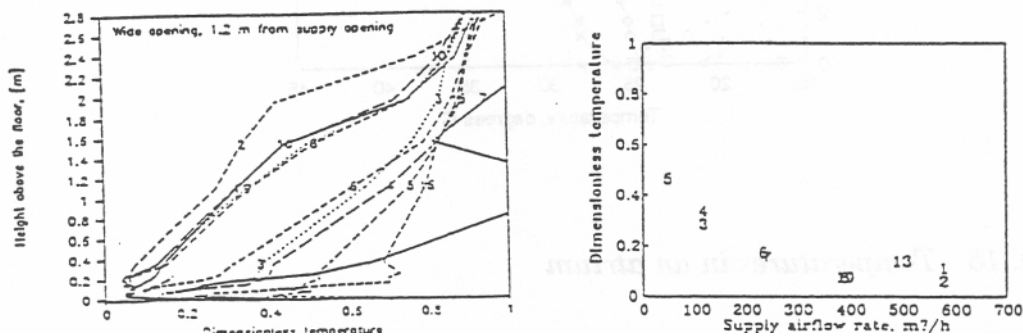


Fig. 14 a) dimensionless temperatures in a room with displacement ventilation plotted against the height above the floor. b) dimensionless temperatures plotted against the supply flow rate. The numbers in a) refer to the numbers in b)

It can be clearly seen from Fig. 14 that the shape of the profile varies from test to test. If the curves are related to the airflow rates as shown in Fig. 14 it is obvious that the shape of the curves depends on the airflow rate. What actually happens is that when the supply airflow rate is reduced the height of the lower zone decreases when the entrainment of the convection flow is constant.

The profiles in fig. 15 are measurements from an atrium under different solar and thermal conditions. In this case the air flow rate is quite constant. The gradient is small during the night with a small heat load and low surface temperatures. During the day, the gradient can be considerable, with temperature near the inlet temperature near the floor and a high temperature (45°C) at the top.

From experimental data it can also be seen that the shape of the profiles is almost the same in all positions. This is due to the poor entrainment of ambient air in the flow. However, the quality and the position of the heat sources and the ceiling height plays an important role for the shape.

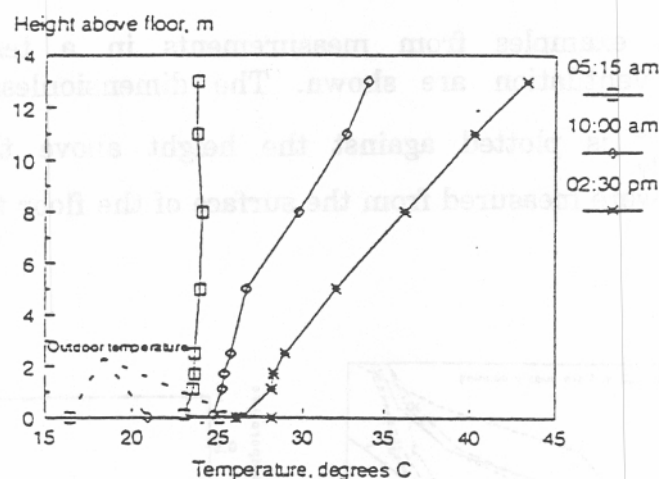
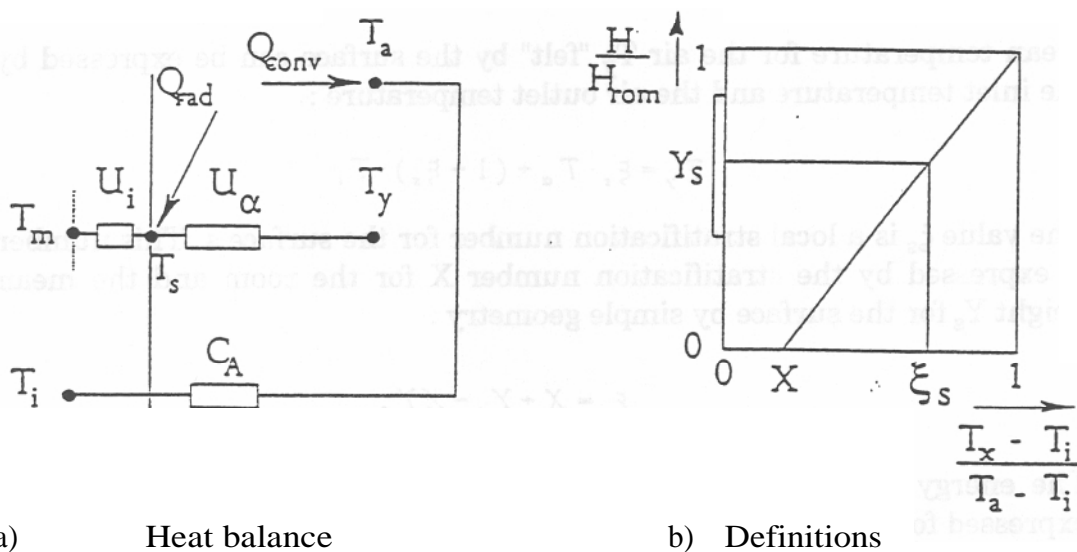


Fig. 15 Temperatures in an atrium

FRES (Flexible Room climate and Energy Simulator see chap 9.) is a dynamic simulation program for multi-zone buildings developed at SINTEF Division of Heating and Ventilation. The program is a tool for HVAC consultants and building designers, widely used in Norway. The objectives are to implement a simple and still reliable model that can improve the existing single-temperature zone model and make it a better tool for atrium simulation.

The proposed linear stratification model is implemented in FRES as described in the previous sections. For calculation of heat transfer between room air and room surfaces, the temperature difference between surface and room air at the mean height of each surface is used.

The convective heat flow to each surface is calculated for the stratified case, ensuring the correct heat balance for the whole building. The stratification will for example make floor and ceiling "feel" different air temperatures. To take care of this, the equation for convective heat flow is modified, taking into account the linear stratification model. This is quite simple, as will be shown here.



a) Heat balance

b) Definitions

Fig 16 The model implemented in FRES

The temperature T_x near the floor is given by the equation

$$T_x = XT_a + (1 - X)T_i$$

where X = Dimensionless temperature near the floor; $X = \frac{T_x - T_i}{T_a - T_i}$
 T_a = Temperature in air outlet
 T_i = Temperature in air inlet

By geometry, mean dimensionless height of a rectangular surface can be expressed by

$$Y_s = \frac{H_1 + H_2}{2H}$$

where H_1 = Height of lower side of rectangle
 H_2 = Height of upper side of rectangle
 H = Height of room

Mean temperature for the air T_y "felt" by the surface can be expressed by the inlet temperature and the air outlet temperature :

$$T_y = \xi_s \cdot T_a + (1 - \xi_s) \cdot T_i$$

The value ξ_s is a local stratification number for the surface s. This number is expressed by the stratification number X for the room and the mean height Y_s for the surface by simple geometry :

$$\xi_s = X + Y_s - XY_s$$

The energy balance for an air volume with one single surface s can be expressed for the surface and the air volume by the equations.

$$U_i(T_m - T_s) + U_a(T_y - T_s) + F_r Q = 0$$

$$C_a(T_i - T_a) + U_a(T_s - T_y) + (1 - F_r)Q = 0$$

where

T_m	=	The neighbour temperature inside the wall	[°]
T_s	=	The surface temperature	[°]
T_i	=	Air inlet temperature	[°]
T_y	=	Air temperature at level Y = Y_s (mean surface height)	[°]
T_a	=	Air temperature at level Y = 1 (Air outlet)	[°]
Q	=	Room heat load	[W]
U_i	=	Heat conductance from surface to nearest wall node	[W/°]
U_a	=	Convective heat transfer coefficient for the surface	[W]
C_a	=	Heat capacity rate of inlet air	[W/°]
F_r	=	Fraction of radiation for room heat load	[W]

This model uses the temperature ($T_y - T_s$) instead of ($T_a - T_s$) as the driving force for the convective heat transfer between room air and the surface. If for example a room faces to the upper part of an atrium and another room faces to the lower part of the same atrium, the model will catch the different conditions of these two rooms.

A combination of the previous equations results in the following equation system, which can be extended to multiroom models with a variable number of walls and a free air flow pattern :

$$\begin{bmatrix} -U_i + U_a & U_a \xi_s \\ U_a & -\xi_s U_a + C_a \end{bmatrix} \begin{bmatrix} T_i \\ T_a \end{bmatrix} + \begin{bmatrix} U_i & U_a(1 - \xi_s) \\ 0 & C_a - (1 - \xi_s)U_a \end{bmatrix} \begin{bmatrix} T_m \\ T_i \end{bmatrix} + \begin{bmatrix} F_r \\ 1 - F_r \end{bmatrix} Q = 0$$

The local stratification number ξ_s must be calculated for every surface in the room for a given X . You will see that $\xi_s = 1$ for the ceiling for all values of X . For the floor, $\xi_s = X$. Further, the case $X = 1$ (no stratification) result in $\xi_s = 1$ for all surface positions. This case reduces the problem to a normal single zone model.

As discussed in the previous section, X is a function of both the airflow rate and the heat load. At the moment, a constant value of X is used. A model for correlation to the floor temperature is implemented as an option. the model is proposed by Mundt, based on a simple energy balance for the air volume close to the floor, neglecting induction of room air into inlet air :

$$C_a(T_i - T_x) + U_a(T_{floor} - T_x) = 0$$

where T_{floor} is the floor surface temperature. This equation is solved for the air temperature T_x near the floor using a mixed air inlet temperature for all air inlets and the floor temperature calculated by FRES. The calculated air temperature T_x is used in the calculations.

3.7.3 Simulations and discussion

An atrium within, the ELA building at the Norwegian Institute of Technology in Trondheim has been simulated over a period and compared to measurements.

A single atrium was modelled. Solar radiation and other climatic data are measured over a 3 day period with quite warm weather and clear sky conditions. Three simulations are presented :

- Ordinary one zone model, $X = 1.0$
- Constant air stratification, $X = 0.2$
- Variable air stratification, $X = f$, calculated according to Mundt's model

The simulations use measured outdoor temperature over a 3 day period as input. A Cloud Cover Factor is chosen so the calculated total radiation on a horizontal surface during a day is close to the measured value.

The results are presented in the figures 17 a, b, c and d. The simulated period is a quite warm period with day temperatures over 20°C, preceded by a colder period. There was no heating demand except during the first night. The controller setpoint in the atrium is 15°C.

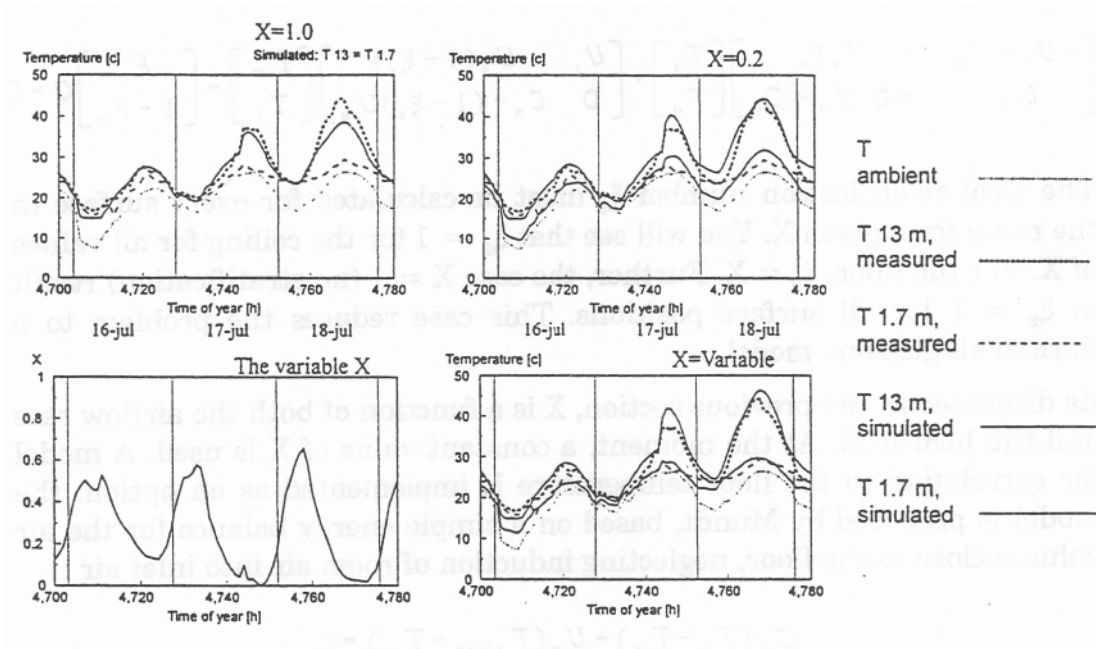


Fig. 17 The simulation results

Fig. 17 shows the temperature using $X = 1.0$. This simulation is identical to a one zone simulation with no air stratification model. The thick line is the simulated air temperature. You can observe the effect of heating during the first night. The air hatches were fully open the first period, using a measured air exchange rate of about 4 ach. At the time $t = 4743$ h, and the rest of the period, the hatches were closed, using a measured air exchange of about 0.45 ach. This results in a temperature rise of 6-7°C which can be found in the graph. In the period with closed hatches, the simulated temperature is slightly lower than the measured value.

Fig 17 shows a simulation with constant $X = 0.2$. This results in two simulated temperatures, one corresponding to the upper level and another corresponding to a level 1.7 m above the floor. The upper level temperatures are higher than the temperatures from the previous simulation with $X = 1.0$, due to the fact that convective heat transfer is connected to the average air temperature outside each surface.

Since this temperature is lower than the upper level air temperature, the calculated heat loss is lower. This results in a higher temperature in the latter case.

The calculated temperature at a level of 1.7 m is too low in the night and too high in the day. The reason for this is that the stratification is connected to the solar load, which varies from zero in the night to a significant value in the day. To correct for this, a model which includes the heat load should be applied.

Fig. 17 shows a simulation using such a model with variable X. The model is described in the previous chapter, and the resulting value of X is presented in fig 17. It varies from close to zero in the day and about 0.6 during the night. The simulated temperature at the 1.7 m level is now much closer to the measured value.

Conclusions

In buildings with stratified room air temperature, improved accuracy in calculated annual energy consumption and air temperatures should be obtained by including a two zone or linear temperature stratification model in building energy simulation programs.

Measurements show that stratification with two separate zones with homogeneous temperature are seldom found. The reason is that heat sources are distributed by radiation to the surfaces in the room. In addition, such a situation is difficult to model.

The proposed model with a linear temperature stratification shows good results using a single example. The model as implemented in FRES is quite robust and flexible, and allows an arbitrary number of surfaces and air flow patterns in the building. Even with a simple correlation of X, the model seems to behave well in a case with variable conditions. A few other cases have also been tested, but more testing work remains before the model can be released.

3.8 Use of standard building dynamic simulation program

The second approach used to model temperature stratification is to divide vertically the atria into different volumes. In each of these volumes the temperature is assumed homogeneous. This method has been used in two dynamic building energy simulation programs without any modifications of the source code :

- TRNSYS → Nuni atrium, ETA atrium (chap 3.10/3.11)
- DEROB → Taman Courtyard (chap. 3.9)

The principle problem with this method is that the different volume must be separated by a wall (surface) within DEROB and TRNSYS. This means that the infrared radiation exchanges are not taken into account in the right way.

With TRNSYS the situation is even worse because the surface which separates the two air zones (volume) can not be defined as a glass panel with 100 % transmission. The solar radiation is then intercepted in this volume and distributed on the surfaces following a surface ratio rule.

A mass transfer between the volumes is possible in the two cases, but the model that calculates it is either very simple (DEROB) or must be implemented (TRNSYS).

3.9 Glazed courtyard at Taman simulated with DEROB-LTH

3.9.1 Description of the analytical model

When the glazed courtyard at Taman was simulated, the model was divided into six different volumes. The courtyard is described by means of four volumes which divide the courtyard vertically. This allows temperatures to be studied at different levels and to compare these with measurements. The lowest volume extends to the level 3.2 m, and the second between 3.2 m and 5.7 m. The two top zones form the volumes just below the roof are triangular in cross section, see figure 25. the two rows of terrace houses along the south and north sides of the courtyard are described in a highly simplified manner as two volumes. In this report no study is made of the energy balances of the surrounding houses, but only of the effect these have on the energy balance in the glazed space. The walls between the surrounding houses and the courtyard are therefore described accurately, while great simplifications have been made in describing those on the outside. Owing to the limitations of the computer program, if the surrounding buildings are to be studied the glazed courtyard must be described in a more schematic manner, for instance without division into several different zones.

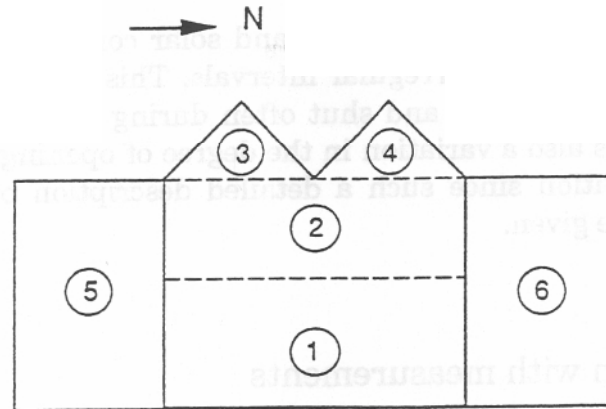


Fig. 18 Division of the analytical model into volumes

In larger volumes temperature stratification may occur, and for this reason it is desirable to have the facility to calculate the temperature at different levels. There is no facility incorporated in DEROB whereby a volume can be divided into different zones. The program makes the temperature equal in the entire volume. In order therefore that it may nevertheless be possible to calculate temperatures at different levels, the glazed space has been divided into a number of volumes, for each of which the program calculates a separate air temperature. Each volume must be delineated by surfaces, and it is therefore desirable that the horizontal division between volumes 1 and 2, volumes 2 and 3 and volumes 2 and 4 should have no effect on the energy balance. The nearest approach that can be made to this is to divide the volumes by a single pane of glass which has 100 % transmission of direct radiation (the transmission of diffuse radiation is then 92 %). By simultaneously allowing air to move between the volumes with the assistance of the thermal driving forces, a model is obtained which gives the best possible description of the glazed courtyard. The long wave radiation between surfaces in the glazed courtyard is not treated entirely correctly, since each volume is calculated separately.

The use of vents and solar control curtains can have a significant effect on the temperature in the glazed space. These must therefore be taken into account in the calculations. The measurements record whether the vents are open and what the positions of the curtains are. Variation in ventilation is represented in DEROB by giving the number of air changes per hour with the external air. The curtains are located horizontally near the roof at the boundary between volumes 2 and 3 and between volumes 2 and 4. In DEROB it is possible to specify variable insulation by stating at what times it is used. Transmission of short wave radiation cannot be stated as input data, and it is at all times 0 %. When the curtains are used for solar control purposes in the calculations, their effect is exaggerated. The measurements show that the curtains transmit about 40 % of global radiation.

As a result of automatic control of vents and solar control curtains, their setting is altered often and at irregular intervals. This applies particularly to the vents which are opened and shut often during the warmer part of the year, and there is also a variation in the degree of opening. This causes difficulties in simulation since such a detailed description of changes in ventilation cannot be given.

3.9.2 Comparison with measurements

As it can be seen in the chapter 3.4.3, there is no big temperature stratification in this atrium. So that this example is not the best case for the performance evaluation of a model which calculate the temperature stratification. In addition the vents situated on the roof of the atrium were often opened during this period. The air exchange rate with outside has been estimated. This constitute a source of error in the calculation which have nothing to do with the temperature stratification model.

The results obtained with this method are represented in the next six figures.

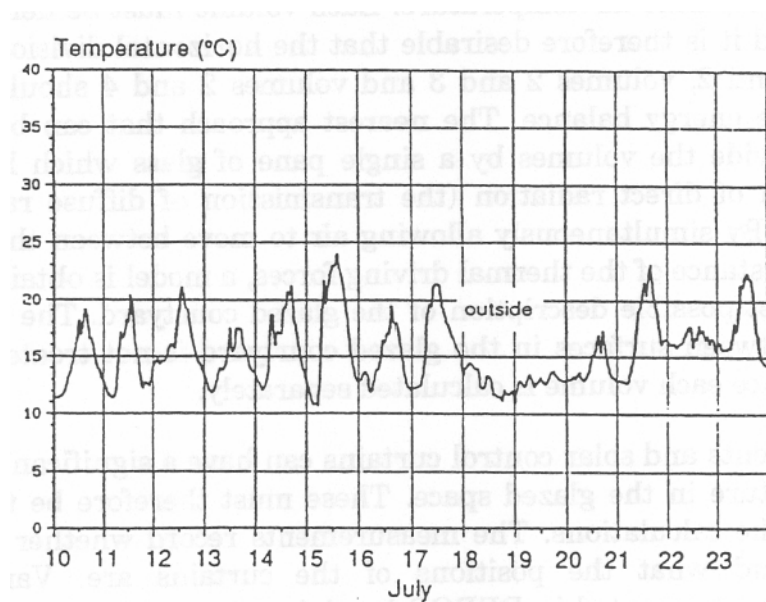


Fig. 19 Outside temperature measured during two weeks in July 1987

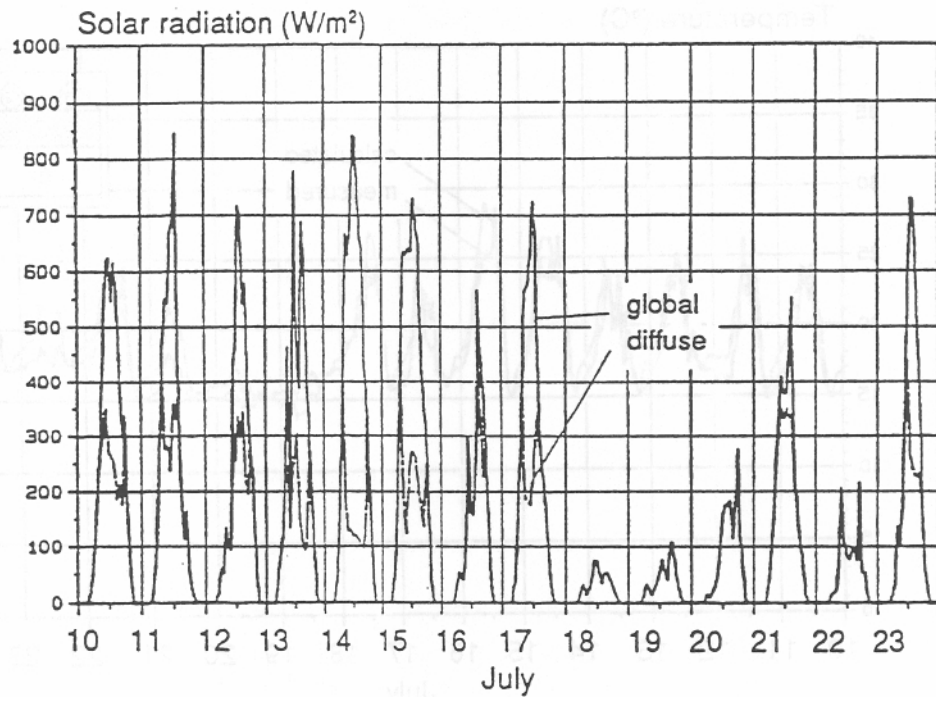


Fig. 20 Solar radiation on a horizontal surface measured during two weeks in July 1987

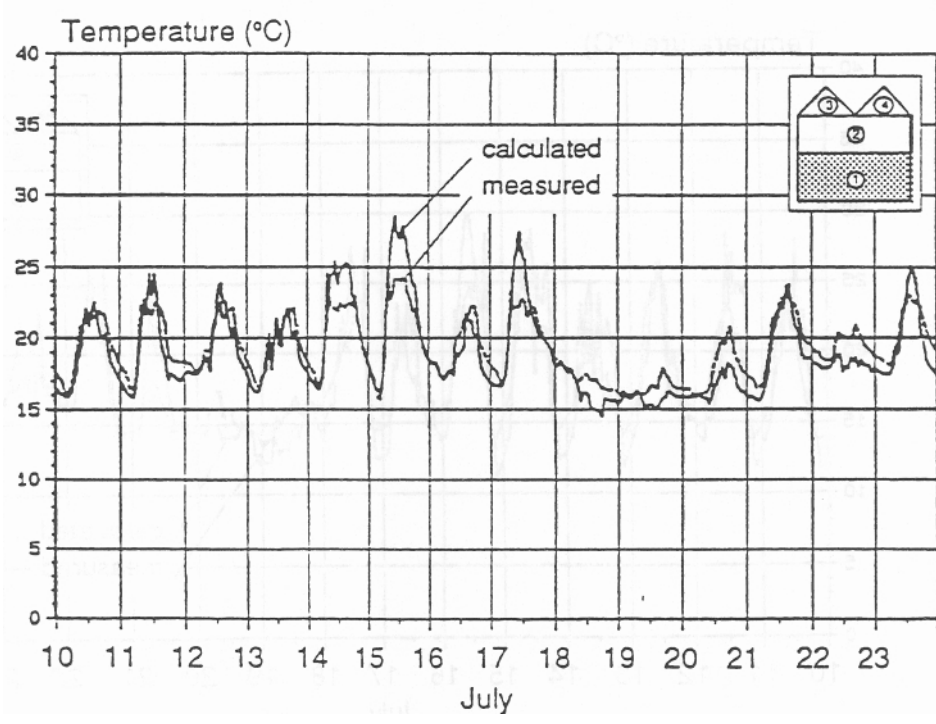


Fig. 21 Calculated and measured temperature in volume 1 during two weeks in July 1987

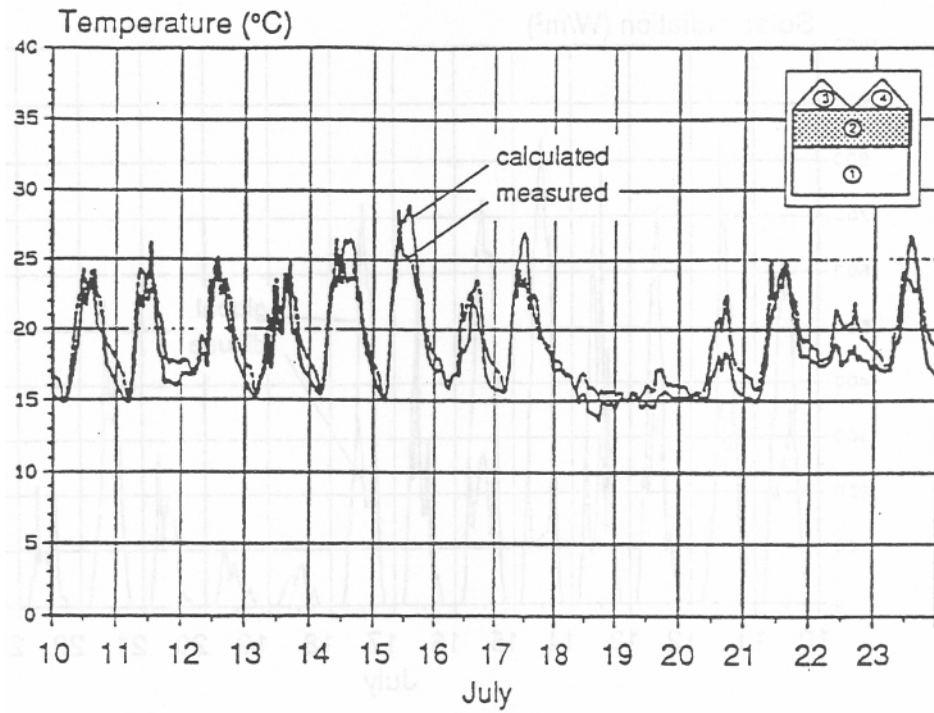


Fig. 22 Calculated and measured temperature in volume 2 during two weeks in July 1987

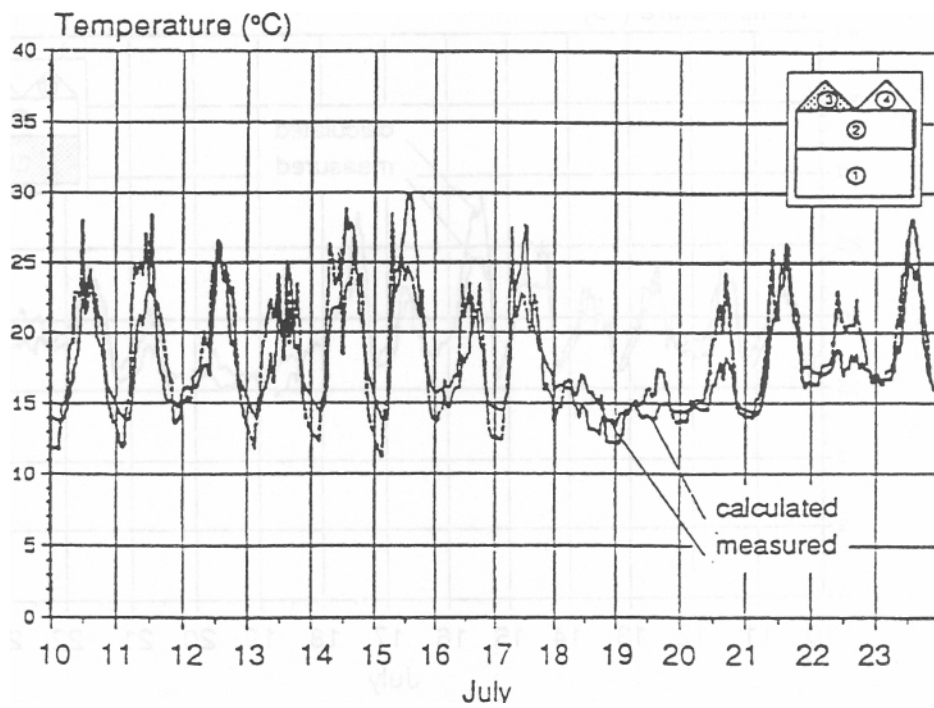


Fig. 23 Calculated and measured temperature in volume 3 during two weeks in July 1987

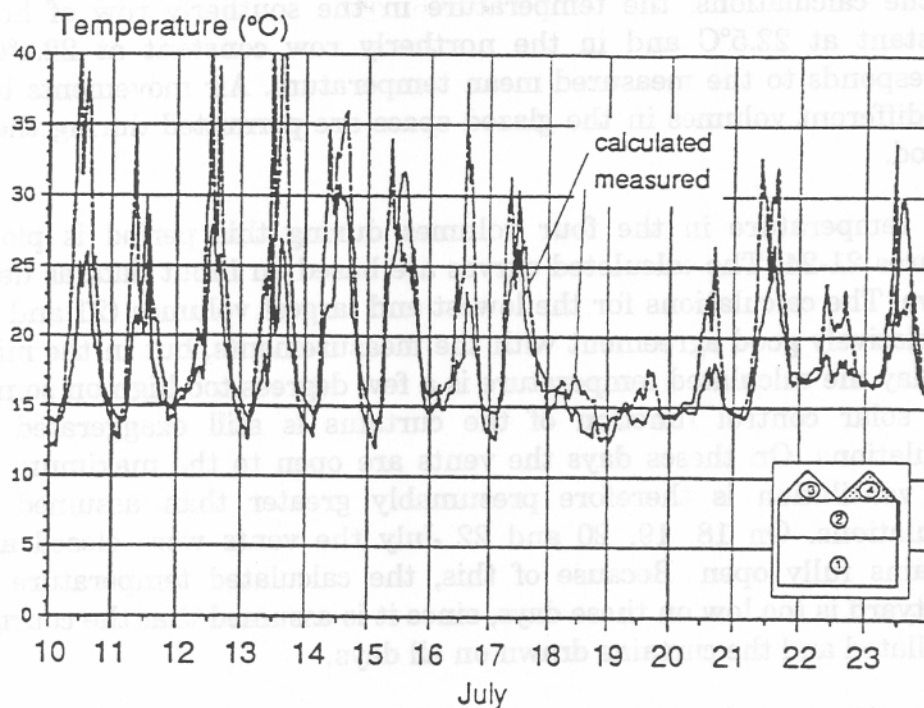


Fig. 24 Calculated and measured temperature in volume 4 during two weeks in July 1987

This period is very difficult to simulate, since the vents and curtains were altered often and with no set pattern. In the calculations ventilation in the lowest volumes i.e. up to a level of 5.7 m, was estimated at 5 air changes per hour between 1000 and 1800 hours and at 2 air changes per hour at other times. The roof vents were fully open during a large part of the day, and it was therefore assumed that in volumes 3 and 4 the air change rate was 10 per hour between 1000 and 1800 hours and 2 per hour at other times. The difficulty is that in reality the opening angle of the vents varied a lot from day to day, and on 18, 19, 20 and 22 July the vents were fully closed. The calculations cannot take account of this, and it has to be assumed that ventilation is the same every day. Unfortunately, it is impossible to find a warm and sunny summer period during which regulation of the curtains and vents is the same every day over a longer period.

In spite of the fact that it was summer, the curtains were drawn in a double layer during the night. During the day the curtains were drawn in a single layer at varying times. As an average, it was decided to have them drawn between 1200 and 1700 hours as input data for the calculations. Note that in the calculations the curtains do not let through any solar radiation, either diffuse or direct. In reality, the transmittance of the curtain for global radiation is approx. 40 %.

In the calculations, the temperature in the southerly row of houses is constant at 22.5°C and in the northerly row constant at 22.4°C. This corresponds to the measured mean temperature. Air movements between the different volumes in the glazed space are permitted during the entire period.

The temperature in the four volumes during this period is plotted in Figures 21-24. The calculated curves are based on input data as described above. The calculations for the lowest and largest volumes (21 and 22) are in relatively good agreement with the measurements, but in the middle of the day the calculated temperature is a few degrees too high on some days. The solar control function of the curtains is still exaggerated in the calculations. On these days the vents are open to the maximum extent, and ventilation is therefore presumably greater than assumed in the calculations. On 18, 19, 20 and 22 July the vents were closed and the curtains fully open. Because of this, the calculated temperature in the courtyard is too low on these days, since it is assumed that the courtyard is ventilated and the curtains drawn on all days.

When allowance is made for the difficulty of simulating such a volume, agreement between measurements and calculations is fairly good in the southerly roof volume, figure 23 In the northerly roof volume, figure 24, the measured temperature is very high during the day and it varies a lot. During some hours the temperature according to the measurements can be 10-15°C higher than the calculated values. It is evident that air movements here have a significant effect on temperature. The large difference may to some extent be due to the fact that the hot air from the lower volumes actually rises along the hottest facade which has a southerly orientation and reaches the roof in volume 4. This is not treated correctly in the calculations. To some extent, the reason for the difference is presumably that the measurement point has no radiation protection and is exposed to powerful insolation.

At the times when the calculated temperature in volume 4 is higher than that measured, this is presumably due to the fact that the vents are in reality fully open on both the leeward and windward sides. This gives rise to a strong draught, and the temperature can suddenly drop to values near the outside temperature.

On the whole, it is difficult to state with certainty why the calculations are different from the measurements. It is very likely that the reason is a combination of the parameters discussed above. One of the most difficult factors to judge is how extensive ventilation is and how it varies in time. This holds not only for this glazed space but for all types of glazed spaces.

If the solar control curtains are not drawn between 1200 and 1700 hours, the calculated temperature in the two lowest volumes is still higher while the roof volumes have a lower temperature, which seems reasonable.

Having the curtains drawn at night in a double layer appears unnecessary in the summer, and can give rise to unnecessarily high temperatures during the day. After all, the idea of having night insulations is to reduce fabric losses to the outside, so that the stored heat remains in the courtyard and raises the temperature level.

In most cases, this is undesirable in the summer. What should be done instead of this is to open the vents at night when the outside temperature is lower so as to reduce the temperature. At Taman this is not so important since there are no problems due to excessive temperatures, but in other glazed spaces where it is difficult to achieve a tolerable temperature level it is important that regulation of curtains and vents should be properly thought out.

3.10 Attached atrium of the University of Neuchatel simulated with the type 56 of TRNSYS

3.10.1 General approach

In order to calculate the vertical temperature profile in an atrium the space is divided vertically in different elements. Each element or volume is assumed as perfectly mixed (homogeneous temperature). Between these "zones" a fiction wall (surface) must be defined, this is the main disadvantage of this method :

- The fiction wall will not allow the floor of the atrium to exchange IR radiation with the ceiling of the atrium for example.
- The solar radiation which is entering volume Nr 3 (figure 25), for example, will be distributed according to the surface ratios to the surfaces of the volume Nr 3. No solar radiation will directly effect volume Nr 2 and Nr 1, except the radiation which is coming in through their own windows.

The problem is illustrated in the next figure

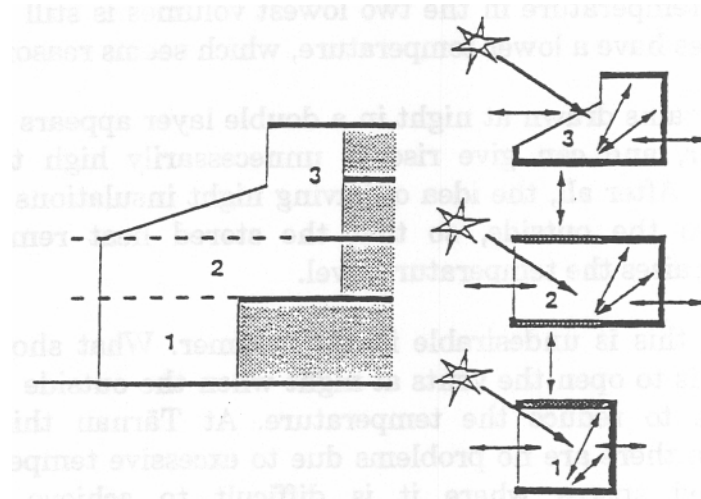


Fig. 25 Zones definition with the TRNSYS standard approach

A mass transfer (air exchange) between the adjacent zones is possible but must be calculated separately by another subroutine.

In order to investigate this method, the three typical days presented in fig. 8 of this report have been used for the comparison.

3.10.2 Third day with temperature stratification (closed hatches, internal shading devices cases)

The volume of the atrium is divided as it is shown in fig. 25.

The first figure gives the temperature evolution of the ground level and of the upper zones (Nr 1 and 3).

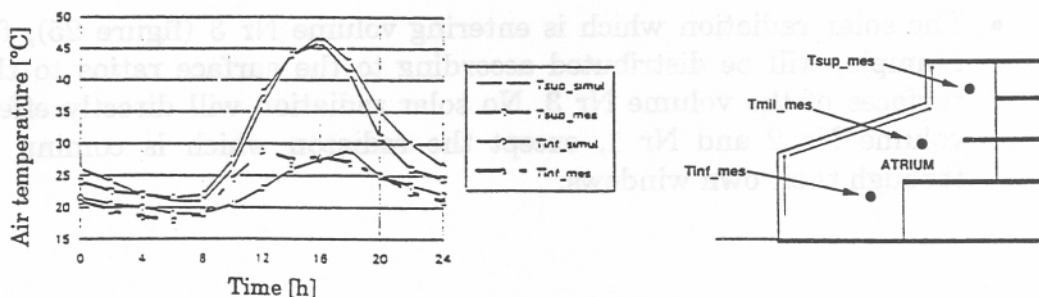


Fig. 26 Comparison between measurements and calculations

3:30

The upper zone temperature is calculated very well. The ground zone temperature is reasonably simulated although, there is a clear inertia problem. The measured temperature in this zone is increasing more rapidly than the one calculated. This can be explained on one hand by the light elements (chairs, tables, metallic structure) which are intercepting solar radiation and gives heat very rapidly to the air and on the other hand by a wrong amount of calculated solar heat gains (too small) applied in this volume. The effect of the light furnitures has not been taken into account in the calculation as the sun is being distributed on the surfaces and especially on the ground (heavy floor D. This failure can be partly eliminated by introducing light "internal" wall as in the zone Nr 1, a part of the solar gains being distributed also on these light surfaces which would play the role of the tables for example.

The second problem due to the wrong calculated amount of solar gains comes from the partitioning of the space. Some solar gain entering through the glasses of zone 3 and 2 will also effect zone 1.

There is also another element which has not been taken into account in the calculation. In fact at about 12 o'clock the lower vents have been opened for half an hour and the mobil wall N° 3 all the afternoon, see figure 27.

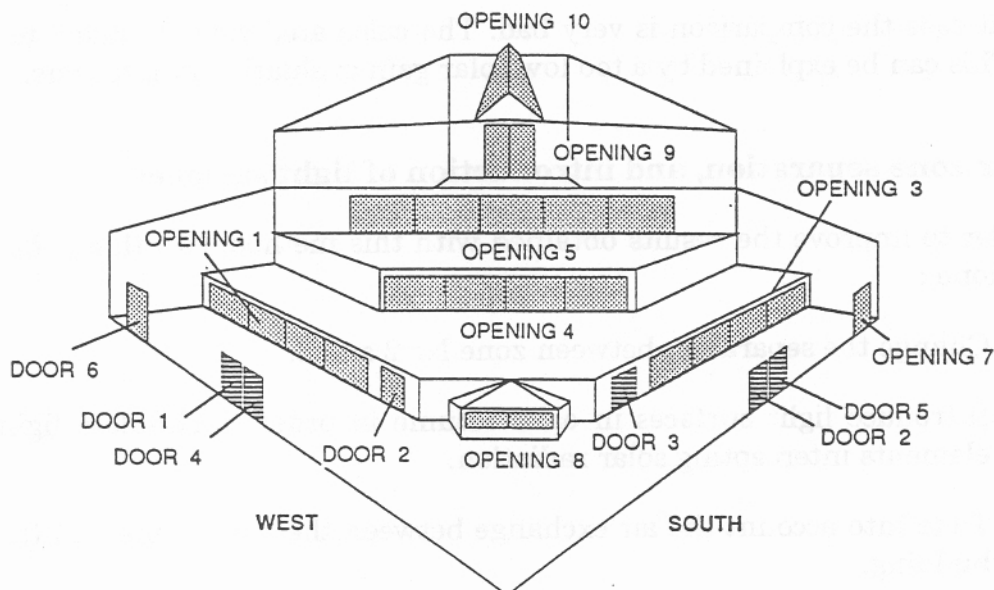


Fig. 27 General view of the openable element against the building

This element explain why the lower space of the atrium remain under 30°C. The air exchange with the building (air at about 20°C) is very important.

The difference between the measurements and the calculations seems not very important, this is due to a compensation effect less solar heat gains but not transfer of air with the building. Of course, this is not acceptable and must be corrected, otherwise the method will be not useful for a designer.

The next figure illustrates the comparison of the element in the middle (Nr 2).

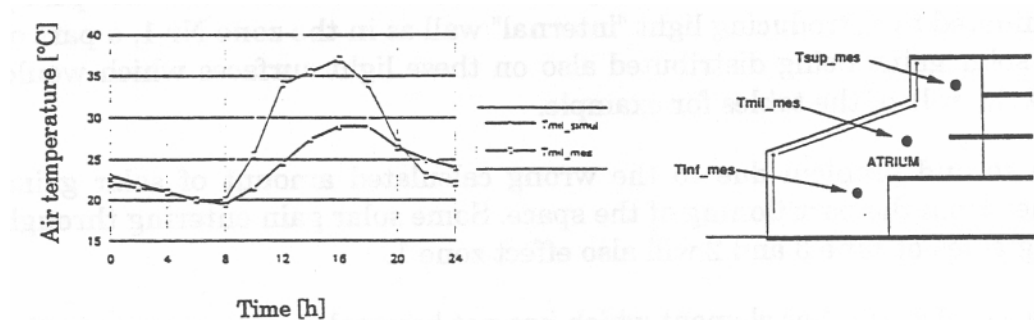


Fig. 28 Comparison between measurements and calculations

In that case the comparison is very bad. The calculated value is much too low. This can be explained by a too low solar gain evaluation in this zone.

Better zone separation, and introduction of light surfaces

In order to improve the results obtained with this method, two things have been done :

- a. Change the separation between zone Nr 2 and 3.
- b. Introduce light surfaces in each volume in order to simulate light elements intercepting solar radiation.
- c. Take into account the air exchange between the lower zone and the building.

a. New zone partitioning

With the first division of the space, zone Nr 3 had a volume of 195 m³ and the zone Nr 2 316 m³. The glazed surface of the volume Nr 3 was 134 m² and the one of the zone Nr 2 only 53 m².

It is clear that the proportion between the volume and glazed surface is not kept, especially with the geometry of the atrium a lot of sun coming through the glazing of the zone Nr 3 will effect the zone Nr 2. The division of the space has therefore been changed in the following way :

Zone Nr 3	Volume	=	100 m ³
	Glazed surface	=	83 m ²
Zone Nr 2	Volume	=	406 m ³
	Glazed surface	=	104 m ²

Half of the inclined glazed surface is incorporated in the second zone!

The new separation is represented in the next figure.

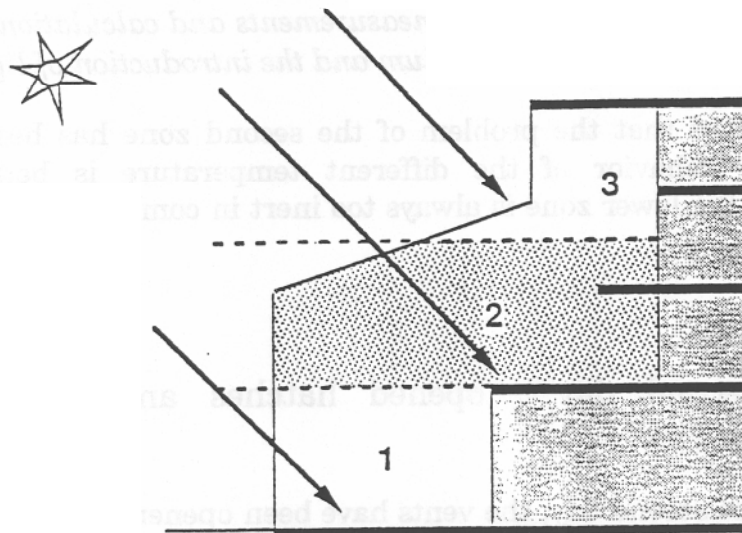


Fig. 29 New space division

b. Introduction of light surfaces

The aim of this introduction is to distribute some part of the solar gain on surfaces with low inertia. These surfaces will be heated very rapidly and will by convection give back some heat into the air rapidly.

The new comparison is presented in the next figure.

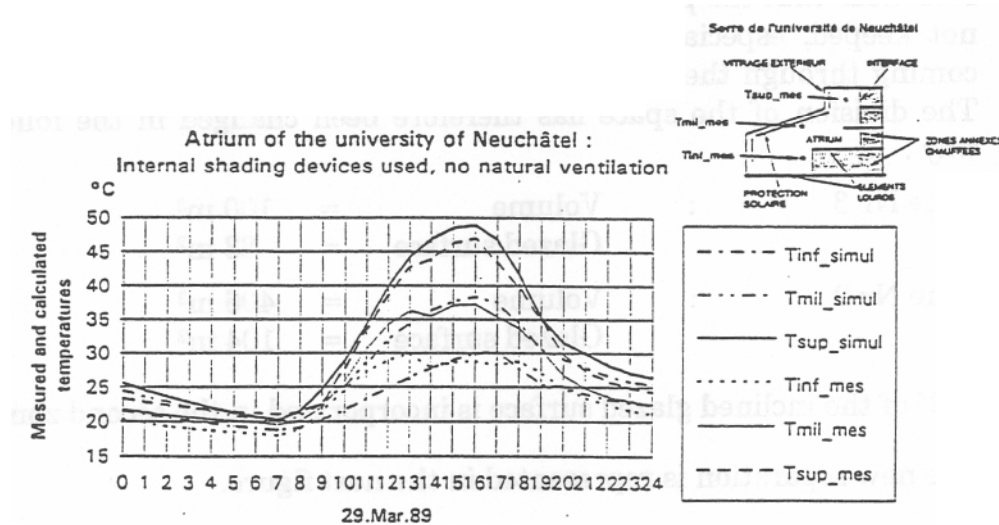


Fig. 30 Comparison between measurements and calculations with the new partitioning of the atrium and the introduction of light surfaces.

It is evident that the problem of the second zone has been solved. The transient behavior of the different temperature is better simulated, although the lower zone is always too inert in comparison to the measured value.

3.10.3 Second day : opened hatches and internal shading devices

During the second day, the vents have been opened from about 11 o'clock since 18 o'clock, and the shading devices were used.

The natural ventilation has been taken into account with the following model :

1. Piston flow : the air coming from the outside through the lower vents is going up to the second volume and finally to the third volume were it leaves the atrium through the upper vents.

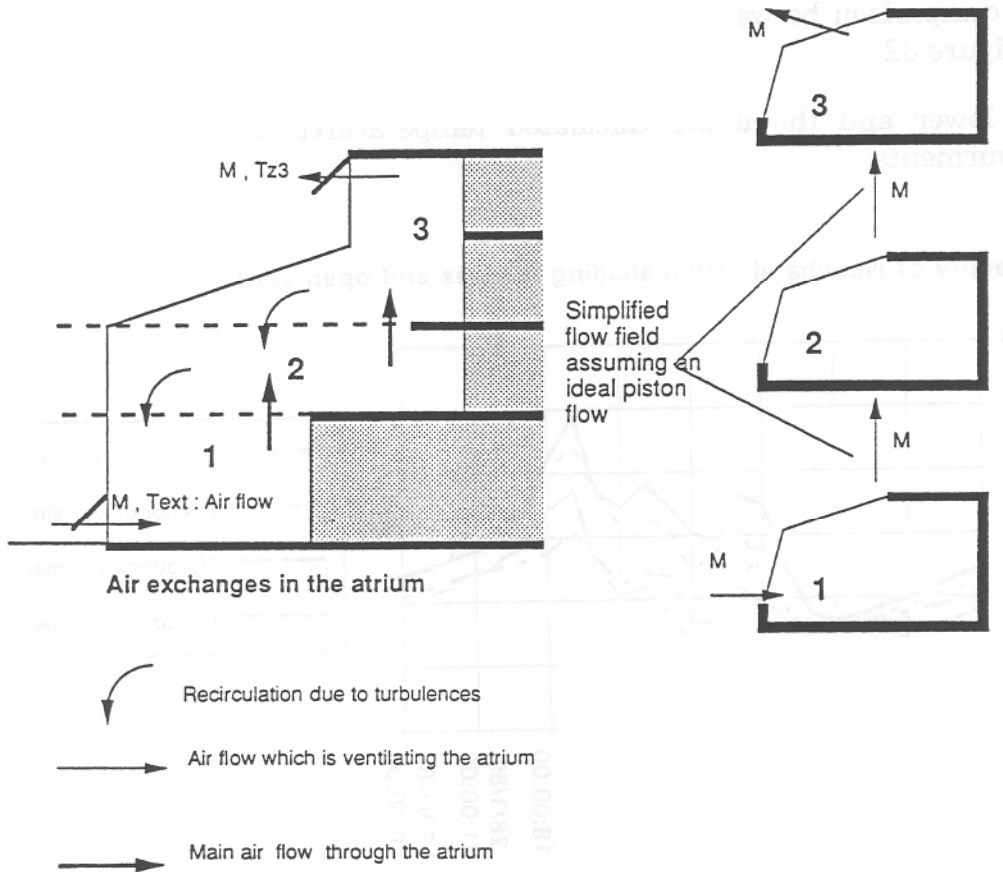


Fig. 31 Piston flow

2. The air exchange rate is calculated in the following way :

- Use of the average internal air temperature $T_{int} = (T_1 + T_2 + T_3)/2$

Air exchange rate :

$$V = S_B CD_B \sqrt{\frac{2 \times g \times H \left| \frac{T_{int} - T_{ext}}{T_{int} + T_{ext}} \right|}{\frac{S_B \times CD_B}{S_H \times CD_H}}} \quad [\text{m}^3/\text{s}]$$

where CD_B and CD_H are respectively the discharge coefficient of the lower and upper vents, the g the gravity, H the difference between the opening height, S_B and S_H respectively the surface at the lower and upper openings.

The comparison between the simulation and the measurement is shown in the figure 32.

The lower and the upper calculated temperatures are compared with measurements

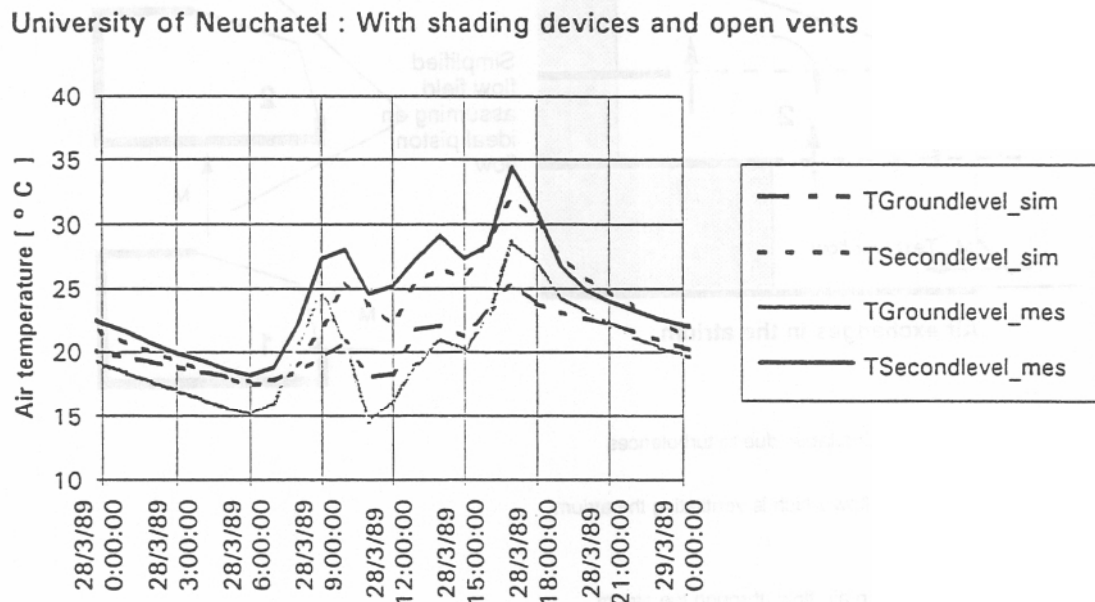


Fig. 32 Comparison of the calculated values with the measurements

The correspondence is good particularly when one think at the complicate air movements in reality and the assumption used in the model.

3.10.4 First day closed hatches without internal shading devices

In this typical situation there will not be any important temperature stratification so that there is no advantages in partitioning the space of the atrium in 3 different zones. With this kind of standard approach we will get a lot of stratification if the air movement between the zones is not implemented.

The problem in this case is to specify the air exchange between the different zones.

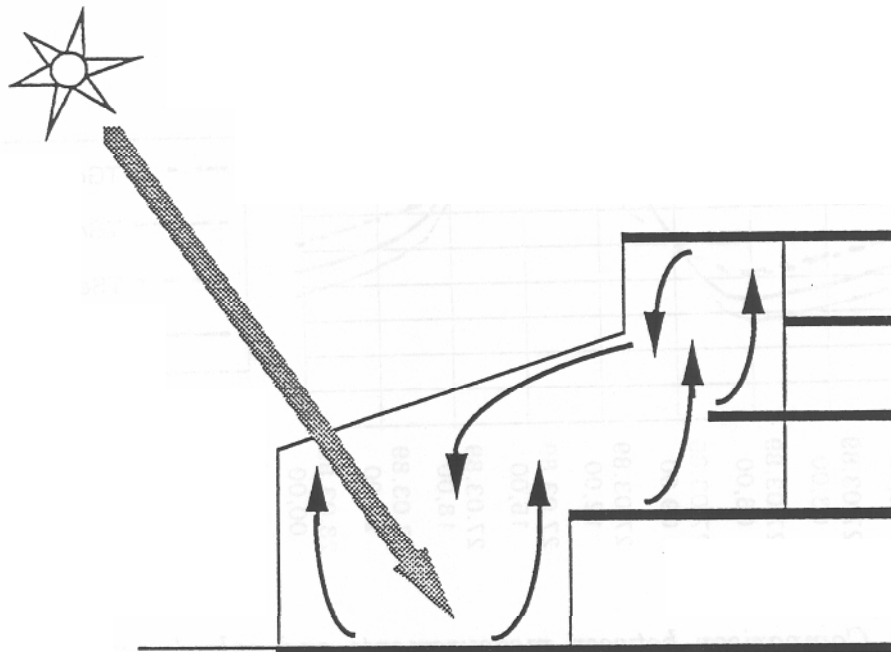


Fig. 33 Air movement in the atrium

In this case we use the relation giving the down draught volume flow created by a cold (or hot vertical) surface in order to make a first estimation of the air flow.

$$V = 0.0029 * \Delta T^{0.4} * B * Z^{1.2} \text{ m}^3/\text{s}$$

where

ΔT = the temperature difference between the air and the surface.

B = the length of the surface

Z = the height of the surface

In our case we assumed :

$$\left. \begin{array}{l} Z = 10 \text{ m} \\ \Delta T = 10^\circ\text{C} \\ B = 20 \text{ m} \end{array} \right\} V = 9000 \text{ kg/h}$$

This mass flow has been used in the simulation and has given good results, as one can see in the figure 34.

University of Neuchatel : No shading devices and no open vents

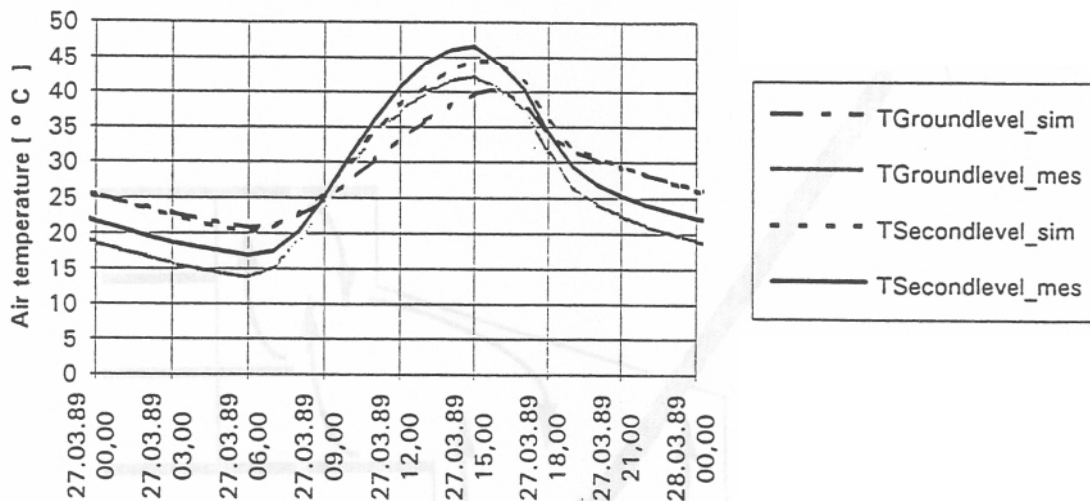


Fig. 34 Comparison between measurements and calculations, University of Neuchâtel with no shading devices and no open vents

3.10.5 First conclusion on the method

The method can be defined as satisfactory in two typical cases :

- 1. No shading devices and no stratification.** By introducing the recirculation of the air the average temperature is well predicted.
- 2. With opened vents (high and low position),** the model based on a piston flow is working and the errors due to the bad solar gain distribution are less predominant than in the case with stratification (internal shading devices used) and no opened vents.

Unfortunately this method cannot be defined as fully appropriate in the stratified case, because it is too sensitive to the zone partitioning (Z direction).

For the design phase, where no information are available, this method can lead to big uncertainties but when some measurements are available and that a validation can be done (as in the case of the university of Neuchâtel) it can be used for some sensitively studies (because a reasonable partitioning can be found in comparison with the measurements).

3.11 ELA atrium of the University of Trondheim simulated with type 56 of TRNSYS

3.11.1 General approach

The same approach that has been used for the atrium of the University of Neuchâtel is tested on the geometry of ELA. The space is divided horizontally also here in three volumes.

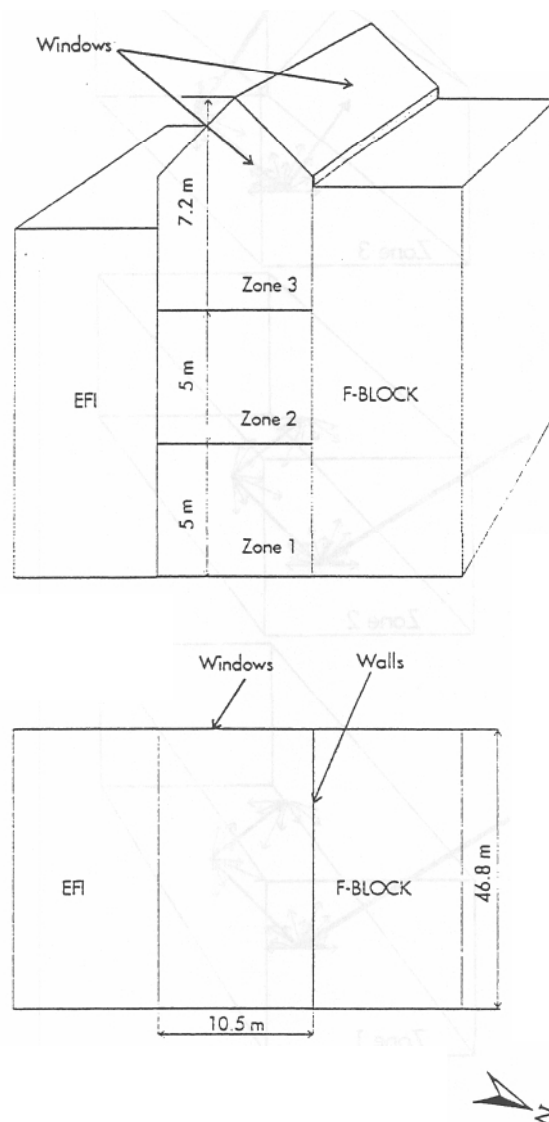


Fig. 35 Vertical Partitioning of the atrium ELA

Two types of calculations will be done on this example :

1. Solar gains distributed in each volume according to the surface ratio rate.

The sun entering in the upper part is distributed only in the upper volume which is not accurate and can lead to problems (see 3.10).

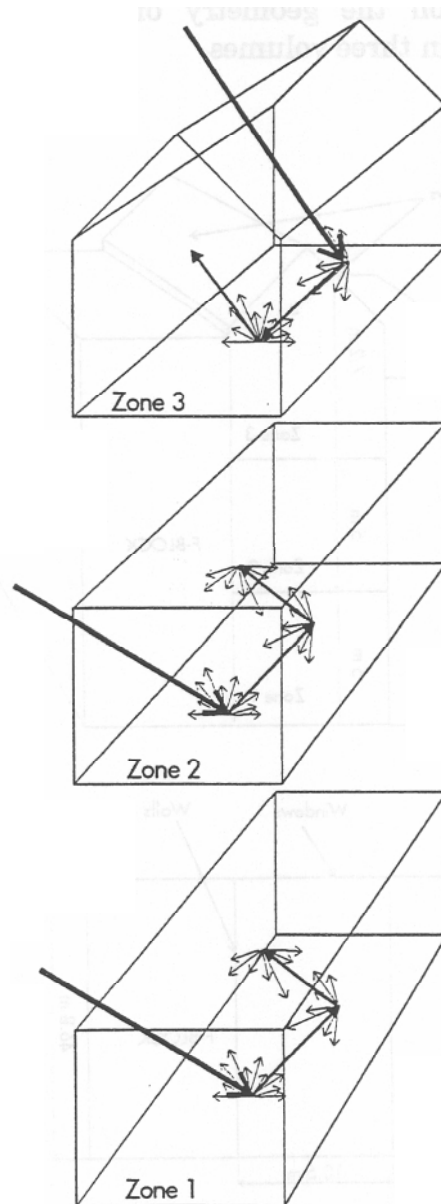


Fig. 36 Solar gains calculations and distribution with the TRNSYS standard model

2. Solar gains distributed according to a more sophisticated model (presented in the chapter 7) which take into account the real part of the sun rays with the first reflection both diffuse and specular.

The solar model of the type 56 is not activated in TRNSYS and the solar gains are distributed in the volume where they hit the surfaces as radiative gains.

Two situations are calculated :

1. The vents are closed, the stratification is important.
2. The vents are opened, the stratification is less important as well as the average temperature.

3.11.2 Standard approach

Closed vents

The measurements are presented in the following figure :

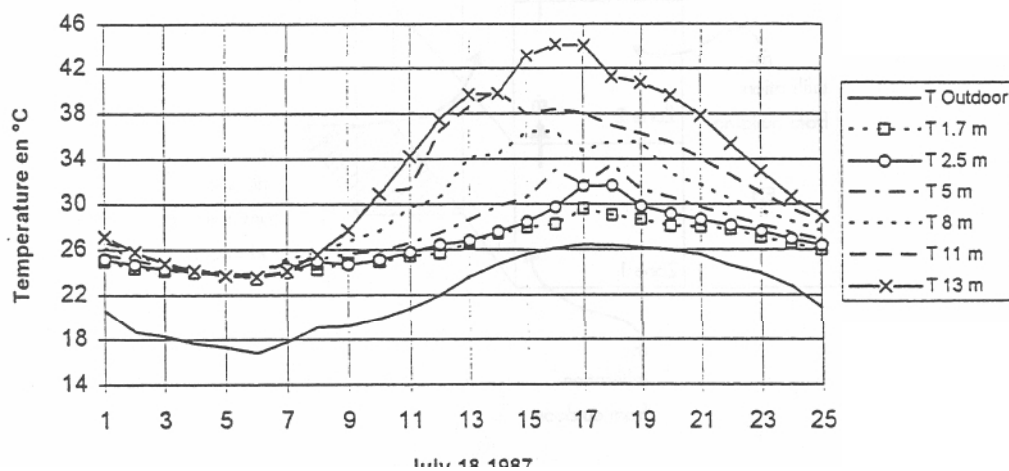


Fig. 37 Measured temperatures with closed vents in the summer

As one can see the stratification of the temperature is relevant.

The method used is described in chapter 3.10

The principal parameters which are important in order to get a good comparison with the measurements are .

- Estimation of the amount of solar gains which enter in the volume but do not stay in it because of the reflection on different surfaces, in that case we assumed that 20 % do not stay in the volume.

Estimation of the air infiltration and exfiltration. In the case of ELA, the window of the offices can be opened in the atrium and there is an open link between the atrium and the office building (which is mechanically ventilated) we have assumed about 1.5 ach coming from outside and from the building, which are going out through the leakages of the roof of the atrium and to the adjacent

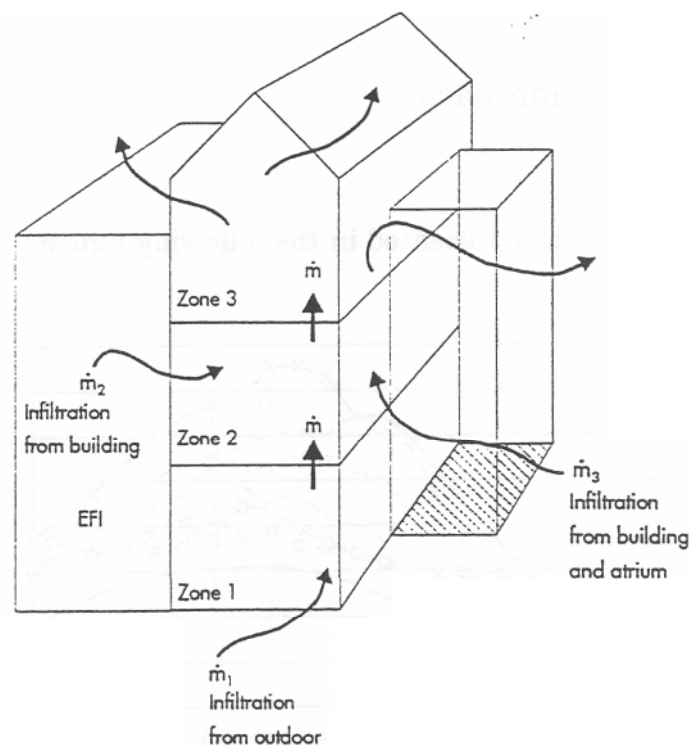


Fig. 38 Simplified infiltration and exfiltration flow field

The results are presented in the following figures. Figure 39 shows the three calculated temperatures.

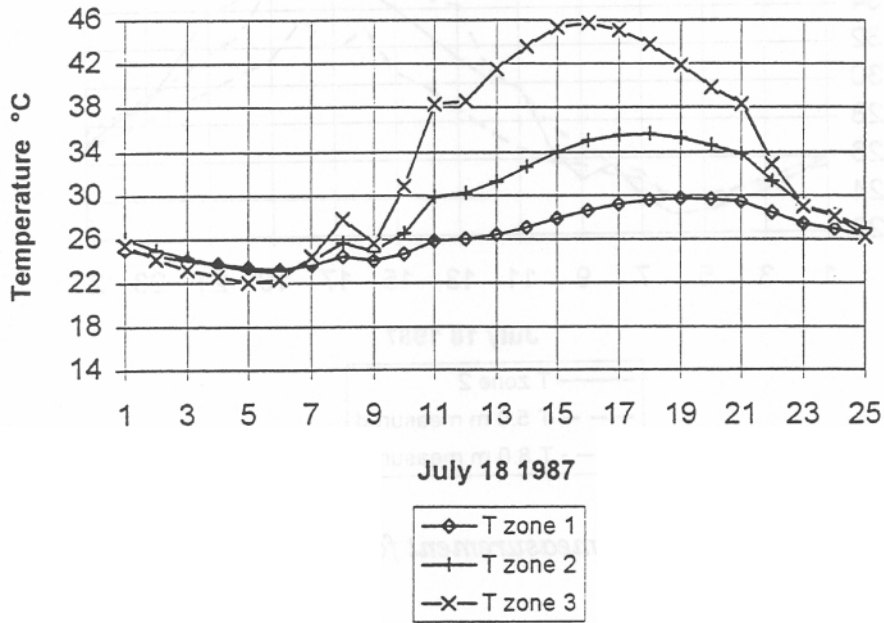


Fig. 39 Calculated average temperature in the 3 zones

The following figures show the comparison with the measured temperatures in the same zone

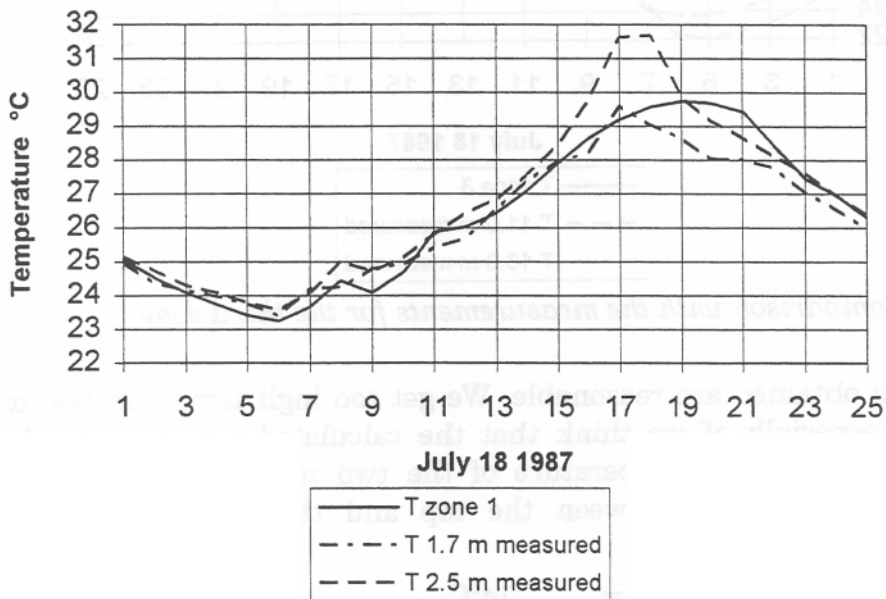


Fig. 40 Comparison with the measurements for the first zone : ground

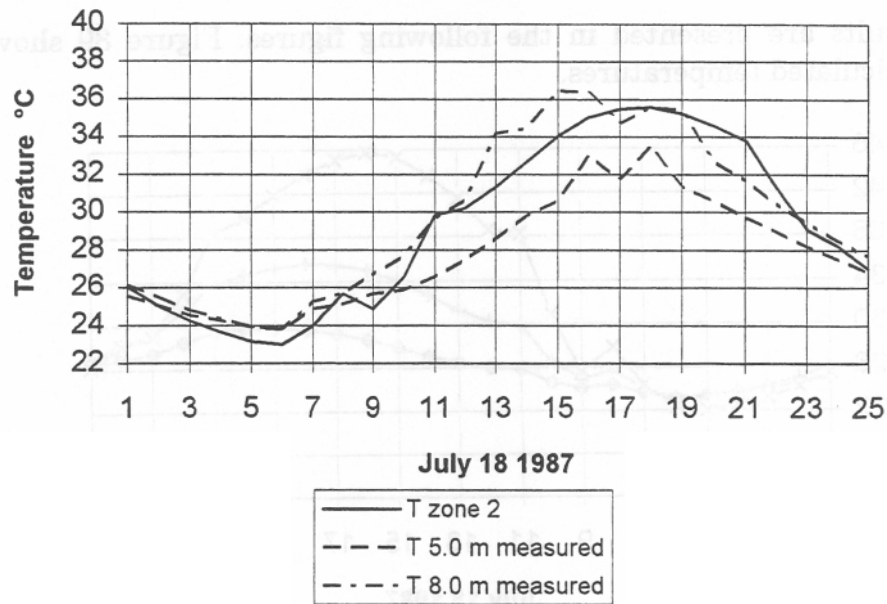


Fig. 41 Comparison with the measurement for the second zone

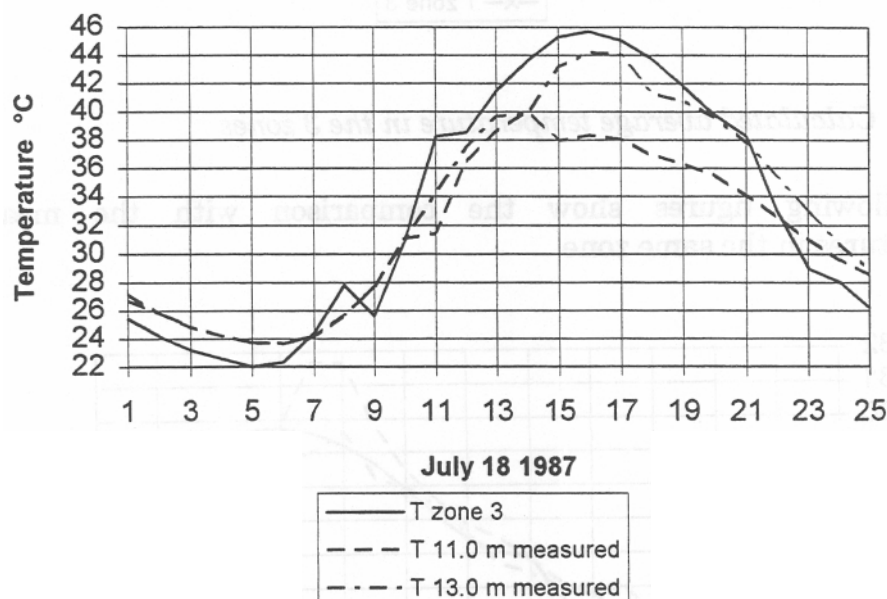


Fig. 42 Comparison with the measurements for the third zone

The results obtained are reasonable. We get too high temperatures in the last zone, especially if we think that the calculated temperature should represent the average temperature of the two measured ones. But the temperature difference between the top and the ground is predicted reasonably.

- $\Delta T_{\text{measured}} = 14^{\circ}\text{C}$
- $\Delta T_{\text{calculated}} = 16^{\circ}\text{C}$

Opened vents

With the vent opened, the air exchange rate with the outside has been evaluated in the same way that has been done for the atrium of the university of Neuchâtel.

The air flow field assumed for the first time is described in the next figure.

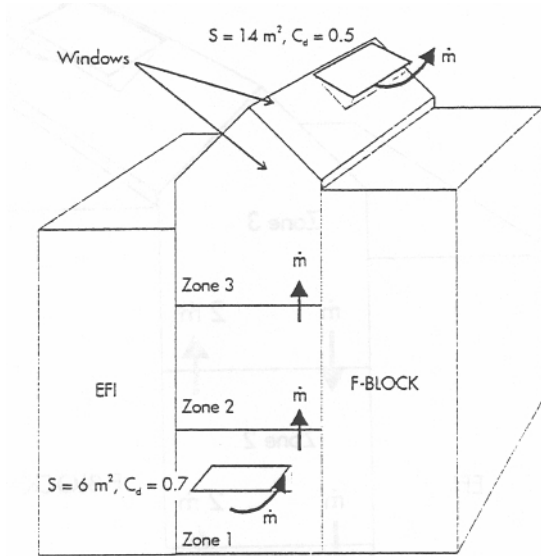


Fig. 43 Piston flow

The velocity of the wind has not been measured precisely, but has been estimated to 2 m/s and coming from the side of the gable which was opened (low : opening of the atrium). The exact opened surfaces of the vents are not clearly documented so that different assumptions have been done.

The measurements of the air temperature in the atrium are presented in the next figure.

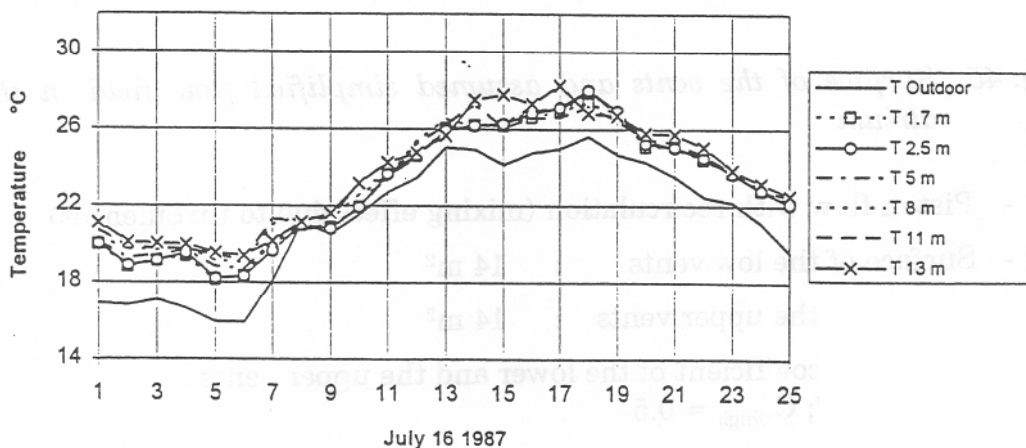


Fig. 44 Measured temperatures with opened vents in the summer.

As one can see there is no stratification any more (only 2 degrees). Except between 13.00 and 17.00 the air temperature in the atrium is well mixed.

The calculation is based on the assumption presented in the figure 45.

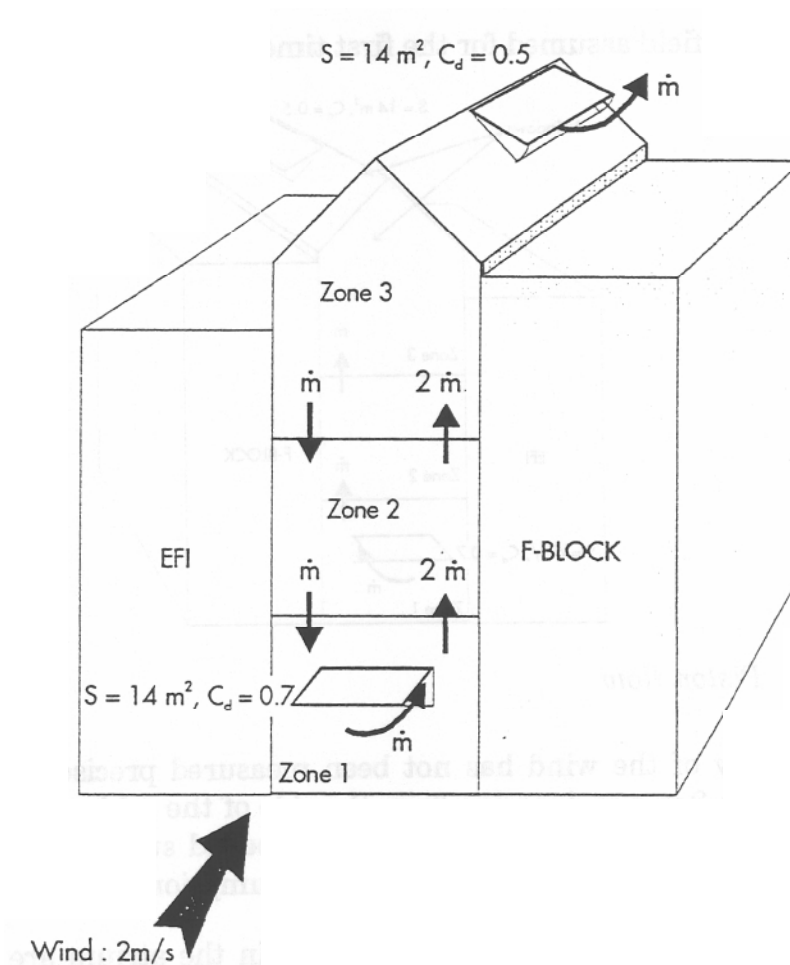


Fig. 45 Surface of the vents and assumed simplified flow field in the atrium

- Piston flow with recirculation (mixing effect due to turbulences)
 - Surface of the low vents 14 m^2
 - Surface of the upper vents : 14 m^2
- Discharge coefficient of the lower and the upper vents :
 - $C_{D\text{low}} = 0.7$; $C_{D\text{high}} = 0.5$
- 2 m/s of wind in the direction of the low opening

The results are presented in the next four figures

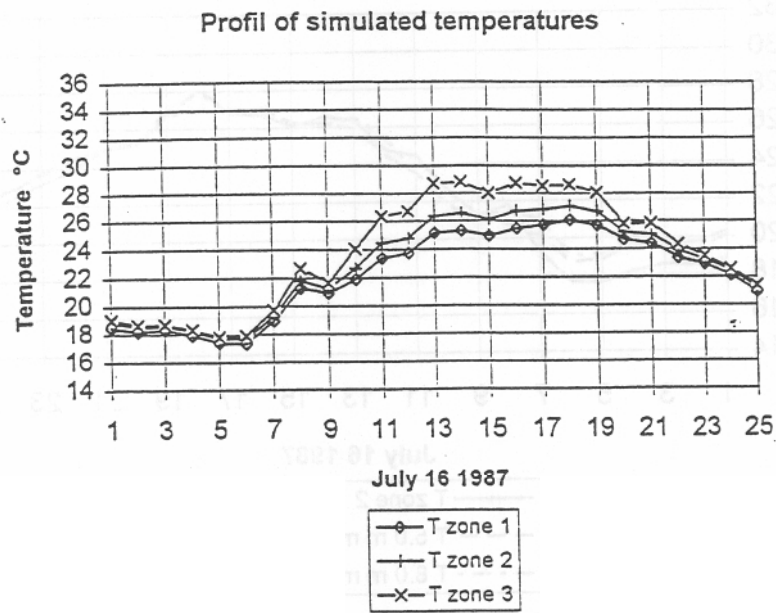


Fig. 46 Calculated temperature in the 3 zones

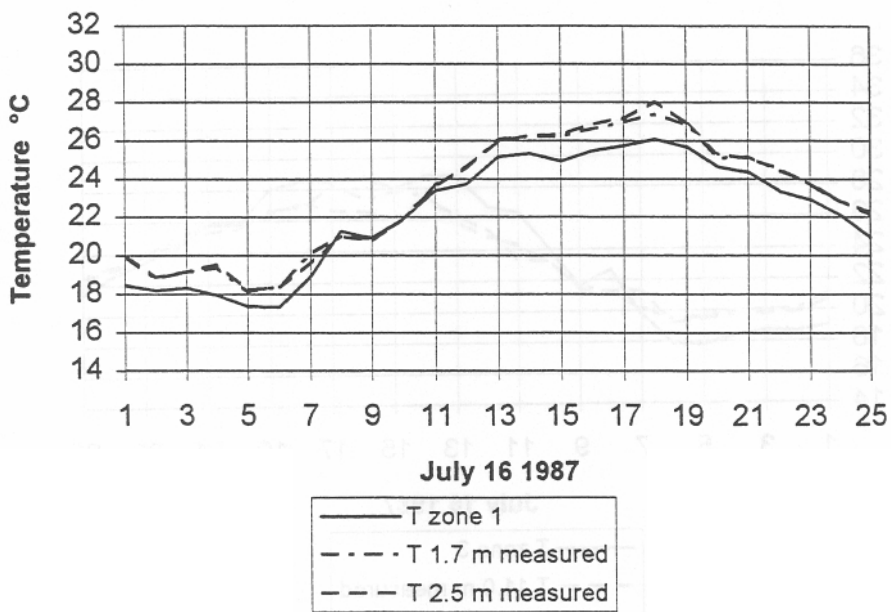


Fig. 47 Comparison with the measurements in the first zone : ground

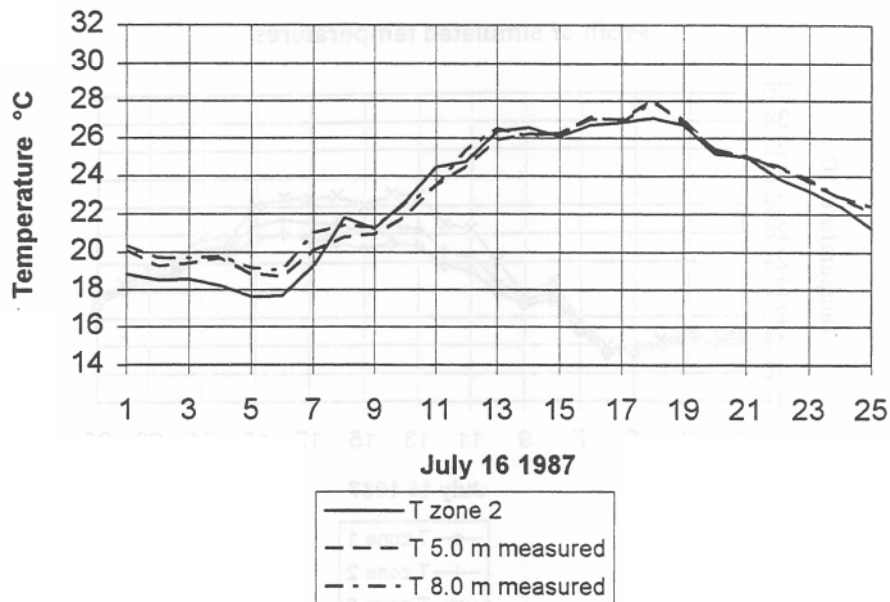


Fig. 48 Comparison with the measurements in the second zone

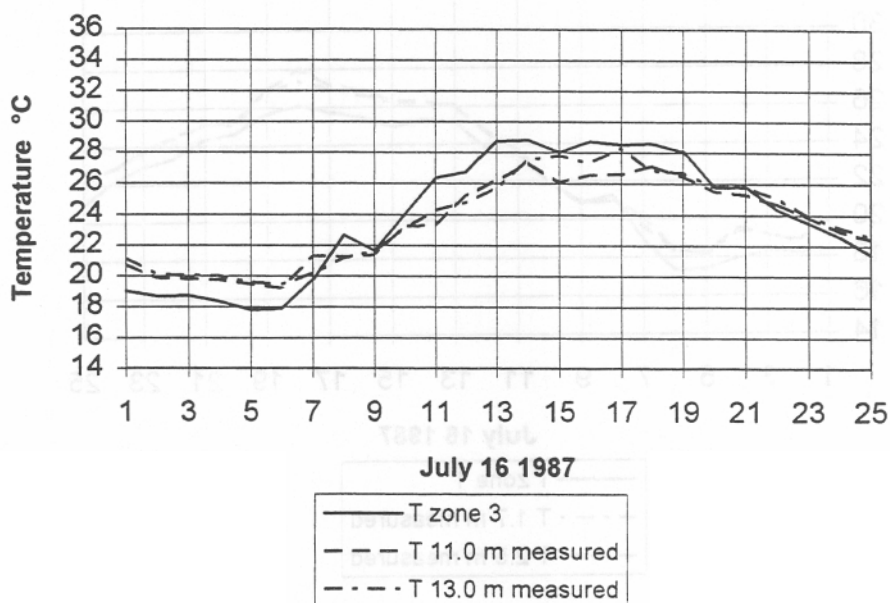


Fig. 49 Comparison with the measurements in the third zone

The results obtained with these new assumption are quite better than the first one. The average temperature and the stratification profile are much closer to the measured values.

3:48

3.11.3 Modified solar distribution approach

The standard distribution method of the solar gains of the program TRNSYS has been modified in the following way.

The first step is to calculate the total amount of the solar gains coming in the whole atrium, see figure 50.

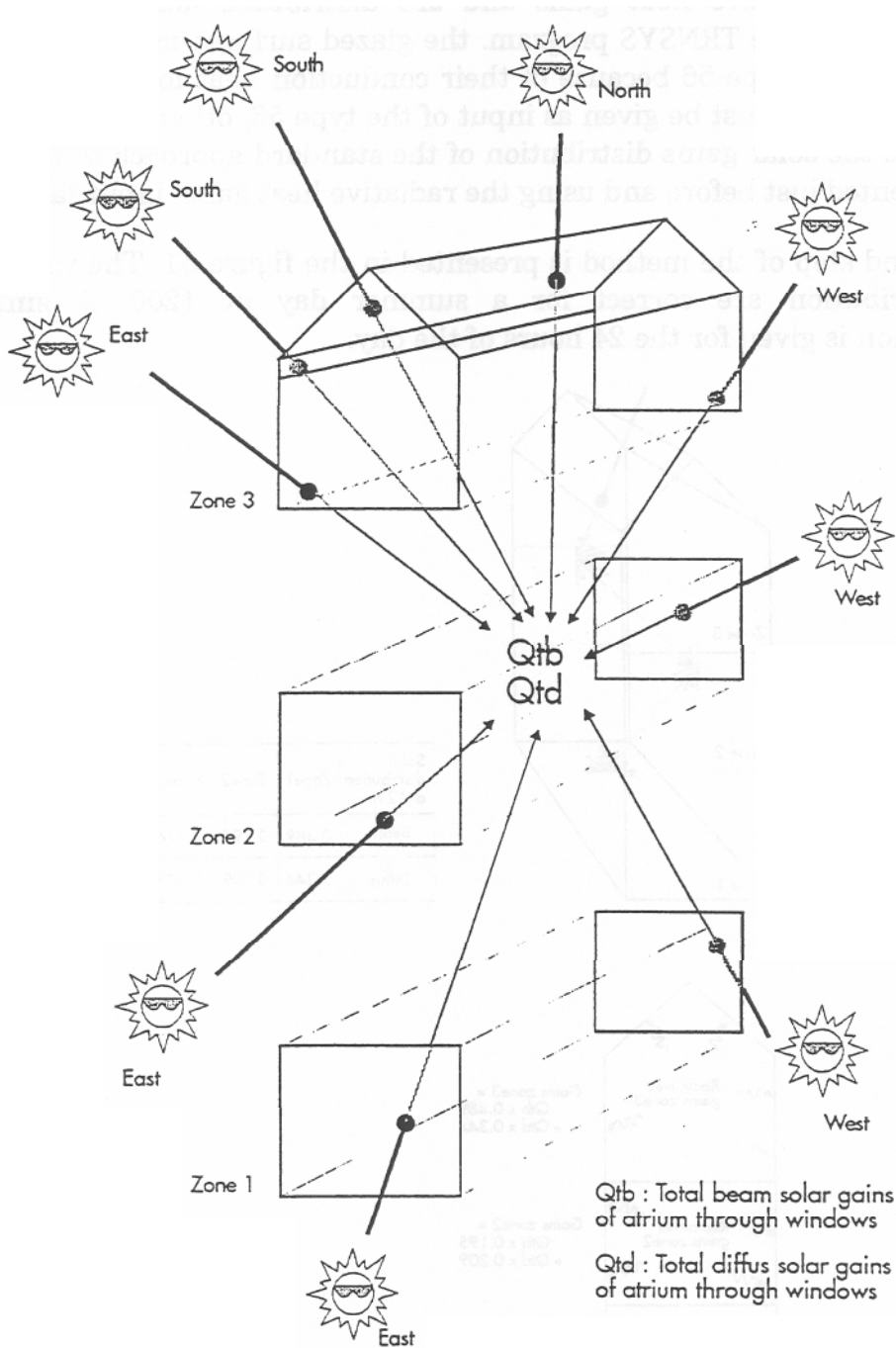


Fig. 50 Step one : calculation of the total amount of solar gain

The second step is using the solar gain distribution obtained with the program presented in chapter 6. The sun penetration in the space and the first reflections both specular and diffuse are calculated correctly. This lead to a power heat distribution on the surfaces of the atrium.

The sum of both the diffuse and the direct radiation which heat the surfaces of each zones is done. This gains are introduced in the Type 56 of TRNSYS as radiative heat gains and are distributed according to the surface ratio of the TRNSYS program. the glazed surfaces must be defined as before in the type 56 because of their conduction heat losses (or gains) but no radiation must be given as input of the type 56, otherwise we would superpose the solar gains distribution of the standard approach to the new one presented just before and using the radiative heat gains input facilities.

The second step of the method is presented in the figure 51. The values of the distribution are correct for a summer day at 1200. A similar distribution is given for the 24 hours of the day.

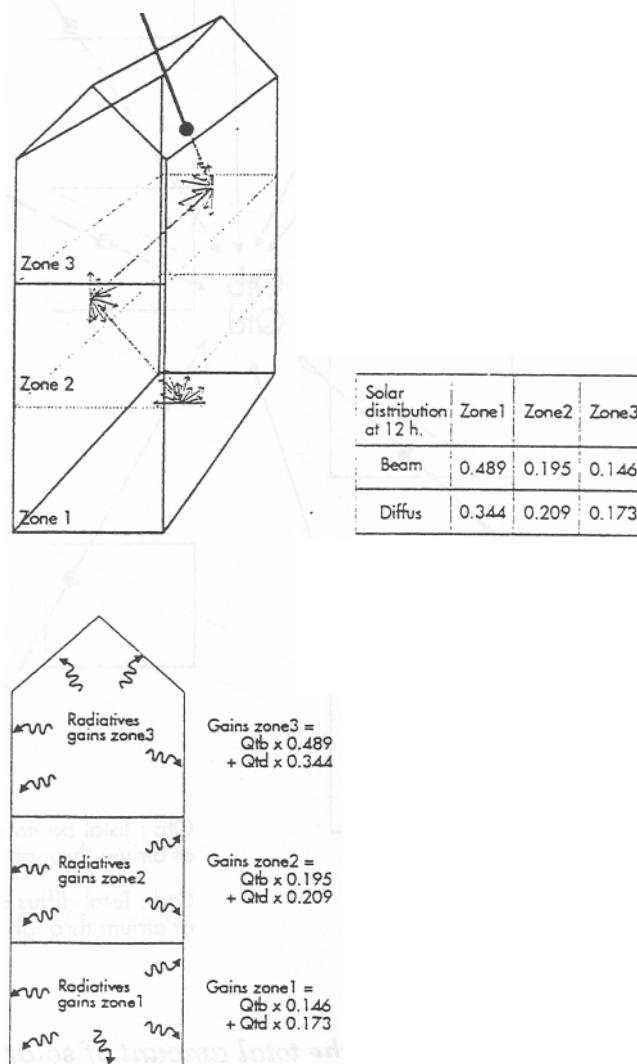


Fig. 51 Second step of the method

3:50

With this method the solar gains which comes from the roof are not only active in the zone number 3 but can effect the ground and the zone 2 of the atrium.

We can also see from this distribution that 17 % of the incoming direct radiation do not stay in the atrium and that 28 % of the diffuse incoming radiation is also not absorbed by the surfaces of the atrium.

Closed vents

The same flow field due to infiltrations which has been used in the standard approach (Chap. 3.11.2) has been used here.

The results of the next figure show the calculated temperature.

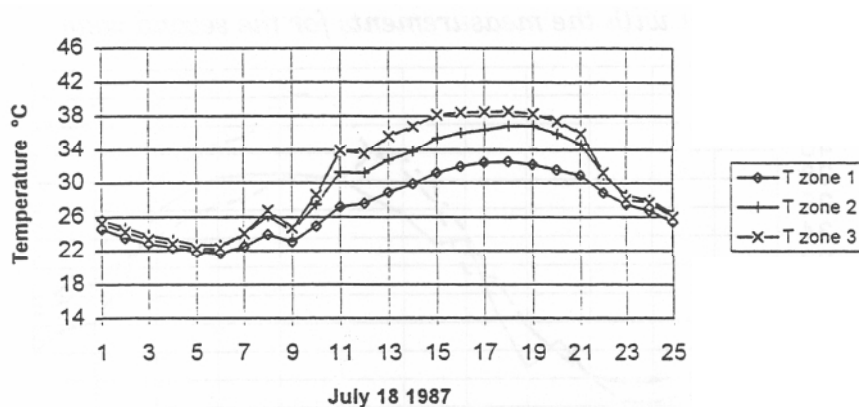


Fig. 52 Calculated average air temperatures in the 3 zones with the new method

The next figures show the comparison with the measured values in the same zones.

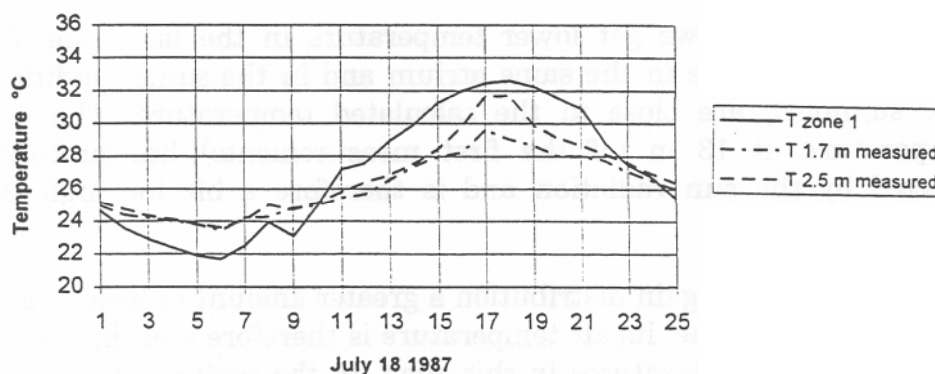


Fig. 53 Comparison with the measurements of the first zone : ground

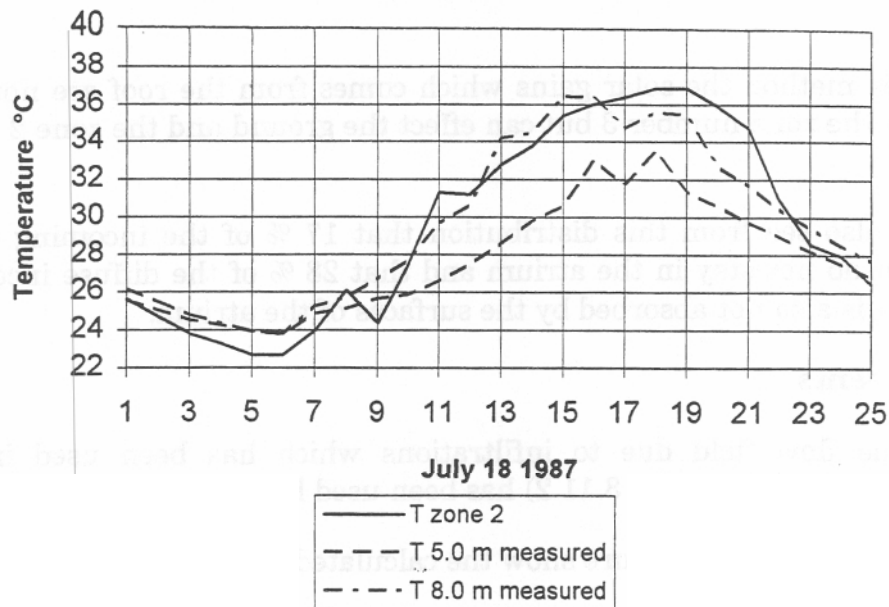


Fig. 54 Comparison with the measurements for the second zone

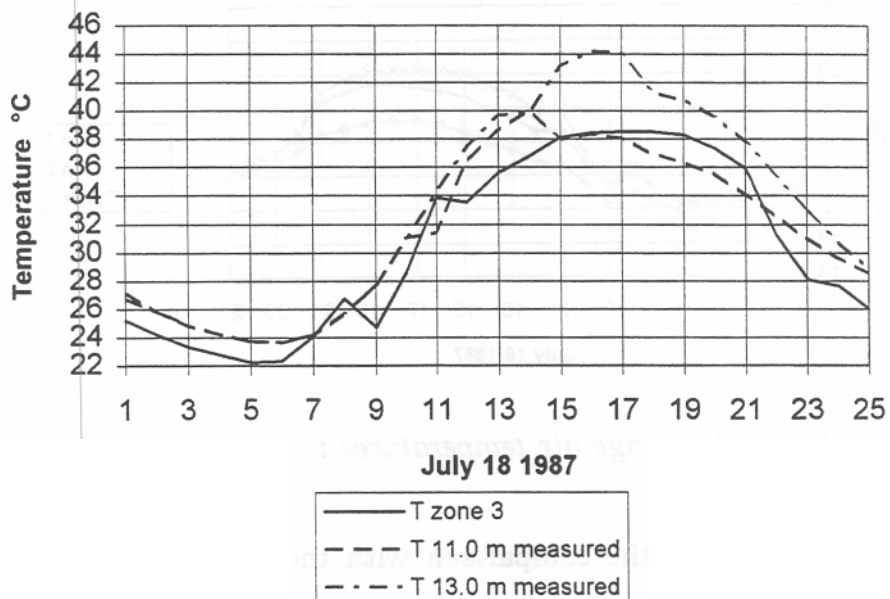


Fig. 55 Comparison with the measurements for the third zone

With this method we get lower temperature in the last zone. But new measurements done in the same atrium and in the same condition (clear day, summer), are close to the calculated temperature. The measured temperature at 13 m (of the first measurements) has probably been affected by the sun radiation and is therefore a bit too high than the reality.

With the new solar gain distribution a greater amount of heat is affected to the first ground zone, its air temperature is therefore a bit higher than the two measured temperatures in this zone. In the reality some interception effects as for example plants and trees which have not been taken into account here could lower the temperature in that zone.

Opened vents

The same distribution method is used here, and the condition of the flow field presented in figure 56 are used.

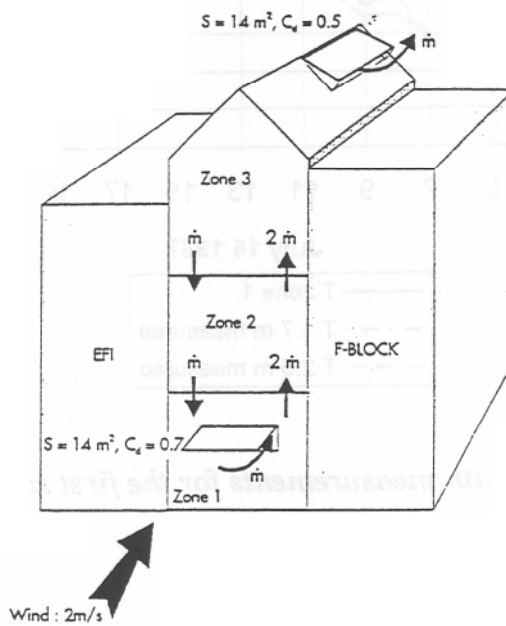


Fig. 56

- Piston flow with recirculation (mixing effect due to turbulences)
- Surface of the low vents : 14 m^2
- Surface of the upper vents 14 m^2
- Discharge coefficient of the lower and the upper vents : $CD_{\text{high}} = 0.5$
 $CD_{\text{low}} = 0.7$
- 2 m/s of wind in the direction of the low opening

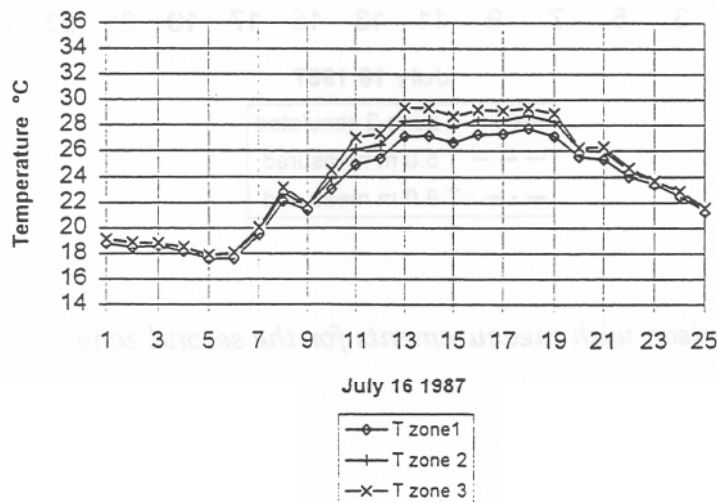


Fig. 57 Calculated temperatures in the 3 zones

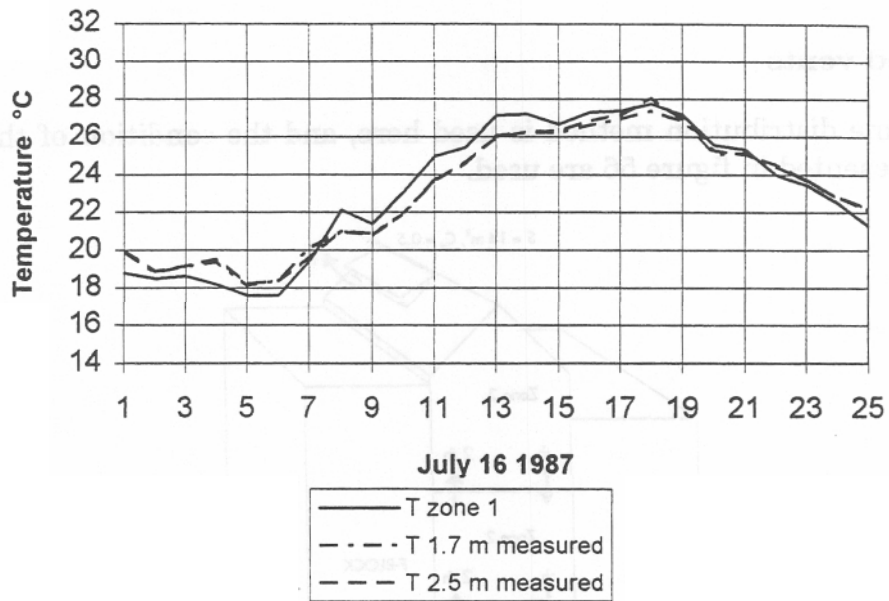


Fig. 58 Comparison with measurements for the first zone

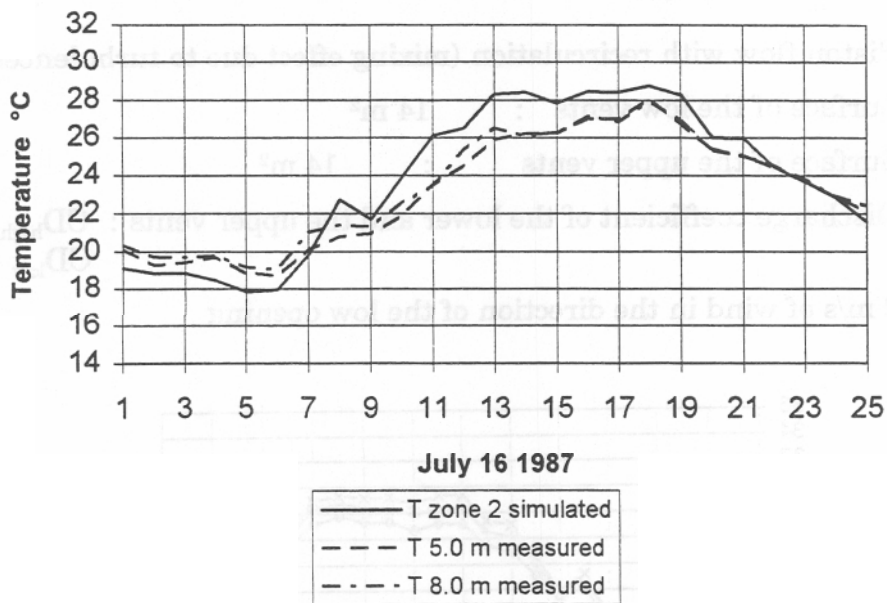


Fig. 59 Comparison with measurements for the second zone

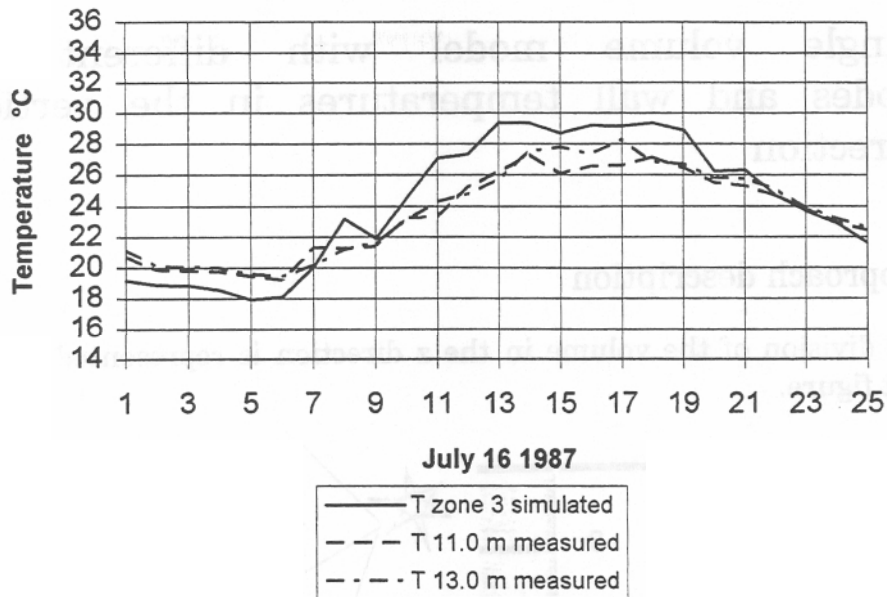


Fig. 60 Comparison with measurements for the third zone

The results obtained in this case are very good. Both the stratification and the average temperature in the atrium are predicted correctly.

3.11.4 Limits of the method

The results obtained with this standard use of building simulation programs are not so bad in the case of the atrium similar to ELA although some important parameters must be assumed, as the amount of solar gain which enter in the volume but are reflected outside afterwards, or the air infiltration in the lower parts of the atrium coming from outside and from the adjacent building. The method can give the designer some important information about the amount of temperature stratification and the surface of vents which is needed in order to ventilate the atrium correctly in the summer.

The results obtained with the correct calculations of the solar gain distribution seem not to be much better than the first one. But they are much more appropriate for the designer because the assumption of the solar gain which are reflected outside the atrium is yet calculated correctly. This precalculation (solar gain distribution) will give much more appropriate results in the case of the atrium of the university of Neuchâtel (attached atrium) than the standard method of the building simulation program. This one is too much sensitive to the volume partitioning of the atrium, and therefore is not appropriate in the general design phase.

3.12 Single volume model with different air nodes and wall temperatures in the vertical direction

3.12.1 Approach description

The division of the volume in the z direction is represented in the next figure.

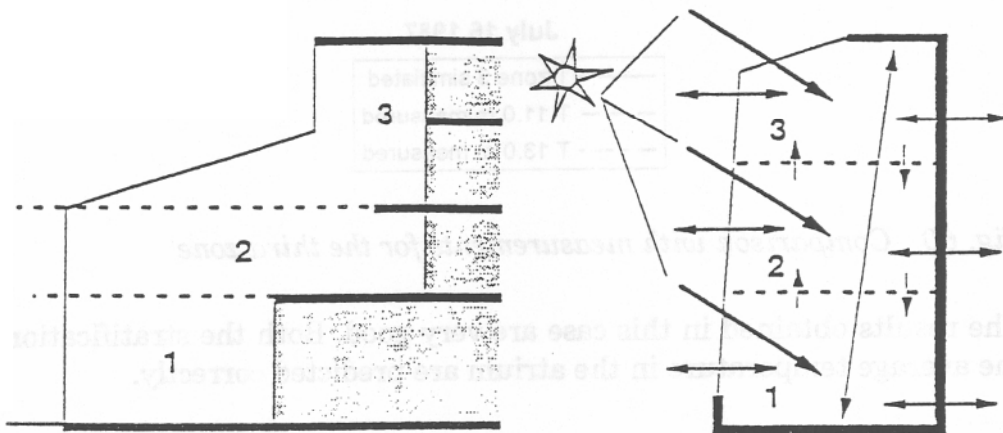


Fig. 61 Single volume model

With this approach the division in the vertical direction is less important because the solar gain distribution is done correctly.

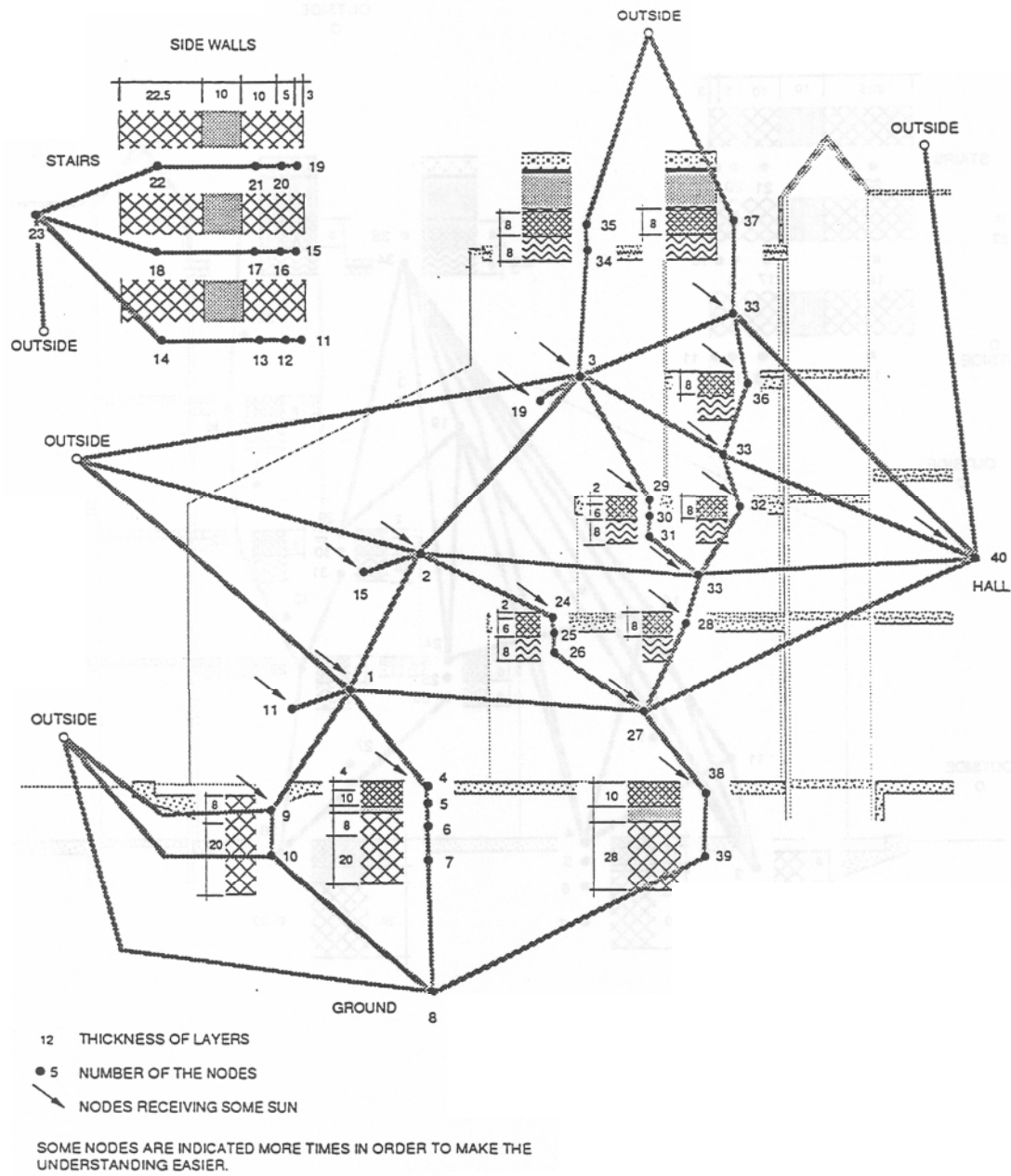
The total amount of energy coming into the atrium is calculated and then distributed on the different surfaces and light elements (air) according to a solar distribution program.

Each hour of the day, a new solar distribution is used according to the season and orientation of the building. Such a distribution program is described in the report dealing with the short wave radiation (chapter 6).

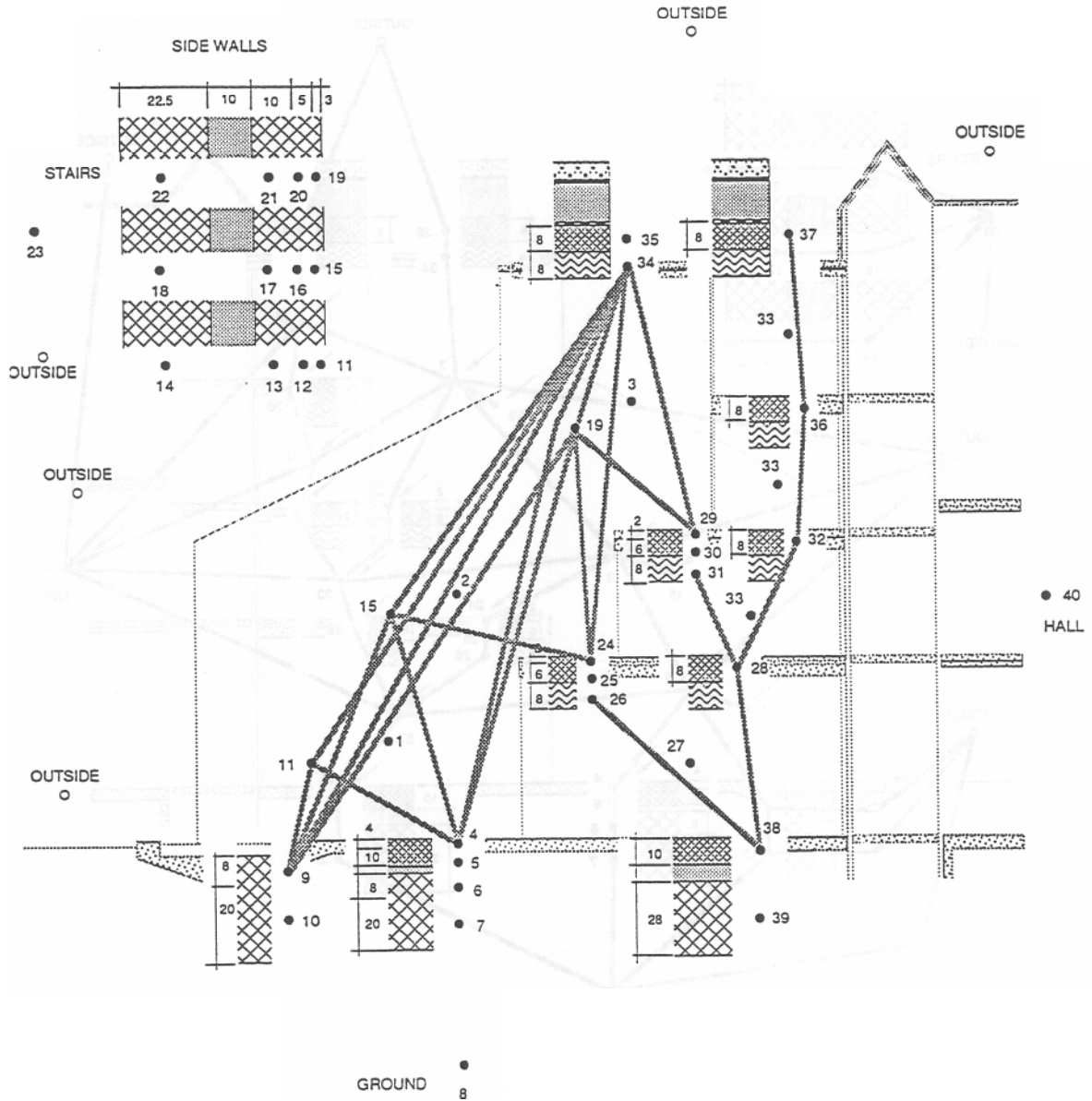
The program used to model the atrium is called MODPAS and has been developed by Sorane SA. It uses a mesh of 40 temperature nodes. These nodes can be the air of a zone as well as the surface or element temperature of a wall. Each nodes is coupled with some other nodes by symmetrical connections (conduction, convection, I.R. radiative exchanges) by non-symmetrical connection (radiative exchanges as short wave (sun) and heat gains), or by connection with the outside.

The atrium is divided in three zones, the connection mesh is presented in the next two pages.

CONDUCTION ET CONVECTION CONNECTIONS



INFRARED RADIATION CONNECTIONS



Two types of air movements are modelled in this program :

- Natural ventilation when the vents are opened
- Mixing due to buoyancy

a) Natural ventilation

When the vents are opened the flow field is assumed as in chapter 3.8 (Piston flow).

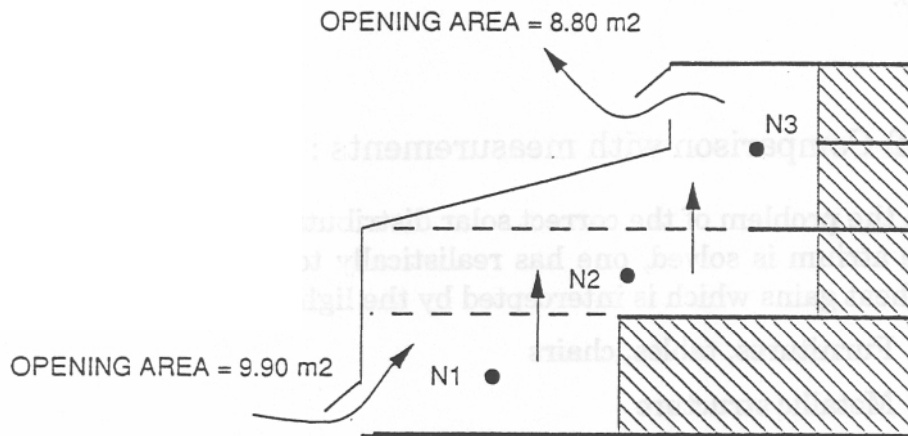


Fig. 62 Piston flow when the vents are opened

The air flow rate entering in the lower zone and going out on the top is calculated using the average air temperature in the atrium ($(T_1 + T_2 + T_3) / 3$) and with the relation presented in chapter 6.4.2.3 $m = f(T_{int}$ and $T_{outside})$

b) Mixing due to

If a lower zone becomes hotter than the zone just above, a convection flow is calculated between the two zones.

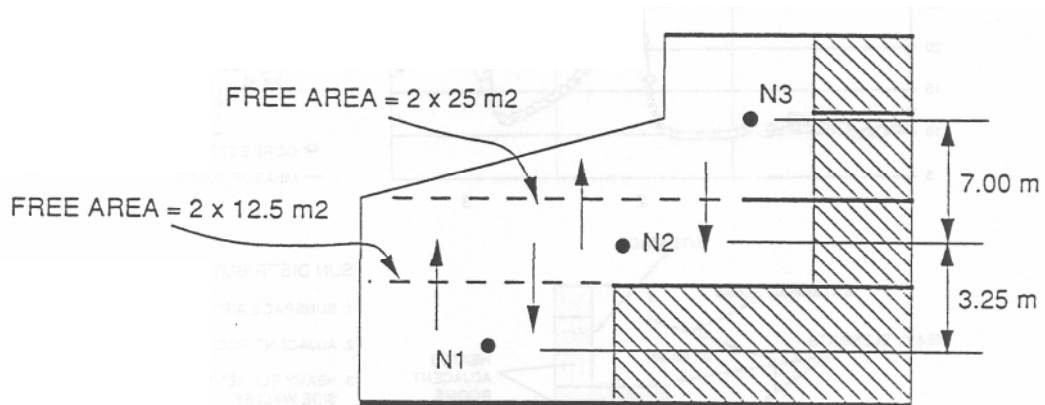


Fig. 63 Buoyant flow

Connection 1-2 : $S = 25 \text{ m}^2$ $\Delta H = 3.25 \text{ m}$
 $Cd = 0.5$

Connection 2-3 : $S = 12 \text{ m}^2$ $\Delta H = 7 \text{ m}$
 $Cd = 0.5$

The flow takes place only if $T1 > T2$ or $T2 > T3$, the mass flow is calculated with the formula based on Bernoulli presented in chapter 3.10.3.

3.12.2 Comparison with measurements : Results

When the problem of the correct solar distribution on the different surfaces of the atrium is solved, one has realistically to evaluate the part of these solar heat gains which is intercepted by the light elements of the atrium :

- Furnitures, tables, chairs
- Metallic structure
- Gates

The consequences of the underestimation of this intercepted part is that the calculated transient behavior and the peak temperature can be wrong.

In the next figure the **average air temperature** in the atrium has been calculated with two intercepted ratios. It can be seen that an error in this evaluation can lead to peak temperature underestimation of about 10°C.

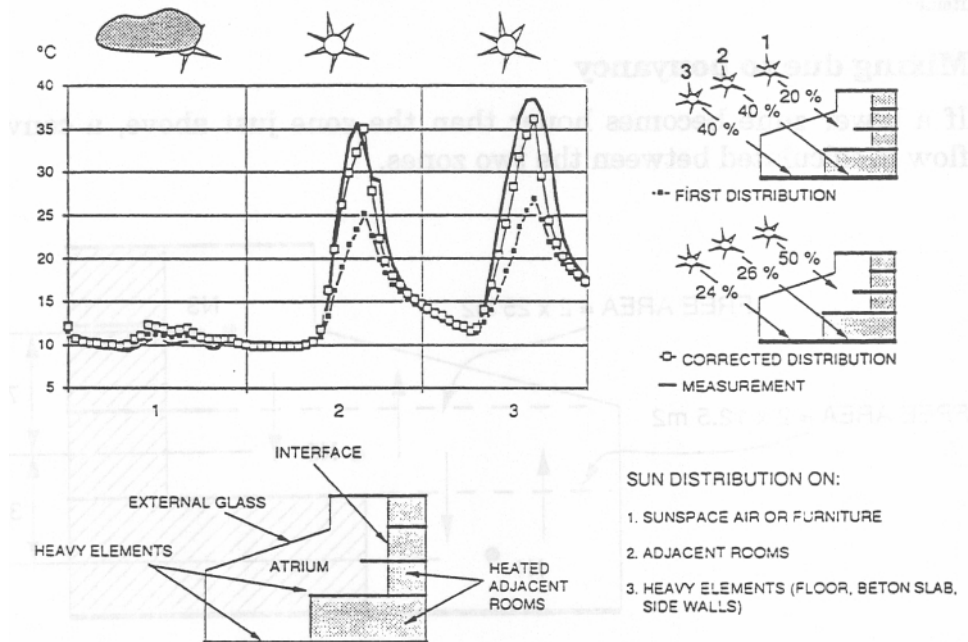


Fig. 64 Importance of the correct evaluation of the solar interception in the atrium

A first period of five days in March has been chosen for the comparison

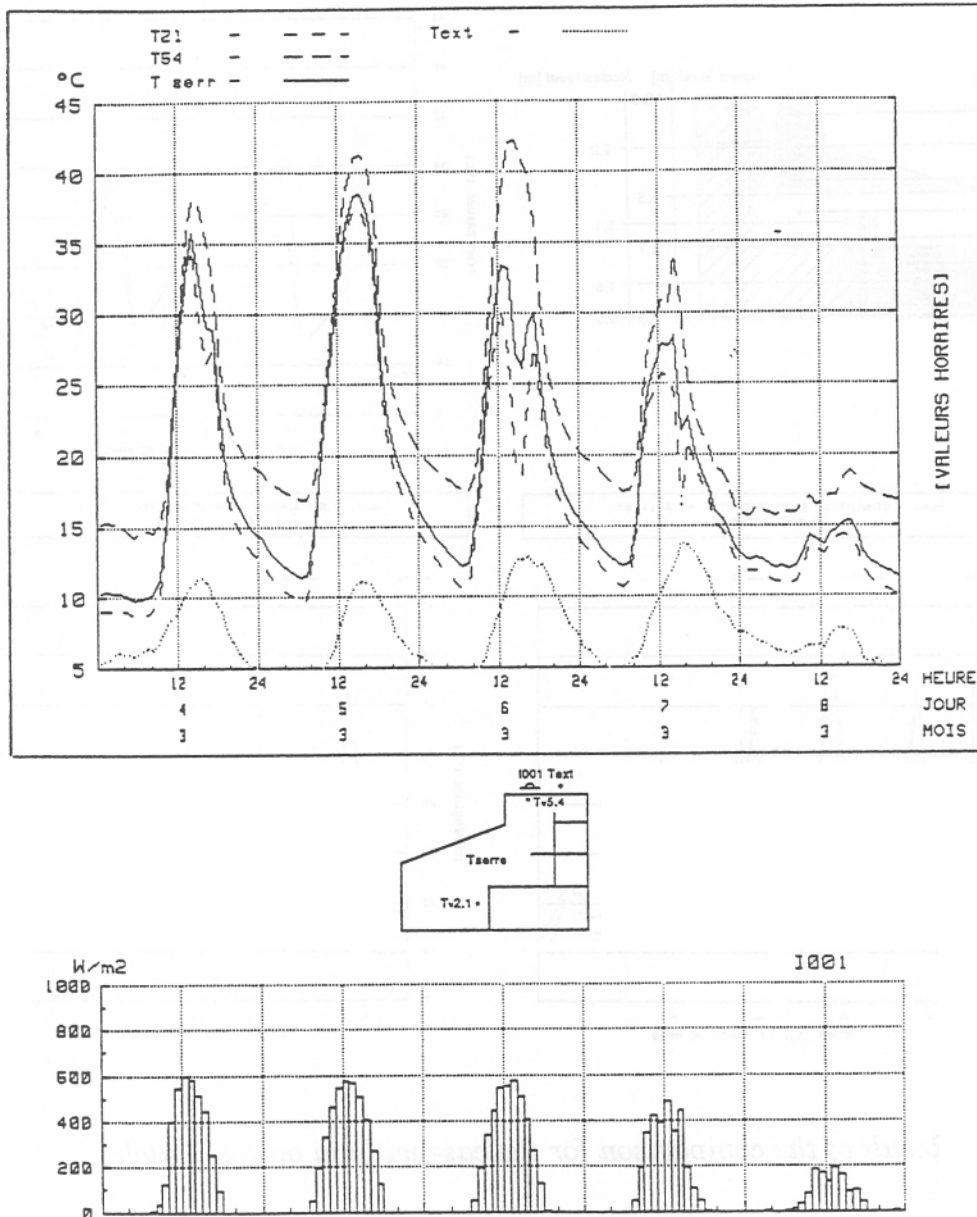


Fig. 65 Measured temperature evolution in the atrium from the 4th to 8th of March 1989

The results of the comparison are shown in the three following figures. The points S1 to S5 refers to measured values, the points N1, N2, N3 to calculated average air temperature in the three volumes.

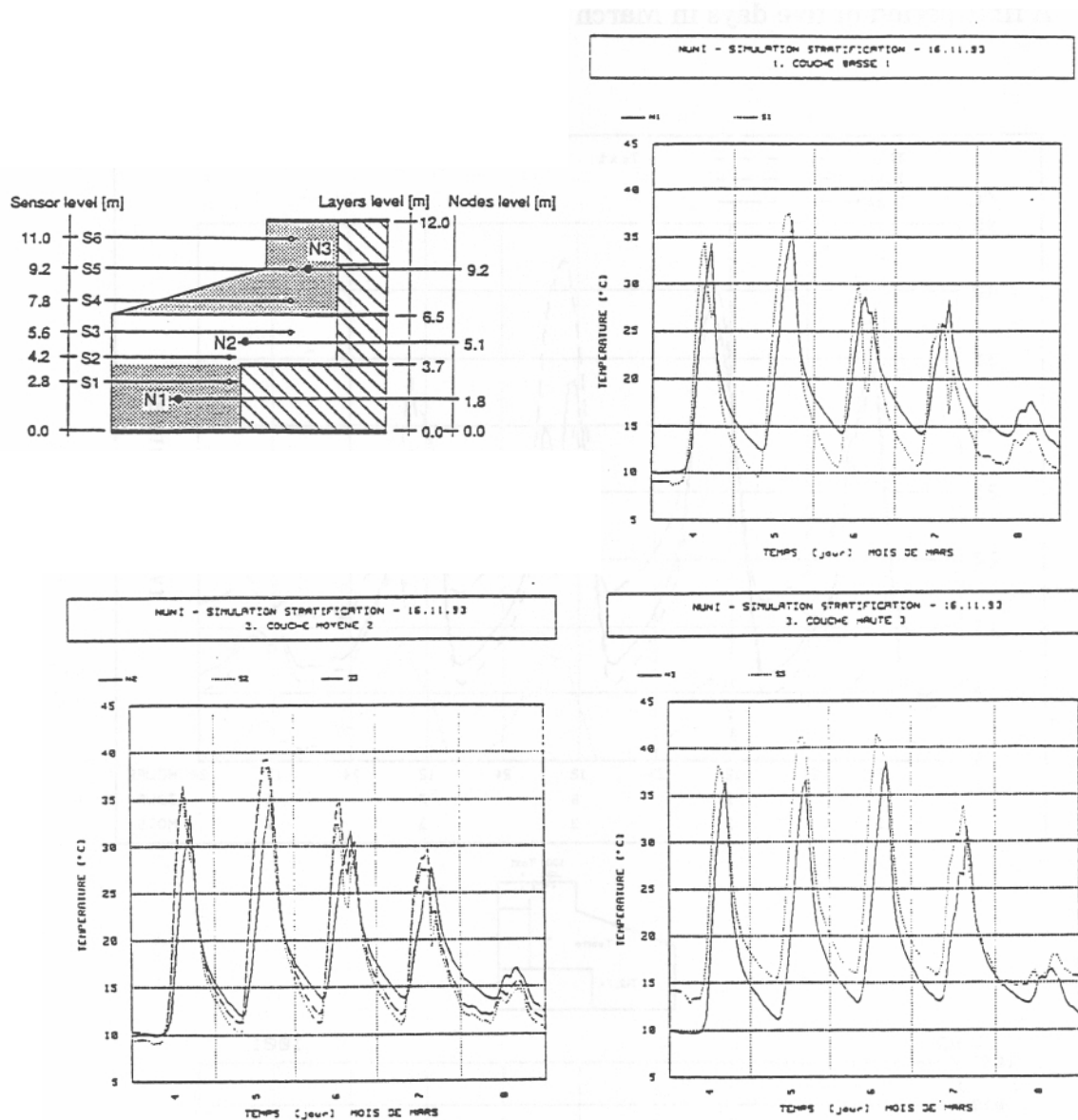


Fig. 66 Result of the comparison for the case without opened hatches

During the two first days the internal shading devices are not used, and the air temperature in the atrium is not stratified very much. During the two next days with the solar protection, the temperature stratification takes place. The calculated values of the different zones are in agreement with the measurements. Some discontinuities in the measured air temperature especially for the lower zone are due to punctual opening of the lower hatches. This small detail has not been taken into account in our calculations.

The second period used is the one already used in the case of the TRNSYS standard approach of chapter 3.10.

The first day (27 of March) is clear and the temperature of the atrium is mixed. No shading devices are used and no vents are opened.

During the second day the shading devices are used as well as the vents opened. The day is also clear (sunny).

During the last day the vents are closed (except the lower ones for about half an hour) and the shading devices are used.

The results of the calculation are presented in the next figure.

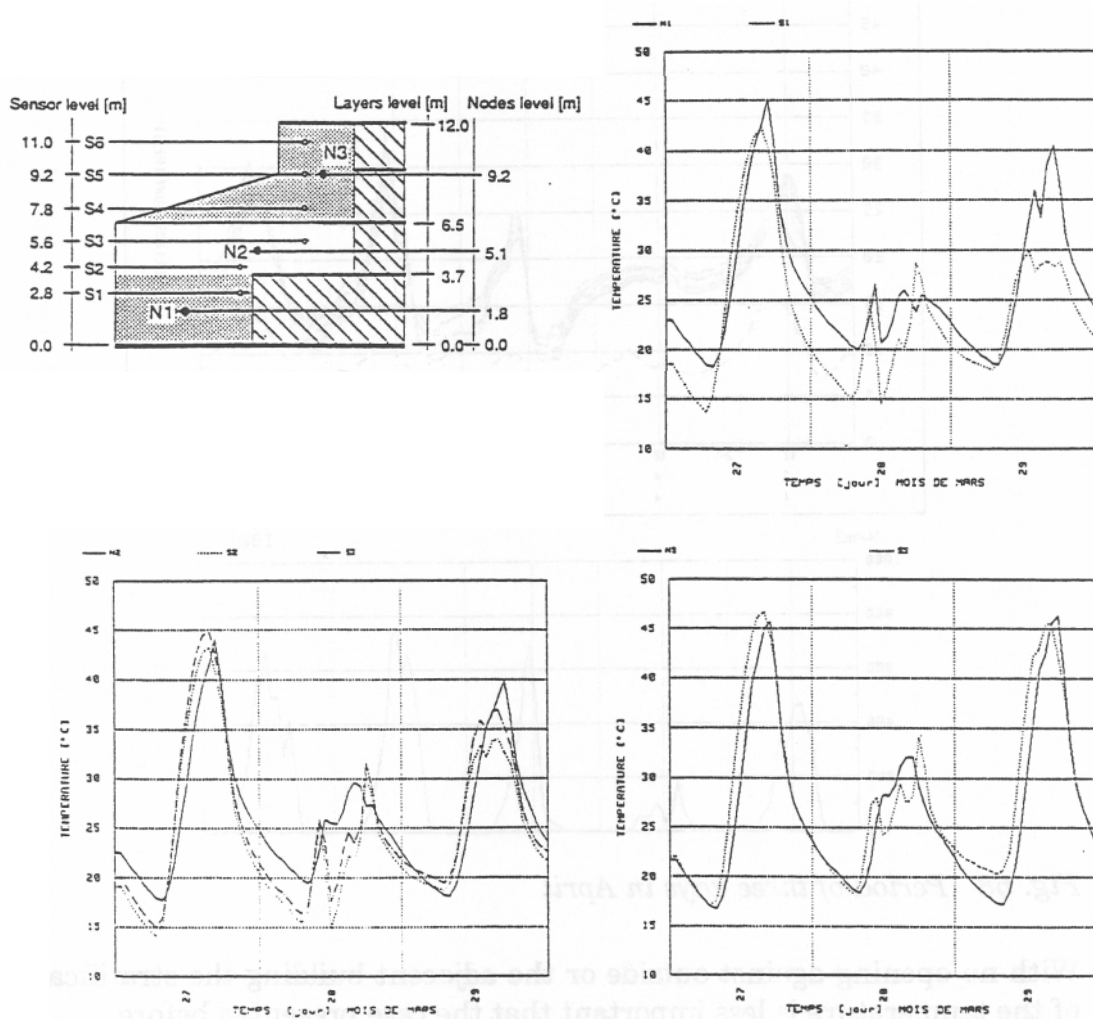


Fig. 67 Results of the comparison for the 27, 28, 29 of March

If the first two days are rather well predicted, the last one is not well predicted in the lower parts. This is not due to the model but simply to the fact that a mobil wall has been opened in the lower part of the atrium. This wall is in direct connection with the building which is at a temperature of 20°C. An important air exchange takes place so that the ground level is maintained at a temperature of 30°C. This effect is not introduced for the moment in the model so that the stratification is not calculated correctly.

The last period is a succession of three days in April. During these days the shading devices are used, the vents are closed and no doors or mobil walls are opened against the building.

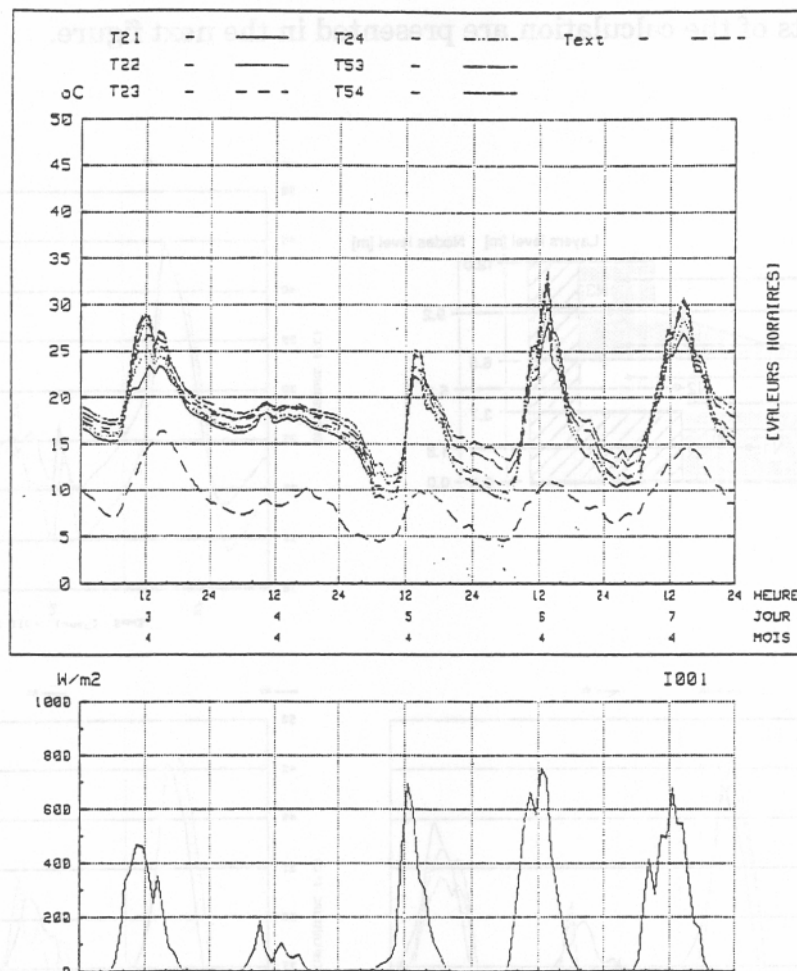


Fig. 68 Period of three days in April

With no opening against outside or the adjacent building the stratification of the temperature is less important than the case presented before.

The comparison of the calculated temperature with the measurements presented in figure 69 are very good and illustrate the validity of the method used.

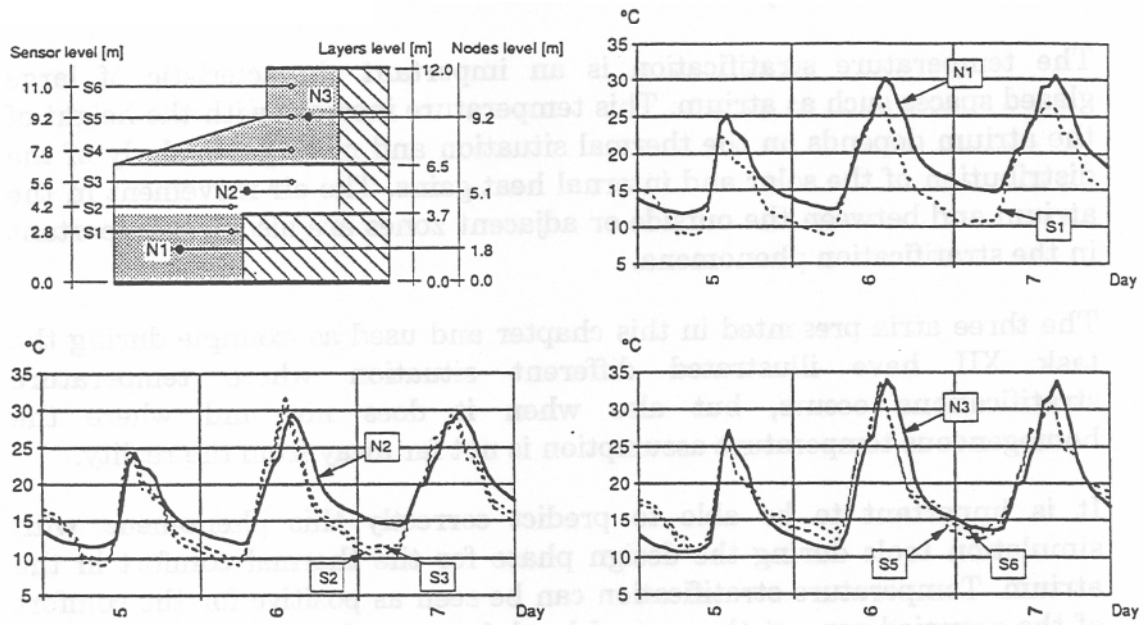


Fig. 69

3.13 Summary and conclusions

The temperature stratification is an important characteristic of large glazed spaces such as atrium. This temperature increase with the height of the atrium depends on the thermal situation and more particularly of the distribution of the solar and internal heat gains. The air movement in the atrium and between the outside or adjacent zones are also very important in the stratification phenomena.

The three atria presented in this chapter and used as example during the task XII have illustrated different situation where temperature stratifications occurs, but also when it does not and where the homogeneous temperature assumption is not far away from the reality.

It is important to be able to predict correctly this phenomena with simulation tools during the design phase for the thermal comfort in the atrium. Temperature stratification can be seen as positive for the comfort of the occupied zone at the ground level, but can also lead to overheating problem if the upper part is also occupied or if adjacent offices are in contact with the upper part of the atrium. In winter time, especially in heated atria the situation is different. Temperature stratification is a disadvantage because it will require more heat in order to obtain comfortable conditions on the ground level.

In fact, the stratification of the temperature in the summer is not very often sufficient to provide comfortable condition at the ground level so that natural ventilation must be used. In that case the stratification decreased, and a simulation tool using the well mixed assumption (homogeneous temperature in the atrium) will give reasonable results.

For the energy consumption prediction it is note quite clear if it is very important to take into account the temperature stratification. Very often, but this is not a rule, heated glazed spaces are not stratified in an important manner, see for example ELA. The reason is that the convectors (heat sources) and the cold surfaces (glasses of the gable and the roofs) are creating a strong air movement which will mixed the air temperature.

In order to illustrate the problem some calculations have been performed on the atrium of the university of Neuchatel. In that case the differences (between the calculation with the all mixed and with the stratification model). In the annual energy consumption of the atrium were not important (maximum difference of 12 %) and the difference for the adjacent space less than 1/2 %. For other atrium and building configuration the result can be a bit different but more sensitivity studies about this subject must be done before a general conclusion can be drawn.

The studies done during the task XII about the modelling of the temperature stratification in an atrium with simplified models have pointed out the following points :

1. The linear temperature stratification model work well in the case of ELA. Of course it assumes a certain temperature profile which is not always valid in other cases. In addition when more opening at different levels are present its use can lead to some problems.
2. When no temperature profile is assumed but the volume simply divided in different horizontally partitioning, the correct distribution of the solar gains in the vertical partitioning is the most important parameter for the correct temperature calculation. Programs which are able in their standard form to predict this distribution correctly as DEROB gives already reasonable results. Other programs as TRNSYS must be corrected as it has been shown in chapter 3.11.3 if one wants to use them in the design phase.
3. Simple flow field assumption are able to give reasonable results, particularly when the vents are opened and the atrium naturally ventilated. Down draft problems cannot be pointed out with these simple flow field models.
4. The effect of the temperature stratification on the energy consumption seems not to be very important in most typical atrium. But more sensitivity studies about this subject must be done before a correct conclusion can be drawn.

3.14 List of symbols

T	=	Temperature	[°C] [°K]
V	=	Volume	[m ³]
S	=	Surface	[m ²]
p	=	Density	kg/m ³
g	=	Gravity	m/s ²
Z	=	Z coordinate, distance	[m]
B	=	Length	[m]
H	=	Height	[m]
t	=	Time	[s]
Q	=	Heat flux	[W]
X	=	Dimensionless temperature near the floor	[-]
U_i	=	Heat conductance from surface to nearest wall node	[W/°]
U_a	=	Convective heat transfer coefficient for the surface	[W]
C_a	=	Heat capacity rate of inlet air	[W/°]
F_r	=	Fraction of radiation for room heat load	[W]
γ_s	=	Local stratification number for surface S	
Y_s	=	Mean height	[m]
C_D	=	Discharge coefficient	[-]
m	=	Mass floor	kg/s

3.15 References

Stein Are Kvikne. 1991. Numerisk Simulering av Termisk Komfort i Glassgarder. Institutt for VVS-Teknikk

Maria Wall. 1992. Glazed courtyard at Taman : Thermal performance of the courtyard and surrounding residential buildings Measurements and calculations. Swedish Council for Building Research

Y. Brügger, P. Chuard and P. Jaboyedoff. 1990. Nouvelle Université de Neuchâtel, mesure de la serre. Office fédéral de l'énergie

Kjell Kolsaker and Hans Martin Mathisen. 1992. Computer simulation of energy use and thermal climate in glazed spaces. Roomvent'92 - Aalborg, Denmark.

4 Natural Ventilation

4.1 Introduction

The purpose of an atrium ventilation system is to ensure the comfort in summer and to remove moisture and other air pollutants in winter with the lowest possible energy consumption. These considerations will determine the maximum and minimum ventilation capacity respectively. Additionally, the inlets and outlets shall be placed and the inlet air velocities shall be chosen so that draft is avoided in the occupancy zone.

For a natural ventilation system, thermal buoyancy and wind are the driving forces, and these forces can effectively be used in atria if only the system is designed and executed in a proper manner as to obtain sufficient ventilation capacity and suitable regulation possibilities.

A natural ventilation system can be designed either as a displacement system or as a mixing system. It is mainly a question of choosing the right position and size of the inlets. With the right size, it is possible to obtain as low an inlet air velocity as 0.1-0.2 m/s for a displacement system.

The critical situation is the hot summer day with no wind. A sufficient ventilation capacity shall then be obtained by the buoyancy alone, and therefore the greatest importance will be attached to thermal buoyancy in this chapter. The wind will contribute to the ventilation capacity. On the other hand, it can give undesired high air velocities and this has to be taken into consideration when designing the control system.

4.2 Ventilation by Thermal Buoyancy

Natural ventilation by thermal buoyancy is the air exchange between two or more zones with different air densities. These differences can be due to different temperatures or different moisture contents. In an atrium the temperature differences will dominate, and therefore moisture differences

will not be taken into account in the following discussion of thermal buoyancy.

Ventilation by air exchange implies openings between the zones, and the opening arrangement can either be separate small openings in different levels or it can be a single large vertical or horizontal opening.

The temperature difference can occur due to heating one or more of the zones. After a period of time, steady state conditions will exist with a balance between the heat supply, the temperature difference, the resulting ventilation capacity and the heat losses. It is this steady-state situation, that will be dealt with in the following discussion.

4.2.1 Ventilation Through Two Separate Openings

The simplest case involves only two small rectangular openings placed above each other as shown on figure 4.1. In both openings an air jet is created as shown on the figure.

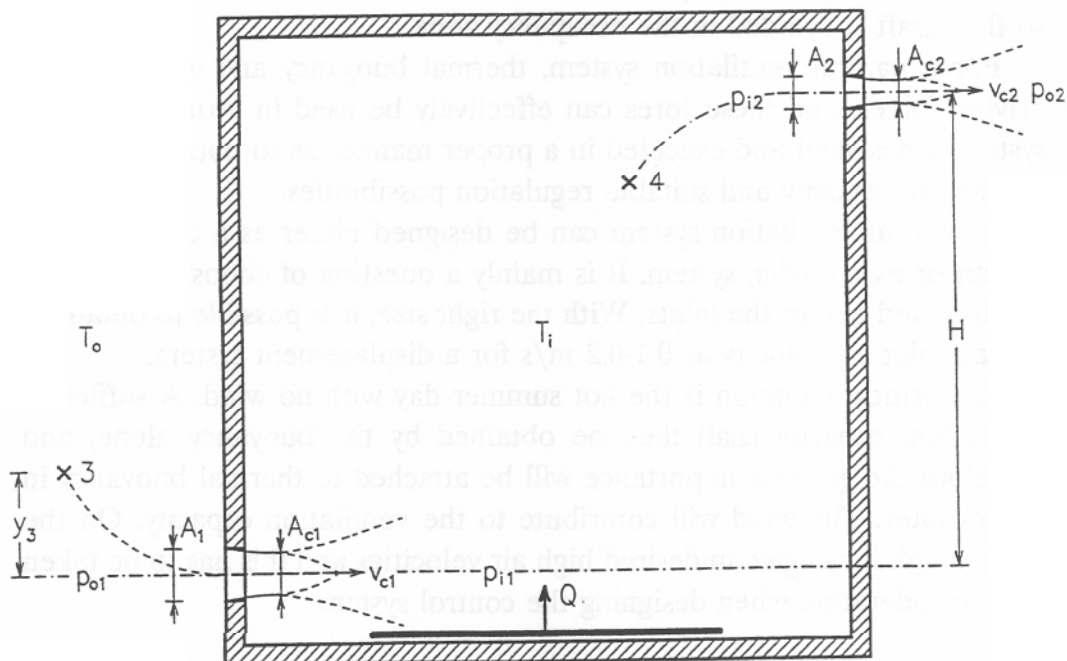


Figure 4.1 Natural ventilation through two openings by thermal buoyancy

The jet passes through the so-called constricted area, where the air pressure is equal to the surrounding pressure and where the air velocity corresponds to, that almost the whole pressure drop across the opening is converted to kinetic energy.

For the flow situation in question, the following equations can be set up:

$$\rho_o c_p A_{cl} v_{cl} \Delta T = Q_s \quad (\text{energy conservation}) \quad (4.1)$$

$$\rho_o A_{cl} v_{cl} = \rho_i A_{c2} v_{c2} \quad (\text{mass balance}) \quad (4.2)$$

$$\Delta p_1 + \Delta p_2 = \Delta \rho g H \quad (\text{momentum in vertical direction}) \quad (4.3)$$

$$\Delta p_1 / \rho_o = v_{cl}^2 / 2 + \zeta_1 v_{cl}^2 / 2 = \psi_1 v_{cl}^2 / 2$$

(modified Bernoulli equation across the inlet) (4.4)

$$\Delta p_2 / \rho_i = v_{c2}^2 / 2 + \zeta_2 v_{c2}^2 / 2 = \psi_2 v_{c2}^2 / 2$$

(modified Bernoulli equation across the outlet) (4.5)

where:

ρ_i and ρ_o are the indoor and outdoor air densities

c_p is the specific heat capacity of the air

A_{c1} and A_{c2} are the constricted inlet and outlet areas

v_{c1} and v_{c2} are the air velocities in the constricted areas

$\Delta \rho$ and ΔT are the differences between indoor and outdoor air density and air temperature

Δp_1 and Δp_2 are the pressure differences across the inlet and outlet

ζ_1 and ζ_2 are the resistance coefficients for the inlet and outlet

Q_s is the surplus heat, i.e. the heat available for heating up the indoor air.

Further relationships are as follows:

$$A_{c1} = C_{c1} A_1 \quad \text{and} \quad A_{c2} = C_{c2} A_2$$

$$v_{c1} = C_{v1} v_{theo} \quad \text{and} \quad v_{c2} = C_{v2} v_{theo} \quad \text{with} \quad v_{theo} = (2 \Delta p / \rho)^{1/2}$$

$$\psi_1 = 1 + \zeta_1 \quad \text{and} \quad \psi_2 = 1 + \zeta_2$$

where:

C_{c1} and C_{c2} are the contraction coefficients for inlet and outlet

C_{v1} and C_{v2} are the velocity coefficients for inlet and outlet.

The unknown quantities are v_{c1} , v_{c2} , Δp_1 , Δp_2 and ΔT or $\Delta \rho$. By using the following relationship between density and temperature:

$$\Delta \rho \sim \rho_i (\Delta T / T_o) = \rho_o (\Delta T / T_i) \quad (4.6)$$

where T_i and T_o are the indoor and outdoor temperatures, respectively, you get the following solution from the eqs. (4.2) - (4.5) :

$$v_{c1} = \left[\frac{2 \Delta \rho g H_1}{\psi_1 \rho_o} \right]^{1/2} = \left[\frac{2 \Delta T g H_1}{\psi_1 T_i} \right]^{1/2} \quad (4.7)$$

$$v_{c2} = \left[\frac{2 \Delta \rho g H_2}{\psi_2 \rho_i} \right]^{1/2} = \left[\frac{2 \Delta T g H_2}{\psi_2 T_o} \right]^{1/2} \quad (4.8)$$

$$\Delta p_1 = \Delta \rho g H_1 = \rho_o \Delta T g H_1 / T_i \quad (4.9)$$

$$\Delta p_2 = \Delta \rho g H_2 = \rho_i \Delta T g H_2 / T_o \quad (4.10)$$

where $H_1 + H_2 = H$, and where again:

$$H_1 = \frac{H}{1 + (T_i / T_o) (\psi_2 / \psi_1) (A_{c1} / A_{c2})^2} \quad (4.11)$$

$$H_2 = \frac{H}{1 + (T_o / T_i) (\psi_1 / \psi_2) (A_{c2} / A_{c1})^2} \quad (4.12)$$

Besides you get from equation (4.1):

$$\Delta T = \frac{Q_s}{\rho_o c_p A_{cl} v_{cl}} \tag{4.13}$$

The result shows, that the aerostatic pressure distribution outside and inside will cross each other somewhere between the openings as shown on figure 4.2. In the crossing point, you have the so called neutral plane or axis where the inside and outside air pressures are equal. There will be an inward air flow through one of the openings and an outward air flow through the other one.

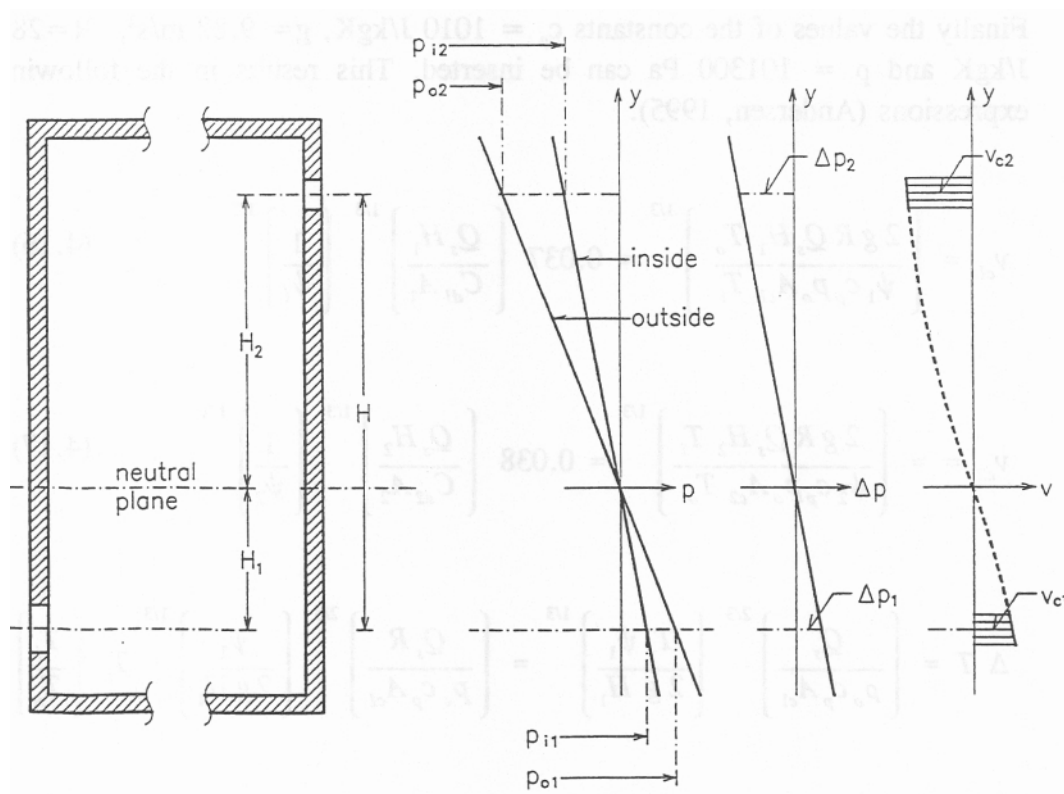


Figure 4.2 Pressures, pressure differences and air velocities at the two openings

The equation (4.13) can be used to eliminate ΔT from the eqs. (4.7) - (4.8). Additionally the following relations between pressure, density and temperature can be used:

$$\rho_i T_o = \rho_o T_o (\rho_i / \rho_o) = (p_o / R) (T_o / T_i) \tag{4.14a}$$

$$\rho_o T_i = \rho_o T_o (T_i / T_o) = (p_o / R) (T_i / T_o) \quad (4.14b)$$

where:

ρ_i and ρ_o are the indoor and outdoor pressures, respectively.

Besides the discharge coefficient can be introduced by (Andersen, 1995):

$$C_d = C_v C_c = C_c / (1 + \zeta)^{1/2} = C_c / \psi^{1/2} \quad (4.15)$$

Finally the values of the constants $c_p = 1010 \text{ J/kgK}$, $g = 9.82 \text{ m/s}^2$, $R = 287 \text{ J/kgK}$ and $p = 101300 \text{ Pa}$ can be inserted. This results in the following expressions (Andersen, 1995):

$$v_{c1} = \left[\frac{2 g R Q_s H_1 T_o}{\psi_1 c_p p_o A_{c1} T_i} \right]^{1/3} = 0.037 \left[\frac{Q_s H_1}{C_{d1} A_1} \right]^{1/3} \left[\frac{1}{\psi_1} \right]^{1/2} \quad (4.16)$$

$$v_{c2} = \left[\frac{2 g R Q_s H_2 T_i}{\psi_2 c_p p_o A_{c2} T_o} \right]^{1/3} = 0.038 \left[\frac{Q_s H_2}{C_{d2} A_2} \right]^{1/3} \left[\frac{1}{\psi_2} \right]^{1/2} \quad (4.17)$$

$$\begin{aligned} \Delta T &= \left[\frac{Q_s}{\rho_o c_p A_{c1}} \right]^{2/3} \left[\frac{T_i \psi_1}{2 g H_1} \right]^{1/3} = \left[\frac{Q_s R}{p_o c_p A_{c1}} \right]^{2/3} \left[\frac{\psi_1}{2 g H_1} \right]^{1/3} T_i \left[\frac{T_i}{T_o} \right]^{2/3} \\ &= 7.1 \cdot 10^{-5} T_i \left[\frac{Q_s}{C_{d1} A_1} \right]^{2/3} \left[\frac{1}{H_1} \right]^{1/3} \end{aligned} \quad (4.18)$$

It is here estimated that

$$T_o / T_i = 1 - \Delta T / T_i \sim 0.95$$

with an error less than 3% so that the expressions are valid with an error less than 2%.

4.2.1.1 Neutral Axis and Air Velocities. The air velocities in the openings are determined by the position of the neutral axis, as can be seen for instance in eqs. (4.7) and (4.8). The position of the neutral axis is again determined by the following ratio, cf. eq. (4.11) and (4.12):

$$n^2 = \frac{T_i}{T_o} \frac{\psi_2}{\psi_1} \left(\frac{A_{c1}}{A_{c2}} \right)^2 = \frac{T_i}{T_o} \left(\frac{C_{d1} A_1}{C_{d2} A_2} \right)^2 \quad (4.19)$$

If for instance $n=1$, you get $H_1 = H_2 = H/2$, and for $n=2$ you get $H_1 = H/5$ and $H_2 = 4H/5$.

Concerning the quantities in eq. (4.19), it should be mentioned that:

- T_i/T_o is almost constant
- ψ_1/ψ_2 can vary a little if changes in A_1 and A_2 result in changes of the flow directions
- C_{c1}/C_{c2} can vary a little if changes in A_1 and A_2 result in changes of the flow through the openings

Changes of the position of the neutral axis is thus first of all dependent on changes of the ratio A_1/A_2 .

If a small inlet velocity is desired in connection with a displacement system, this can be obtained by making H_1 small, and this can again be done by making the area ratio A_1/A_2 large.

A higher inlet air velocity is required by a mixing ventilation system and this can be obtained by increasing H_1 . On the other hand, instability problems may occur near the outlet due to wind, if H_1 has a value close to H .

4.2.1.2 Ventilation Capacity and Opening Areas. The ventilation capacity will be:

$$V = v_{cl} A_{cl} = A_{cl} (2 \Delta T g H_1 / (\psi_1 T_i))^{1/2} \quad (4.20a)$$

and by inserting eq. (4.8) you obtain:

$$V = 0,037 (Q_5 H^1)^{1/3} (C^{dl} A_I)^{2/3} \quad (4.20b)$$

If the outlet area is kept fixed and the inlet area is varied, there will not be proportionality between the ventilation capacity and the inlet area. For instance, a doubling of the inlet area, so that $n = A_1/A_2 = 2$, will only increase the ventilation capacity by 26% if the temperature difference is kept constant and only by 17% if the net heat input is kept constant. By a six fold increase of the inlet area, the increase in ventilation capacity is 39% and 25% respectively. The reason is that by increasing the inlet area the neutral plane moves downward decreasing the pressure difference across the inlet and if the net heat input is kept constant, it results in a lower temperature difference which further decrease the pressure difference (or the "driving forces").

The ratio between a reference ventilation capacity V_{ref} with $A_1/A_2 = 1$ and fixed A_1 and the capacity with any other area ratio is, when ΔT is kept constant (cf. Equation (4.20a) together with Equations (4.11) and (4.19)) :

$$\frac{V_1}{V_{ref}} = \left(\frac{2}{1 + n^2} \right)^{1/2}$$

For fixed outlet area A_2 and constant ΔT you get similarly:

$$\frac{V_2}{V_{ref}} = \left(\frac{2}{1 + 1/n^2} \right)^{1/2}$$

These relationships between ventilation capacity and area ratio are illustrated on figure 4.3a.

The condition that ΔT is kept constant is not realistic in practice as it implies that the net heat input is increased with the same rate as the ventilation capacity. In practice the net heat input will rather be constant. This leads to, cf. Equation (4.20a) together with Equations (4.11) and (4.19):

$$\frac{V_1}{V_{ref}} = \left(\frac{2}{1 + n^2} \right)^{1/3}$$

$$\frac{V_2}{V_{ref}} = \left(\frac{2 n^2}{1 + n^2} \right)^{1/3}$$

This relationship is likewise shown in figure 4.3a

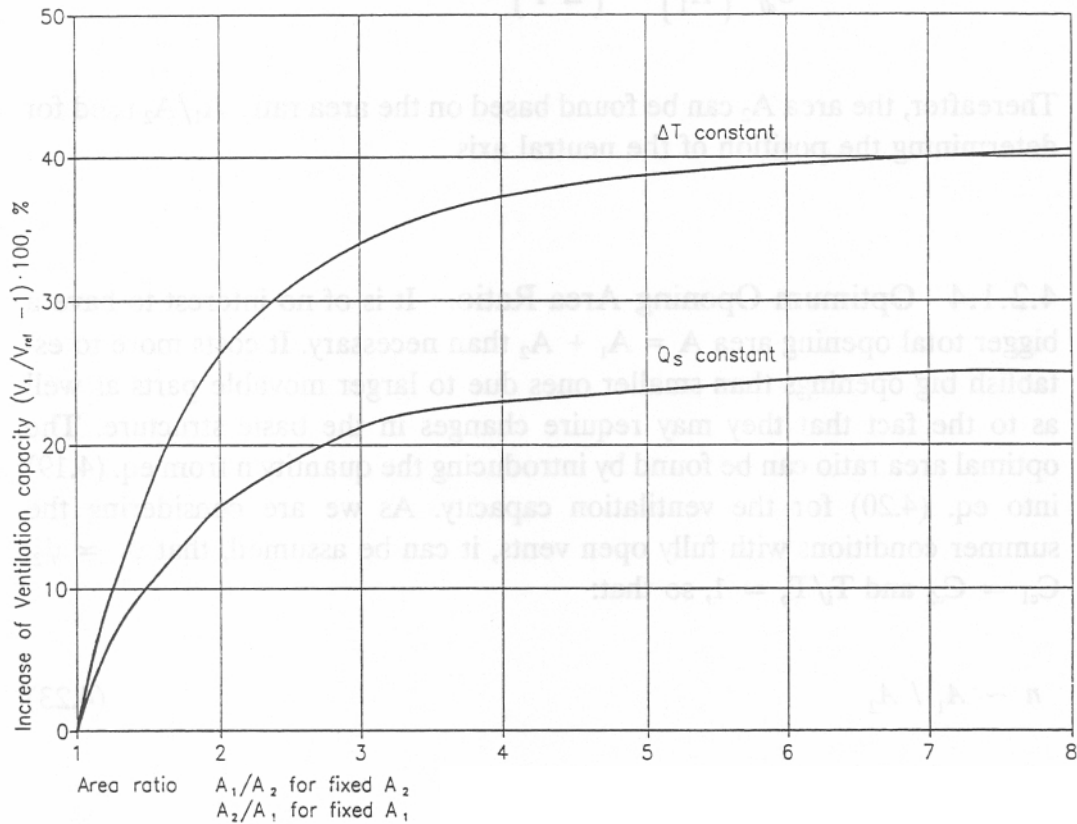


Figure 4.3a Increase in flow for increased inlet or outlet area by constantly kept temperature difference or net heat input.

4.2.1.3 Required Opening Area. The usual design task is to determine the opening areas so that a certain ventilation capacity or a certain temperature difference can be obtained under summer conditions. For this purpose, you get from the eqs. (4.20) and (4.18) the following expressions for the inlet area in dependence on either the ventilation capacity or the temperature difference:

$$A_1 = 140 \frac{V^{3/2}}{(Q_s H_1)^{1/2} C_{dl}} \quad (4.21)$$

$$A_1 = 6.0 \cdot 10^{-7} \frac{Q_s}{C_{dl}} \left[\frac{1}{H_1} \right]^{1/2} \left[\frac{T_i}{\Delta T} \right]^{3/2} \quad (4.22)$$

Thereafter, the area A_2 can be found based on the area ratio A_1/A_2 used for determining the position of the neutral axis.

4.2.1.4 Optimum Opening Area Ratio. It is of no interest to have a bigger total opening area $A = A_1 + A_2$ than necessary. It costs more to establish big openings than smaller ones due to larger movable parts as well as to the fact that they may require changes in the basic structure. The optimal area ratio can be found by introducing the quantity n from eq. (4.19) into eq. (4.20) for the ventilation capacity. As we are considering the summer conditions with fully open vents, it can be assumed, that $\psi_1 \approx \psi_2$, $C_{e1} \approx C_{e2}$ and $T_i/T_o \approx 1$, so that:

$$n \sim A_1 / A_2 \quad (4.23)$$

and besides you have, when $A_1 + A_2 = A$:

$$A_1 = \frac{A_1}{A_1 + A_2} A = \frac{A_1/A_2}{A_1/A_2 + 1} A = \frac{n}{n + 1} A \quad (4.24)$$

This results in:

$$V = 0.037 \left[\frac{n}{n + 1} \right]^{2/3} \left[\frac{1}{1 + n^2} \right]^{1/3} (C_{dl} A)^{2/3} (Q_s H)^{1/3} \quad (4.25)$$

As Q_s is fairly constant, the only variable is n , and it can be found that there is only one extreme value, and that is for $n = 1$ resulting in a maximum value for V as shown on figure 4.3b. If the inlet and the outlet have the same shape, the optimal opening ratio from a ventilation capacity point of view is thus obtained, when the two openings are of equal areas.

It should be mentioned that the ventilation capacity is not particularly sensitive to changes in n . It can thus be seen from figure 4.3b that:

$$V \geq 0.9V_{\max} \text{ for } 0.5 \leq n \leq 2.0. \quad (4.26)$$

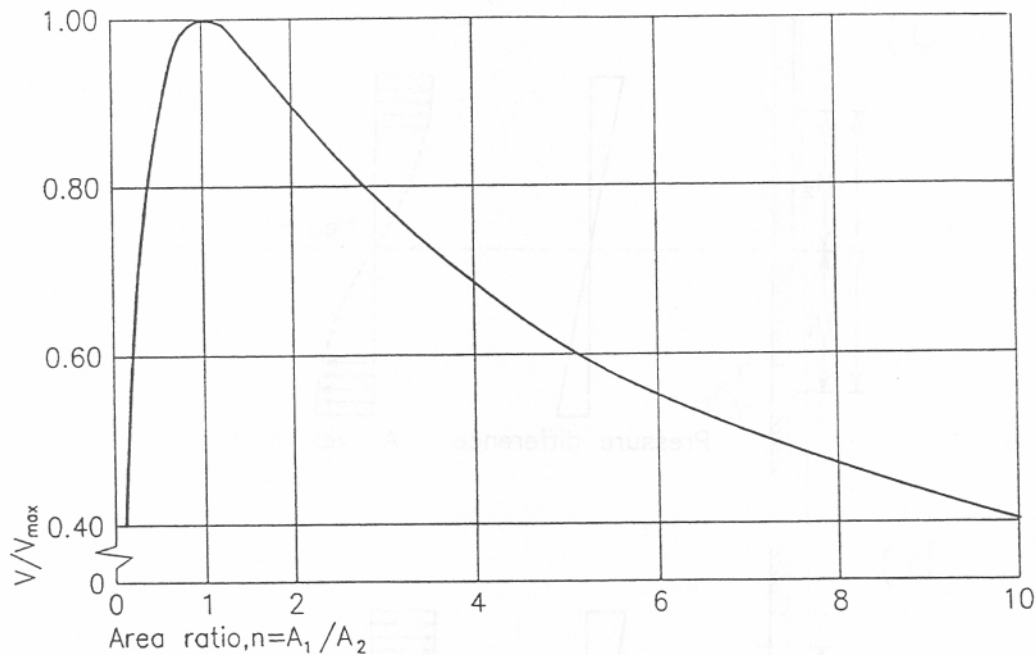


Figure 4.3b The ventilation capacity as a function of the area ratio when the total opening area is kept constant

4.2.1.5 Threshold Position. Bidirectional Flow. The neutral axis moves downward for increasing area ratio A_1/A_2 , cf. eq. (4.11). At the same time the vertical velocity distribution over the opening goes from being almost constant to becoming more and more parabolic. When the neutral axis passes below the upper edge of the inlet, air starts to move outward through the part of the inlet between the neutral axis and the upper edge as shown on figure 4.4.

The neutral axis coinciding with the upper edge of the inlet is thus a threshold position for having an uni- or a bidirectional flow through the inlet. For this position the ventilation capacity can be determined by:

$$V_{thres} = \int_A v dA = \frac{2}{3} A_{cl} v_{cmax} = (2/3) C_{dl} A_1 (2 \Delta \rho g h_1 / \rho_o)^{1/2} \quad (4.27)$$

If the air velocity is assumed constant and with a value corresponding to the pressure difference in the middle of the inlet you obtain the following capacity, c.f. eg. (4.7):

$$V = v_{cl} A_{cl} = C_{dl} A_1 (2 \Delta \rho g (h_1/2) / \rho_o)^{1/2} \quad (4.28)$$

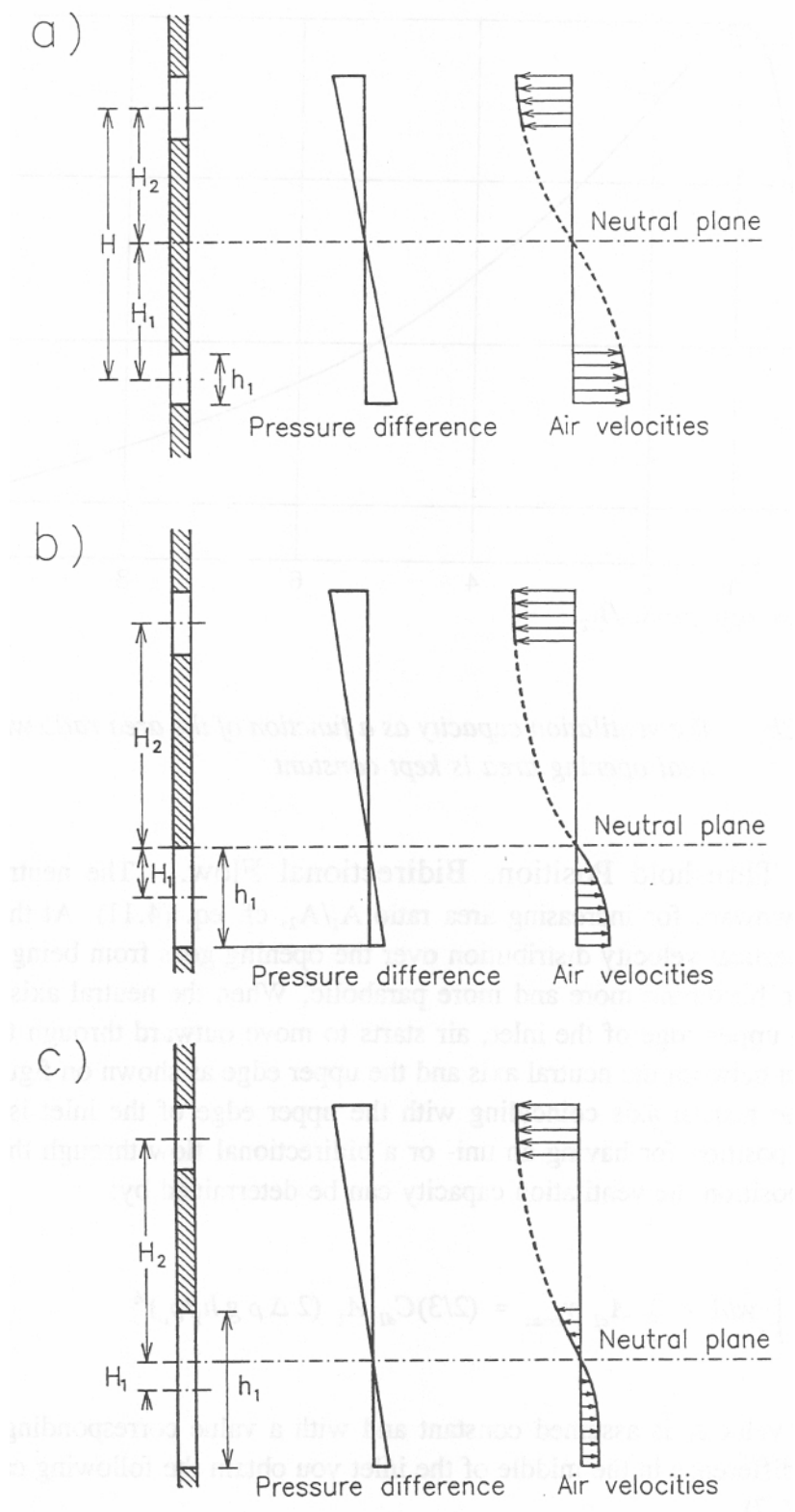


Figure 4.4 The position of the neutral axis by different area ratios with corresponding pressure differences and air velocities.

The ratio between the two capacities is:

$$\frac{C_{d1}}{C_{d2}} = 0,94$$

The error in using the ventilation capacity expression (4.20) is thus small and therefore the expressions derived so far can be used with good approximation as long as the neutral axis position is not below the threshold position, i.e. the upper edge of the inlet (or above the lower edge of the outlet).

In order to be sure beforehand that the neutral axis is above the threshold position, a certain requirement can be put on the opening height h_i of the inlet. This height shall be smaller than the height determined by the following mass balance equation:

$$(2/3) \rho_o C_{d1} (b_1 h_1) (2 \Delta \rho g h_1 / \rho_o)^{1/2} = \rho_i C_{d2} A_2 (2 \Delta \rho g (H - h_1/2) / \rho_i)^{1/2}$$

As $(\rho_i / \rho_o)^{1/2} \sim 1$ and by assuming that $C_{d1} \sim C_{d2}$, this can be reduced to:

$$2/3 b_1 h_1^{3/2} = A_2 (H - h_1/2)^{1/2} \quad (4.29)$$

By squaring you get an equation in 3. degree for determining the threshold value of h_1 . A first guess can be obtained by omitting $h_1/2$ from the parenthesis leading to:

$$h_1 \sim \left[\frac{3A_2}{2b_1} \right]^{3/2} H^{1/3} \quad (4.30)$$

A similar expressions can be derived for the threshold outlet height.

4.2.1.6 Temperature Stratification. In a heated room, the air temperature can have one of the four vertical distributions as shown in figure 4.5.

- curve A, downward curved, by strong heating from a centrally placed, concentrated heat source
- curve B, a straight line, which is often used when only the temperature differences between inside and outside in top and bottom are known
- curve C, upward curved, when the heat source is close to the floor, and when there is a good mixing of the incoming air just above floor level.

curve D, constant temperature, used when all the incoming air becomes well mixed shortly after the entrance.

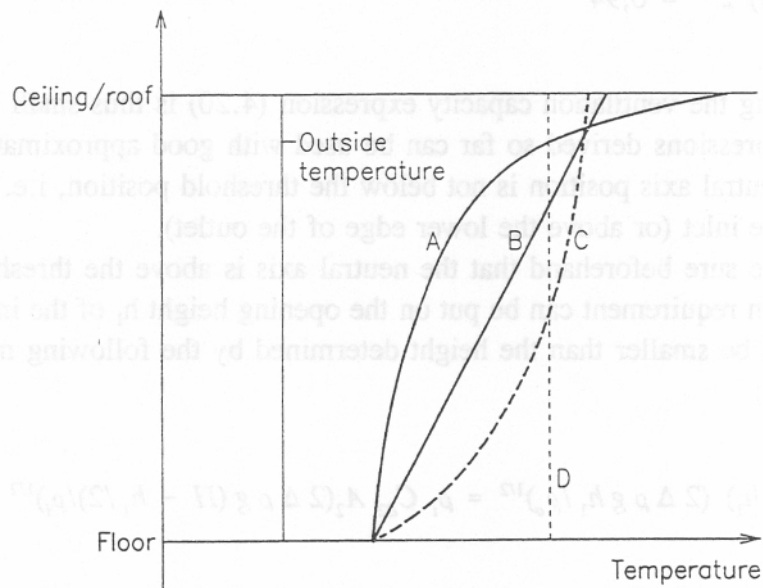


Figure 4.5 Possible vertical temperature distributions in a heated room represented by the curves A, B, C and D.

Temperature measurements in atria have shown a temperature distribution similar to curve A, when inlets and outlets are almost closed, similar to curve B, when they are slightly open and similar to curve D, when they are fully open.

For the straight line distribution, you in principle get pressure distributions as shown on figure 4.6. They will cross each other in order to get the mass balance fulfilled.

Taking the crossing point (or the neutral axis) as the starting point where $T_i = T_{io}$, the temperature distribution can be expressed by:

$$T_i = T_{io} + az \tag{4.31}$$

so that the density becomes:

$$\rho_i = \rho_{io} T_{io} / T_i = \rho_{io} T_{io} / (T_{io} + az) \tag{4.32}$$

The following pressure difference between outside and inside can then be derived (Andersen, 1995) :

$$\begin{aligned} \Delta p &= p_o - p_i = (\rho_o - \rho_{io}) g y + 0,5 g \rho_{io} (a/T_{io}) y^2 \\ &= \Delta \rho_o g y + b g y^2/2 \end{aligned} \tag{4.33}$$

where:

$$b = \rho_{io} a/T_{io} = \rho_{io} (\Delta T_{12}/H) / T_{io} \tag{4.34}$$

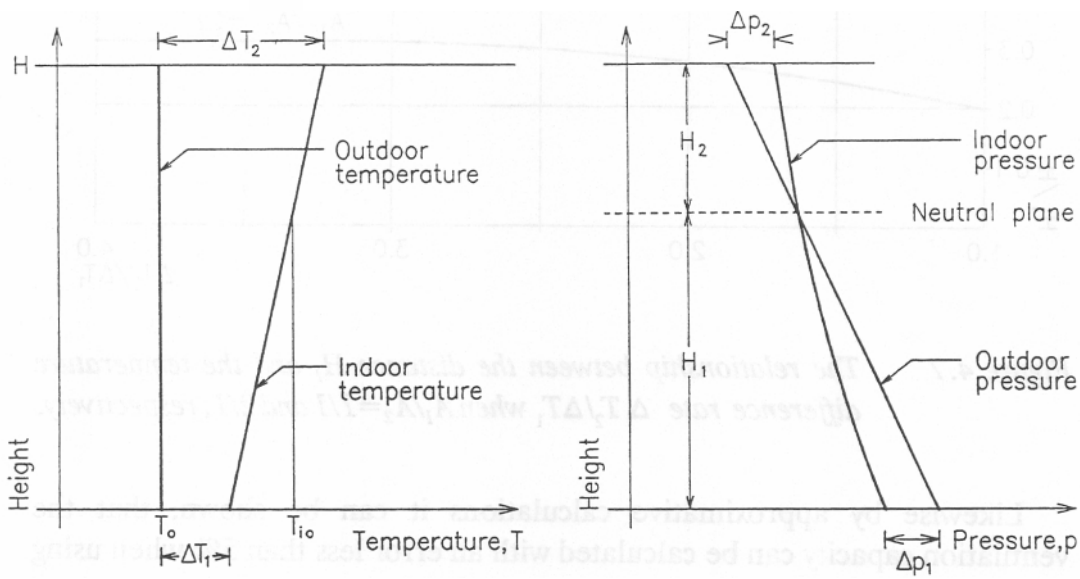


Figure 4.6 Pressure conditions by linear indoor temperature distribution

By calculating first Δp_1 and Δp_2 across the two openings from eq (4.33), next the corresponding velocities by using eqs. (4.4) and (4.5) and then inserting these velocities into a squared mass balance equation, eq. (4.2), you get the following equation for determining the position of the neutral axis, when assuming $\rho_i/\rho_o \approx 1$, $\psi_1 \approx \psi_2$ and $C_{e1} \approx C_{e2}$:

$$A_1^2 (\Delta \rho_o g H_1 - b g H_1^2/2) = A_2 (\Delta \rho_o g H_2 + b g H_2^2/2) \tag{4.35}$$

As $H_2 = H - H_1$ this results in an equation of 2. degree in H_1 , but with $\Delta \rho_o$ being dependent on H_1 .

Approximate calculations with $A_1 = A_2$ and $A_1 = 2A_2$, respectively, result in the neutral axis position shown on figure 4.7 in dependence of the ratio $\Delta T_1/\Delta T_2$. For ΔT_1 moving towards zero (or $\Delta T_2/\Delta T_1$ moving towards infinity) you find $H_1/H = 0.71$ and 0.45 for $A_1/A_2 = 1/1$ and $2/1$, respectively. The

temperature stratification results in a bigger pressure difference at the outlet and a smaller one at the inlet, and this means again that the neutral axis moves above the position valid for constant indoor temperature.

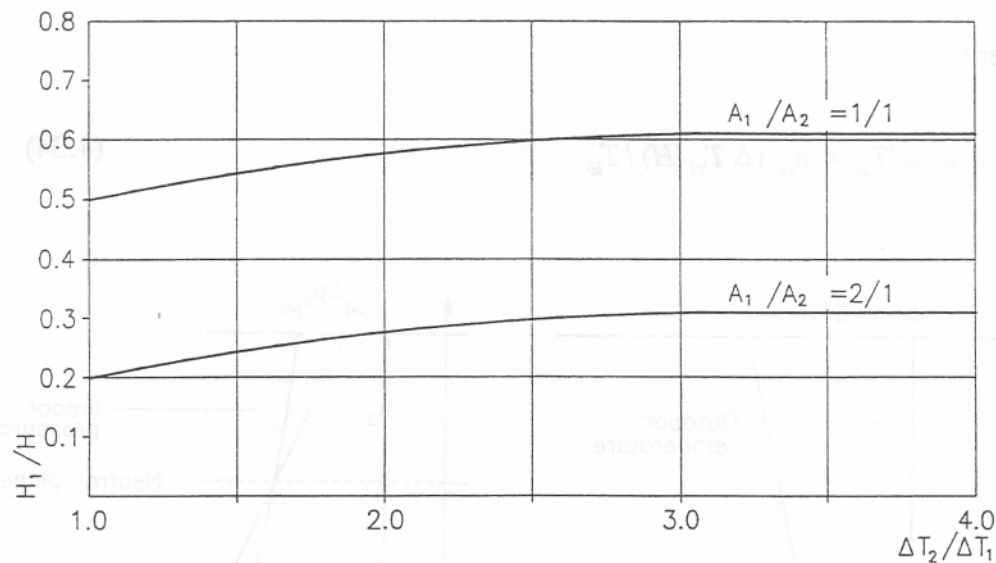


Figure 4.7 The relationship between the distance H_1 and the temperature difference rate $\Delta T_2/\Delta T_1$ when $A_1/A_2 = 1/1$ and $2/1$, respectively.

Likewise by approximative calculations it can be shown, that the ventilation capacity can be calculated with an error less than 5% when using the eq. (4.20) with an indoor temperature (mean temperature) determined by:

$$T_i = T_o + (\Delta T_1 + \Delta T_2)/2 \quad (4.36)$$

The reason for the good approximation is that the indoor pressure distribution is very close to a straight line even with a ratio $\Delta T_2/\Delta T_1 = 4/1$. The curved indoor pressure distribution shown on figure 4.6 is thus strongly exaggerated.

4.2.1.7 Opening Orientation. The two openings may be placed horizontally or one may be placed vertically and the other horizontally, or they may be placed more or less sloped. The determining equations will remain unchanged, so that the same will be case for the solution. The air velocities, the ventilation capacities etc. are thus independent of the orientation of the openings, unless the orientation makes changes in the coefficients for velocity and contraction.

4.2.1.8 Surplus Heat. The heat quantity Q_s in eq. (4.1) is the amount of sensible heat available for creating the temperature difference between inside and outside. This amount can under steady state conditions be determined by a heat balance equation, which includes added heat from heating system, electrical equipment, people, adjacent rooms, sunshine etc and heat losses due to infiltration and heat transmission.

Some of the heat sources are dependent on the indoor temperature, and the heat losses are usually dependent on the temperature difference between inside and outside. The surplus heat thus becomes dependent on the inside as well as the outside temperature.

4.2.1.9 Coefficients of Interest. In the equations derived above, coefficients are involved which take the friction loss into account (the velocity and the resistance coefficient) as well as the contraction of the jet (the contraction coefficient). Additionally, there is a coefficient taking both effects into account (the discharge coefficient).

The Velocity Coefficient C_v takes into account that the air velocity will not be completely constant across the contracted area due to friction along the opening edge. You get a mean velocity defined by:



where v is the velocity obtained if the whole pressure drop is converted into kinetic energy. The coefficient C_v will be about 0.97 - 0.99 for sharp-edged openings, corresponding to a friction loss of 2 - 5 %. The coefficient may be markedly lower (Massey, 1989) for sharp-edged openings where the thickness is not negligible.

The Resistance Coefficient C_r describes the friction loss as a pressure drop defined by:



By using the modified Bernoulli equation (which takes the friction into account), you find the following relationship between the velocity and the resistance coefficient (Andersen, 1995) :

$$C_v = 1 / (1 + \zeta)^{1/2} \quad (4.39)$$

or

$$\zeta = (1 / C_v)^2 - 1 \quad (4.40)$$

For $C = 0.95$, you get $\zeta = 0.11$.

In practice you may see resistance coefficient values of 1.8 - 2.8 or even higher for sharp-edged openings. These higher values include the contraction and/or the remaining kinetic energy. They may also include a vent that is partly closed, resulting in very high resistance coefficients. It is in fact artificial resistance coefficients, which are created with the purpose to simplify the calculations.

The Contraction Coefficient C_c takes the reduction of the flow cross section in the constricted area into account.

The contraction coefficient has a value between 0.5 (for a so-called Borda opening) and 1.0 (for a well-curved opening). For a sharp-edged opening, the value will be about 0.6.

The Discharge Coefficient C_d is frequently used in practice. It is defined as the ratio between the actual flow (measured) and the theoretical one, i.e.:

$$C_d = \frac{V_{actual}}{V_{theo}} = \frac{A_{cl} v_{cl}}{A_1 v_{theo}} = \frac{A_1 C_c C_v v_{theo}}{A_1 v_{theo}} = C_c C_v \quad (4.41)$$

By replacing the velocity coefficient with the resistance coefficient, you obtain, cf. eq. (4.39):

$$C_d = \frac{C_c}{(1 + \zeta)^{1/2}} = \frac{C_c}{\psi^{1/2}} \quad (4.42)$$

4.2.1.10 Calculation Considerations. The surplus heat Q_s will as mentioned before usually be dependent on the temperature conditions. Therefore, the calculation of the ventilation capacity often has to be carried out iteratively to get the heat balance equation fulfilled.

In some cases the constant contributions to the heat balance are so dominating, that it is acceptable to consider Q_s as constant. This is for

4:18

instance the case in the summer situation when determining the necessary opening areas. The heat transmission and the infiltration losses can then be considered as so small that they can be omitted, and the surplus heat will be the sum of the heat from machinery, electrical equipment, people, the sun etc..

In winter the ventilation system should be designed to remove the air pollution.

If it for instance concerns removal of moisture in order to keep a certain moisture content or relative humidity of the indoor air, the necessary ventilation capacity is determined by:

$$D = G$$

This gives a ventilation heat loss, when ρ :

$$Q_v = \rho_i c_p V \Delta T = c_p G \Delta T / (x_i - x)$$

which has to be included in the heat balance equation. The heat balance may still be positive indicating that further ventilation is needed if an increased indoor temperature can not be accepted. It may also be negative and then more heat should be added if a lower indoor temperature is not acceptable.

4.2.2 Ventilation Through Several Separate Openings

Several separate openings will not change the inside linear pressure distribution. But you must know the position of the neutral axis to be able to calculate the air velocities through the openings. This position can be determined by the mass balance equation:

$$\sum \rho_o A_{cr} v_{cr} - \sum \rho_i A_{cs} v_{cs} = 0 \quad (4.43)$$

where index r and s indicates inlets and outlets respectively and where for instance the inlet velocities can be determined by:

$$\Delta p_r / \rho_o = \Delta \rho g |y_r| = \psi_r v_{cr}^2 / 2 \quad (4.44)$$

By inserting (4.44) into (4.43), you obtain the the following equation for determining the position of the neutral axis when assuming that

$$\rho_i \approx \rho, \psi_r \approx \psi_s \text{ and } C_{cr} \approx C_{cs}: \quad (4.45)$$

$$\sum A_r |y_r|^{1/2} - \sum A_s y_s^{1/2} = 0$$

For instance for four openings as shown on figure 4.8 you get:

$$A_1 H_1^{1/2} + A_2 (H_1 - L_1)^{1/2} - A_3 (H - H_1 - L_3)^{1/2} - A_4 (H - H_1)^{1/2} = 0 \quad (4.46)$$

where the neutral pressure plane height H_1 is the only unknown quantity. The equation can be solved iteratively. A good first guess can be obtained by solving the equation only taking the highest and lowest opening into account, as they usually contribute most to the equation.

In case the neutral axis goes through one of the openings, this opening can be omitted by the next step in the iteration, as the contribution from that opening to the equation will be almost zero.

When the position of the neutral axis is determined, you can find the air velocities and the ventilation capacity. For the above mentioned case with four openings, you obtain, when assuming that the neutral axis is placed between opening no. 2 and 3 and when using eq. (4.20a) on opening no. 1 and 2:

$$V = C_{d1} A_1 \left(\frac{2 g \Delta T H_1}{T_i} \right)^{1/2} + C_{d2} A_2 \left(\frac{2 g \Delta T (H_1 - L_1)}{T_i} \right)^{1/2} \quad (4.47)$$

By introducing:

$$A_2 = n A_1, y_2 = H_1 - L_1 = m_2 H_1, \text{ and } C_{d2} = q_2 C_{d1}$$

you obtain:

$$V = C_{d1} A_1 \left(\frac{2 g \Delta T H_1}{T_i} \right)^{1/2} (1 + n^2 m_2^2 / q_2^2)^{1/2} \quad (4.48)$$

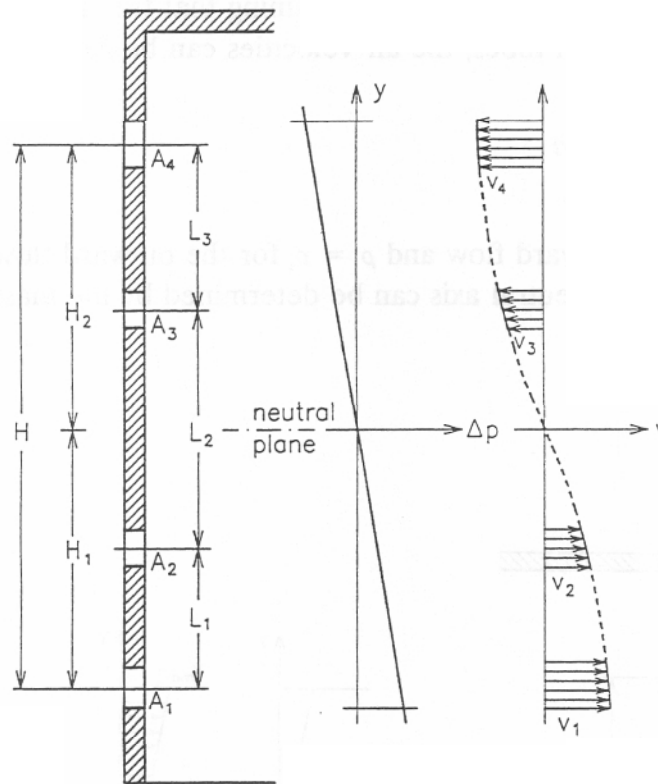


Figure 4.8 Pressure difference and air velocities by four openings

It is further possible to use the eqs. (4.18) and (4.20)-(4.22) for temperature difference, ventilation capacity, and opening areas, if only the quantity H_1 is replaced by:

$$H_1^* = H_1 (1 + n_2^2 m_2/q_2) \quad (4.49)$$

More generally, i.e. for more than four openings, the same equations can be used by replacing H_1 with:

$$H_1^* = H_1 (1 + n_2^2 m_2/q_2 + n_3^2 m_3/q_3 + \dots) \quad (2.50)$$

where only openings with inward flow are included, and where H_1 is the distance between the neutral plane and the centre of the lowest opening.

4.2.3 Ventilation Through One Rectangular, Vertical Opening

For a large vertical opening as shown on figure 4.9, an aerostatic pressure will exist outdoors as well as indoors, and under steady state conditions, the inside and outside pressure distribution will cross each other somewhere in

the opening. This gives an inward air flow in the lower part of the opening and an outward flow in the upper part. Assuming that the flow takes place in thin, horizontal stream tubes, the air velocities can be determined by:

$$V = (2 \Delta \rho g |y| / (\rho \psi))^{1/2} \quad (4.51)$$

where $\rho = \rho_o$ for the inward flow and $\rho = \rho_i$ for the outward flow.

The position of the neutral axis can be determined by the mass balance equation, and you find:

$$h_1/h_2 = (T_o/T_i)^{1/3} \quad (4.52)$$

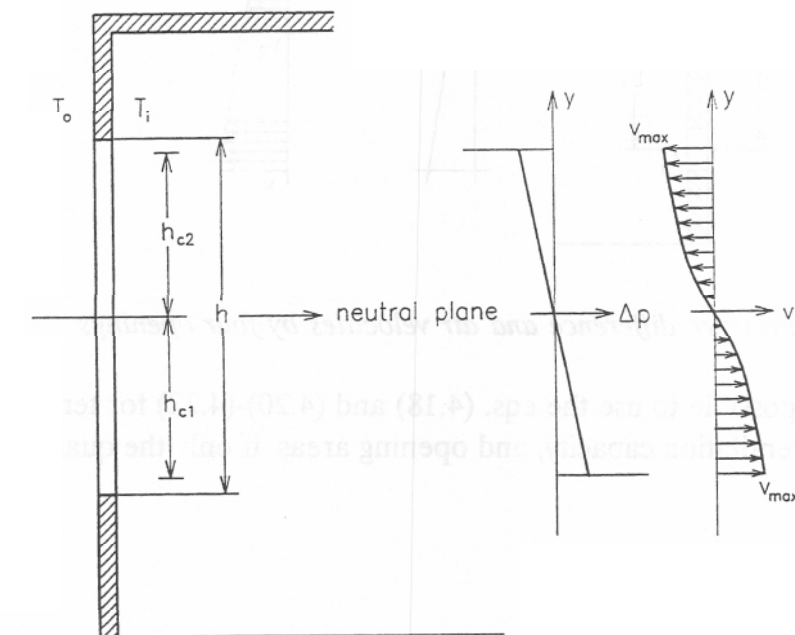


Figure 4.9 Distribution of pressure difference and air velocity by one vertical opening

As $T_o > T_i$ the position of the neutral axis will be close to the middle of the opening, and you obtain the following maximum velocities at the lower and upper edges of the opening:

$$v_{\max} = \left[\frac{2 g \Delta T h_c / 2}{T_i \psi} \right]^{1/2} = \left[\frac{g \Delta T h_c}{T_i \psi} \right]^{1/2} \quad (4.53)$$

The velocity distribution being parabolic, the ventilation capacity becomes:

$$V = \frac{2}{3} b_c (h_c/2) v_{\max} = \frac{1}{3} A_c v_{\max} \quad (4.54)$$

By using the energy equation (4.1) you get:

$$\Delta T = \frac{Q_s}{\rho_o c_p V} = \frac{3 Q_s}{\rho_o c_p v_{\max} A_c} \quad (4.55)$$

which can be used to eliminate ΔT in eq. (4.53). Together with eq. (4.14a) and by inserting the values of the constants you get successively:

$$v_{\max} = \left[\frac{3 Q_s g R h_c}{c_p p_o C_d A} \right]^{1/3} \left[\frac{T_o}{T_i} \right]^{1/3} \left[\frac{1}{\psi} \right]^{1/2} = 0,043 \left[\frac{Q_s h_c}{C_d A} \right]^{1/3} \left[\frac{1}{\psi} \right]^{1/2} \quad (4.56)$$

$$\begin{aligned} \Delta T &= \left[\frac{3 Q_s R}{c_p p_o C_d A} \right]^{2/3} \left[\frac{1}{g h_c} \right]^{1/3} \left[\frac{T_o}{T_i} \right]^{1/3} T_o \\ &= 2.0 \cdot 10^{-4} T_o \left[\frac{Q_s}{C_d A} \right]^{2/3} \left[\frac{1}{h_c} \right]^{1/3} \end{aligned} \quad (4.57)$$

$$V = \frac{1}{3} A_c \cdot 0.043 \left[\frac{Q_s h_c}{C_d A} \right]^{1/3} \left[\frac{1}{\psi} \right]^{1/2} = 0.014 (C_d A)^{2/3} (Q_s h_c)^{1/3} \quad (4.58)$$

The requirement to the opening dimensions to get a certain ventilation capacity or a certain temperature difference can then be determined by, when assuming $h_c \approx 0.8$ h:

$$b^{2/3} h = 79.4 V / (Q_s^{1/3} C_d^{2/3}) \quad (4.59)$$

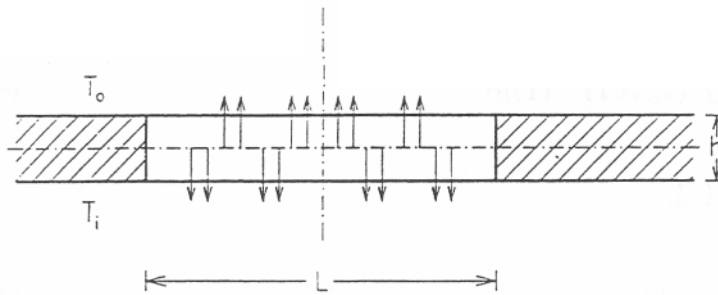


Figure 4.10 Air flow through one horizontal opening

By using the energy equation (4.1) these expressions can be turned into:

$$\begin{aligned}
 V &= (0.18 A)^{2/3} \left[\frac{Q_s g h}{c_p \rho_o T_i} \right]^{1/3} = (0.18 A)^{2/3} \left[\frac{Q_s R g h}{c_p P_o} \right]^{1/3} \left[\frac{T_i}{T_o} \right]^{1/3} \\
 &= 0.0098 A^{2/3} (Q_s h)^{1/3} \quad \text{for } 0,1 < h/A^{1/2} < 0,7 \quad (4.65)
 \end{aligned}$$

$$\begin{aligned}
 V &= (0.06 A)^{2/3} \left[\frac{Q_s g A^{1/2}}{c_p \rho_o T_i} \right]^{1/3} = (0.06 A)^{2/3} \left[\frac{Q_s R g A^{1/2}}{c_p P_o} \right]^{1/3} \left[\frac{T_i}{T_o} \right]^{1/3} \\
 &= 0.0047 A^{5/6} Q_s^{1/3} \quad \text{for } h/A^{1/2} < 0,1 \quad (4.66)
 \end{aligned}$$

By combining (4.63) with (4.65) and (4.64) with (4.66) you get:

$$\Delta T = 3.0 \cdot 10^{-4} (Q_s/A)^{2/3} T_i (1/h)^{1/3} \quad \text{for } 0,1 < h/A^{1/2} < 0,7 \quad (4.67)$$

$$\Delta T = 6.2 \cdot 10^{-4} Q_s^{2/3} T_i (1/A)^{5/6} \quad \text{for } h/A^{1/2} < 0,1 \quad (4.68)$$

From eqs. (4.65) - (4.68) it is finally possible to determine the required opening area as to get a certain ventilation capacity or temperature difference, respectively, and you get for $0,1 < h/A^{1/2} < 0,7$:

$$\Delta p = \psi \rho v_c^2 / 2$$

or

$$v_c = ((f_o - f_i) / \psi)^{1/2} v_w \quad (4.76)$$

4.3.1 Wind Velocities and Pressure Coefficients

The wind velocity depends on the height above terrain and the terrain type, and it can be expressed by, cf. figure 4.11:

$$v_w = K v_{10} \ln(h/h_o) \quad (4.77)$$

where h_o is the roughness factor indicating the height above terrain where the wind velocity still can be considered to be zero. The constant K is dependent on x_w , because $K \ln(10/h_o) = 1.0$.

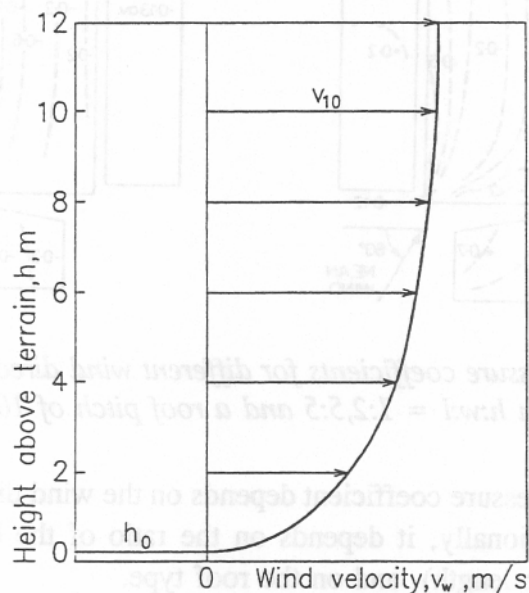
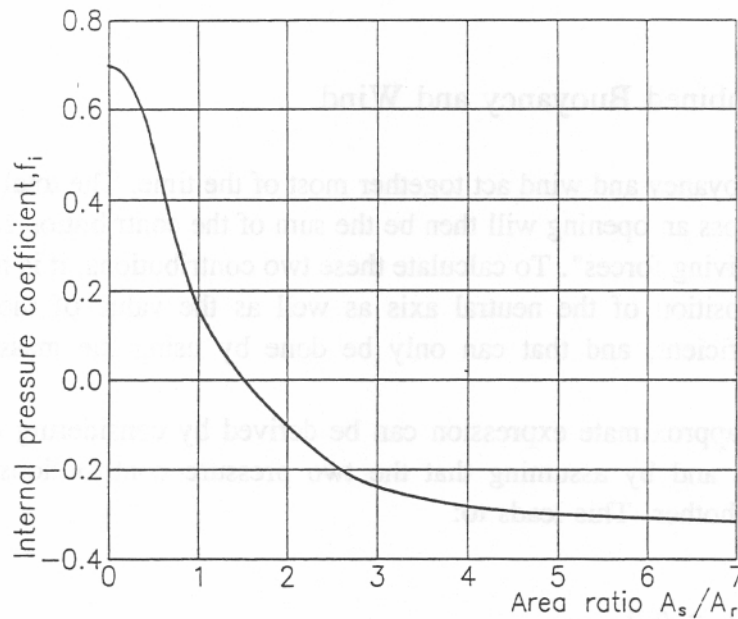


Figure 4.11 Wind speed in dependence of the height above terrain.

or by using eq. (4.76) and assuming that $\rho_i \approx \rho_o$:

$$\sum ((f_{or} - f_i)/\psi_r)^{1/2} A_{cr} = \sum ((f_i - f_{os})/\psi_s)^{1/2} A_{cs} \quad (4.79)$$

On figure 4.13 are shown calculated values for the internal pressure coefficient in dependence of the area ratio A_s/A_r and when assuming an external pressure coefficient of 0.75 on windward side and of -0.35 on leeward side of the building.



4.13 The internal pressure coefficient as function of the ratio between the outlet and the inlet area, A_s/A_r

4.3.2 Ventilation Capacity

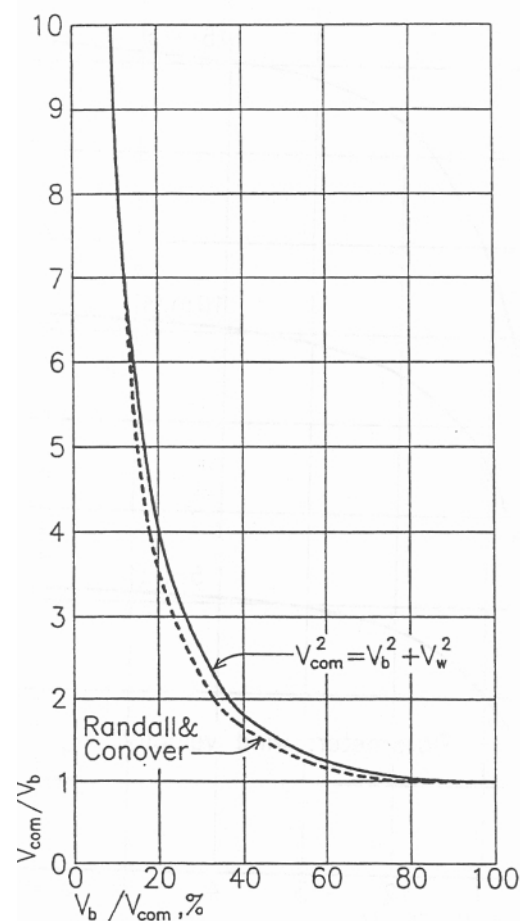
The ventilation capacity can be found as:

$$\begin{aligned} V &= \sum A_{cr} v_r = \sum A_{cr} ((f_{or} - f_i)/\psi_r)^{1/2} v_w \\ &= \sum C_{dr} A_r (f_{or} - f_i)^{1/2} v_w \end{aligned} \quad (4.80)$$

Because the wind ventilation capacity is independent of the temperature, it may

The expression is valid with good accuracy when either the buoyancy or the wind is dominating, and this will always be the case in an atrium design situation.

On figure 4.14 is shown the comparison between eq. (4.83) and the mean value of the calculation results found by Randall and Conover (1931) on several buildings under different conditions. Taking all their results into consideration you find, that the error by using the eq. (4.83) is biggest, reaching about 20-25%, when the two contributions are almost equal. From a design point of view, this is in fact not critical, as the error can be adjusted by the control system.



4.14 Comparison of eq. (4.83) with the mean curve for the calculations done by Randall and Conover (1931).

4.3.4 Control Possibilities

The internal pressure coefficient is strongly dependent on the distribution of the opening areas on the windward and leeward side of the building. If the openings are placed mainly on the windward side the internal pressure coefficient will

the leeward gable and an outward flow through the openings near the windward gable. This may create draft problems if the control system is not able to cope with this situation. A possibility is to make the openings controllable section-wise along the building.

4.4 Infiltration

Air infiltration is the uncontrolled air exchange through cracks and other leakages in the building envelope. The air flow is caused by the pressure differences between inside and outside created by the temperature differences (i.e. thermal buoyancy) and by the wind.

4.4.1 Theoretical Considerations

The flow through the cracks may be laminar or turbulent depending on the crack width and the air velocity. By narrow cracks or low air velocity (by small pressure differences) the flow is laminar and the air flow through the cracks can be determined by the Poiseuille law:

$$V_{crack,l} = \alpha_{lam} \Delta p \quad (4.83)$$

where α_{lam} is a flow coefficient which includes the crack dimensions and the viscosity of the air. For wider cracks or higher velocities, the flow will be turbulent and you have:

$$V_{crack,t} = \alpha_{tur} \Delta p^{1/2} \quad (4.84)$$

The total air flow through the cracks will depend on the pressure differences as well as the distribution of the cracks on the building envelope. It is not possible to know the crack dimensions and their distribution beforehand and therefore the infiltration is frequently expressed by:

$$V_{infil} = \alpha_{tur} \Delta p^{\beta} \quad (4.85)$$

where the exponent β has a value of 0.5 or 1.0. Measurements indicates that β has a value of 0.6-0.75 for a long range of Δp (Blomsterberg 1990) or $13 \sim 2/3$. In practice it is usual to measure the tightness of a building by a certain pressure difference Δp_{ref} . By any other pressure difference, you then have

Table 4.1 Airtightness measured in atria at an overpressure of 50 Pa.
(Wall and Blomsterberg, 1994)

Building	Completed, year	ach by 50 Pa	Surrounding build- ings
Kabi Pharmacia	1991	1.1	Offices
Scandinavian Center	1991	0.8	Offices/shops
Siriushuset	1992	1.0	Offices
Oncological Clinic	1992	0.7	Wards, hos-pital
Piggvaren	1986	14	Residential ¹
Tärnan	1983	8.8	Residential ²

(Blomsterberg, 1993)

² (Wall, 1992)

4.5 Use of formula. Implementation

The set of formulas can be used in the following ways:

- Directly in the design of the natural ventilation system and for analysis purposes for instance in connections with the design of the control system.
- Implemented into computer programs for thermal simulation of buildings.
- Determination of certain starting values for calculations with CFD-programs (Computational Fluid Dynamics).

It is first of all the formulas for thermal buoyancy which are of interest as the extreme design situations occur by calm weather. A survey of formulas to be used under such conditions are shown in table 4.2 based either on the density difference, on the temperature difference or on the net heat input.

The wind can be coupled through formulas (4.82) and (4.83). The wind will act as a supplement to the thermal buoyancy driven ventilation. The combination of thermal buoyancy and wind ventilation will influence the design of the control system.

4.5.1 Direct Use

The design situation, where the required maximum opening areas are to be determined, occurs in calm summer weather. Then the sufficient ventilation

capacity has to be obtained by thermal buoyancy alone. If a required temperature difference not to be exceeded is known, the net heat input can be determined by the heat balance equation and then the required opening areas can be found by eq.(4.22). If you know the air exchange to be obtained, eq. (4.21) can be used.

A minimum ventilation is required in winter when a certain amount of air pollution or moisture has to be removed. This removal requires a certain minimum ventilation capacity. Besides, a certain indoor temperature has to be obtained and then the net heat input can be determined. Finally, the minimum opening areas can be determined by eq. (4.21) and these areas are of interest in connection with the design of the control system.

The formulas in table 4.2 are also suitable for analysis purposes, for instance the air velocities in the openings in connection with comfort considerations under various conditions, or the opening areas in connection with designing the control system.

4.5.2 Implementation in Thermal Simulation Programs

The thermal simulation programs developed to date attach the greatest importance on the indoor climate during winter and on the energy consumption in that connection. The exchange of fresh air is therefore dealt with in a very simple manner, as it can be seen in the description in chapter 9 of some existing used simulation programs, and that is usually sufficient under winter conditions.

In summer natural ventilation is a cooling measure and a high ventilation capacity may be needed. The ventilation capacity varies strongly with opening geometry, opening position and with heat load, and no model for this variation is found as an integrated part of any simulation program. Some programs (like FRES and TRNSYS, see chapter 9) use precalculated data which are introduced into the program as a variable. Other programs (like tsbi3, see chapter 9) use a simple formula for the air change rate per hour depending on temperature difference and wind velocity and including 2-3 constants to be assumed by the program user. But the user or the designer gets no help for determining the necessary opening areas.

The formula (4.22) would be very useful as a subroutine in the simulation programs for determination of the needed opening areas. If the temperature difference ΔT not to be exceeded is known, then also the indoor temperature $T_i = T_o + \Delta T$ will be known, and the net heat input can be taken from the heat balance in the program. The subroutine can step by step follow the calculations and will give the needed opening areas stepwise, so that the maximum value can be determined. If, for instance, a certain maximum opening area should not be exceeded from a structural or another point of view the consequences can be determined by the simulation program.

4.6 Summary

Natural ventilation can be used as a mean to cool atria and the adjacent building. Both buoyancy and wind cause natural ventilation effects. This chapter provide formulas to study natural ventilation by buoyancy and wind separate and together. It also gives data on infiltration in existing and new atria.

Thermal buoyancy can be calculated for two separate, a single vertical, and a single horizontal opening, respectively. For two separate openings, neutral axis and air velocities and ventilation capacity as a function of opening area can be studied. Required and optimum opening area can be calculated. The influence of thermal stratification on natural ventilation is also shown. Resistance and contraction values for the openings are suggested.

Calculation of natural ventilation can be performed by hand or as a part of a simulation in a CFD-program (Computational Fluid Dynamics) or a building energy simulation program.

Suffices

- b = buoyancy
- c = contracted
- d = discharge
= indoor
- o = outdoor
- io = indoor value at neutral plane level
- w = wind
- 1 = inlet (by two openings)
- 2 = outlet (by two openings)
- r = inlet (by several openings)
- s = outlet (by several openings)

5. Surface Heat Transfer Coefficients

5.1 Introduction

Heat is transferred between a building surface and its surroundings by radiation and convection. These two modes of heat transfer act independently of each other, and by the temperatures relevant in connection with building surfaces, the heat transfer per unit surface area can be expressed by:

$$Q/A_s = h_r (T_s - T_{a1}) + h_c (T_s - T_{a2}) \quad (5.1a)$$

or, if $T_{a1} = T_{a2} = T_a$:

$$Q/A_s = (h_r + h_c) (T_s - T_a) = h(T_s - T_a) \quad (5.1b)$$

where:

h is the surface heat transfer coefficient

h_r is the radiation heat transfer coefficient

h_c is the convection heat transfer coefficient

A_s is the area of the surface in question

T_s is the temperature of the surface

T_{a1} , T_{a2} , T_a are reference temperatures for the surroundings.

The surface heat transfer coefficient is dependent on temperatures as well as on air velocities close to the surface. For normal insulated building surfaces

$$\Delta Q_r / Q_r = ((\Delta T_{12} / 2) / T_m)^2 \quad (5.5)$$

so that the error is less than 1% if ΔT_{12} is smaller than 50 K.

Figure 5.1 shows the correct value of the factor $hr/\sigma\epsilon_{12}$ (sometimes called the temperature factor and equal to $(T_1^4 - T_2^4)/(T_1 - T_2)$) as a function of the mean temperature (or the temperature level) and with the temperature difference as a parameter. It can be seen that even for reasonable big temperature ranges the factor is almost independent of Δt . Besides, it is almost linear, and this linearity can be found by expanding T in the following way:

$$T_m^3 = (T_o + T_m - T_o)^3 = T_o^3(1 + (T_m - T_o)/T_o)^3 \sim T_o^3(1 + 3(T_m - T_o)/T_o)$$

where T_o is a fixed temperature in the middle of the linearity range. The coefficient h_r can thus in a certain range be expressed by:

$$h_r \sim 4\epsilon_{12}\sigma T_o^3 (1 + 3(T_m - T_o)/T_o) \quad (5.6)$$

The radiant heat exchange between building surfaces and their surroundings can often be considered as taking place between the surfaces in a so-called enclosure, where one of the surfaces is plane or convex (i.e. it can not "see" any parts of itself) and is totally surrounded by the other surface as shown on Figure 5.2. In this case the effective emissivity can be determined by (Wong, 1977):

$$1/\epsilon_{12} = 1/\epsilon_1 + (A_1/A_2)((1/\epsilon_2) - 1) \quad (5.7)$$

Some relevant emissivity values are shown in Table 5.1. It can be seen that the emissivities of building surfaces usually have a value of 0.9-0.95, unless they are painted or clad with something bright metallic.

5.2.1 Interior Radiation

Inside the building, the radiant heat exchange takes place between the outer and the inner walls. Unless one of the inner walls is heated for instance by the sun, it can be assumed that the surface temperature of all inner walls is equal to the inside air temperature. You then get following expression for the heat exchange:

$$Q_{\dot{n}} = h_{\dot{n}}(T_i - T_s)A_1 \quad (5.8)$$

where A_1 is the area of the outer wall surface, T_i is the inside air temperature, and T_s is the outer wall surface temperature.

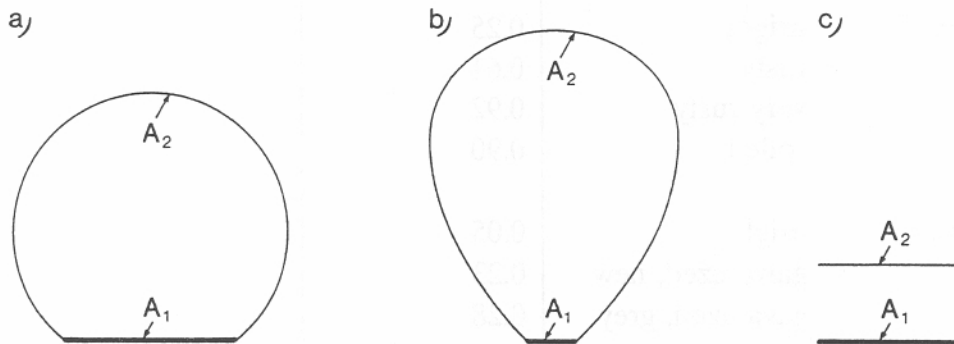


Figure 5.2 Positions of two radiant surfaces.

If the room has only one outer wall, its surface is part of an enclosure for which the effective emissivity can be found from eq. (5.7). For $\epsilon_2 \sim \epsilon_1$ you get:

$$\epsilon_{12} = \epsilon_1 / (1 + (A_1/A_2)(1 - \epsilon_1)) \quad (5.9)$$

Further, with only one outer wall you have that $A_1/A_2 < 1/5$ and you get:

$$\epsilon_{12} \sim \epsilon_1 \quad (5.10)$$

with an error less than 2%, and $h_{\dot{n}}$ can then be determined as:

$$h_{\dot{n}} = 4 \epsilon_1 \sigma T_m^3 \quad (5.11)$$

Under normal conditions, T_m will have a value of 283 K - 303 K. In this range and for $T_o = 293$ K, you get from eq. (5.6):

$$\begin{aligned} h_{\dot{n}} &= 4 \cdot \epsilon_1 \cdot 5.67 \cdot 10^{-8} \cdot 293^3 (1 + 3(T_m - 293)/293) \\ &= 5.7 \cdot \epsilon_1 (1 + 0,010(T_m - 293)) \end{aligned} \quad (5.12)$$

It can further be seen, that a constant value:

$$h_{r,i} = 5.7 \cdot \epsilon_i \quad (5.13)$$

can be used in the range 288 K - 298 K with an error less than 5-7%, and in the range 283 K - 303 K with an error less than 10-12%.

If one of the inner walls is heated by the sun, equation (5.8) can be used, but now with A_1 as the area of the heated surface, and T_i as the temperature of the remaining surfaces (including the outer wall surface) and assumed to be equal to the inside air temperature. Besides, the radiation heat transfer coefficient can be considered as constant similar to eq.(5.13), but with an about 15% higher value due to the higher temperature level, cf. figure 5.1.

For two outer wall surfaces forming an angle you have to distinguish between if the angle is convex or concave seen from the inside. By a convex angle, eq. (5.8) can be used with A_1 as the total area of the two surfaces and with h_r as a constant value similar to eq.(5.13) but adjusted to the temperature level. If the two outer surfaces form a concave angle each of the outer surfaces has to be treated separately with its own view factor, which can be found in a relevant textbook.

5.2.2 Exterior Radiation

The exterior heat exchange takes place between the exterior building surfaces and the sky, the ground, and the surrounding buildings and vegetation. The heat exchange can be expressed by:

$$Q_{ro} = h_{ro} (T_s - T_{eq}) A_s \quad (5.14a)$$

where h_{ro} is the exterior radiation heat transfer coefficient, T_s is the temperature of the exterior surface in question with the surface area A_s , and finally T_{eq} is an equivalent temperature representing the surroundings.

5.2.2.1 Sky Temperature. When calculating the radiant heat exchange with the sky, a so-called sky temperature is often introduced in order to simplify the calculations. From a thermal radiation point of view, the sky is then considered as a hemispherical, black surface with a temperature T_{sky} , which gives a radiation equal to the actual measured radiation T_{sky} , i.e.:

content of the air and thereby the dew point temperature is almost constant during 24 hours.

The sky temperature can be found by inserting the expressions for ρ_{sk} into eq. (5.14d). This is done for the equations (5.14e) - (5.14g) in the outdoor air temperature range -20°C to 10°C with a relative humidity of 90%. The resulting sky temperatures are shown on figure 5.3 together with some sky temperatures based on sky emissivities found by other authors.

The measurements behind the sky temperatures on figure 5.3 are carried out on the country side far from towns except for Brown (1956) and Berdahl and Fromberg (1982). The figure shows higher sky temperatures for areas close to towns than on the country side. This is understandable from the point of view, that increasing air pollution increases the sky emissivity. It indicates that it might be reasonable to distinguish between country side, and town areas, when it concerns sky temperatures. For the country side you get the following linear approximate relationship between sky temperature and outdoor air temperature with the last mentioned being in the range -20°C to 10°C :

$$t_{sky} = -24 + 1,2 t_o \quad (5.15a)$$

or

$$T_{sky} - 273 = -24 + 1,2 (T_o - 273) \quad (5.15b)$$

or

$$T_{sky} = -79 + 1,2 T_o \quad (5.15c)$$

For town areas, figure 5.3 indicates the following relationship:

$$t_{sky} = -14 + 1,2 t_o \quad (5.16a)$$

or

$$T_{sky} = -69 + 1,2 T_o \quad (5.16b)$$

For totally cloudy skies the equivalent radiant temperature becomes much closer to the ambient temperature as shown on Figure 5.4. In this case you get the following approximate expression:

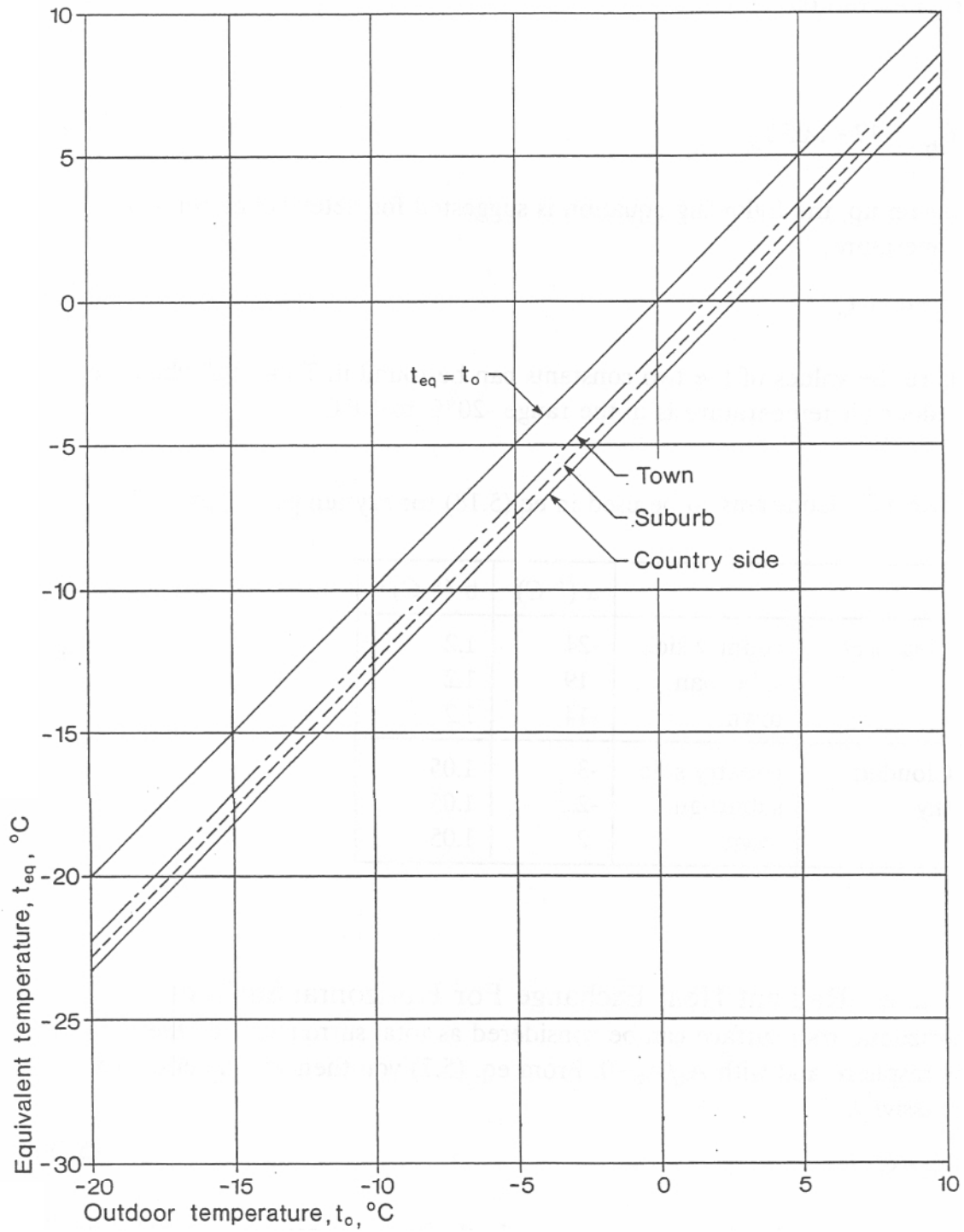


Figure 5.4 Sky temperatures in nights with clouded sky.

K to 243 K with a medium value of 253 K. This results in the following linear expression for the outside radiation heat transfer coefficient with an error less than 1%:

$$h_{ro} = 4\epsilon_1 \cdot 5.67 \cdot 10^{-8} \cdot 253^3 (1 + 3(T_m - 253)/253) = 3.7\epsilon_1 (1 + 0,012(T_m - 253)) \quad (5.20)$$

A constant value of:

$$h_{ro} = 3.7\epsilon_1 \quad (5.21)$$

can be used in the range $248 \text{ K} < T_m < 258 \text{ K}$ with an error less than 9-10% and in the range $261 \text{ K} < T_m < 271 \text{ K}$ with an error less than 14-15%.

With clouded sky and an assumed outdoor temperature range of zero to -10 °C, the sky temperature will be -3 °C to -13 °C and the mean temperature will have a medium value of about 267 K. This gives the following linear expression for h_{ro} valid for $261 \text{ K} < T_m < 271 \text{ K}$:

$$h_{ro} = 4.3\epsilon_1 (1 + 0,011(T_m - 267)) \quad (5.22)$$

For the same temperature range the constant value

$$h_{ro} = 4.3\epsilon_1 \quad (5.23)$$

can be used with an error less than 10%.

5.2.2.3 Radiant Heat Exchange For Vertical Surfaces. A vertical surface can be considered as a part of an enclosure together with a half sky hemisphere and the ground. Assuming a view factor of 0.5 for the sky as well as for the ground you can derive a equivalent radiant temperature $T_{r,eq}$ for the surroundings determined by:

$$T_{r,eq} \sim (T_{sky} + T_g)/2 \quad (5.24a)$$

where T_g is the ground temperature. Assuming the ground temperature to be close to the outdoor temperature, eq. (5.24a) gives results close to what was found by Brown (1956) and which is shown on figure 5.5.

For an outdoor temperature in the range of zero to -20 °C, the equivalent radiant temperature will approximately be in the range of -10 °C to -30 °C. Then t_m will be in the range of -5 to -5 °C with a medium value of -5 °C. This gives the following linear expression for h_{ro} :

A constant value of

$$h_{ro} = 3.9 \epsilon_1 (1 + 0.012(T_m - 259)) \quad (5.25)$$

A constant value of

$$h_{ro} = 3.9 \epsilon_1 \quad (5.26)$$

can be used with an error less than 10%.

With clouded sky the values of h_{ro} given by eqs. (5.22) and (5.23) can be used.

5.2.2.4 Radiant Heat Exchange For Sloping Surfaces. For sloping roof surfaces the radiant heat exchange decreases. Petersen (1966) suggest the following reduction factor:

$$f_{red} = (1 + \cos \alpha)/2 \quad (5.27)$$

where α is the angle between the surface and the horizontal. The radiation contribution from the ground can be neglected as the ground temperature will be close to the exterior surface temperature.

By 20 degree roof slope, you then get $f_{red} = 0.98$ and by 45 degrees you get $f_{red} = 0.85$. The reduction is thus of minor importance for roofs.

5.3 Convective Heat Transfer Coefficients

By convective heat transfer, the heat energy is transported from one place to another by a moving fluid. In the case discussed here, the moving fluid is air.

The air movement may be induced by buoyancy forces which arise from density differences, which again are caused by temperature differences in the air. This is called free (or natural or buoyant) convection. The air movement may also be caused by external means like fans or atmospheric wind, and this is called forced convection.

The heat transfer from the surface to the moving air takes place in the so-called boundary layer, which is the thin layer closest to the surface, where changes in air velocities and in temperature differences take place.

At the beginning of the surface (by the so-called leading edge), the flow will be laminar, i.e. the flow particles move in layers parallel to the surface, and if

k is the conductivity of the air

ν is the kinematic viscosity of the air

The quantities representing the air properties, i.e. c_p , k , and ν , should principally be evaluated by the average temperature of the moving air. For building surfaces, where the temperature difference will not be larger than 20-30°C, it is sufficiently accurate to evaluate the air properties at the temperature of either the surface or the undisturbed air.

It should be noticed, that the Pr number is a pure fluid property constant. For air with a temperature in the range of -20 °C to 50 °C the magnitude of Pr is 0.70 - 0.72. Therefore a value of $Pr = 0.71$ will be used in the following.

The equation (5.27) contains some constants and they are found by correlating the equation to experimental data.

An equation similar to eq.(5.28) can be derived for the local Nusselt number and the only difference is that the characteristic length has to be replaced by the distance x from the leading edge to the point in question. There is a definite relationship between the local and the average Nusselt number, which can be found by integrating the local heat transfer coefficient along the whole surface.

5.3.1 Free Convection

By free convection, the flow velocity is determined by the temperature difference so that the Reynold number is not an independent parameter in this case. When using eq.(5.28) for free convection, the Reynold will disappear and you get for the average Nusselt number:

$$Nu_{av} = f(Gr_L, Pr) \quad (5.29)$$

The flow will always be laminar in the beginning, but a transition to turbulent flow may take place. It takes place if instabilities in the flow are not damped sufficiently, and this depends on the ratio between the buoyant and the viscous forces in the flow, which again can be expressed by the product of the Grashof and the Prandtl number. The transition value of this product depends on the direction of the surface as well as of the heat flux compared to the direction of the gravity.

It should be mentioned that the air velocities by free convection on building surfaces will not be much higher than 1 m/s, and that a convection heat transfer coefficient much larger than 4 W/m²K should not be expected. By

For large values of $Gr_L Pr$, for instance a value of 10^{11} , the laminar region can be neglected, and the following equations can be used with an error smaller than 5%:

$$Nu_{av} = 0.13(Gr_L Pr)^{1/3} \quad (5.35)$$

and

$$h_c = 1.5(\Delta T)^{1/3} \quad (5.36)$$

For the local values you get:

$$Nu_x = 0.13(Gr_x Pr)^{1/3} \quad (5.37)$$

and

$$h_{cx} = 1.5(\Delta T)^{1/3} \quad (5.38)$$

A survey of the equations for vertical surfaces is given in table 5.3.

5.3.1.2 Inclined Surfaces. By inclined surfaces the direction of the heat flux has to be taken into account as it influences significantly the magnitude of the heat transfer coefficient. In that connection it is convenient to consider the components of the buoyancy forces normal and parallel to the surface. If the normal component has direction towards the surface it will maintain the boundary layer. If having a direction away from the surface, separation of the boundary layer from the surface will occur, where parcels of air moving away from the surface continuously will be replaced by ambient air, which again results in an increased heat transfer.

The component parallel to the surface is in any case reduced with a factor $\cos\Theta$ compared to its value by vertical surfaces, and where Θ is the angle between the surface direction and the vertical. This gives a similar reduction in the boundary layer velocities and thereby in the convection heat transfer coefficient, as long as the boundary layer follows the surface.

By a heated bottom surface or a cooled top surface, in practice corresponding to a heated ceiling or a supercooled roof, the normal component of the buoyancy force acts towards the surface, and the surface guides the air movements in the boundary layer so that you mainly will have laminar flow. Experimental data confirm, that the equations used for the

Table 5.4 Natural convection on inclined surfaces, isothermal or uniformly heated (Churchill, 1990a, Kreith and Bohn, 1993).

	Laminar regime 1)	Turbulent regime 2)
COLD TOP SURFACE, WARM BOTTOM SURFACE 3)		
Nusselt no:		
Local	$Nu_x = 0.44 (Gr \cos \theta Pr)^{1/4}$	No fully developed turbulence
Average	$Nu_{av} = 0.59 (Gr_L \cos \theta Pr)^{1/4}$	has been measured
Heat transfer coefficient:		
Local	$h_{\alpha} = 1.1 (\Delta T \cos \theta / x)^{1/4}$	
Average	$h_{car} = 1.5 (\Delta T \cos \theta / L)^{1/4}$	
WARM TOP SURFACE COLD BOTTOM SURFACE 4)		
Nusselt no:		
Local	$Nu_x = 0.44 (Gr_x \cos \theta Pr)^{1/4}$	$Nu_x = 0.13 (Gr \cos \theta Pr)^{1/3}$ for $\theta < 45^\circ$ $Nu_x = 0.13 (Gr \sin \theta Pr)^{1/3}$ for $\theta > 45^\circ$
Average	$Nu_{av} = 0.59 (Gr_L \cos \theta Pr)^{1/4}$	$Nu_{av} = 0.13 (Gr_L \cos \theta Pr)^{1/3} - 25.0 \cos \theta$ for $\theta < 45^\circ$ $Nu_{av} = 0.13 (Gr_L \sin \theta Pr)^{1/3} - 130 \sin \theta + 105 \cos \theta$ for $\theta > 45^\circ$
Heat transfer coefficient:		
Local	$h_{\alpha} = 1.1 (\Delta T \cos \theta / x)^{1/4}$	$h_{\alpha} = 1.5 \Delta T \cos \theta$ for $\theta < 45^\circ$ $h_{\alpha} = 1.5 \Delta T \sin \theta$ for $\theta > 45^\circ$
Average	$h_{cav} = 1.5 (\Delta T \cos \theta / L)^{1/4}$	$h_{\alpha} = 1.5 \Delta T \cos \theta - 0.6 \cos \theta / L$ for $\theta < 45^\circ$ $h_{\alpha} = 1.5 \Delta T \cos \theta - 3.1 \cos \theta / L + 2.5 \sin \theta / L$ for $\theta > 45^\circ$

1) θ = angle between surface and vertical

3) e.g. cold floor or warm ceiling

5) Transition takes place for $Gr \cos \theta Pr \sim 10^5 e^{9 \cos \theta}$

2) Valid for $\theta < 87^\circ$

4) e.g. warm floor or cold ceiling

indicates that a laminar as well as a turbulent regime has to be considered. A survey of equations of interest is shown in table 5.5.

Table 5.5 Natural convection for horizontal surfaces, isothermal or uniformly heated. (Incropera and De Witt, 1990, Churchill, 1990a).

	Laminar regime 2)	Transition	Turbulent regime
		$Gr_x Pr$	
COLD TOP SURFACE, WARM BOTTOM SURFACE 1) Nusselt no: Local Average Heat transfer coefficient: Local Average	$Nu_x = 0.29 (Gr_x Pr)^{1/5}$ $Nu_{av} = 0.49 (Gr_L Pr)^{1/5}$ $h_{cx} = 0.29 (\Delta T/x^2)^{1/5}$ $h_{cav} = 0.49 (\Delta T/L^2)^{1/5}$	10^{10}	No fully developed turbulence has been measured
WARM TOP SURFACE, COLD BOTTOM SURFACE 3) Nusselt no: Local Average Heat transfer coefficient: Local Average	$Nu_x = 0.41 (Gr_x Pr)^{1/5}$ $Nu_{av} = 0.70 (Gr_L Pr)^{1/5}$ $h_{cx} = 0.41 (\Delta T/x^2)^{1/5}$ $h_{cav} = 0.70 (\Delta T/L^2)^{1/5}$	10^5	$Nu_x = 0.12 (Gr_x Pr)^{1/3}$ $Nu_{av} = 0.12 (Gr_L Pr)^{1/3}$ $h_{cx} = 1.5 \Delta T^{1/3}$ $h_{cav} = 1.5 \Delta T^{1/3}$

- 1) Finite surface with escape possibilities at the edges, e.g. supercooled roof
- 2) $L = \text{area/perimeter}$
- 3) e.g. warm roof, heated floor, or cooled ceiling

Table 5.6 Forced convection on flat surface parallel to the flow.
 (Incropera and De Witt, 1990, Mills, 1992, Wong 1977).

	Laminar regime	Transition	Turbulent regime
		Re_x	
ISOTHERMAL		$2 \cdot 10^5 - 5 \cdot 10^5$	
Nusselt no:			
Local	$Nu_x = 0.33 Re_x^{1/2} Pr^{1/3}$		$Nu_x = 0.029 Re_x^{0.8} Pr^{1/3}$
Average	$Nu_{av} = 0.66 Re_L^{1/2} Pr^{1/3}$		$Nu_{av} = 0.036 (Re_L^{0.8} - 23000) Pr^{1/3}$
Heat transfer coefficient:			
Local	$h_{cx} = 1.9 (v/x)^{1/2}$		$h_{cx} = 4.6 v^{0.8} x^{-0.2}$
Average	$h_{cav} = 3.7 (v/L)^{1/2}$		$h_{cav} = 5.7 v^{0.8} L^{-0.2} - 18.2/L$
UNIFORMLY HEATED		$\sim 5 \cdot 10^6$	
Nusselt no:			
Local	$Nu_x = 0.45 Re_x^{1/2} Pr^{1/3}$		$Nu_x = 0.031 Re_x^{0.8} Pr^{1/3}$
Average	$Nu_{av} = 0.68 Re_L^{1/2} Pr^{1/3}$		$Nu_{av} = 0.037 (Re_L^{0.8} - 23000) Pr^{1/3}$
Heat transfer coefficient:			
Local	$h_{cx} = 2.6 (v/x)^{1/2}$		$h_{cx} = 4.9 v^{0.8} x^{-0.2}$
Average	$h_{cav} = 3.8 (v/L)^{1/2}$		$h_{cav} = 5.9 v^{0.8} L^{-0.2} - 18.7/L$

5.3.3 Combined Free and Forced Convection

In the discussion of forced convection, it has been assumed that free convection did not occur. This is an idealization, as any heat transfer process requires a temperature gradient and thereby density differences when fluids are involved, and this results in free convection. Likewise there will usually be some air movements in a room and around a building due to mechanical ventilation, windforces, etc. so that forced convection may occur in connection with free convection. Therefore, an interaction between free and forced convection has to be considered in order to find out when free or forced convection can be neglected, and when both of them have to be taken into account.

The combined effect of free and forced convection is strongly influenced by the direction of the two contributions relative to each other. They may have the same direction (assisting flow, or have opposite direction (opposing flow), or be perpendicular to each other (transverse flow). These directions may also influence on the start of turbulence. Assisting flow can delay the start whereas opposing flow can promote it.

The combined effect of free and forced convection can be found from the following superposition rule:

$$(Nu_{com})^n = (Nu_{free})^n \pm (Nu_{forc})^n \quad (5.43)$$

where the exponent n varies according to the specific case to be combined

A theoretical analysis shows that the magnitude of the ratio Gr_L/Re_L^2 , representing the ratio between the buoyancy and the inertia forces, can give a qualitative indication on whether one of the contributions can be neglected or both of them have to be taken into consideration.

5.3.3.1 Vertical Surfaces. Laminar Flow. For laminar, combined convection, experimental data indicate that the best correlation is obtained with an exponent n=3 (Churchill 1990b) in the equation (5.43), so that you get:

$$(Nu_{com})^3 = (Nu_{forc})^3 \pm (Nu_{free})^3 \quad (5.44)$$

5.3.3.2 Vertical Surfaces. Turbulent Flow. No correlating equation has been found. According to Incropera and Witt (1990) the contribution from free convection can usually be neglected, when the forced flow is turbulent.

5.3.3.3 Horizontal Surfaces. By a forced horizontal flow above a heated horizontal top surface or a cooled bottom surface, the buoyant forces will increase the heat transfer. For a cooled top surface or a heated bottom surface, the heat transfer will be decreased.

For laminar flow, Churchill (1990b) recommend the following equation for the combined heat transfer:

$$(\text{Nu}_{\text{com}})^{7/2} = (\text{Nu}_{\text{forc}})^{7/2} \pm (\text{Nu}_{\text{free}})^{7/2} \quad (5.45)$$

where the positive sign is applicable for heated top and cooled bottom surfaces (e.g. heated floor or cooled ceiling) and the negative sign is for cooled top and heated bottom surface.

If the buoyant forces assist, the free convection can be neglected according to Gebhart (1971) when $\text{Gr}_L/\text{Re}_L^{5/2} < 0.08$.

If the buoyant forces oppose, eq.(5.45) results in a zero solution for $\text{Nu}_{\text{forc}} = \text{Nu}_{\text{free}}$. However, separation occurs before Nu_{free} exceeds Nu_{forc} (Mills, 1992), so that the equation is only valid for positive Nu_{comb} .

For turbulent flow, no analysis or experimental data are available. Referring to vertical surfaces, it is reasonable to assume that the contribution from free convection is so small, compared to turbulent forced convection, that it can be neglected.

5.4 Interior Building Surfaces

The convection heat transfer coefficients discussed so far are all derived by theoretical considerations supported by experimental data found under controlled laboratory conditions. Under practical conditions, air currents will always appear, which will disturb the convection process, which again usually will increase the convective heat transfer. By interior surfaces, the air currents may for instance be induced by the ventilation system or by vertical and horizontal temperature gradients.

$$\text{Gr}_x \text{Pr} = 10^8 \Delta T x^3 \quad (5.50)$$

The range of this quantity will be from 5×10^8 and upward, so that laminar as well as turbulent free convection has to be considered.

5.4.2.1 Walls. For walls, it is necessary to distinguish between the inner surfaces of insulated and uninsulated outside walls and of unheated and heated inside walls, respectively. Further, the height of the wall has to be taken into account.

For insulated outside walls up to a height H of about 3 m, the quantity $\text{Gr}_H \text{Pr}$ ($x = H$) will have a value up to 10^9 resulting in laminar free convection, so that the convection heat transfer coefficient is determined by, cf. table 5.3:

$$h_{ci} = 1.5(\Delta T/H)^{1/4} \quad (5.51)$$

For insulated walls higher than 3 m, the free convection becomes partly turbulent so that you get:

$$h_{ci} = 1.5(\Delta T)^{1/3} - 0.6/H \quad (5.52)$$

or for $H > 6$ m:

$$h_{ci} \sim 1.5(\Delta T)^{1/3} \quad (5.53)$$

For uninsulated outside walls like glass facades, the temperature difference will be so large that you get values of $\text{Gr}_H \text{Pr}$ of about 10^{10} , so that the convection becomes turbulent and so that eq.(5.53) can be used even for heights down to 2.5 - 3.0 m.

For unheated inside walls the temperature difference will be so small that laminar convection can be assumed even for wall heights above 6 m, so that eq.(5.51) should be used.

For heated inner walls, for instance heated by the sun, temperature differences similar to those for uninsulated outside walls can be expected and even larger, so eq.(5.53) can be used for any height.

5.4.2.2 Cold Floors or Warm Ceilings. In this case, almost no convection should occur. It can therefore be assumed that the convection heat transfer coefficient will be considerably smaller than found by the equation in table 5.5, which is valid for horizontal surfaces where the air can escape along the edges. If a halving is assumed, you get:

Further, they measured the heat transfer from a horizontal free-edged plate with the heated surface facing downward and suspended 1.5 m above the floor. In that case they found a convection heat transfer coefficient about four times larger than the one found for the heated ceiling.

Khalifa and Marshall (1990) made their measurements in a test cell divided into a hot and a cold zone. The wall between the two zones thus functioned as an outside wall. The hot zone had a floor area of $2.95 \times 2.35 \text{ m}^2$ and the room height was 2.05 m. The four walls and the ceiling in this zone were covered with aluminium foil in order to minimize the effect of the longwave radiation exchange. Heat was supplied from the floor or from heat panels covering the wall opposite to the outside wall, or from a radiator either placed along the outside wall or along the inside wall opposite to the outside wall. The difference between inside air temperature and surface temperature was in the range 0.5 - 3.5 °C.

For the floor heating case, they found:

$$\begin{aligned} \text{Walls: } h_{ci} &= 2.1(\Delta T) \\ \text{Floor: } h_{ci} &= 2.3(\Delta T) \\ \text{Ceiling: } h_{ci} &= 2.7(\Delta T)^{0.13} \end{aligned}$$

For the wall heating case the found:

$$\begin{aligned} \text{Outside wall: } h_{ci} &= 2.3(\Delta T)^{0.25} = \\ \text{Wall with heat panels : } &\text{no result was obtained} \\ \text{Floor: } &\text{not measured} \\ \text{Ceiling: } h_{ci} &= 3.1(\Delta T)^{0.17} \end{aligned}$$

For the case with radiator placed opposite to the outside wall, they found:

$$\begin{aligned} \text{Outside wall: } h_{ci} &= 2.2(\Delta T) \\ \text{Wall with radiator: } h_{ci} &= 2.4(\Delta T) \\ \text{Floor: } &\text{not measured} \\ \text{Ceiling: } h_{ci} &= 2.8(\Delta T) \end{aligned}$$

Delaforce et al. (1993) made their measurements in an outside test cell with an inside floor area of $2.03 \times 2.03 \text{ m}^2$ and a height of 2.33 m. The heat was supplied by an air heating system and the temperature difference was in the range of 0.5 - 4.0 °C. When the heat was supplied continuously, they found (with rather large dispersion):

by the circular air flow pattern in the room with air moving upward by the warmer wall and downward by the colder one.

The measurements or Delaforce et al. (1993) are also carried out by such temperature differences and surface dimensions that laminar flow is to be expected, but their result are rather dispersed. However, it is of interest to notice their increased values by intermittent heat supply.

Summarizing, it can be stated that the approximate, theoretical solutions for the convection heat transfer coefficients represented by the equations (5.51) - (5.55) are in reasonable good accordance with the available full-scale measurements. Only should the constants in front of the equations be increased by 20 - 25%. Besides, it should be taken into consideration, that the coefficients should be increased further by 15 - 20% by unsymmetrical heat supply.

5.4.5 Recommended Values

The following recommendations are estimates based on the knowledge available.

Outside walls:

$$\text{insulated, } H < 3 \text{ m: } h_i = 5.0 + 2.0(\Delta T)^{1/4} \quad (5.56)$$

$$\text{insulated, } 3 \text{ m} < H < 6 \text{ m: } h_i = 5.0 + 2.0(\Delta T)^{1/3} - 0.8/L \quad (5.57)$$

$$\text{insulated } H > 6 \text{ m: } h_i = 5.0 + 2.0(\Delta T)^{1/3} \quad (5.58)$$

$$\text{uninsulated: } h_i = 5.0 + 2.0(\Delta T)^{1/3} \quad (5.59)$$

Inside walls:

$$\text{unheated: } h_i = 1.0 + 2.0(\Delta T)^{1/4} \quad (5.60)$$

$$\text{heated: } h_i = 1.0 + 2.0(\Delta T)^{1/3} \quad (5.61)$$

Cold floor or warm ceiling:

$$h_i = 1.0 + 0.2(\Delta T/L^2)^{0.2} \quad (5.62)$$

Warm floor or cold ceiling:

$$h_i = 1.0 + 2.0(\Delta T)^{1/3} \quad (5.63)$$

By unsymmetrical heat supply, the convective part should be increased by 20%.

In any other cases, a more detailed analysis has to be carried out.

Walls, insulated: $\Delta T \sim 5 - 10^\circ\text{C}$
 uninsulated: $\Delta T \sim 0 - 5^\circ\text{C}$
 Roofs, insulated: $\Delta T \sim 10 - 15^\circ\text{C}$
 uninsulated: $\Delta T \sim 5 - 10^\circ\text{C}$

The surfaces of the uninsulated walls and roofs are less supercooled due to the larger heat transfer from the inside when a heated building is considered.

In nights with clouded sky, the surface temperature will only be a few degrees above the outdoor air temperature when heated buildings are considered.

It is the situations with low surface temperatures which are of interest (condensation problems, heat losses etc.). Therefore, only the conditions in nights will be discussed in the following.

The equations for determining if the free or the forced convection can be neglected, or if the boundary layer flow is laminar or turbulent, are the equations (5.49) and (5.50). Further you have the following equation for the transition by forced convection:

$$\text{Re}_x = vx/\nu \sim 7 \cdot 10^4 vx \quad (5.64)$$

The values of the constants in these equations do not vary more than about 10% in the temperature range 0 - 30°C

5.5.2.1 Walls. For vertical surfaces, the free convection can be neglected if $\text{Gr}_L/\text{Re}_L < 0.3$ (cf. section 5.3.3.1) almost independent of, if the free convection assists or opposes the forced convection. The boundary value of 0.3 corresponds to (cf.eq.(5.49)):

$$0.034\Delta TH/\nu^2 < 0.3$$

or

$$\nu^2 > 0.1\Delta TH$$

For the forced convection you get with the air velocity $v > 0.4$ m/s and with the wall height $H > 3$ m :

$$\text{Re}_L > 7 \times 10^4 \times 0.4 \times 3 \sim 10^5$$

For a supercooled, insulated wall you get, when assuming $\Delta T = 8^\circ\text{C}$, that eq.(5.68) is valid for $H/v^2 > 1$, or $v^2 < H$, and this results in $v < 2$ m/s for a 4 m high wall, and $v < 3$ m/s for a 10 m high wall.

For larger air velocities, the free convection can be neglected, and the convection heat transfer coefficient can then be determined by eq.(5.70).

It should be noticed that eqs.(5.68) and (5.69) indicate a zero solution, but experimental data show that the lowest Nu-number is $Nu = 0.8$ (Churchill, 1990).

For a supercooled, uninsulated wall with $\Delta T \sim 4^\circ\text{C}$, you get $H/v^2 > 2$ or $v^2 < 0.5H$.

By nights with cloudy sky with $\Delta T \sim 2^\circ\text{C}$, you get $H/v^2 > 5$ or $v^2 < 0.2H$.

By transverse flow, i.e. when the wind direction is inclined compared to the building direction, the boundary value for Gr_L/Re_L is about 0.7, cf. section 5.3.3.1, and this means again that free convection can be neglected by air velocities that are 30% smaller than the velocities found above.

5.5.2.2 Horizontal Roofs. For horizontal surfaces, the free convection can be neglected if $Gr_L/Re_L < 0.1$ almost independent of, if the free convection is assisting or opposing the forced convection. This corresponds to :

$$\Delta TH/v^2 < 3$$

or

$$v^2 > 0.3 \Delta TH$$

Compared to the walls it means an almost doubling of the air velocities before the free convection can be neglected.

For the forced convection, similar considerations can be done as for the walls and you find that the forced convection is only fully laminar by calm weather.

The free convection is strongly dependent on the direction of the heat flux. For a supercooled roof you get from table 5.5:

$$\sim 0.5(\Delta T/L^2)^{0.2} \quad (5.71)$$

Contrary to a cold floor or a heated ceiling, no reduction will be done, because the surface can be considered as finite with escape possibilities at the roof edges.

$$h_c = a + bv \text{ for } v < 5 \text{ m/s} \quad (5.73)$$

$$h_c = cv^d \quad \text{for } v > 5 \text{ m/s} \quad (5.74)$$

A frequently seen reference in textbooks is Jürges (1924), who found the following values for the constants for a rolled surface:

$$a = 5.8 \quad b = 3.9 \quad c = 7.1 \quad d = 0.78$$

For polished surfaces he found about 5% smaller values and for more rough surfaces he found about 10% larger values. These values of the constants have on the whole been confirmed by later researchers up through the 1930'es and 1940'es.

Rowley et al (1930a) (cited by Cole and Sturrock, 1977) also examined the influence of the mean temperature (i.e. the average between the air and the surface temperature), and they found a slightly higher convection coefficient by a higher mean temperature.

Rowley et al (1930b) examined the influence of the surface texture. Getting a fair agreement with Jürges (1924) for smooth surfaces, they found an about 25% higher coefficient for more rough surfaces made of plaster, bricks and concrete.

Parmelee and Huebscher (1947) measured on a vertical plate parallel to the flow. They found results similar to those of Jürges (1924). Besides, they found that the length of the surface influenced on the coefficient by giving decreasing values for increasing lengths.

5.5.3.2 Non-parallel flow. A few experiments are carried out with inclined surfaces in wind tunnels. Rowley and Eckley (1933) found with a $0.38 \times 0.38 \text{ m}^2$ surface that an inclination angle between 15° and 90° resulted in a smaller coefficient than by parallel flow, but the value was independent of the angle as long as the air velocity was below 7 m/s. For higher velocities the coefficient was only slightly reduced compared to its value by parallel flow. They concluded that for practical purposes, the coefficient for parallel flow was sufficient accurate also for inclined surfaces.

Sturrock (1971) (cited by Cole and Sturrock, 1977) measured the convection coefficient on a 230 mm cube. He found, that the orientation of the surface had a significant influence on the coefficient. Besides, his coefficient values were significantly higher than those found by previous researchers. His results in the velocity range 3 - 10 m/s could be expressed by:

texture is understandable from the point of view that a more rough surface induces an earlier and a higher degree of turbulence, which again increases the heat transfer.

The influence of the length found by Pamelee and Huebscher (1947) is in accordance with what can be found when considering the forced part of eq.(5.68) for sufficiently large air velocities.

The results of Rowley and Eckley, indicating that the inclination angle has almost no influence in a certain range of angles is in good accordance with the results of Tien and Sparrow (1979) mentioned in section 5.3.2.2.

The high coefficient values of Sturrock (1971) can partly be explained by the fact, that he did not eliminate the radiation effects. An other reason might be the different flow pattern around an immersed cube compared to the pattern above a plate mounted flush to one of the surfaces of a wind tunnel.

5.5.4 Full-Scale Measurements

Full-scale measurements are carried out by Sturrock (1971), Ito et al (1972), Nicol (1977), and Sharples (1984). The measurements are carried out in the night to avoid the effect of solar radiation.

Besides, the long wave radiation contribution is subtracted in all the results except those of Sturrock (1971).

Sturrock (1971) made his measurements on a 26 m high building and found for the windward walls:

$$h_{co} = 11.4 + 5.7v_w \quad (5.76)$$

where v_w is the wind speed measured in the main stream above the roof.

Ito et al (1972) did their measurements on a six storey building and they relates their coefficients to the wind speed measured 8 meter above the roof as well as to the air velocities measured close to the walls. The coefficients related to the wind speed, are rather dependent on the distance from the edges, whereas when related to the surface air velocities, the coefficients are almost independent of this distance. For the surface air velocities they found:

$$v_s \sim 0.2v_w \quad \text{for windward surfaces and far from edges}$$

$$v_s \sim 0.3v_w \quad \text{for windward surfaces closer to edges}$$

5.5.4.1 Discussion of Full-scale Measurements. It is natural to compare the full-scale results with the results of the wind tunnel experiments. In this connection it should be pointed out that the velocity in these results is the velocity close to the surface just outside the boundary layer and has nothing to do with the wind speed in the main stream above the roof or 10 m above the terrain.

The work of Ito et al is the most comprehensive of the four full-scale experiments discussed here. His surface air velocities are consistent with what you can get when using relevant pressure coefficients in eq.(5.42). His expression for the air velocities by surfaces far from edges thus corresponds to a pressure coefficient of about 0.95. His expression for the convection coefficient is in fair accordance with the wind tunnel experiments. Only, the temperature difference between the surface and the ambient air is missing. Therefore, it is not possible to evaluate his constant $a \sim 6 \text{ W/m}^2\text{K}$, which is determined by this temperature difference.

The results of Nicol (1972) are likewise in reasonable accordance with the wind tunnel experiments, when taking into account that for low-rise buildings, you have a pressure coefficient of 0.5-0.6 on the windward side. This gives a surface air velocity of $v_s \sim 0.7v_1$.

In the eq.(5.76) of Sturrock (1971), the velocity is the wind speed measured in the main stream above the roof. Therefore, he gets convection coefficients, which are about the double of what is found by the other researchers. One reason for these high values is probably, that he did not eliminate the long wave radiation to the sky.

Sharpies (1984) finds rather small convection coefficients. It seems as if problems have occurred in connection with his velocity measurements.

5.5.5 Recommended Values

It is necessary to distinguish between the radiation and the convection contribution when considering the heat transfer between an exterior surface at its surroundings. The recommendations for the radiation part is given in section 5.5.1. Therefore, only the convection part will be discussed in the following.

It should be noticed that the amount of full-scale measurements on exterior surfaces is rather modest, and measurements on roofs are totally lacking.

As to the wall measurements, the results of Ito et al (1972) seems most reliable, and together with the wind tunnel results, they indicate that the semi-

20% should be added in order to take the uncontrolled effects by full-scale measurements compared with laboratory experiments into account.

For a supercooled, insulated wall, (e.g. by a calm, clear night) the free and forced convection are almost equal, and they oppose each other in principle. But, as the air currents around the building will be rather changing in this case, a certain assisting flow may be assumed, and the expression for free, turbulent convection from table 5.3 will be proposed with an increase of 30%. By further adding 20% as mentioned above, you get:

$$h'_{co} \sim 1.2 \times 1.3 \times 1.5(\Delta T)^{1/3} = 2.4(\Delta T) \quad (5.81)$$

For windy weather, the free convection can be neglected, and you get by using eq.(5.70) and eq.(5.80) and adding 20%:

$$h_{co} = 1.2 \times 5.0(0.4 + 0.64v) = 2.4 + 3.8v \quad (5.82)$$

This equation can be considered as valid for a very smooth surface like glass. For a more rough one, an increase of about 50% should be considered.

For a supercooled, uninsulated wall an analysis gives the same result as for the insulated wall.

For a warm, insulated and uninsulated wall (e.g. cloudy weather) the two convection contributions assist each other. In calm weather this leads to, when taking a certain forced contribution of about $2.5 \text{ W/m}^2\text{K}$ into account:

$$h'_{co} \sim 1.2 \times (2.5^3 + (1.5(\Delta T)^{1/3})^3)^{1/3} (28.0 + 5.9 T)$$

For windy weather eq.(5.82) can be used unchanged.

Summarizing, the following equations for the convection heat transfer coefficient for exterior walls can be recommended based on the knowledge available:

Smooth walls:

Calm weather, supercooled wall:

$$h = 2.4(T)^{1/3}$$

warm wall:

$$h_{co} = (28 + 6 T)^{1/3}$$

$1 \text{ m/s} < v_s < 7 \text{ m/s}$:

$$= 2.4 + 3.8v,$$

$7 \text{ m/s} < v_s$:

Rough walls:

Increase the smooth-values with 50%

5.6 Summary

The surface heat transfer is composed of radiation and convection. This chapter contains a description of the theoretical and practical interior and exterior surface heat transfer coefficients.

The principle of radiative heat transfer between surfaces is described. For interior surfaces emissivity values are suggested. For exterior surfaces sky temperature studies are presented and values suggested. The influence of surface slope is also shown.

The theory of free convection on vertical, inclined and horizontal surfaces is presented. The location of the heat source or warm surface is also discussed. Formulas are presented for both forced and combined free and forced convection.

For interior surfaces a method to combine radiation and convection coefficients into one coefficient is presented. Results of laboratory and full scale measurements are presented. Recommendations are given on values for radiation and convective coefficients for warm and cold ceilings, floors and walls.

For exterior surfaces it is suggested not to combine radiation and convection. Results are presented on wind tunnel and full scale measurements and recommended values are given for walls and roofs.

5.8 References

- Berdahl P., og Fromberg R.; The Thermal Radiance of Clear Sky. *Solar Energy*, 29, 229-314. 1982
- Brown, G.: Värmeövergång vid byggnaders yttertor. Statens nämnd för Byggnadsforskning. Handlingar nr. 27. Stockholm 1956.
- Brunt, D.: Notes on radiation in the atmosphere. 1. *Quarter Journal of the Royal Meteorological Society*, 58 (1932): 389-420.
- Brunt, D.: *Physical & dynamical meteorology*. Cambridge 1934.
- Churchill, S.W.: Free Convection around Immersed Bodies. In: *Hemisphere Handbook of Heat Exchanger Design*. Hemisphere Publishing Corporation. New York, 1990a.
- Churchill, S.W.: Combined Free and Forced Convection Around Immersed Bodies. In: *Hemisphere Hand Book of Heat Exchanger Design*. Hemisphere Publishing Corporation. New York, 1990b.
- Cole, R.J.: The longwave radiation incident upon the external surface of buildings. *Building Services Engineer*, 44 (1976): 195-206.
- Cole, R.J. and Sturrock, N.S.: The Convective Heat Exchange at the External Surface of Buildings. Review Paper. *Building and Environment*. Vol 12, 207-214. 1997.
- Delaforce, S.R. et.al.: Convective Heat Transfer at Internal Surfaces. *Building and Environment*, Vol 28, 211-220, 1993.
- Eckert, E.R.G. and Drake, R.M.: *Heat and Mass Transfer*. McGraw-Hill, New York 1959.
- Ede, J.E.: Advances in Free Convection. In: *Advances in Heat Transfer*. Academic Press, New York, 1967.

Mills, A.F.: Heat Transfer. Irwin Inc., Boston. 1992.

Min, T.C. et.al.: Natural Convection and Radiation in a Panel-heated Room. Trans. ASHRAE 62. 337-358. 1956.

Nicol, K.: The Energy Balance of an Exterior Window Surface, Inuik, N.W.T., Canada. Building and Environments, Vol 12, 215-219. 1977.

Parmelee G.V. and Huebscher, G.: Forced Convection Heat from Flat Surfaces. Trans. ASHRAE, 58, 85-106, 1947.

Philipps, H.: Zur Theorie der Wärmestrahlung in Bodennähe. I: Gerlands Beiträge zur Geophysik, Band 56. Leipzig 1940, pp. 229-319.

Raman, P.K.: Heat radiation from the clear atmosphere at night. Indian Academy of Sciences. Proceedings, 1 (1935): 815-821.

Rowley, F.B. et.al: Effects of Air Velocity on Surfaces Coefficients. Trans. ASHRAE, 36. 123. 1930 a.

Rowley, F.B. et.al.: Surface Conductances as Affected by Air Velocity, Temperature and Character of Surface. Trans. ASHRAE, 36. 429. 1930 b.

Rowley, F.B. and Eckley, W.A.: Surface Coefficients as Affected by Wind Direction. Trans. ASHRAE, 38. 1932.

Schlichting, H.: Boundary-Layer Theory, McGraw-Hill, New York, 1979.

Sharples, S.: Full-Scall Measurements of Convective Energy Losses from Exterior Building Surfaces. Building and Environments, Vol 19, no. 1, 31-39, 1984.

Sparrow, E.M. and Geiger, G.T.: Local and Average Heat Transfer Characteristics for a Disk Situated Perpendicular to a Uniform Flow. J. of Heat Transfer, Vol. 107, 321-326, 1985.

Sparrow, E.M. and Gregg, J.L.: Buoyancy Effects on Forced-Convection Flow and Heat Transfer. J. of Applied Mechanics, Sec.E. Vol. 81, 133-135, 1959.

6 Solar radiation

This chapter gives a description of solar radiation physics and an overview of how different building energy simulation programs deal with this.

In order to distinguish how the different algorithms for solar radiation will influence the results of calculated incident, transmitted and distributed solar radiation in atrium buildings, calculations with different programs are made and compared for a simple building with a glazed space.

A simplified method to estimate solar energy utilisation in glazed spaces is also presented.

6.1 Incident solar radiation

Full treatment of the effect of solar radiation on buildings considers the surfaces of building components as parts of a thermodynamic system comprising the atmosphere, the ground and any buildings in close proximity.

The solar radiation which is received outside the atmosphere by a surface perpendicular to the direction of radiation, the solar constant, is 1.94 Ly/min (1353 W/m^2). The solar constant varies during the year, depending on the varying distance between the sun and the earth, from 1.979 to 2.02 Ly/min. At perihelion, in the beginning of January, the maximum value is 1400 W/m^2 and at aphelion, in the beginning of July, the minimum value is 1309 W/m^2 .

Over a year, the breakdown of the radiation which the earth receives from the sun is approximately as follows (Tasler, 1972; Seller, 1965)

Incident radiation at the limit of the atmosphere	100%
Reflection and scatter towards space	30%
Absorption in the atmosphere	17%
Scattered radiation towards the surface of the earth	22%
Direct radiation towards the surface of the earth	31%

wave radiation. The net outward radiation from the ground surface is the difference between the radiation emitted by the ground and counter-reflection from the atmosphere.

The sum of global radiation and the radiation reflected by the ground and other parts of the environment is called total radiation. All these radiant heat transfers occur in the short wave region. When the entire thermodynamic interaction between the surface of a building and the atmosphere is to be studied, the long wave radiation from the atmosphere, the ground and surrounding surfaces must also be included.

Figure 6.1 illustrates the energy fluxes at the surface of a building. These fluxes consist of a convective component

$$q = h_c (T_a - T_s)$$

where

- h_c = surface heat transfer coefficient ($\text{W/m}^2 \text{ } ^\circ\text{C}$)
- T_a = air temperature ($^\circ\text{C}$)
- T_s = surface temperature ($^\circ\text{C}$)

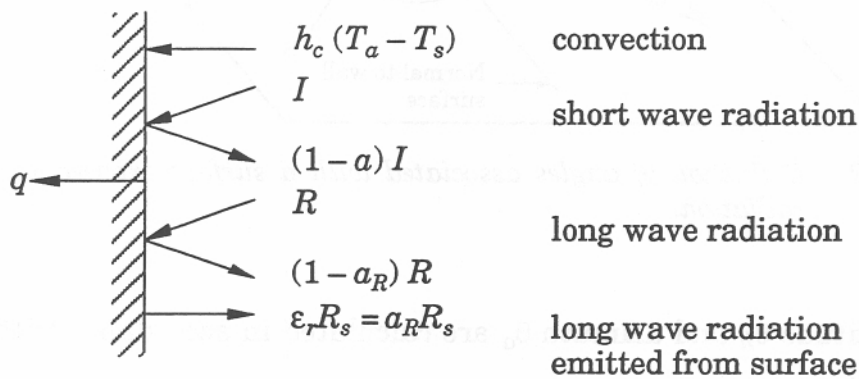


Figure 6.1 Energy fluxes at the surface of a building exposed to solar radiation.

Of the short wave radiation I , the proportion aI is absorbed and the remainder is reflected. The same applies for long wave radiation, i.e. proportion $a_R R$ is absorbed and the remainder, $(1 - a_R) R$ is reflected. Finally, the surface emits the long wave radiation $\epsilon_r R_s$, where R_s corresponds to the radiation from a black surface with the same temperature T_s as the surface of the building.

By constructing a heat balance for the surface, the following expression is obtained

$$q = h_c (T_a - T_s) + aI + \epsilon_r (R - R_s) \quad (\text{W/m}^2) \tag{6.1}$$

$$\begin{aligned}\theta_d = & 0.33281 - 22.984 \cos w_N N_d - 0.34990 \cos 2 w_N N_d \\ & - 0.13980 \cos 3 w_N N_d + 3.7872 \sin w_N N_d \\ & + 0.03205 \sin 2 w_N N_d + 0.07187 \sin 3 w_N N_d \quad (^\circ)\end{aligned}\quad (6.4)$$

where

$$\begin{aligned}w_N &= 2 \pi / 366 \\ N_d &= \text{day number}\end{aligned}$$

Since the solar altitude and azimuth are to be calculated by Equations (6.2) and (6.3) on the basis of civil time, the hour angle must be corrected in accordance with Equation (6.5)

$$\theta_H = 15 (H - k_m + k_{lH} - 12) \quad (^\circ) \quad (6.5)$$

where

$$\begin{aligned}H &= \text{time (civil time)} \quad (\text{h}) \\ k_m &= \text{correction in hours in accordance with Equation (6.6)} \quad (\text{h}) \\ k_{lH} &= \text{correction in hours for the local time deviation from the time} \\ &\quad \text{meridian} \quad (\text{h})\end{aligned}$$

The correction is to be made both in view of the position of the locality in relation to the standard meridian and with regard to the time equation. The time equation gives the difference between true solar time and mean solar time and varies over the year owing to the fact that the orbit of the earth round the sun is elliptical and that this orbit is not in the plane of the equator.

The time equation is given by

$$\begin{aligned}k_m = & 0.0072 \cos w_N N_d - 0.0528 \cos 2 w_N N_d - 0.0012 \cos 3 w_N N_d \\ & - 0.1229 \sin w_N N_d - 0.1565 \sin 2 w_N N_d - 0.0041 \sin 3 w_N N_d \quad (\text{h})\end{aligned}\quad (6.6)$$

With the angles defined in Figure 6.2, the intensity of solar radiation on a surface of arbitrary orientation can be written as

$$I = I_{DN} \cos \theta_i \quad (6.7)$$

where

$$\begin{aligned}I_{DN} &= \text{intensity of radiation in the direction of radiation} \quad (\text{W/m}^2) \\ \theta_i &= \text{angle between the normal to the surface and the direction} \\ &\quad \text{of radiation} \quad (^\circ)\end{aligned}$$

The coefficient α_r describes Rayleigh scatter and is a function of wavelength in accordance with

$$\alpha_r = \lambda^{-4} 0.00816 \quad (6.10)$$

The coefficient α_d is a function of wavelength and is subject to a high degree of variation depending on the turbidity of the atmosphere

$$\alpha_d = \lambda^{-1.3} \beta \quad (6.11)$$

where

β = coefficient of turbidity according to Table 6.1.

Table 6.1 Coefficient of turbidity according to Taesler (1985) and Taesler & Andersson (1985).

Month	Month
Jan 0.040	July 0.065
Feb 0.040	Aug 0.060
March 0.050	Sep 0.055
April 0.060	Oct 0.050
May 0.070	Nov 0.040
June 0.070	Dec 0.040

Optical air mass is a function of solar altitude θ_h and, according to Taesler and Andersson (1985) and Liljequist (1979), can be approximated as follows

$$m = \frac{1}{\sin \theta_h} \quad \text{when } \theta_h > 10^\circ \quad (6.12)$$

$$m = 1.22 \left(\frac{1.0144}{\sin(\theta_h - 1.44)} - 0.49 \right) \quad \text{when } \theta_h \leq 10^\circ \quad (6.13)$$

Using the coefficients of absorption in accordance with Equations (6.10) and (6.11), coefficients of turbidity in accordance with Table 6.1 and the optical air mass as determined by Equation (6.12) or (6.13), the intensity of radiation at the surface of the earth is calculated in accordance with Equation (6.9) for an arbitrary wavelength. By integrating (6.9) over the wavelength region of interest, 0.2-10 μm , we obtain the intensity of direct radiation in the direction of the normal as

The intensity of radiation calculated by Equation (6.14) is reduced due to absorption by water vapour on its passage through the atmosphere. The absorption is a function according to Liljequist (1979)

$$F = f(w \cdot m) \quad (\text{W/m}^2) \quad (6.15)$$

where

w = quantity of water which can be precipitated (kg/m^2)

m = optical air mass according to Equation (6.12) or (6.13)

The way in which the quantity of precipitable water is calculated on the basis of radio sonde data is described in Liljequist (1979). This reference also describes a simplified method of empirically determining the absorption according to Fowle, in which the quantity of precipitable water is represented by the vapour pressure at the surface. The following expression is given

$$F = 70 + 2.8 e m \quad (\text{W/m}^2) \quad (6.16)$$

where

e = vapour pressure at the surface (mbar)

The absorption according to (6.16) is related to the mean distance of the earth from the sun.

The direct radiation in the direction of the normal, corrected for the appropriate distance between the earth and the sun, and with respect to the absorption in water vapour, is obtained from

$$I_{DN} = (I'_{DN-F}) \quad (6.17)$$

where

= correction factor in accordance with Equation (6.18)

The correction factor k_e which takes account of the eccentricity of the earth's orbit around the sun, is obtained from

$$k_e = \frac{1}{1353} (1353 + 45.326 \cos w_N N_d + 0.88018 \cos 2 w_N N_d - 0.00461 \cos 3 w_N N_d + 1.8037 \sin w_N N_d + 0.09746 \sin 2 w_N N_d + 0.18412 \sin 3 w_N N_d) \quad (6.18)$$

$$I_{dH} = \frac{\eta}{1-\eta} I_{DN} \sin \theta_h \quad (6.25)$$

6.1.2 Short wave radiation from a cloudy sky

In the SOLTIMSYN model (Taesler and Andersson, 1985), solar radiation in conjunction with a cloudy sky is calculated on the basis of synoptic data obtained from meteorological observations.

On the basis of information concerning cloud cover in eights of the sky and the quantities of the different types of cloud, a resultant albedo (reflection) for cloud is calculated by

$$A_c = \frac{N_l A_l + N_m A_m + N_h A_h}{8} \quad (6.26)$$

where

A_c = resultant albedo of cloud

N_l = amount of low cloud, stratus stratocumulus

N_m = amount of middle cloud

N_h = amount of high cloud

A_l = 0.75, albedo for low cloud

A_m = 0.45, albedo for middle cloud

A_h = 0.40, albedo for high cloud

According to Liljequist (1979), global radiation in cloudy weather can be calculated on the assumption that the sky is covered by a homogeneous layer of cloud and that no absorption occurs either inside or below the cloud. It is further assumed that the sky is cloudless above the cloud cover.

Of the global radiation which is incident on the top of the cloud, the proportion $A_c I_H$ is reflected. The remainder, $(1 - A_c) I_H$, passes through the cloud and reaches the surface of the earth. Repeated reflection will occur between the surface and the cloud base. The total downward radiation is the global radiation at the surface. The sum is an infinite geometric series, and can be written as

$$I_{H,c} = I_H \frac{1 - A_c}{1 - A_g A_c} \quad (6.27)$$

where

$I_{H,c}$ = global radiation for a cloudy sky (W/m^2)

A_g = albedo of ground

If the effect of the amount of cloud is also included, then, in analogy with Equation (6.28), Equation (6.31) is modified to

$$t_a = \left(\frac{I_{DN} (1 - N_c/8)}{I_o} \right)^{\frac{1}{m}} \quad (6.32)$$

Diffuse solar radiation in the direction towards the sun is treated geometrically in the same way as direct solar radiation, and background radiation is assumed to be wholly diffuse. With the aid of Equation (6.32), diffuse radiation in a direction towards the sun can be written as

$$I_{dN,c} = t_a I_{dH,c} \quad (6.33)$$

where

$$I_{dN,c} = \text{diffuse solar radiation in the direction towards the sun (W/m}^2\text{)}$$

The remaining diffuse radiation is background radiation, given by

$$I_{dB,c} = I_{dH,c} - I_{dN,c} \sin \theta_h \quad (6.34)$$

The diffuse radiation incident on a surface of arbitrary inclination can now be written as the sum of the contributions of diffuse radiation in the direction towards the sun, background radiation and radiation reflected from the ground

$$I_{di,c} = I_{dH,c} t_a \cos \theta_i + I_{dB,c} \frac{1 + \cos \theta_t}{2} + A_g I_{H,c} \frac{1 - \cos \theta_t}{2} \quad (6.35)$$

where the two last terms account for the correction for partially screened horizon and ground surface respectively. See e.g. Brown and Isfält (1974, pp 97-101)

where

$$\theta_t = \text{inclination of surface to the horizontal plane } (\theta_t = 90 - \theta_\gamma) \quad (^\circ)$$

water vapour and carbon dioxide. The emission bands of water vapour are very wide, and atmospheric radiation is to a high degree determined by the temperature in the lower layers of the atmosphere and by the water vapour content of the air. Carbon dioxide has a very wide emission band which is of significance, and radiation in this wavelength interval is approximately equal to that received from an ideal black body.

In e.g. Liljequist (1979) atmospheric radiation is given by the expression

$$R_A = f(e) \sigma T_a^4 \quad (6.38)$$

where

$f(e)$ = a function which is dependent on the humidity of the atmosphere

T_a = air temperature at ground level (the Stevenson cage) (K)

The average vapour pressure in the atmosphere has a characteristic variation with height above the surface. It is thus possible, in lower layers of the atmosphere, to have the vapour pressure e represent the humidity profile of the atmosphere. The contribution made by carbon dioxide is represented by a constant which is included in the function $f(e)$.

In the literature, different expressions are given for the function $f(e)$. The following relationship according to Brunt (1952) has been used

$$R_A = (0.52 + 0.065 \sqrt{e}) \sigma T_a^4 \quad (6.39)$$

where

e = vapour pressure in mbar at the level of the Stevenson cage

Equation (6.39) is valid only for a cloudless sky and average conditions regarding the variation of temperature and humidity with the height above ground level. The expression is thus not valid when there is e.g. powerful surface inversion or inversion at a height (Liljequist, 1979).

6.2.2 Long wave radiation from a cloudy sky

When the sky is cloudy, radiation conditions change because the cloud base emits thermal radiation. The cloud base can be regarded as an ideal black body (Liljequist, 1979). In the same way as when the sky is clear, radiation is affected by water vapour and carbon dioxide in the atmosphere.

$$R_{A,Nc} = \frac{N_c}{8} ((1 - k_\lambda) R_G + k_\lambda R_A) + \left(1 - \frac{N_c}{8}\right) R_A \quad (6.43)$$

where

$R_{A,Nc}$ = long wave radiation from the atmosphere for an amount N_c of cloud (W/m^2)

6.2.3 Long wave radiation on inclined surfaces

The total long wave radiation incident on a building surface of arbitrary orientation is then calculated using Equation (6.36), R_A being replaced by $R_{A,Nc}$ in order to take cloud cover into account

$$R = R_{A,Nc} \frac{1 + \cos \theta_t}{2} + R_G \frac{1 - \cos \theta_t}{2} \quad (6.44)$$

If account is also taken of reflection from the ground, Equations (6.42)—(6.43) are modified. Atmospheric radiation in cloudy weather must be corrected by the term

$$\omega = \frac{1}{1 - (1 - \varepsilon_g)(1 - k_\lambda)} \quad (6.45)$$

Equation (6.44) also includes atmospheric radiation reflected from the ground as expressed by the term R_G . Radiation emitted from the ground when there is broken cloud cover, allowing for atmospheric radiation reflected from the ground, is defined as

$$R_{G,Nc} = \varepsilon_g T_G^4 + (1 - \varepsilon_g) R_{A,c} \quad (6.46)$$

Properties for a non-polarised wave can, due to the random fluctuations, be obtained as the average of two polarised waves with their electrical planes perpendicular to each other. The transverse electric (*TE*) wave, also called the parallel component and the transverse magnetic (*TM*) wave, also called the perpendicular component normally are used. The first of these has its electrical plane and the other its magnetic plane parallel to the plane of incidence on an interface between two media.

An optically thick layer has a thickness which is so large compared to the wavelength of the radiation that interference phenomena can be neglected. Commonly used materials in windows, glass or plastic sheets, with a thickness of some millimetres can be treated as optically thick layers. Thin film coatings on glass must often be assumed as optically thin layers as the thickness approaches the wavelength of the radiation, thus interference effects become important. These type of layers are not discussed further.

The refraction index n is defined as the ratio of wave speed in vacuum c_0 to the speed in the media c .

$$n = \frac{c_0}{c} = \sqrt{\mu\gamma} \quad (6.46)$$

where μ is the magnetic permeability and γ the electrical permittivity of the media. This index is valid for media with infinite resistivity and can be used in most cases, e.g. for normal glass we have ≈ 1.5 . Note that the refraction index may vary with the wavelength.

To quantify the absorption within a media an extinction coefficient k is used. For a given path length x in a media, the absorption in a single pass through the media is given by Bouger's law (also referred to as Beer's law).

$$a = 1 - e^{-k_g x} \quad (6.47)$$

For some glass types $k_g \approx 23.3 \text{ m}^{-1}$ is used and 19.6 m^{-1} is often seen for float glass. In this case no reflection is assumed in the media and according to thermodynamic equilibrium we get the transmission:

$$t = 1 - a \quad (6.48)$$

The gaps between the panes in windows are often filled with air. In some cases a heavy gas is used in a sealed unit to reduce the U value. Air, as well as commonly used gases, can be treated as vacuum when calculating solar radiation through windows and within buildings. Absorption, scattering et cetera in gases are only needed to take into account when looking at the propagation through the atmosphere, thus we can use a refraction index $n = 1$ and an extinction coefficient $k = 0$ for all gases.

$$r_{TM} = \left(\frac{n_1 / \cos \theta_1 - n_2 / \cos \theta_2}{n_1 / \cos \theta_1 + n_2 / \cos \theta_2} \right)^2 \quad (6.55)$$

With two semi-infinite media there are no multiple reflections nor any absorption at the interface. Thus, according to thermodynamic equilibrium, we get the transmission through the interface.

$$t_{TE} = 1 - r_{TE} \quad \text{and} \quad t_{TM} = 1 - r_{TM} \quad (6.56)$$

6.3.2 Single panes, optically thick layers

The radiation in an optically thick layer between two semi-infinite media is illustrated in Figure 6.4. The incident radiation from media 1 is partly transmitted to media 2 and partly reflected back. In the layer multiple reflections will occur causing multiple reflected beams back into media 1 and multiple transmitted beams into media 2.

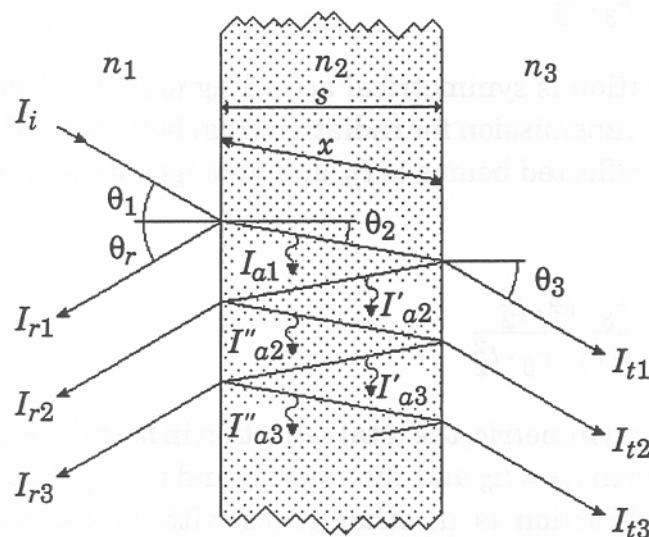


Figure 6.4 The radiation in an optically thick layer between two semi-infinite media.

For a given incident angle θ_1 at the first surface, Eq 6.49 gives the reflection angle θ_r and Eq 6.50 the refraction angle θ_2 which then will be the incident angle at the second surface were the same equation gives the next refraction angle θ_3 . According to Eq 6.49 all waves reflected inside media 2 have the same reflection angle θ_2 , thus all waves transmitted back into media 1 and those transmitted into media 3 have the directions θ_r and θ_3 respectively.

$$a_b = \frac{I_{ba}}{I_{bi}} = \frac{a_2 \cdot t_3 \cdot (1 + r_1 \cdot t_2)}{1 - r_1 \cdot r_3 \cdot t_2^2} \quad (6.62)$$

To meet the requirement of thermodynamic equilibrium we have

$$t + r_f + a_f = 1 \quad \text{and} \quad t + r_b + a_b = 1 \quad (6.63)$$

This relation is sometimes referred to as Kirchoff's law and can be used to replace e.g. Eqs 6.61 and 6.62 in order to save some calculation work.

The above equations must first be determined for each of the *TE* and *TM* waves, then the averages give the final result for a non-polarised wave, e.g. the reflection is given by

$$r = 0.5 (r_{TE} + r_{TM}) \quad (6.64)$$

These averages can not be used in a multi pane window, in which case all panes must be taken into account before the average values are determined.

If the refraction indices vary with wavelength we then have to integrate over the solar spectrum, and by integration over the hemisphere the parameters for diffuse radiation can be found.

6.3.3 Multiple pane windows

Up to now, we have only dealt with single layers surrounded by semi-infinite media. We will now place two or more layers in a combination. The thickness of the layers and the gaps between them are assumed to be small compared to other dimensions so the assumption of infinite reflections is still valid.

For each layer, the above discussed reflection, absorption and transmission will now be referred to as single layer's parameters, thus for the layer *j* alone in its semi-infinite surrounding:

- $r_{f,j}$ = reflection of forward incident radiation
- $r_{b,j}$ = reflection of backward incident radiation
- $a_{f,j}$ = absorption of forward incident radiation
- $a_{b,j}$ = absorption of backward incident radiation
- t_j = transmission of forward or backward incident radiation

As noted above, these parameters should be those for *TE* or *TM* waves, not the average for non polarised radiation.

$$t_c = I_{f,N+1} / I_{f,1} \quad (6.68)$$

$$r_c = I_{b,1} / I_{f,1} \quad (6.69)$$

and the absorption in each layer by Eq 6.67 and

$$a_{c,j} = I_{a,j} / I_{f,1} \quad (6.70)$$

In order to avoid the operations in Eqs 6.68 - 6.70, $I_{f,1} = 1$ can be used as boundary condition.

Transmission through the combination is always symmetrical but reflection and absorption may depend on the direction. In these cases, the same method could be used again but with different boundary conditions.

In Method 2 another common technique is used. The two first layers are combined to a fictive layer with all reflections taken into account in a similar way as in a single layer. We get for this fictive layer

$$t'_1 = \frac{t_1 \cdot t_2}{1 - r_1 \cdot r_2} \quad (6.71)$$

$$r'_1 = r_1 \frac{r_2 \cdot t_1^2}{1 - r_1 \cdot r_2} \quad (6.72)$$

and for each layer under influence of the other layer

$$a'_1 = a_1 \left(1 + \frac{r_2 \cdot t_1}{1 - r_1 \cdot r_2} \right) \quad (6.73)$$

$$a'_2 = \frac{t_1 \cdot t_2}{1 - r_1 \cdot r_2} \quad (6.74)$$

In case of more layers, the first fictive layer is combined in the above way with next layer giving a new fictive layer containing three layers et cetera. However, the complexity in calculation of the absorption in each layer will grow quickly with the number of layers.

In Method 3 a quite different technique, suggested by Källblad, 1973, is to use Eqs 6.65 - 6.67 in a method well suited for computer calculation. Rewriting Eq 6.66 gives

$$I_{f,j} = (I_{f,j+1} - r_{b,j} I_{b,j+1}) / t_j \quad (6.75)$$

Starting by setting $I_{f,N+1}$ to an arbitrarily positive value and $I_{b,N+1} = 0$ we can use the Eqs 6.75, 6.65 and 6.67 in that order for $j = N, N - 1$ et cetera until we get $I_{f,1}, I_{b,1}$ and $I_{a,1}$. Finally we get the overall coefficients with the Eqs 6.68, 6.69 and 6.70.

In ASHRAE (1993), the above quantity is called solar heat gain and is used e.g. when defining the Shading Coefficient.

Most programs assume an empty room when any of the above methods are used, but in some programs a part of the transmitted radiation can be assumed as convective heat gain to the room air. This is an approximate way to treat radiation absorbed in furniture

6.4.2 Direct radiation

Many simulation programs treat the direct radiation within rooms in a simplified way. The simplest is to assume that all radiation transmitted through a window is diffused by curtains etc. This assumption was defended by that the programs were used to estimate cooling load at situations where curtains or blinds always were used. With this assumption, the direct radiation is treated as described above.

As for the diffuse radiation, user defined or calculated time independent factors describing the distribution of the direct radiation are sometimes used. Some programs also treat a part of the transmitted direct radiation as convective heat gain to the room air.

The above simplified methods may introduce great errors, especially as the distribution vary by the solar position. In order to get more accurate results, one must determine in which surfaces the direct radiation is absorbed.

The direct radiation transmitted through a window can primarily hit many surfaces in a building, eventually after transmission through openings or glazed parts of inner walls and doors. How much of the radiation that will hit a specific surface may be calculated in a similar way as shading for a window. For each inner surface, all other surfaces may be shading or partly transparent screens. Thus the primarily incident direct radiation on all surfaces can be determined.

Next problems are the treatment of the absorbed and reflected parts of the primarily hit. Normally the radiation is smoothed out over the whole surface and the reflected part is treated as a diffuse radiative source. This allows treatment of the reflected radiation in the same way as described above for the diffuse radiation. In many cases, this approximation is acceptable, especially if walls, floors and ceilings are divided into small parts.

Caution has to be taken in rooms with large areas having specular reflection, e.g. glazed parts. If the solar altitude is low, most of the direct radiation may be reflected and then transmitted out from the building. Assuming diffuse reflections in these cases may lead to the conclusion that most of the radiation will be absorbed in inner surfaces. However, if one wants to treat specular reflections, an elaborate direct tracing has to be

6.5 Solar processor in DEROB-LTH

6.5.1 Input data to the solar processor

DEROB-LTH uses a climate data file containing hourly values day by day for one year or a period of a year covering the whole period of simulation. Climate data for days preceding and following the simulation period is allowed.

To calculate the solar radiation the DEROB-LTH program needs the following types of input data:

Location of site and time of simulation:

- Latitude of the site , positive to the North and negative to the South of the equator (°)
- Day of the year
- Hour of the day

Hourly values for solar radiation :

- Normal solar radiation (W/m²)
- Diffuse solar and sky radiation on horizontal surface (W/m²)

6.5.2 Solar altitude and azimuth

The position of the sun is calculated for each hour of the day in the middle of each month of the simulation period. The position of the sun is described by

- solar altitude angle $\theta_h = 90 - \theta_z$
- solar azimuth angle θ_a

Consider a coordinate system whose origin coincide with the center of the earth, and its x-y plane describes the equational plane and its z-y plane coincide with the direction of the incoming solar radiation. In this coordinate system the earth rotates about the z axis.

The position of a point on the surface of the earth for a given hour of the day is given by

$$\hat{r} = r_a (\sin \Phi_l \cos \Phi_H \hat{i} + \sin \Phi_l \sin \Phi_H \hat{j} + \cos \Phi_H \hat{k}) \quad (6.78)$$

6.5.3 Incident solar radiation on exterior surfaces

The insolation of solar radiation on exterior surfaces is calculated from measured hourly values of normal solar radiation, I_{DN} , and diffuse solar and sky radiation on horizontal surface, I_{dh} .

The total insolation on exterior surfaces includes three different sources :

- direct solar radiation
- diffuse solar and sky radiation
- direct, diffuse and sky radiation reflected from the ground surface

The calculation of insolation of direct solar radiation is based on the fact that each surface in the building model is divided into a regular grid of 25 elements. To determine the insolation of direct solar radiation on a surface, each of its elements is tested for any obstruction, opaque or transparent, between the center of the grid element and the sun's position. This approximation is used to calculate an effective area, $A_{E,i}$, for each surface i . $A_{E,i}$ is defined as follows:

$$A_{E,i} = \left(\sum_j tr_{ij} \right) \cdot \cos \theta_i \cdot \Delta A_i \quad (6.86)$$

tr_{ij} = progressive transmission through all obstructions between the grid element and the sun's position. For an opaque obstruction like a shading wall $tr_{ij} = 0$.

θ_i = solar incident angle on surface i

ΔA_i = the true area of the grid element of surface i

The insolation of direct solar radiation, I_D , is calculated as

$$I_D = A_{E,i} \cdot I_{DN} / A_i \quad (6.87)$$

A_i = the true area of surface i

The insolation of diffuse solar and sky radiation, I_{d1} , is calculated as

$$I_{d1} = 0.5 \cdot (1 + \cos \theta_t) \cdot I_{dH} \cdot C_{\theta z} \quad (6.88)$$

θ_t = the tilt angle of the surface to horizontal

$C_{\theta z}$ = the direct cosine of the sun in the zenith direction

I_{dH} = diffuse radiation on a horizontal plane

The insolation of solar radiation on a transparent surface is transmitted in two ways depending on the presence of shading devices like curtains or not.

If no shading device is active the transmitted solar radiation includes both a diffuse and a direct component as follows :

$$I_{dt} = 0.92 \cdot t_c \cdot (I_{d1} + I_{d2}) \quad (6.94)$$

$$I_{Dt} = t_{ci} \cdot I_D \quad (6.95)$$

I_{dt} = the transmitted part of insolation of diffuse solar radiation (W/m²)

t_{ci} = the transmittance t_c adjusted for the angle of incidence (-)

I_{Dt} = the transmitted part of insolation of direct solar radiation (W/m²)

If shading device is active, the direct component is treated as a diffuse source and the transmitted solar radiation is calculated as follows :

$$I_{dDt} = 0.92 \cdot k_{ec} \cdot t_c \cdot (I_{d1} + I_{d2} + I_D) \quad (6.96)$$

k_{ec} = a reducing factor for shading device like curtains (-)

I_{dDt} = the transmitted part of insolation of diffuse and direct solar radiation (W/m²)

6.5.5 Internal solar distribution within a zone

Solar radiation taking part in the internal distribution in a zone emanate from two different types of loadings

- diffuse solar radiation transmitted through a transparent surface into the zone
- direct solar radiation transmitted into the zone and reflected at a surface

Both types of loadings will be distributed as a diffuse source as follows:

$$P_{eci} = \sum_j I_{lum,ij} \cdot S_j \quad (6.97)$$

$I_{lum,ij}$ = the illumination factor that describes the fraction of the radiation from the surface j that arrives at surface i after all the reflections have been accounted for. (m²)

S_j = the strength of the loading at surface j (W/m²)

P_{eci} = the radiation received by surface i (W)

6.6 Solar processor in FRES

FRES uses the method from ASHRAE Fundamentals (1985) for the calculation of solar altitude and azimuth from location, day and local time, and is not referred here.

For the calculation of direct and diffuse radiation, a method based upon the cloud cover factor is used, and it is briefly described below. Simple geometry for external shading is also available, and is not described in detail.

6.6.1 Input data to the solar processor

FRES needs data for the location and time to calculate the hourly solar position. For calculation of solar radiation, the cloud cover ($0 < N_{CC} < 10$) is input from a weather file or from a constant value (24-hour simulations). FRES gets cloud cover from a special weather data file, which must be specially produced for new locations. The current version of FRES cannot use measured values for global solar radiation directly.

6.6.2 Solar altitude and azimuth

The method is completely described in ASHRAE Fundamentals and needs no repetition here.

6.6.3 Incident solar radiation on exterior surfaces

On a cloudy day, the Cloud Cover Factor N_{CCF} (Kimura and Stephenson, 1969) is used. The total radiation $I_{H,c}$ on a horizontal surface on a cloudy day is expressed as

$$I_{H,c} = I_H \cdot N_{CCF} \quad (6.98)$$

where I_H is total radiation on a horizontal surface a clear day. N_{CCF} is the cloud cover factor and is expressed by

$$N_{CCF} = k_P + k_Q \cdot N_{CC} + k_R \cdot N_{CC}^2 \quad (6.99)$$

where k_P , k_Q and k_R are constants or dependent of time of year, and N_{CC} is cloud cover ($0 < N_{CC} < 10$). The value k_P is called "Clearness index" and is treated as a site-dependent constant input by the user. k_Q varies as a

6.6.4 Transmitted solar radiation

A window is modelled as a single surface with direct transmittance t_{dir} and equivalent absorptance a_{eq} . Equivalent absorptance is calculated from the values for total and direct transmittance found in the manufacturer's data for any multi-pane window construction.

The angular dependence of the absorptance and transmittance is modelled using the coefficients for DSA Glass (ASHRAE Fundamentals, 1985).

Transmitted and absorbed solar heat load is calculated for every facade of every window in the building model. Absorbed heat is added directly to the window surface. Transmitted heat to each room is summed for every window facing away from a window facade. In case of inner facades, the heat taken from windows with facades facing towards the room is subtracted. A warning is issued if more than 30% direct transmitted heat is subtracted (retransmitted).

Windows facing towards other rooms are treated as outer facades in this first step of the calculation. Reduction in incident radiation of inner facades due to other windows must be done manually by providing some constant shading. Room geometry must be individually modelled for each facade by specifying overhang, side-fins and front obstruction.

6.6.5 Internal solar distribution within a zone

The net transmitted heat load is distributed to the surfaces by two artificial reflections.

1. Net transmitted radiation is focused only to the opaque surfaces, and a fraction (specified for the room) is evenly must be taken to have big enough opaque surfaces. The rest is reflected. Default value of the absorptance factor is 0.7.
2. Net reflected from 1. is evenly distributed to all surfaces. Opaque surfaces absorb all heat, and windows absorb a fraction $1-TU$, where TU is the mean resulting direct transmittance for all windows. The rest is "lost" from the model. Re-transmittance at this stage leaves the model even for windows with inner facades.

6.7 Solar processor in SUNREP (TRNSYS)

SUNREP computes the distribution of solar radiation into a room. Another program, the solar processor, computes the solar energy entering the room through the windows.

The solar processor used for the Shoebox test (see section 6.10) is the solar processor of MODPAS, a thermal simulation program. This processor is derived from the TRNSYS processor, based on J.A.Duffie and W.A.Beckman (1974).

6.7.1 Input data to the solar processor

For calculation of the solar radiation the following data are used by the solar processor.

- θ_l = Latitude of the site (North positive) ($^{\circ}$)
- A_g = Surface albedo (-)
- N_d = The day of the year, the julian day (1 - 366) or the day of the month and the month
- H = The hour of the day (1 - 24)
- I_{DH} = Horizontal direct solar radiation (W/m^2)
- I_{dH} = Horizontal diffuse solar radiation (W/m^2)
- θ_v = South azimuth of the surface (South = 0, -90 = East, +90 = West) ($^{\circ}$)
- θ_t = Angle between the horizontal and the surface (the slope) ($^{\circ}$)
- S_c = Shading coefficient of the window glass (=1 for a clear 3 mm glass)

In the solar distribution program input data are needed for the room, windows, subdivisions of walls (panels) and obstructions.

The rooms are defined by the geometry and the front wall azimuth. The windows are defined by number, geometry and position in the walls. The glass can be transparent or partly translucent (diffusing glass).

The walls are defined by geometry and position. Each wall can be paneled to refine the distribution. Internal windows between zones can be treated as panels: they have a coefficient of absorption of 0.90 and a coefficient of specular reflection of 0.10. With these values the solar energy absorbed by the window is the sum of the energy absorbed by the glass (— 0.10) and the energy passing through the glass (— 0.90) and entering another room.

The surfaces for each wall and panel are defined by two coefficients: one coefficient of absorption of the light and one coefficient of specular reflection. A perfect diffusing surface has a specular reflection of zero.

θ_i = Angle of incidence of beam radiation on the surface ($^\circ$)

The direct and diffuse incident solar radiation is calculated as

$$I_{Di} = \text{MAX} (0 , \cos \theta_i / \cos \theta_z) \cdot I_{DH} \quad (6.117)$$

$$I_{di} = R_d \cdot I_{dH} + R_g \cdot (I_{DH} + I_{dH}) \quad (6.118)$$

where

I_{DH} = Horizontal direct solar radiation (W/m^2)

I_{dH} = Horizontal diffuse solar radiation (W/m^2)

I_{Di} = Incident direct solar radiation on the surface (W/m^2)

I_{di} = Incident diffuse solar radiation on the surface (W/m^2)

The ratios R_d and R_g are given by

$$R_d = 1 + \cos \theta_t / 2 \quad (6.119)$$

$$R_g = \rho \cdot (1 - \cos \theta_t / 2) \quad (6.120)$$

6.7.4 Transmitted solar radiation

The transmitted and absorbed solar radiation is calculated in accordance with Stephenson (1965).

For the direct solar radiation, we have

$$t_D = - 0.00885 + 2.71235 \cos \theta_i - 0.626062 (\cos \theta_i)^2 - 7.07329 (\cos \theta_i)^3 + 9.75995 (\cos \theta_i)^4 - 3.89922 (\cos \theta_i)^5 \quad (6.121)$$

$$a_D = - 0.01154 + 0.77674 \cos \theta_i - 3.94657 (\cos \theta_i)^2 + 8.57881 (\cos \theta_i)^3 - 8.38135 (\cos \theta_i)^4 + 3.0118 (\cos \theta_i)^5 \quad (6.122)$$

where

t_D = Direct solar transmittance: solar radiation through a single glass (clear 3 mm)

a_D = Direct solar absorptance: solar radiation absorbed in a single glass (clear 3 mm)

6.7.5 Internal solar distribution within a zone

The direct solar radiation distribution is computed for each wall, panel and window for each hour of a day. Generally the calculation is made for one day in the month. A typical computing gives the direct solar distribution of the middle day of the 12 months of a year and one diffuse solar distribution for the year (independent of the hour and the day).

The results can be stored in files. The solar distribution files can be integrated in thermal simulation programs. The thermal simulation program calculates, with its own solar processor, the solar energy entering the room through the windows. The program SUNREP only distributes this solar energy on the internal surfaces.

The windows are divided into a number of rectangular subsurfaces. Two different calculations are made: one each hour of each day for the direct radiation, one for the diffuse radiation.

For the direct solar radiation, all the rays are parallel, for the diffuse solar radiation an hemisphere (the sky) is divided in 208 elements (isotropic diffuse solar distribution).

The attenuation due to the angle of incidence of the sun rays on the window glass can be included (angle modifier factor: algorithms of Stephenson, see chapter 6.7.4)

The method of calculation is a simplified ray tracing technique. The intersection between a ray entering the room and an internal surface (walls, panels or opposite windows) is geometrically calculated (three-dimensional). The sun ray striking a surface is divided into three parts:

- the absorbed part
- the diffuse reflected part
- the specular reflected part

All the surfaces are considered as composite reflecting elements. The coefficient of absorption and the coefficient of specular reflection determine the three parts.

- compound reflection
- diffuse reflection
- specular reflection

The solar energy which is not absorbed by the first stroked surface is reflected diffusely on all the other internal surfaces and is reflected as a beam to one surface. The second reflection is always diffuse. The diffuse reflection is calculated with the method of the view factors between the stroked surface and the other internal surfaces.

6.8 Solar processor in TSBI3

6.8.1 Input data to the solar processor

Climate data to be used by TSBI3 must exist in a special binary format. Data supplied as ascii-files can be converted to this binary TSBI3-format by use of the TRYCVE program developed by the Danish Building Research Institute.

The climate must be described by hourly values, day by day for the whole year, or day by day for periods of the year. The extension of the climate file must be *.TRY.

For calculation of the solar radiation the following data are used by TSBI3:

Location of the site the climate data belongs to:

- Latitude of the location, θ_l ($^\circ$), positive to the North
- Longitude of the location, θ_g ($^\circ$), positive to the East
- Standard time meridian. (hours). positive to the East.

Data concerning solar irradiation:

- Direct radiation at normal incidence, I_{DN} (W/m^2)
- Diffuse sky radiation on horizontal, I_{dH} (W/m^2)
- Cloud cover (octas) scale 0-8 or fraction, N_c (-).

The radiation and cloud cover data used by TSBI3 can be calculated by the TRYCVE program from any pair of solar data of which one excludes the diffuse sky radiation and the other includes the diffuse radiation.

TSBI3 uses the cloud cover for determination of the distribution of the diffuse solar radiation.

6.8.2 Solar altitude and azimuth

The position of the sun in relation to the building to be simulated is calculated hour by hour for one day (the 3rd day) in each week of the year, according to algorithms by Lund (Lund, 1977). The position is described by the sun's height angle over the horizon and its azimuth, the angle from north of the sun's beam projection on the horizontal plane.

The equation of time is estimated for the relevant day number of the year from:

$$\cos \theta_\alpha = -(\sin \theta_l \cdot \cos \theta_d \cdot \cos \theta_{ts} + \cos \theta_l \cdot \sin \theta_d) / \cos \theta_h \quad (6.131)$$

The position of the sun is calculated for every half hour of the third day in each week of the year.

The times for sunrise and sunset are also calculated, as well as the optical solar height $\theta_{h,opt}$ in which the real solar height is adjusted for the refraction in the atmosphere, according to the following:

$$\text{For } \theta_h > -0.005 \text{ rad} \quad \theta_{h,opt} = \theta_h + 0.0000225 / (\theta_h + 0.23) \quad (6.132)$$

$\theta_{h,opt}$ is the optical solar height (rad)

θ_h is the solar height (rad)

6.8.3 Incident solar radiation on exterior surfaces

The *total solar irradiance* on a surface is regarded to consist of 3 contributions, i.e.:

direct solar radiation (from the sun), I_{DN}

radiation from the sky (diffuse sky radiation), I_{dH}

reflected radiation from the surface of the ground, I_{Ag}

The *direct solar radiation* on a sloping surface can be calculated from the radiation at normal incidence:

$$I_{D,\theta_i} = I_{DN} \cdot \cos \theta_i \quad (6.133)$$

$\cos \theta_i$ is the cosine to the angle of incidence, calculated from:

$$\cos \theta_i = \cos (\theta_\alpha - \theta_w) \cdot \cos \theta_h \cdot \sin \theta_t + \sin \theta_h \cdot \cos \theta_t \quad (6.134)$$

θ_α is the solar azimuth angle (°)

θ_w is the orientation of the surface (°)

θ_h is the solar height angle (°)

θ_t is the slope of the surface, measured from horizontal (°), tilt angle

When the optical solar height is negative, the direct radiation is set to zero.

The *diffuse radiation* on a sloping surface I_{d,θ_i} can be expressed (Petersen, 1982) in comparison with diffuse radiation on the horizontal I_{dH} , with a factor f :

$$I_{d,\theta_i} = f \cdot I_{dH} \quad (6.135)$$

For surfaces, the direct solar radiation is set to 0 at times (in half-hours) where the sun is positioned lower than the defined sky-line. For windows, the direct radiation is adjusted by the fraction of the window being in the shade of the shadow or sky-line.

Like all other "systems" in TSBI3 a shadow is connected to a *schedule* for which it is possible to describe variations in the shading coefficient over the day and over the year.

Building obstructions, *overhang and side fins* are specified, which can shade for solar irradiation on a window. It can be described as a horizontal overhang which juts out over the window or vertical side fins at the left hand or right hand side of the window (or both), seen from face 2 (i.e. normally from outside).

Data for overhang and side fins are used for calculation of shading of the direct and the diffuse radiation. During definition of overhangs, which are large in comparison with the dimensions of the glazing, uncertainty is increased regarding the calculated solar irradiation, amongst other things because it does not make allowance for reflection of radiation from the overhangs.

The *total solar irradiation* on exterior surfaces is the sum of the contributions from direct sun radiation, diffuse sky radiation, and radiation reflected from the ground, calculated from the expressions above:

$$I_{tot,\theta_i} = I_{D,\theta_i} + I_{d,\theta_i} + I_{Ag,\theta_i} \quad (6.142)$$

6.8.4 Transmitted solar radiation

The transmission of the direct solar radiation through windows is calculated (Johnsen and Grau, 1994) from the coefficient for transmission at normal incidence from:

$$f_{\theta_i} = f_{(\perp)} \cdot (1.0 - 0.04 \cdot (\theta_i/100) - 2.933 \cdot (\theta_i/100)^6 + 2.13 \cdot (\theta_i/100)^{12}) \quad (6.143)$$

$f_{(\perp)}$ is the transmission coefficient for direct solar radiation at normal incidence

θ_i is the angle of incidence (°)

The transmission of the diffuse solar radiation is simply calculated as

$$f_d = 0.9 \cdot f_{(\perp)} \quad (6.144)$$

f_d is the transmission coefficient for diffuse solar radiation

To surfaces is the part of the radiation distributed between the individual constructions in the floor, walls and ceiling. The total solar radiation is distributed according to a "distribution key" which expresses the relative solar intensity (W/m^2) to floor, walls and ceiling respectively.

The parameter "*max to other zones*" is only relevant for windows in internal walls, and is described in the following section.

6.8.6 Internal solar distribution between zones

The program calculates principally the solar radiation through a window in an internal wall, as if it were placed in an external wall. The solar radiation which strikes the window in the internal wall must first pass through the windows in the zone in front and often it is only a small part of the solar radiation to the first zone, which passes on. How great an amount will pass on is calculated on the basis of the following:

Size and orientation of the windows, transmittance for radiation through the windows in the outer wall and in the internal wall, as well as data for "overhang" and "side fins" around the internal window and the shadows from this.

A pre-requisite for the solar radiation being calculated with an acceptable accuracy is therefore that the geometric conditions and the total shading effect of the zone which lies in front of the internal window, can approach the effect of the overhang, side fins and shadows on the window. The ceiling in the zone in front must thus be described as an overhang over the internal window, the walls and side fins or shadows, whilst other shading elements, for example, minor wall surfaces, window bars etc., in the outer walls must be taken account of as a reduction in the total transmittance of solar radiation which both passes through the external zone and through the internal window.

Max to other zones is a parameter for definition of how great a part of the solar radiation in the current zone can as a maximum be assumed to pass through internal windows to adjacent zones.

Under certain conditions, the program can calculate the solar radiation through windows in internal walls. As this calculation of the solar radiation will often be encumbered with a relatively large uncertainty, this parameter is used to ensure that calculation errors do not lead to results which are physically impossible, for example, a zone which 'passes on' more solar energy than it receives itself.

When clipping polygons, two polygons are involved at a time. The polygon to be clipped is referred to as the *subject polygon* and the clipping polygon as the *clip polygon*. In the case of shadings on a window, the window is the subject polygon, and the shading polygon is the clip polygon.

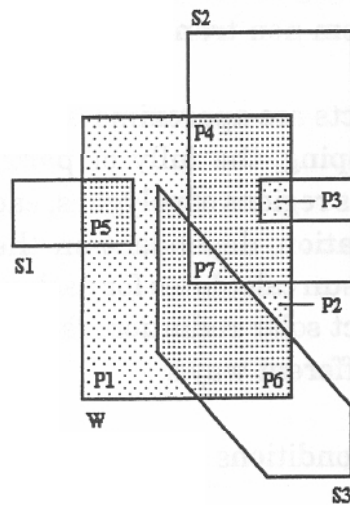


Figure 6.7 Region and polygons.

An area of a certain property, e.g. the radiated part(s) of a window, is referred to as a *region*. A region is described as a collection of zero, one or more non-overlapping polygons.

In Figure 6.7 the window polygon W is partly shaded by the convex polygons S1 and S3, and the concave polygon S2. If all the shadings are opaque, the resulting radiated region consists of the polygons P1, P2 and P3. However, if the shading polygons are transparent, the resulting radiated region consists of the polygons P1, P2, P3, P4, P5, P6 and P7.

The factor of transparency for a resulting polygon is the product of the factor of transparency of the overlapping polygons. The factor of transparency for P7, for example, will be the product of the factors of transparency for P4 and P6.

6.9.3 Application

An algorithm for clipping a concave polygon to the boundaries of another concave polygon has been developed in the context of hidden surface removal for applications in Computer Graphics (Weiler and Altherton, 1977) and (Rogers, 1985). The same algorithm can be used when determining shaded regions of windows or solar collectors.

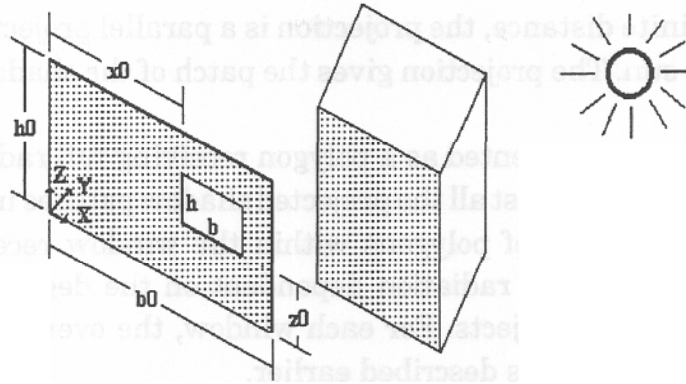


Figure 6.8 Coordinate system, definition of windows and shading objects.

3. Definition of the windows in the wall, i.e. the position of the windows in the wall and their shape. The window can be defined as any polygon or circular shape. The position of the window, as well as the overhang and side fins are defined according to the measures indicated in Figure 6.9. The overhang and side fins can be transparent in any degree.

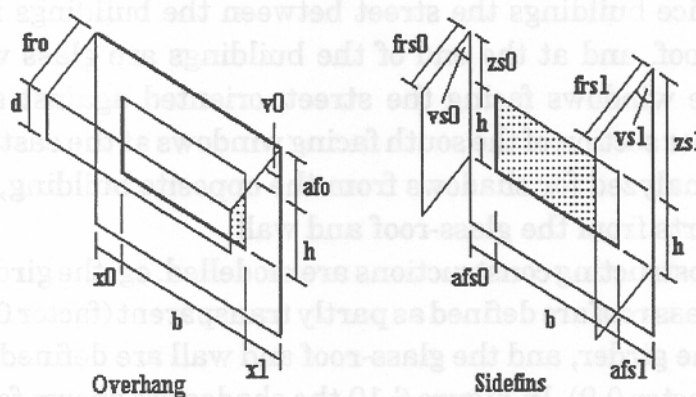


Figure 6.9 Definition of window overhang and sidefins.

4. Definition of remote shading objects. Each object is approximated by a number of plane polygons, each of which is attached with a factor of transparency. The polygons are defined in the chosen coordinate system, cf. Figure 6.8.

Calculation of incident solar radiation on windows is a complex problem to handle. It includes the following tasks:

First, the position of the sun is calculated for a certain day of the year at a given time. According to the sun's position, the shading objects are projected onto the surface with the windows (or solar collectors). As the

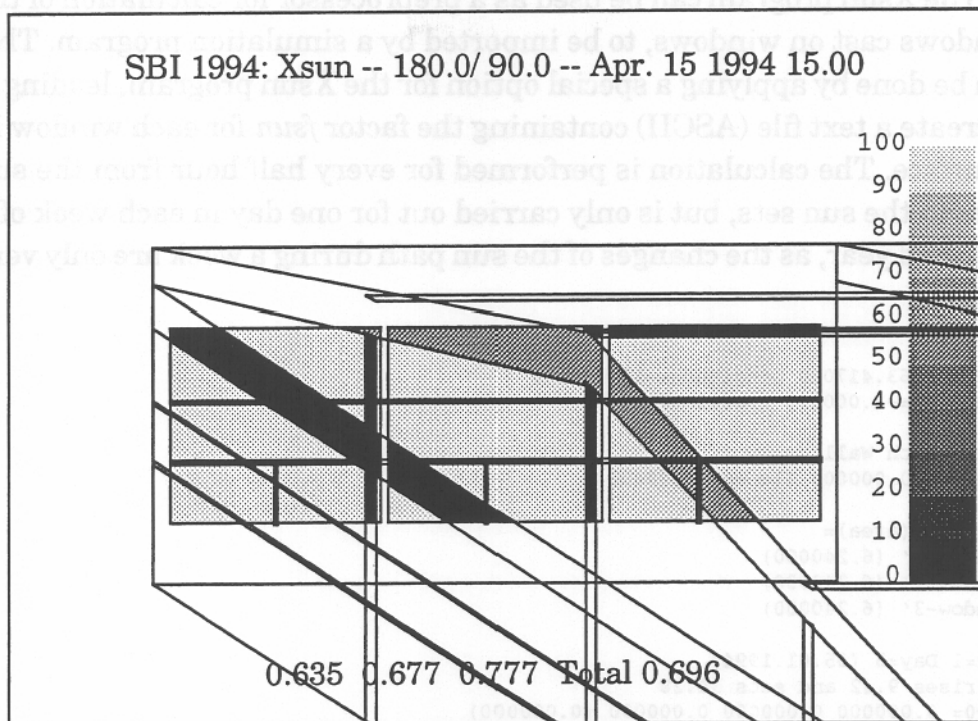


Figure 6.10 Shadings on windows in facades to overglassed street.

6.9.5 Shadow calculations for thermal simulation programs

In thermal simulation programs the calculation of shadows cast by exterior objects on the windows are often relatively crude. The same is the case for shadows caused by the surroundings nearby the windows, approximated by side fins and overhang. This, of course, also leads to inaccurate calculations of the direct solar irradiation on the windows, and thus, a crude prediction of the solar heat gains.

Many thermal simulation programs do not allow for definition of the surroundings in great detail, and therefore, implementation of more precise algorithms in the programs can not improve the precision of the shadow calculations without extending the data input considerably. However, by performing the shadow calculations through a detailed program, external to the simulation program, and later importing the results into a simulation program, a better precision without extending the data input needed for the simulation program can be obtained. Extending a simulation program with ability for importing a file is rather simple compared to extensions with more complicated input and implementation of new and more complicated calculation algorithms.

6.10 The shoebox study

This study was made in order to compare different methods of calculating the solar radiation and its distribution in a sunspace and a building connected to the sunspace. Calculations have been made for a simple room with two windows to the south and then for the same room combined with a sunspace in front of the south facade.

6.10.1 Description of the shoebox

The basic geometry of the studied building is the same as used in IEA Task 12B/Annex 21C, in the BESTEST study (Judkoff and Neymark). This building only consists of one room with two large windows to the south. The room is 48 m² and the windows are each 6 m² and double glazed, see Figure 6.12.

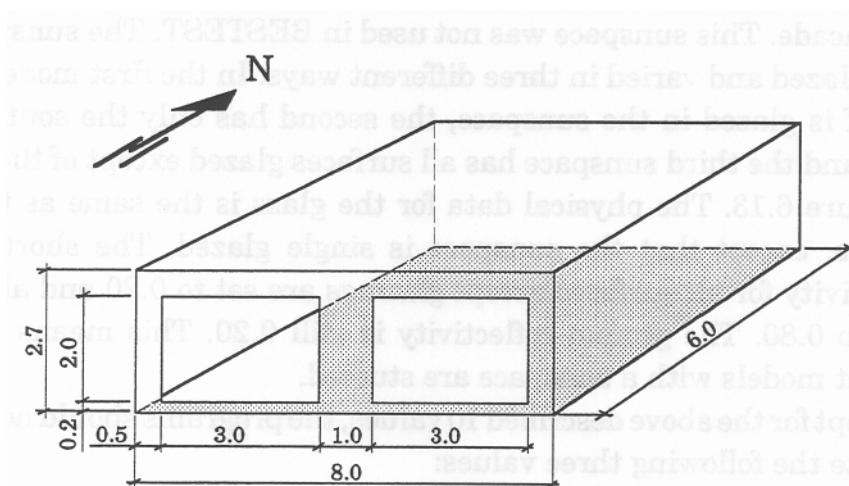


Figure 6.12 The shoebox.

The absorptivity of short wave radiation was set to 0.5 for all surfaces except glazings. Each pane of the window has the absorptance 0.06, reflectance 0.08 and transmittance 0.86 at perpendicular incidence. The ground reflectivity was set to 0.20.

The used simulation programs (FRES, DEROB-LTH, TSBI3 and TRNSYS/SUNREP) were to give hourly values of the following.

- P_{tot} total incoming short wave radiation to the outside of the windows (W)
- P_{trans} total short wave radiation transmitted to the room (W)
- P_{net} the part of P_{trans} that stays in the room. (%)

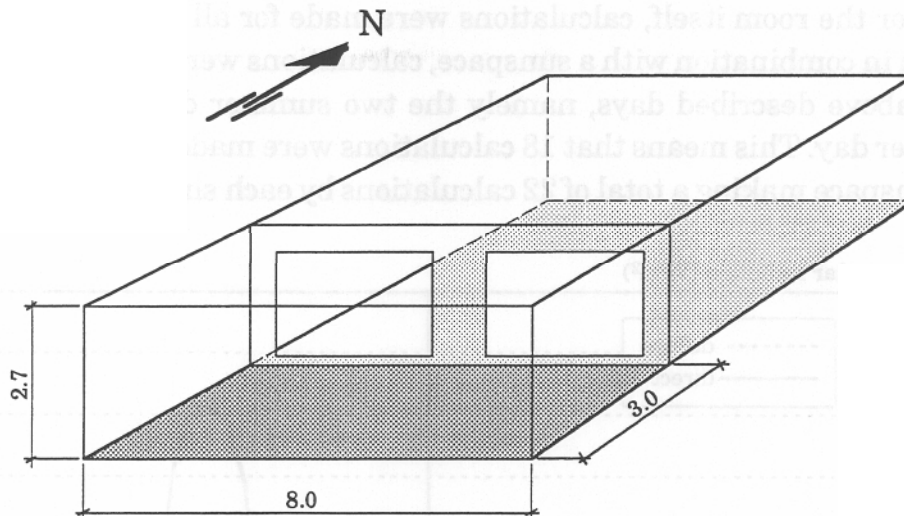


Figure 6.13 The shoebox with a sunspace.

A certain amount of solar radiation is hitting the outside of the sunspace. A part of this is transmitted into the sunspace, some of this is reflected out again, some passes through into the room behind and the rest is absorbed in the sunspace. A part of the radiation that is transmitted to the room is reflected out into the sunspace again and the rest is staying in the room. The net radiation is the part of the solar radiation that is staying in the sunspace, alternatively the room, and then used in the energy balance in order to calculate temperatures, energy needs and so on. In this study we are just comparing the calculation of the distribution of solar radiation to different volumes and surfaces. There are no calculations made of temperatures or energy needs.

6.10.3 Climatic data

Climatic data from Copenhagen, Denmark, is used, two winter days and two summer days from the Danish Test Reference Year (TRY). The latitude for Copenhagen is 56.0°N . One clear day and one overcast day were chosen for each season. The 19th and the 22nd of December are chosen as winter days, see Figure 6.14 showing the solar radiation. The 19th of December is a totally cloudy day with only diffuse solar radiation and the 22nd of December is a clear winter day. In Figure 6.15, the solar radiation in the overcast summer day (19th of May) and the clear summer day (7th of June), is shown.

6.10.4 Results for the shoebox without a sunspace

At the different programs first calculated the solar radiation hitting the two windows when no sunspace was placed in front of the building. The transmitted solar radiation and its distribution to different surfaces in the room were also calculated. Only some examples are shown in this chapter.

In Figure 6.16 the total solar radiation hitting the outside of the two windows during the clear winter day is shown. The sum of the total solar radiation hitting the windows during the day is 37.1 kWh according to TSBI3, 36.8 kWh with DEROB-LTH, 34.3 kWh with TRNSYS and 32.5 kWh with FRES.

In Figure 6.17 the transmitted solar radiation is shown. The transmitted radiation is 27.3 kWh calculated with TSBI3, 27.2 kWh by DEROB-LTH, 26.3 kWh by TRNSYS and 25.0 kWh by FRES during the clear winter day.

When the weather is clear, that is when the solar radiation contains both a direct and diffuse part of radiation, the part of solar radiation hitting a specific surface in a room will vary during the day. In Figure 6.18 the part of the transmitted solar radiation hitting the floor in the room during the clear winter day is shown. The four different programs estimate that about 25-35% of the transmitted solar radiation will hit the floor. TSBI3 and FRES have constant values during the day and TRNSYS/SUNREP and DEROB-LTH have hourly variations. The part that hits the west wall in the room is shown in Figure 6.19. The difference between the programs is considerable. The solar radiation will directly hit the west wall in the morning and the east wall in the afternoon. Note that in TSBI3, the distribution factors are input data, i.e. they are defined by the user.

During the clear summer day, the solar radiation is more intense. However, as the sun in the middle of the day is higher up in the sky, the resulting incident radiation to the vertical windows is not higher than in the middle of the winter day. The total incident radiation during a day is however much higher in the clear summer day than in the winter day, as the sun is shining several more hours per day. In Figure 6.20 the total solar radiation hitting the outside of the windows is shown. In this case, TRNSYS and DEROB-LTH give almost the same results, TRNSYS 55.0 kWh during the day and DEROB-LTH 54.4 kWh. TSBI3 gives the highest value, 58.4 kWh and FRES the lowest, 49.6 kWh. There is also a time difference of 1 hour between TSBI3 and the other programs, which also is seen in other calculation cases.

The transmitted radiation is shown in Figure 6.21 and here TRNSYS is the highest with 37.0 kWh, TSBI3 35.6 kWh, DEROB-LTH 34.7 kWh and FRES 34.3 kWh.

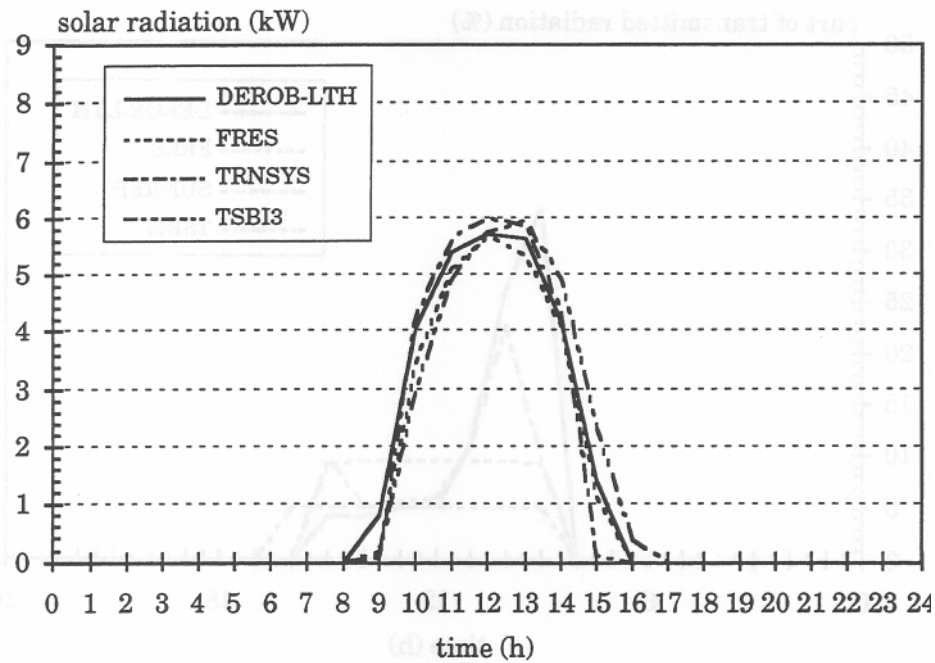


Figure 6.17 Transmitted solar radiation through the two windows during the clear winter day.

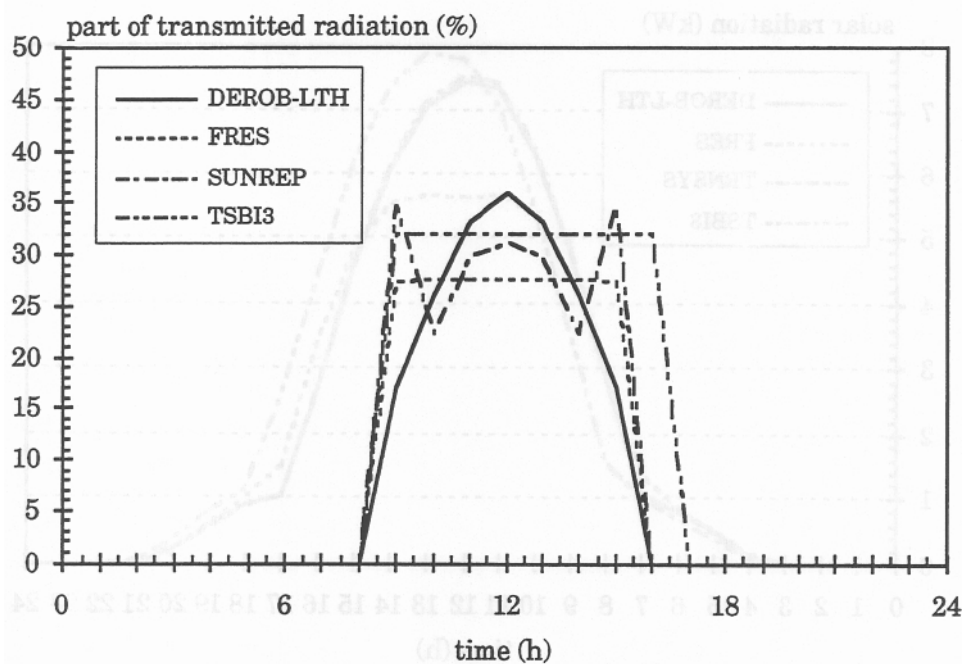


Figure 6.18 Part of the transmitted radiation hitting the floor of the shoebox during the clear winter day.

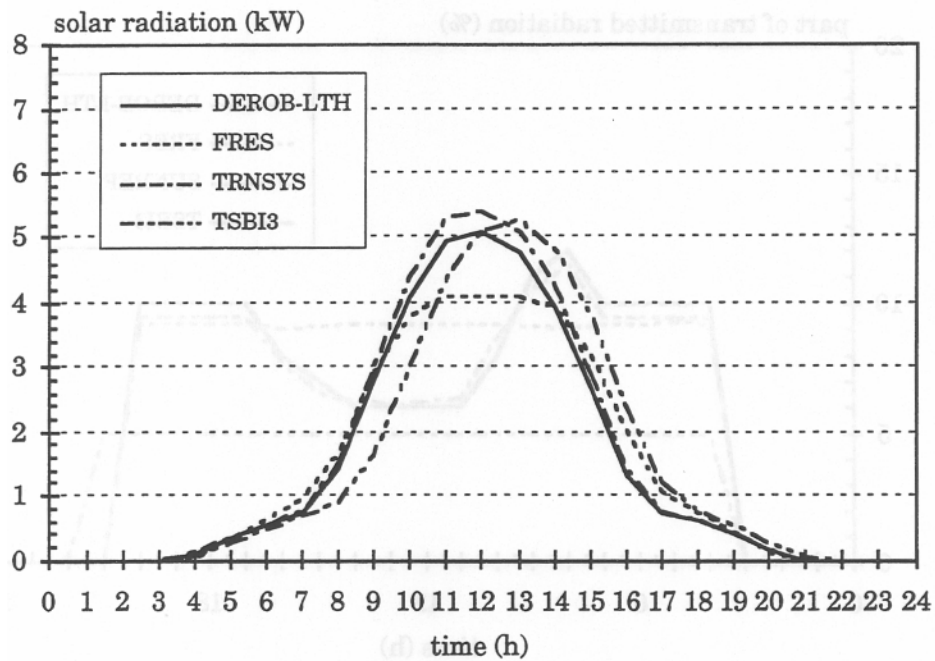


Figure 6.21 Transmitted solar radiation through the two windows during the clear summer day.

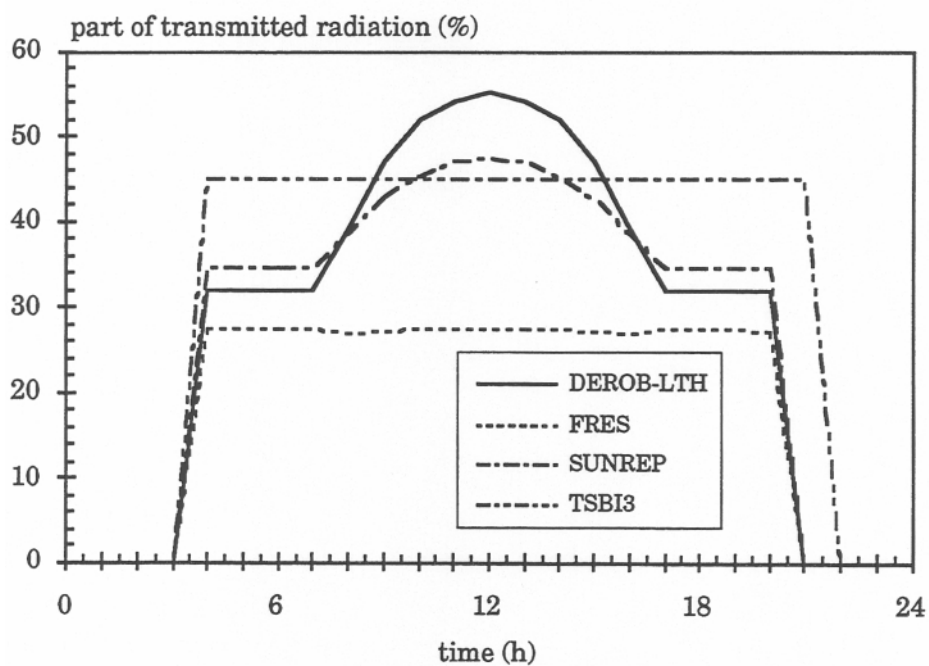


Figure 6.22 Part of the transmitted radiation hitting the floor of the shoebox during the clear summer day.

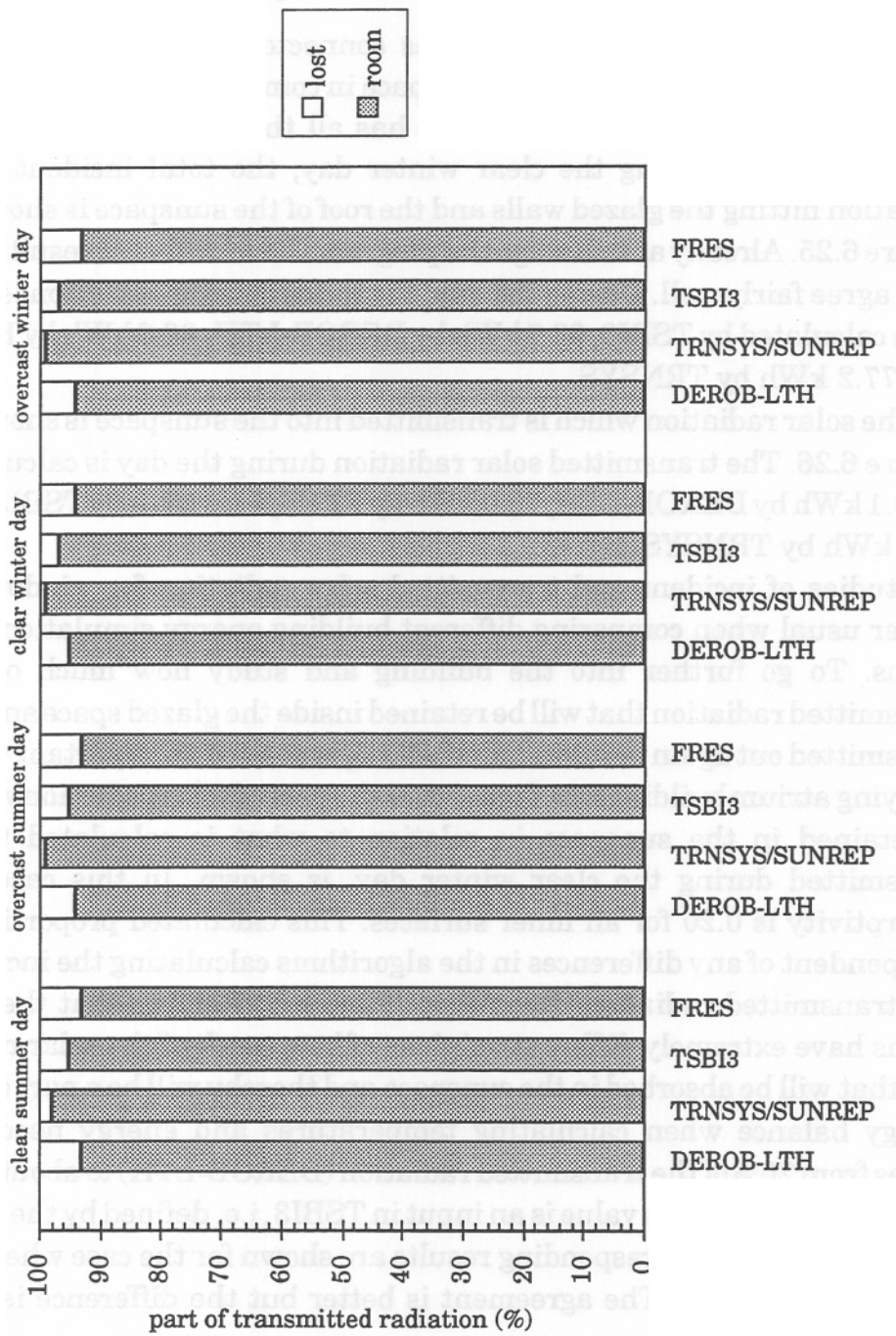


Figure 6.24 Solar energy balances for the shoebox.

the clear winter day is calculated to be 14.7 kWh by DEROB-LTH. By TRNSYS/SUNREP it is 21.9 kWh, by TSBI3 33.7 kWh and by FRES 42.4 kWh. With a higher absorptivity, 0.80, the result from TRNSYS/SUNREP is 29.8 kWh absorbed solar radiation, DEROB-LTH 32.7 kWh, TSBI3 42.3 kWh and FRES 46.2 kWh. The differences are smaller with a higher absorptivity. If everything would have been absorbed, the absorbed solar radiation would have been the same as the transmitted radiation.

The total solar energy balance, calculated for the clear winter day is shown in Figure 6.31. The transmitted solar radiation into the sunspace is defined as 100%. This is then divided into the part that is absorbed in the sunspace, the part that is absorbed in the room and the part that is lost to the outside by short wave radiation. The difference is very large between the programs as shown also in earlier figures.

The corresponding calculations for the clear summer day have also been made. In Figure 6.32 the calculated solar radiation hitting the outside of the sunspace with all surfaces glazed, is shown. It is almost impossible to see more than three curves, depending on that TRNSYS and DEROB-LTH have almost the same result. The total incident solar radiation during the day is calculated to 413 kWh by FRES, 387 kWh by TSBI3, 382 kWh by DEROB-LTH and 379 kWh by TRNSYS. In Figure 6.33 we can see that the difference is larger between the programs when calculating the transmitted radiation. The transmitted solar radiation is calculated to 354 kWh by FRES, 302 kWh by DEROB-LTH, 294 kWh by TSBI3 and 270 kWh by TRNSYS. Even if this should be acceptable, the difference between the calculated absorbed solar radiation in the sunspace is not, see Figure 6.34. This calculations are made for light surfaces, i.e. when the short wave absorptivity is 0.20. In Figure 6.35 the absorptivity is 0.80. In this case FRES and TSBI3 has similar results as well as TRNSYS/SUNREP and DEROB-LTH. Note that the percentage part of the transmitted solar radiation that will be absorbed in the sunspace and not lost to the outside, is input data in TSBI3. This means that the user has to make an assumption or use calculation results from other programs.

If the results are shown as absorbed solar energy during the summer day, it becomes obvious that the contribution from the sun is differing very much, see Figure 6.36 and 6.37. In Figure 6.36 the absorptivity is 0.20 and in this case the total solar radiation absorbed during the day is 63.9 kWh by DEROB-LTH, 102.2 kWh by TRNSYS/SUNREP, 176.4 kWh by TSBI3 and 267.5 kWh by FRES. With the absorptivity 0.80 the absorbed radiation is 145.3 kWh by TRNSYS/SUNREP, 165.5 kWh by DEROB-LTH, 213.3 kWh by TSBI3 and 291.6 kWh by FRES.

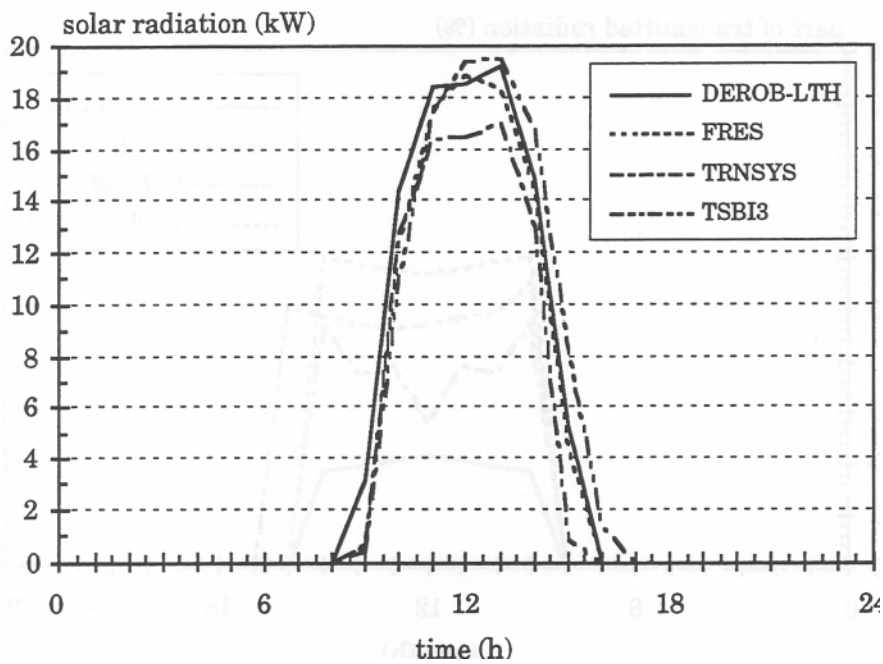


Figure 6.25 Incident solar radiation for the sunspace with all surfaces glazed during the clear winter day.

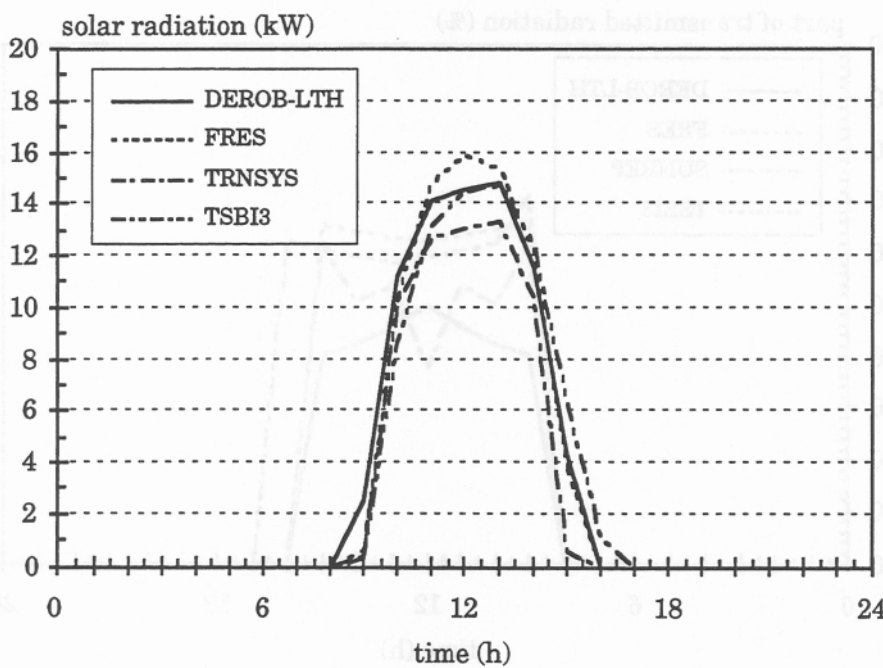


Figure 6.26 Solar radiation transmitted to the sunspace with all surfaces glazed during the clear winter day.

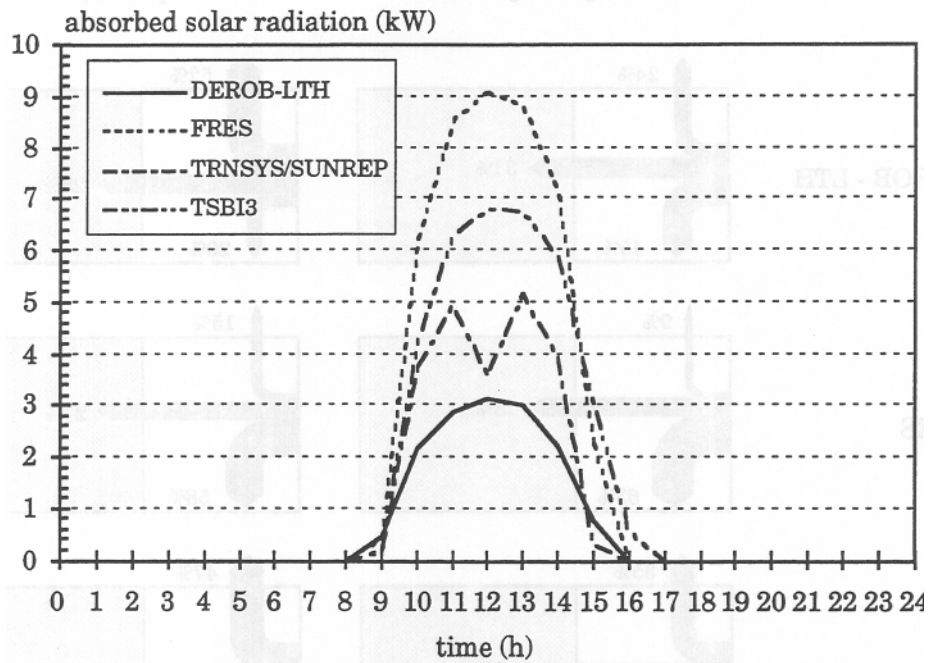


Figure 6.29 Absorbed solar radiation in the sunspace during the clear winter day. Absorptivity = 0.20.

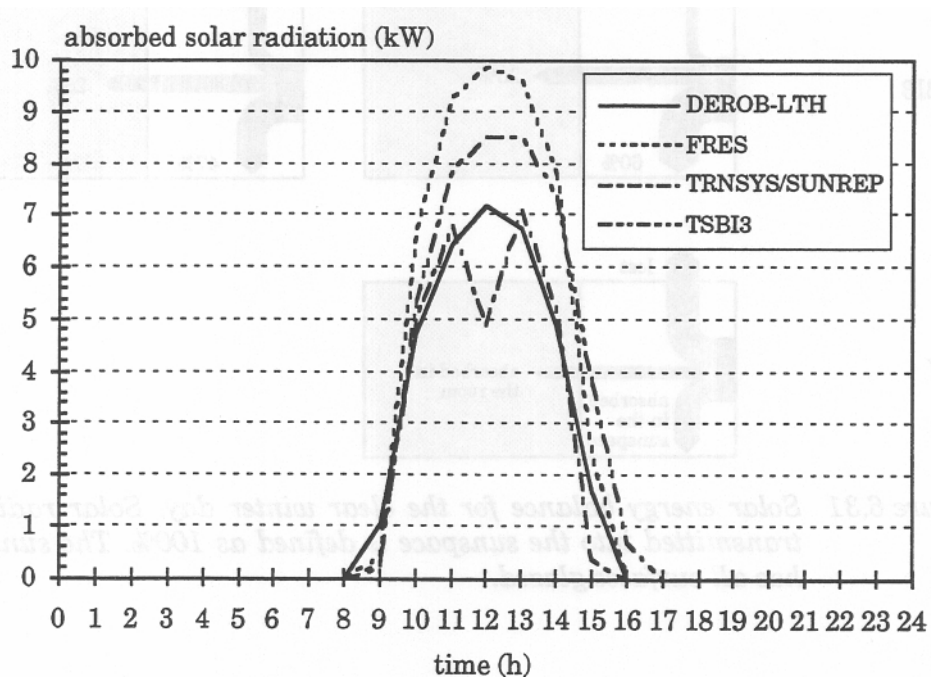


Figure 6.30 Absorbed solar radiation in the sunspace during the clear winter day. Absorptivity = 0.80.

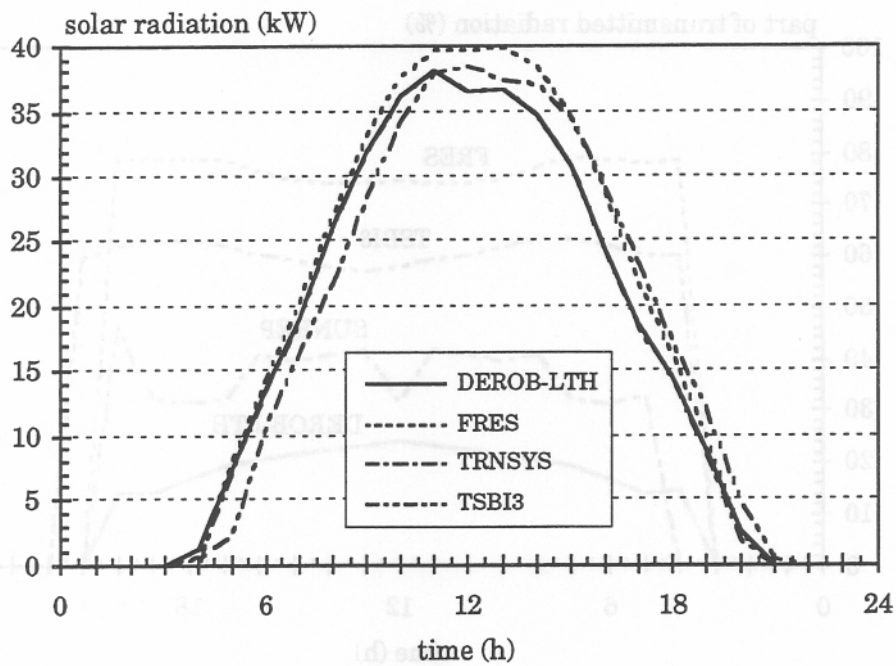


Figure 6.32 Incident solar radiation for the sunspace with all surfaces glazed during the clear summer day.

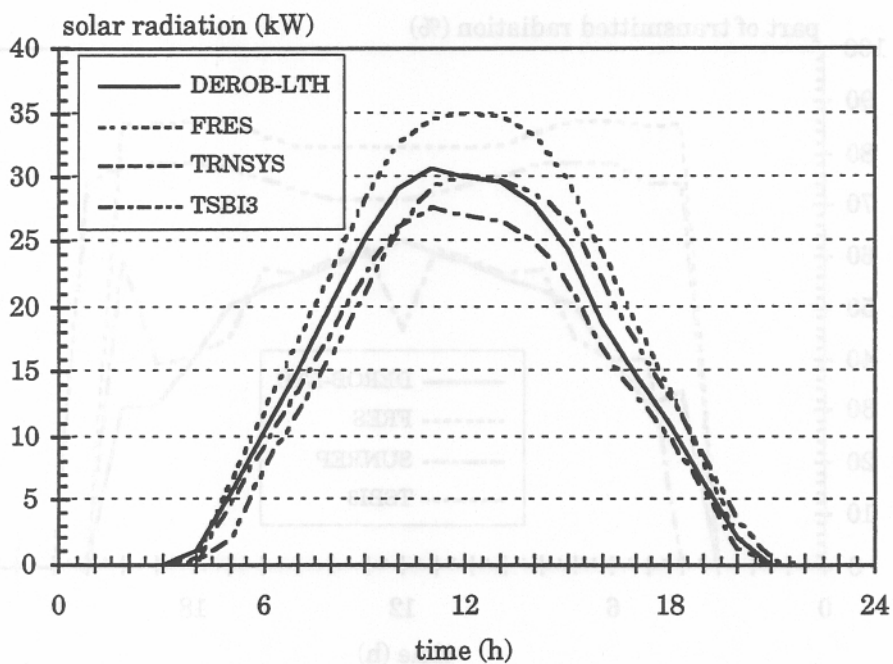


Figure 6.33 Solar radiation transmitted to the sunspace with all surfaces glazed during the clear summer day.

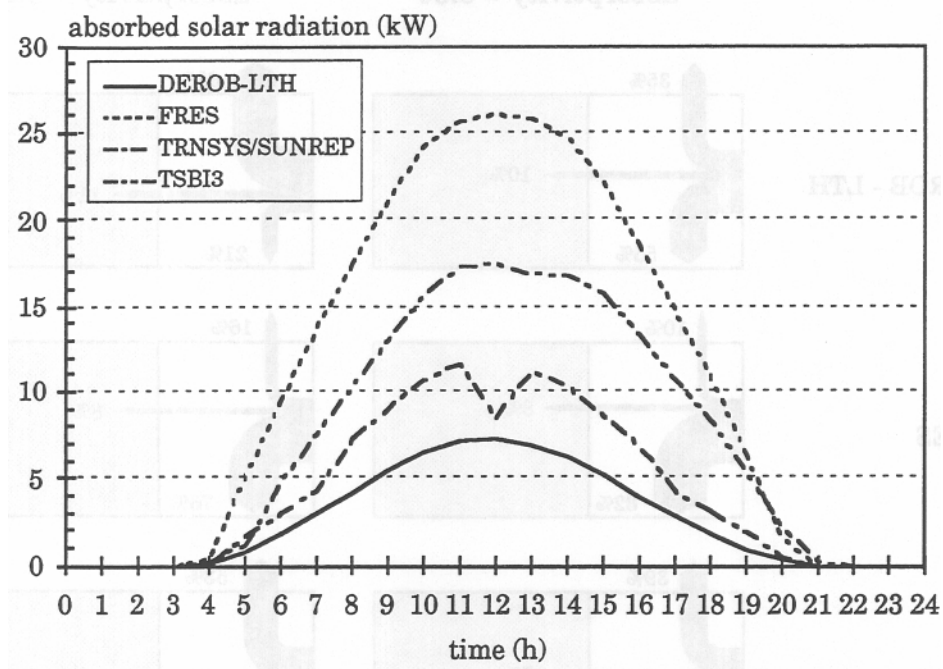


Figure 6.36 Absorbed solar radiation in the sunspace during the clear summer day. Absorptivity = 0.20.

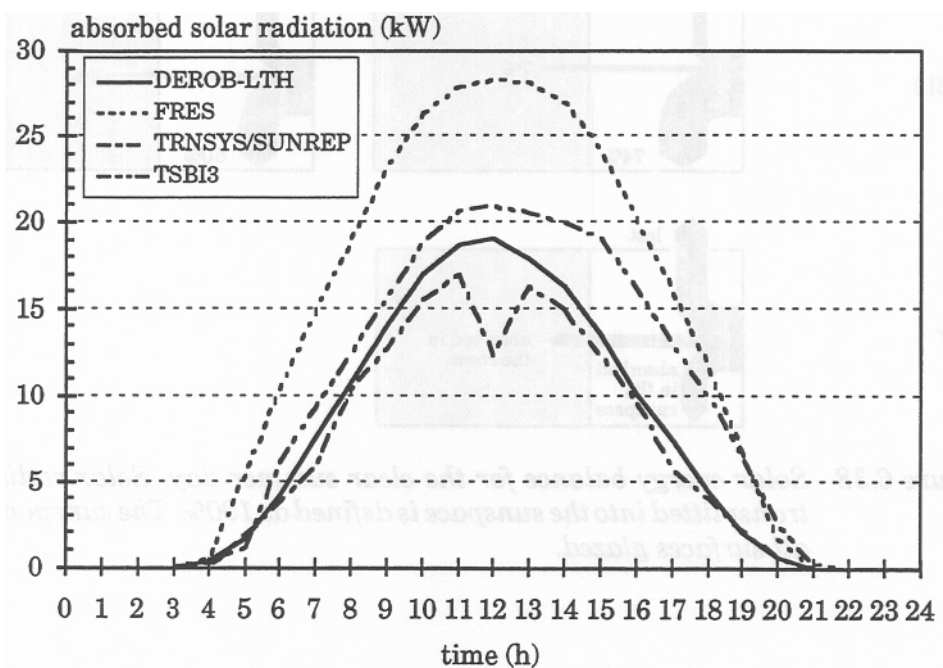


Figure 6.37 Absorbed solar radiation in the sunspace during the clear summer day. Absorptivity = 0.80.

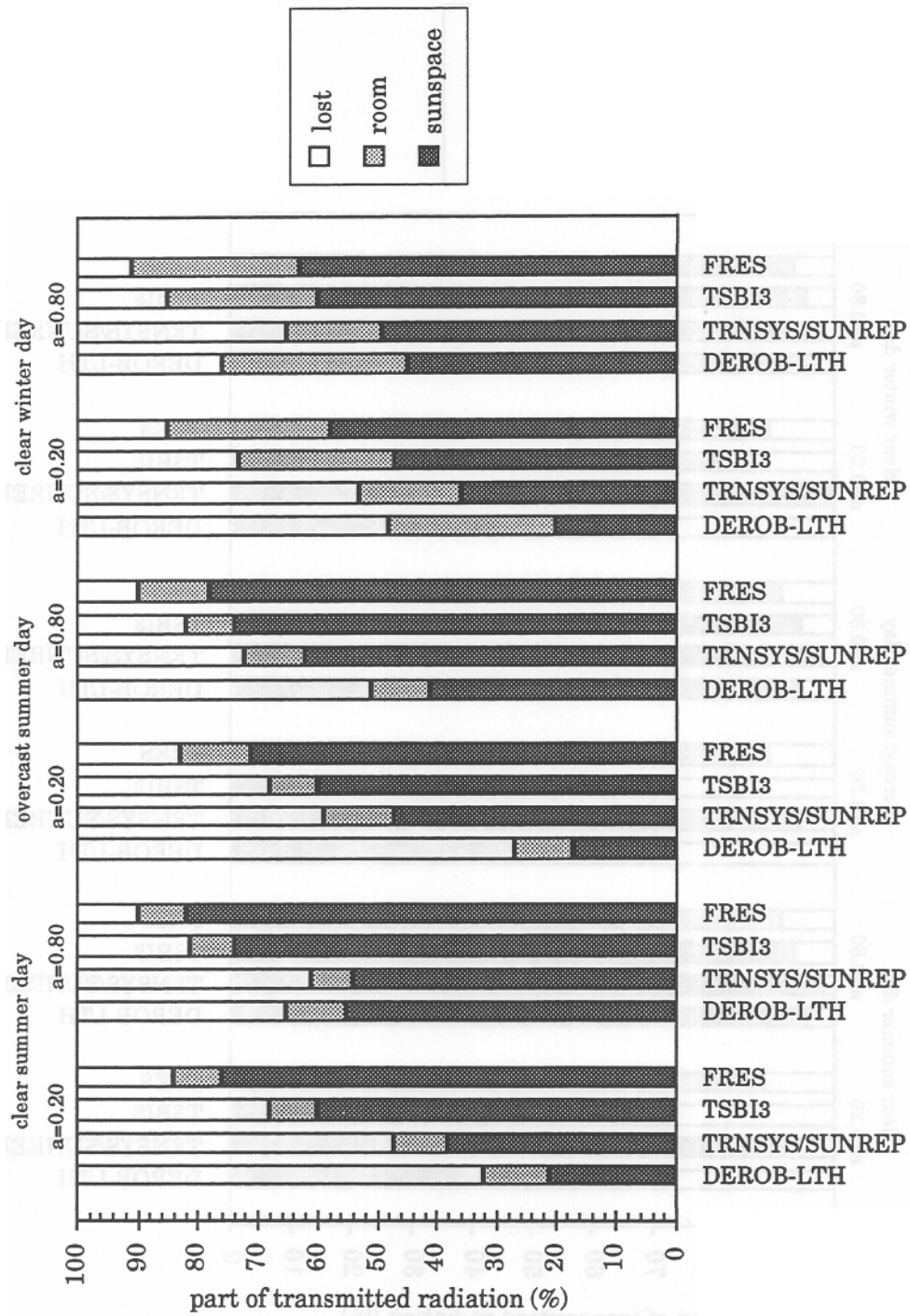


Figure 6.39 Solar energy balances for the shoebox combined with a sunspace with all surfaces glazed.

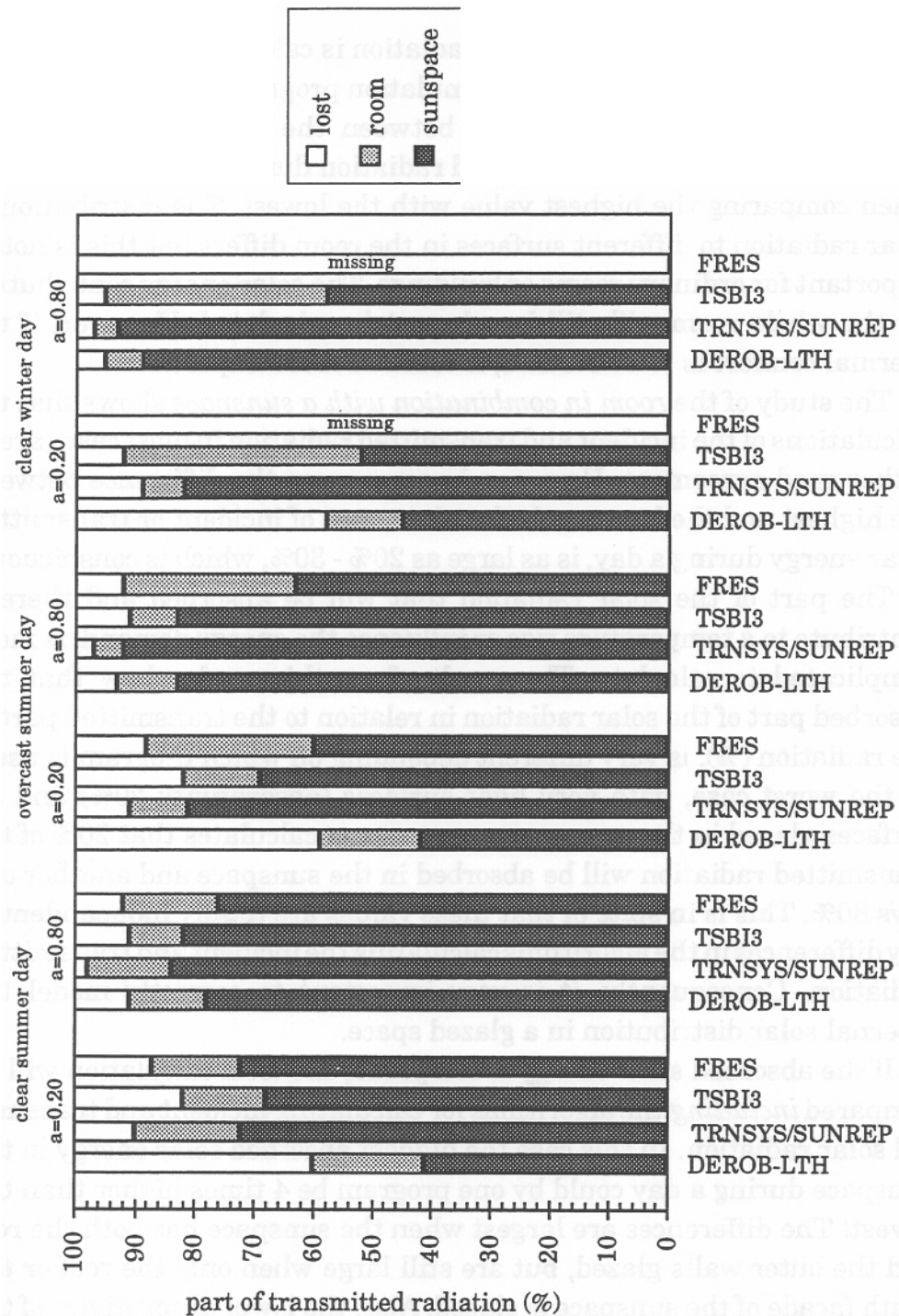


Figure 6.41 Solar energy balances for the shoebox combined with a sunspace with only the roof glazed.

In FRES, the transmitted solar radiation is absorbed in two steps. In the first step, the transmitted radiation is evenly absorbed only in the opaque surfaces, taken into account the absorptivity factor. The part that is not absorbed will be reflected. In the second step, the reflected radiation from step one will be evenly distributed to all surfaces. The opaque surfaces absorb all heat and the windows will absorb the part which is not transmitted. No further reflections will occur. This method is adequate for an ordinary room with relatively small windows (like the test room). The problem occurs when a large part of the room is surrounded by glazed surfaces, like a sunspace or an atrium. As the transmitted radiation in the first step only is distributed to opaque surfaces, the absorbed energy will be overestimated.

DEROB-LTH and SUNREP are using a geometrical description of the buildings in order to calculate which surfaces that will be hit by the sun and calculate absorption and reflections using view factors to distribute the solar radiation.

The results from DEROB-LTH and TRNSYS/SUNREP give in general significantly lower energy contribution from the sun than TSB13 and FRES. If atrium buildings or other types of glazed spaces are to be studied, it is essential to base the calculations on a geometrical description, taking into account transmission, reflections and absorptivity so that solar radiation can be transmitted out again directly or by reflection. Building energy simulation programs used for ordinary buildings are definitely not automatically suitable for atrium buildings.

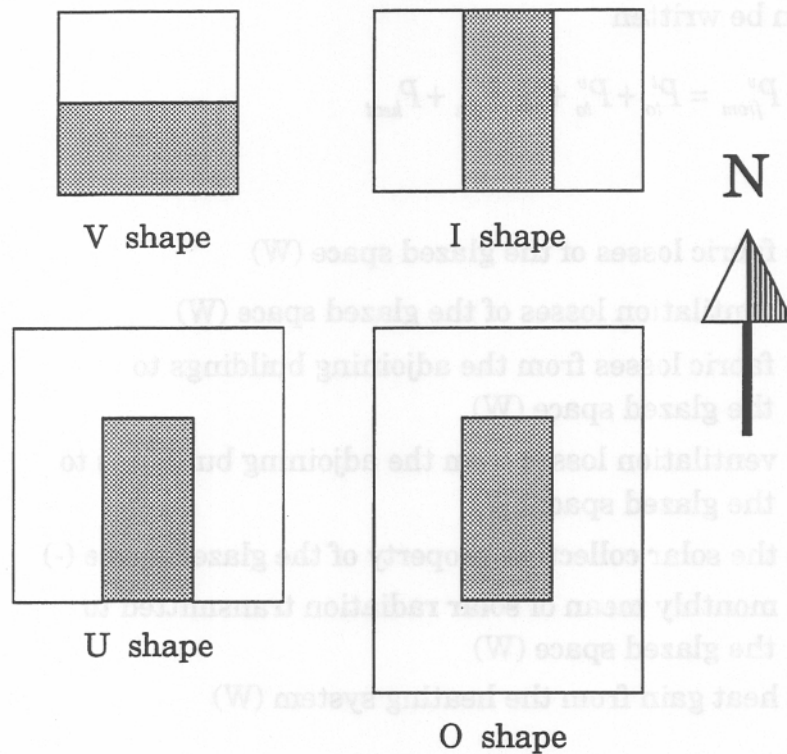


Figure 6.42 Plan and orientation of the studied glazed spaces.

Table 6.4 Properties of the glass types for perpendicular incidence.

Glass type	Trans- mission	Reflec- tion	Absorp- tion	U value (W/m ² °C)
single glass	0.85	0.08	0.07	5.88
double glass	0.72	0.13	0.15	2.94
triple glass	0.62	0.17	0.21	1.96

The study showed that the effect of the investigated factors can be ranked in the following order of significance. The ones at the top have the greatest significance, and those at the bottom the least.

- Absorptivity for short wave radiation of the inside surfaces of the glazed space (i.e. dark or light surfaces)
- The geometry of the space and the proportion of glazed surfaces
- The properties of the glazed construction
- Orientation
- Time of year
- Geographical position (latitude)

This means that the solar collection property S need not be calculated for different latitudes. It can also be considered constant over the year. On the other hand, the properties of the glazed space with regard to transmission of solar radiation cannot be ignored, nor can the geometry or the absorptivity of the inside surfaces.

The solar collection property S has therefore been calculated for the different types of glazed spaces for single, double and triple glazing. The value of S must also be calculated as a function of absorptivity. Obviously, there are many different variants of glazed space design, but all these cannot be predicted or shown here. The examples are intended to give an idea of the solar collection properties which different types of glazed spaces have, so that an approximative assessment of temperatures and energy requirement may be made.

6.11.3 Summary of solar collection property for variable absorptivity and geometry

The mean value of the solar collection property S over the year has been calculated for different values of absorptivity for the walls and floor which adjoin the glazed space. Climatic data from Lund, Sweden, for 1988 have been used (latitude 55.72°N , longitude 13.22°E), and the orientations are as shown in Figure 6.42. The results can however be used for other locations and for other orientations, see Wall (1994).

Values of the solar collection property S as a function of absorptivity are plotted for the four types of glazed space in Figure 6.43-6.46. The glazed spaces are described earlier in this chapter. Calculations have been made for single, double and triple glazing in the roof and glazed facades

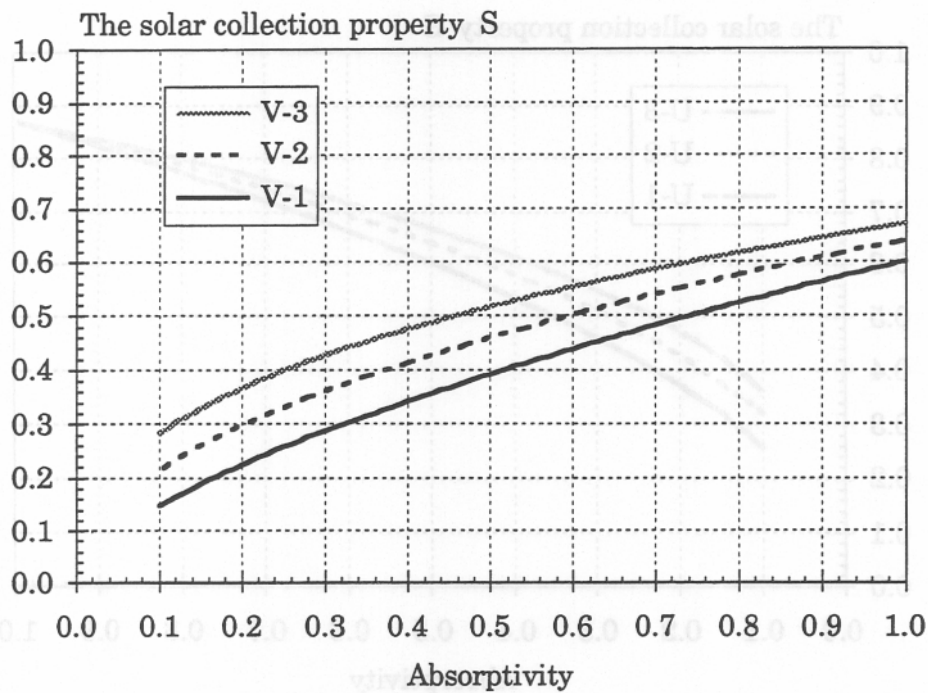


Figure 6.43 Solar collection property as a function of absorptivity for the glazed space with a building on one side.

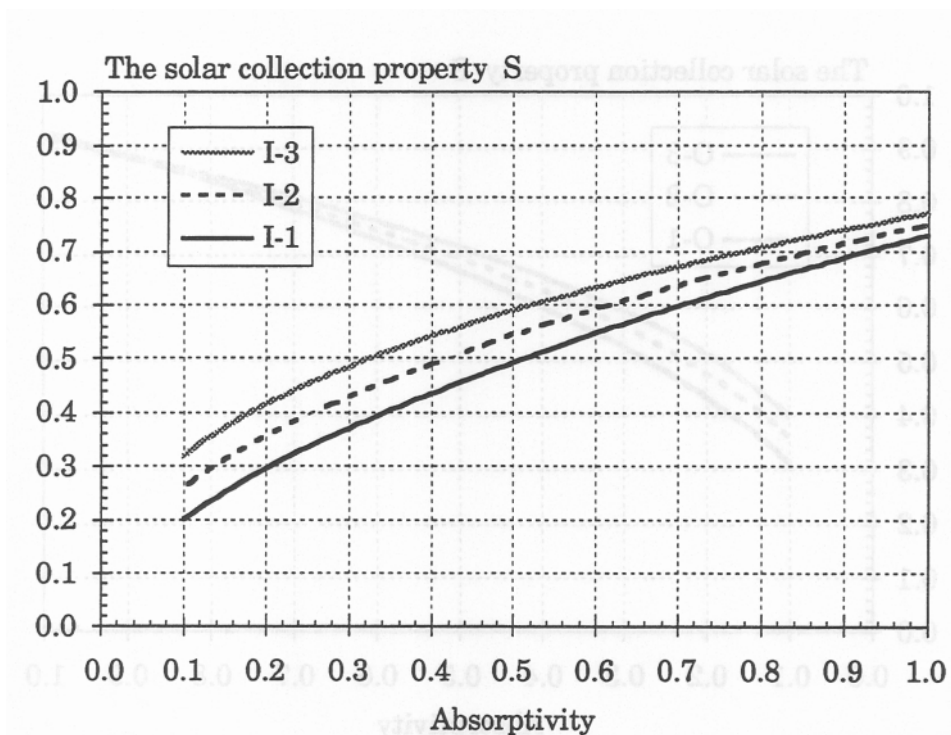


Figure 6.44 Solar collection property as a function of absorptivity for the glazed space with buildings on two sides.

6.11.4 The effect of inclined surfaces

To see how the solar collection property is influenced by the angle of the roof, calculations were also made with a 30° pitched roof. The results show that the solar collection property S is reduced with about 0.05-0.10 compared with a horizontal roof, when the glazed space has buildings on two, three or four sides.

The calculation error of the utilised solar radiation will be minimized if the above calculated values of S is used in combination with transmitted solar radiation for a simplified horizontal roof. With this simplified geometry, the calculation error of the utilised solar energy will be less than 1% with single glazing. With triple glazing, the error will be about 3-4%.

The solar collection property S for the glazed space with a building on only one side, will increase with about 0.05 when the roof has an angle of 30° or the glazed wall an angle of 60° instead of a horizontal roof or vertical walls. In this case the transmitted solar radiation should be calculated for the actual angle of the surfaces. In combination with the above calculated values of S , the utilised solar radiation will be underestimated with about 10%. In order to reduce this error further, add 0.05 to the chosen value of S in Figure 6.43, then the error will be minimal.

evaluated. The method is based on calculations with DEROB-LTH, which is a building energy simulation program using a geometrical description of the buildings to calculate the solar radiation.

An example of a method calculating shadows is also presented. The method has been implemented in a PC software application, called Xsun, which can function as a stand-alone design tool or maybe integrated with programs for thermal simulation of buildings or solar systems. An example is given where Xsun is integrated with the thermal simulation tool TSBI3.

H	time (civil time) (h)
H_{τ}	the current half hour (h)
H_{ts}	the true solar time (h)
h_c	surface heat transfer coefficient ($\text{W/m}^2\text{C}$)
$h_k, k=0$	total outside film coefficient ($\text{W/m}^2\text{K}$)
$h_k, k>0$	total conductivity between the pane k and $k+1$ ($\text{W/m}^2\text{K}$)
I	short wave radiation (W/m^2)
I_i	incident radiation (W/m^2)
I_{fi}	forward incident radiation (W/m^2)
I_a	absorbed radiation (W/m^2)
I_{fa}	absorbed part of forward incident radiation (W/m^2)
I_{fj}	forward directed radiation in front of layer j (W/m^2)
I_{fr}	reflected part of forward incident radiation (W/m^2)
I_{ft}	transmitted forward directed radiation (W/m^2)
I_{Ag}	reflected radiation from the surface of the ground (W/m^2)
$I_{Ag,\theta i}$	reflected radiation from the surface of the ground, angle of incidence (W/m^2)
$I_{Ag,\theta t}$	reflected radiation from the surface of the ground, sloped surface (W/m^2)
I_{ba}	absorbed part of backward incident radiation (W/m^2)
I_{bi}	backward incident radiation (W/m^2)
I_{bj}	backward directed radiation in front of layer j (W/m^2)
I_{br}	reflected part of backward incident radiation (W/m^2)
I_D	insolation of direct solar radiation (W/m^2)
I_{Dt}	transmitted direct solar radiation (W/m^2)
I_{dt}	transmitted diffuse solar radiation (W/m^2)
I_{dDt}	transmitted diffuse and direct solar radiation (W/m^2)
I_{d1}	incident diffuse solar radiation (W/m^2)
I_{d2}	total reflected solar radiation from the ground (W/m^2)
$I_{d,\theta i}$	diffuse solar radiation on a sloping surface (W/m^2)
I_{dV}	diffuse solar radiation on a vertical surface (W/m^2)
I_{di}	total incident diffuse solar radiation on the surface (W/m^2)
I_{Di}	total incident direct solar radiation on the surface (W/m^2)
$I_{Di,c}$	total incident direct solar radiation on the surface with an amount of cloud N_c (W/m^2)
$I_{D,\theta i}$	direct solar radiation on a sloping surface (W/m^2)
$I_{D\theta,C}$	direct solar radiation on an arbitrary surface (W/m^2)
$I_{dB,c}$	diffuse background radiation (W/m^2)
I_H	global solar radiation (W/m^2)
$I_{H,c}$	global solar radiation, cloudy sky (W/m^2)
I_{dH}	horizontal diffuse solar radiation (W/m^2)
$I_{dH,c}$	horizontal diffuse solar radiation, cloudy sky (W/m^2)
I_{DH}	horizontal direct solar radiation (W/m^2)
$I_{DH,c}$	horizontal direct solar radiation, cloudy sky (W/m^2)
I_{DN}	direct solar radiation, normal incidence (W/m^2)
$I_{DN,C}$	direct solar radiation at normal incidence, cloudy sky (W/m^2)
I'_{DN}	direct solar radiation, normal incidence, dry atmosphere (W/m^2)
I_o	the solar constant (W/m^2)

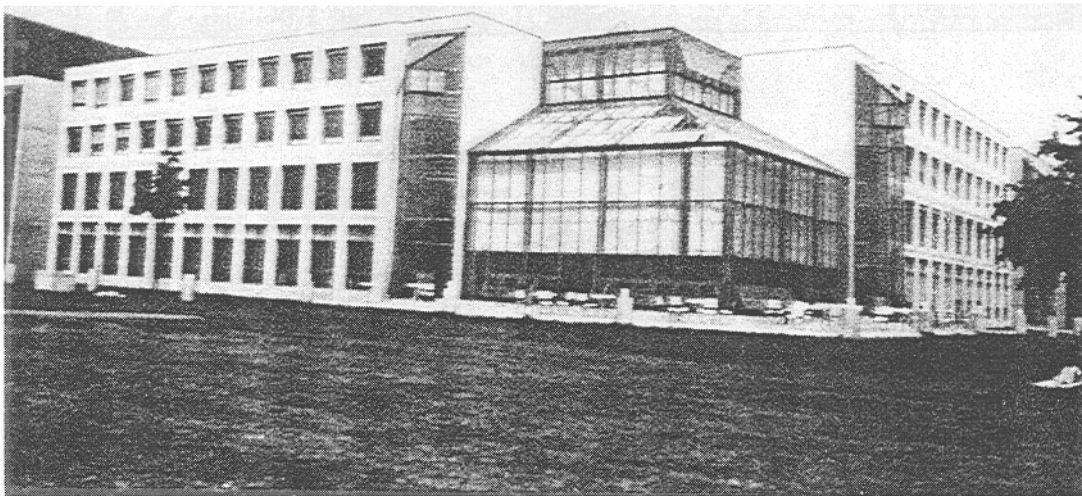
P_{tot}	total incoming short wave radiation to the windows (W)
$P_{tot,gl}$	total incoming short wave radiation to the outside of the glazings of the sunspace (W)
P_{trans}	total short wave radiation transmitted to the room (W)
$P_{trans,gl}$	total short wave radiation transmitted to the sunspace (W)
P_{eci}	the radiation received by surface i (W)
P_{ceil}	resulting short wave radiation to the ceiling, part of P_{trans} (%)
P_{east}	resulting short wave radiation to the east wall, part of P_{trans} (%)
P_{floor}	resulting short wave radiation to the floor, part of P_{trans} (%)
P_{north}	resulting short wave radiation to the north wall, part of P_{trans} (%)
P_{south}	resulting short wave radiation to the south wall, except for windows, part of P_{trans} (%)
P_{west}	resulting short wave radiation to the west wall, part of P_{trans} (%)
P_{win}	resulting short wave radiation to the windows (inside), part of P_{trans} (%)
P_{net}	the part of P_{trans} that stays in the room (W)
$P_{net,gl}$	the part of $P_{trans,gl}$ that stays in the sunspace (%)
P_{to}^t	fabric losses from the adjoining buildings to the glazed space (W)
P_{from}^t	fabric losses of the glazed space (W)
P_{to}^v	ventilation losses from the adjoining building to the glazed space (W)
P_{from}^v	ventilation losses of the glazed space (W)
P_{heat}	heat gain from the heating system (W)
P_{sun}	monthly mean of solar radiation transmitted to the glazed space (W)
\hat{p}_1	position of the sun in a coordinate system (-)
\hat{p}_2	position of the sun in a cardinal coordinate system (-)
q	energy flux at a surface (W/m^2)
R	long wave radiation (W/m^2)
R_A	atmospheric long wave radiation (W/m^2)
$R_{A,c}$	atmospheric radiation when the sky is completely covered by cloud (W/m^2)
R_{A,N_c}	long wave radiation from the atmosphere for an amount N_c of cloud (W/m^2)
R_G	long wave radiation from the ground (W/m^2)
R_{G,N_c}	long wave radiation from the ground at broken cloud cover (W/m^2)
R_{Geff}	effective thermal radiation from the ground, clear sky (W/m^2)
$R_{Geff,c}$	effective thermal radiation from the ground, cloudy sky (W/m^2)
R_s	radiation from a black surface (W/m^2)
R_d	a ratio for calculation of incident solar radiation (Eq. 6.119) (-)
R_g	a ratio for calculation of incident solar radiation (Eq. 6.120) (-)
r	reflectance (-)
r_1	reflectance, 1st media (-)
r_2	reflectance, 2nd media (-)
r_3	reflectance, 3rd media (-)
r_b	reflection of backward directed radiation (-)
$r_{b,j}$	reflection of backward directed radiation at layer j (-)
r_c	the reflectance at normal incident for the window (-)
r_f	reflection of forward directed radiation (-)

α_d	coefficient of absorption for particulate scatter (-)
α_r	coefficient of absorption for molecular scatter (-)
β	coefficient of turbidity
ε_g	long wave emissivity of ground (-)
ε_r	long wave emissivity of surface (-)
Φ_H	$2\pi (t-6) / 24$ (rad)
Φ_l	$(90^\circ - \text{latitude}) \cdot \pi / 180$ (rad)
γ	electric permittivity (As/Vm)
η	coefficient used for calculation of diffuse solar radiation (Eq. 6.21)
κ	constant between 0.30 and 0.35 (Eq. 6.19) (-)
λ	wavelength (μm)
μ	magnetic permeability (Vs/Am)
$\theta_1, \theta_2, \theta_3$	plane angles (rad)
θ_α	the solar azimuth angle ($^\circ$)
θ_β	the horizontal angle between the normal and the direction of radiation ($^\circ$)
θ_d	declination of the sun ($^\circ$)
θ_γ	the angle between the normal to the surface and the horizontal plane ($^\circ$)
θ_g	longitude of the locality ($^\circ$)
θ_l	latitude of the locality ($^\circ$)
θ_H	hour angle ($^\circ$)
θ_h	the solar height angle (rad)
$\theta_{h,opt}$	the optical solar height (rad)
θ_i	the angle of incidence ($^\circ$)
θ_r	angle of reflection ($^\circ$)
θ_s	sunrise hour angle ($^\circ$)
θ_t	inclination of surface to the horizontal plane ($^\circ$)
θ_{ts}	the true solar time (rad)
θ_v	south azimuth of the surface ($^\circ$)
θ_w	the orientation of the surface ($^\circ$)
θ_z	zenith angle ($^\circ$)
σ	Stefan-Boltzmann constant, $(5.70 \cdot 10^{-8} \text{ W/m}^2\text{K}^4)$
v_1	solar angle with the south ($^\circ$)
v_2	solar angle with the east ($^\circ$)
w	quantity of water which can be precipitated (kg/m^2)
w_N	$2\pi / 366$ (rad)

- Källblad, K. (1973). *Strålning genom glaskombinationer, Principer och datorprogram* (In Swedish) (Report 1973:12). Lund (Sweden): Department of Building Science, Lund Institute of Technology.
- Liljequist, G. H. (1979). *Strålning* . (*Radiation*). (In Swedish). Uppsala (Sweden): University of Uppsala, Department of Meteorology.
- Lund, H. (1977). *SOLIND - Program til beregning af solindfald*, (SOLIND - Program for calculation of solar irradiation) (In Danish). Lyngby: DTH, Thermal Insulation Laboratory.
- Petersen, E. (1982). *Solstråling og dagslys, - målt og beregnet*. (Solar Radiation, - Measured and Calculated) (In Danish) (Report 34). Lyngby: Lysteknisk Laboratorium.
- Rogers, D. F. (1985). *Procedural Elements for Computer Graphics*, pp. 179-185, McGraw-Hill Book Company.
- Seller, W. D. (1965). *Physical climatology*. University of Chicago Press, Chicago & London.
- Stephenson, D.G. (1965). Equations for Solar Heat Gain through Windows. *Solar Energy*, Vol 9 Nr 2 april-june 1965.
- Taesler, R. & Andersson, C. (1985). *En metod for beräkning av solstrålning från normala meteorologiska observationer. (A method for the calculation of solar radiation from normal meteorological observations)*. (In Swedish) (SEAS Sheet No 1). Stockholm (Sweden): Royal Institute of Technology, Department of Heating and Ventilation.
- Taesler, R. (1972). *Klimatdata för Sverige (Climatic data for Sweden)*. (In Swedish). Stockholm (Sweden). Swedish Council for Building Research.
- Taesler, R. (1985). *Klimatberoendet i bebyggelsens energibudget. Data och beräkningsmetoder (The dependence of the energy budget of buildings on climate. Data and calculation methods)*. (In Swedish) (Report No R116:1985). Stockholm (Sweden): Swedish Council for Building Research.
- Thekaekara, M. P. (1973). *Solar Energy*, 14, 107-27. Pergamon.
- Wall, M. (1994). *Projekteringshjälpmedel för inglasade rum. Klimat och energi. (A design tool for glazed spaces. Climate and energy)*. (In Swedish). Lund (Sweden): University of Lund - Lund Institute of Technology, Department of Building Science.

7. Test studies

7.1 Neuchâtel University - NUNI



Building type	Education
Passive solar features	Direct daylighting Sunspace
Occupancy date	October 1986
Floor area	8.100 m ²
Annual delivered fuel	Heating energy 215 MJ/m ² (estimated)
Architects	NCL Architecture-urbanisme
Energy consultant	Sorane SA
Client	Canton de Neuchatel

7.1.1 Summary

The new building of the faculty of literature of the University of Neuchatel has a heating energy demand of only 215 MJ/m²,an. The symmetrical building has a central courtyard and attached sunspace. It is heated by a heatpump with backup on extremely cold days from district heating. The prominent large sunspace was conceived as a passive solar heated space. The building is deliberately not air conditioned and only special rooms have mechanical ventilation. The glazed space is tempered in summer through natural ventilation and evaporative cooling from pools of water.

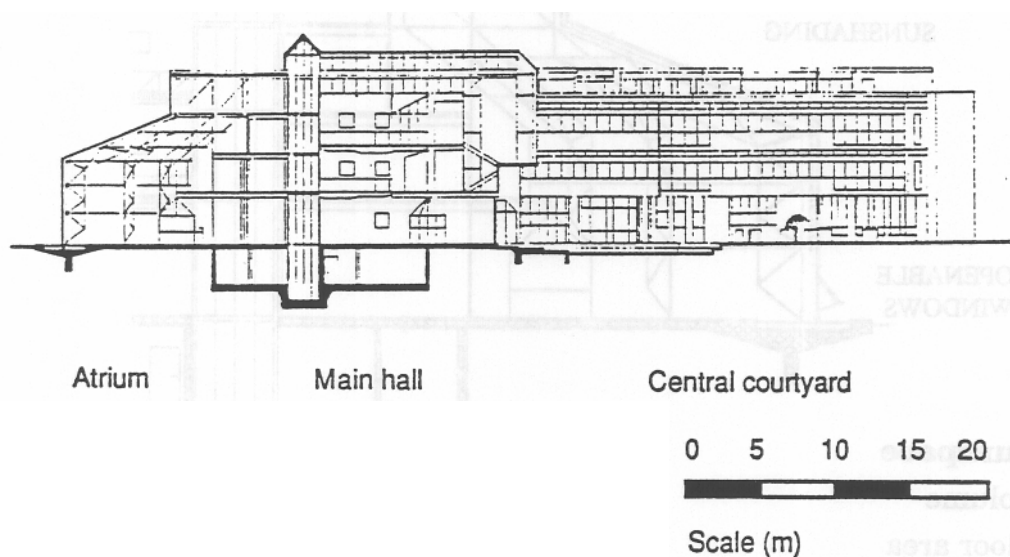
7.1.3 Building form

The 3-4 story building complex, organized around a central court, is comprised of six blocs :

- Four nearly identical blocks housing a library, class rooms and offices
- A 12 x 12 x 12 m sunspace with 160 m² of vertical glass and 130 m² of sloping glass
- A central block with the entry hall, cafeteria and commons area

A pedestrian axis passing diagonally through the building connects the town to the open park land foreseen for festivals. This axis passes through the commons area which can be used independently from the normal operations of the building.

Volume	Gross 24'600 m ³
Floor area	Gross 8'100 m ²
Number of levels	4 + basement



7.1.4 Building construction

The concrete framing, ductwork and other services are all exposed rather than hidden with a suspended ceiling. the construction is based on a 7.2 m grid. The sunspace is single glazed to the outside and to the building side.

U-Values (W/m ² K)	
Windows	3.10 and 1.60
Walls	0.35
Building	0.70

7.1.7 Costs

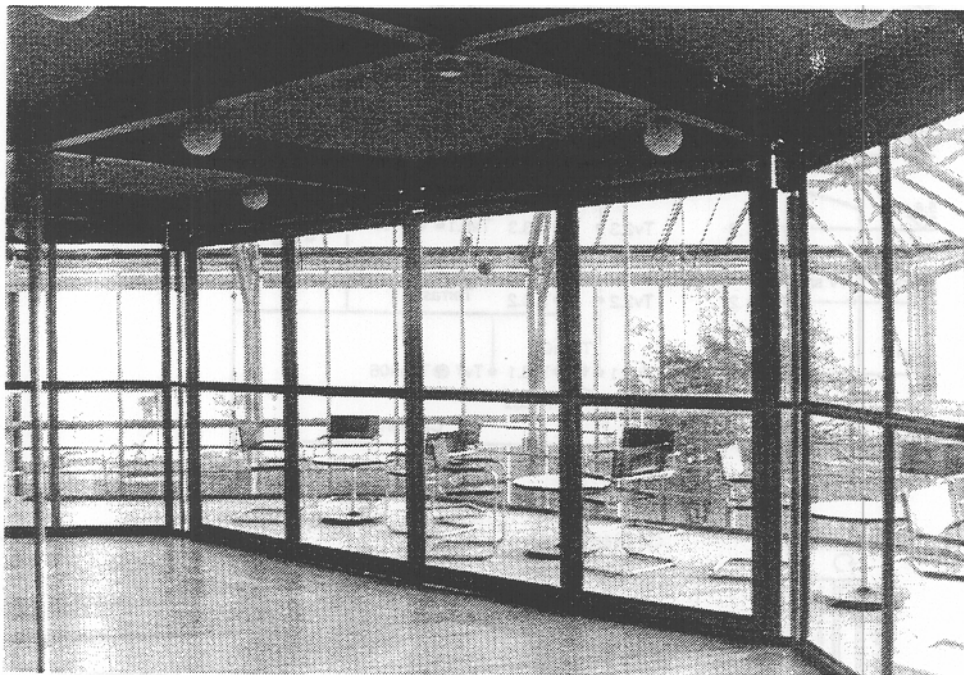
The entire building complex was estimated to cost Sfr. 17,500,000. Actual costs were 20 percent higher. Part of this overcost included additional insulation, decided upon during the course of construction.

7.1.8 Energy performance

The estimated annual energy consumption for heating is 215 MJ/m²,a.

7.1.9 Human factors

The frequent and full occupancy of the sunspace proves its success as a gathering space. Students are apparently willing to accept cooler temperatures of the space in the winter in order to enjoy the amenity of the "outdoor" character of the space.



7.1.10 Energy saving achieved by the atrium

In winter the atrium is not heated, it is used as a buffer zone. In this way the amount of energy saved has been evaluated to 28 MWh/year.

This correspond to 4 % of the annual energy consumption of the whole university building (654 MWh/an).

7.1.12 Typical internal air temperature profiles

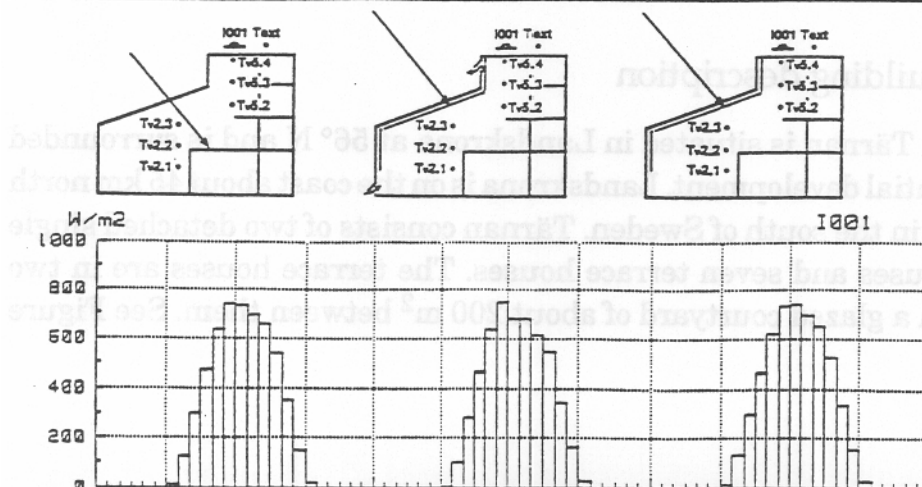
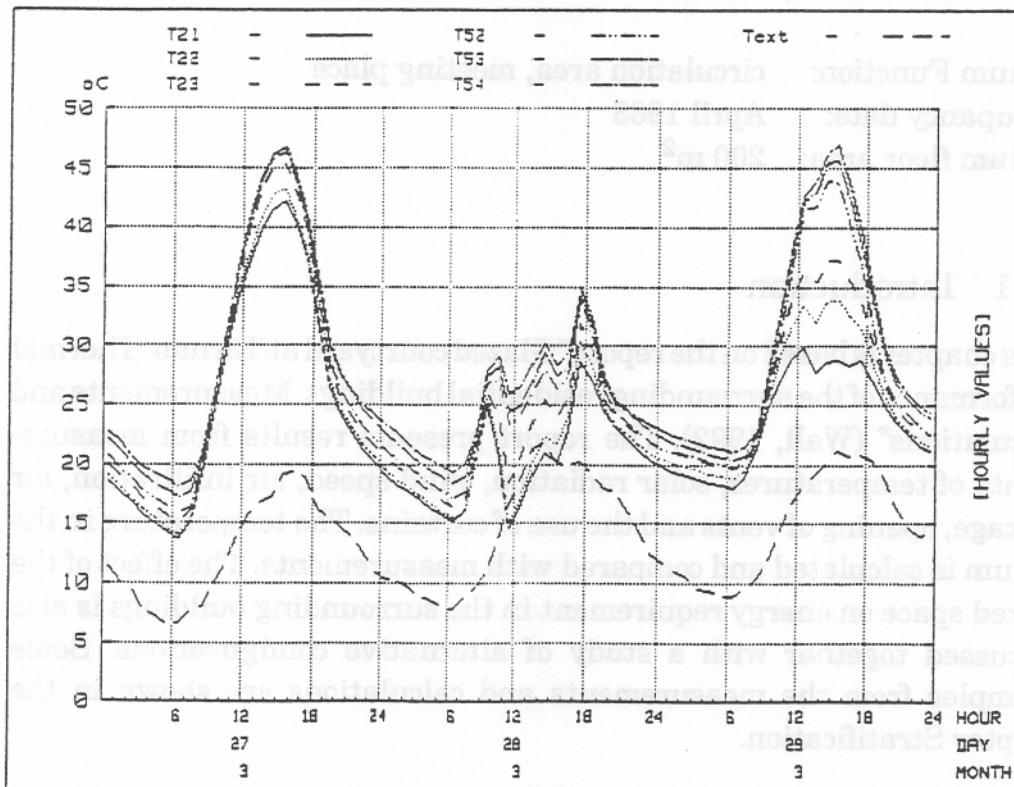
In the next figure three typical sunny days are presented.

During the **first day** no internal shading as well as no natural ventilation (opened hatches) are used.

The air temperature is not very stratified (only 4 degrees).

During the **third day**, the hatches are closed but the internal shading devices are used, in this way if the peak temperature in the upper part of the atrium has not changed in comparison to the first day, the lower part is 15K under the peak temperature !

Finally during the **second day** the internal shading devices are used and the hatches opened (from 10.30 a.m.). In this way, the stratification is reduced (8-10°C) and the temperature in the occupied zones becomes comfortable.



7.2.1 and 7.2.2. Together, they form a tenant-owner association. The terrace houses are on 2.5 storeys with a floor space of 123 m² and contain 5 rooms plus kitchen. In the vicinity of the dwellings there is a communal refuse storage room/store and a building housing the heat pumps.

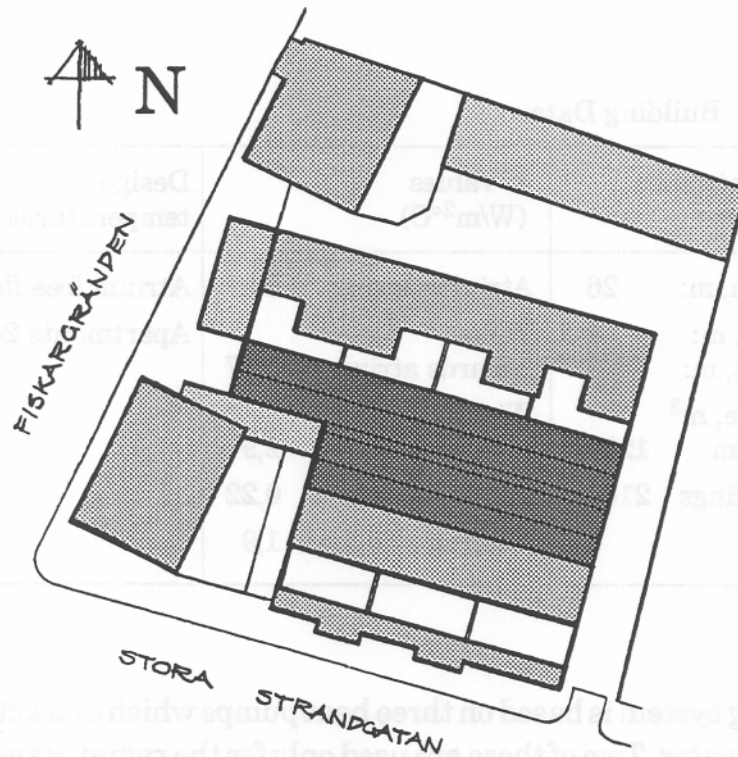


Figure 7.2.2 Layout plan, Tärnan.

The loadbearing walls of the buildings consist of prefabricated concrete units with cast-in timber studs. Between the studs the wall units contain mineral wool which is covered by a plastics foil and gypsum plasterboard.

The facades towards the external air consist mainly of painted concrete units with internal mineral wool insulation and gypsum plasterboard. Towards the courtyard the walls are clad with minerite fibre cement slabs, with mineral wool and gypsum plasterboard on the inside. The U value of the walls towards the courtyard is 0.27 W/m²°C (145 mm mineral wool) and the windows are reduced to double glazing. Towards the external air the windows are triple glazed, and the walls towards the external air, which have extra insulation, have a U value of 0.22 W/m²°C (45+145 mm mineral wool).

The floors consist of prefabricated concrete units with cast-in studs, with the concrete on the bottom. The ground floor slab has 195 mm mineral wool, and the intermediate floor 50 mm.

Vents are provided in both the roof and the gables. About 25% of the roof surface can be opened. In the roof there are horizontal curtains of acrylic fabric which are used both as insulation and for solar control.

The vents and curtains are controlled automatically by means of a special control equipment made by Dansk Gartneri Teknik (DGT) Sweden AB. This system has long been used in greenhouses. The control equipment is connected to temperature sensors and a smoke detector in the courtyard, and to humidity (rain), light and wind sensors outside.

When the temperature in the courtyard reaches a certain preset value, the vents are opened. If it begins to rain, the vents are half shut, and if there is strong wind, they are shut so that they have 10% opening area. The vents on the leeward side are opened first. These vents are opened to a larger angle than those on the windward side. The side which is to the leeward is determined by measurement, but it can also be set on the controls manually.

When the temperature in the courtyard reaches a certain (high) level, the curtains are drawn across in one layer, see Figure 7.2.3. A gap is left in the middle so that warm air can easily rise and leave through the open vents. The curtains are also controlled by a light meter.

At night when it is dark and cold, the curtains are drawn across in two layers to provide insulation, see Figure 7.2.3. The curtains can also be used as insulation in daytime when it is very cold outside. If the curtains were drawn during the night, they are opened in stages in the morning so that the cold downdraught should not be too strong for the plants. On the whole, the control of the vents and curtains can to a large extent be tailor-made for each project.

In principle, the courtyard is unheated. However, in order that the plants should survive, two 9 kW building driers have been used to prevent the temperature dropping below freezing.

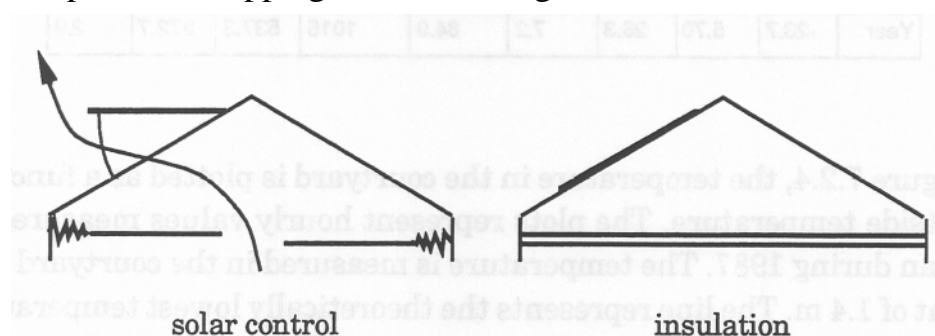


Figure 7.2.3 Use of the curtains as solar control and as insulation.

measurements deviate from the line. The reason for this is that two 9 kW building driers have been placed in the courtyard in order to maintain the temperature above freezing so that the plants can survive.

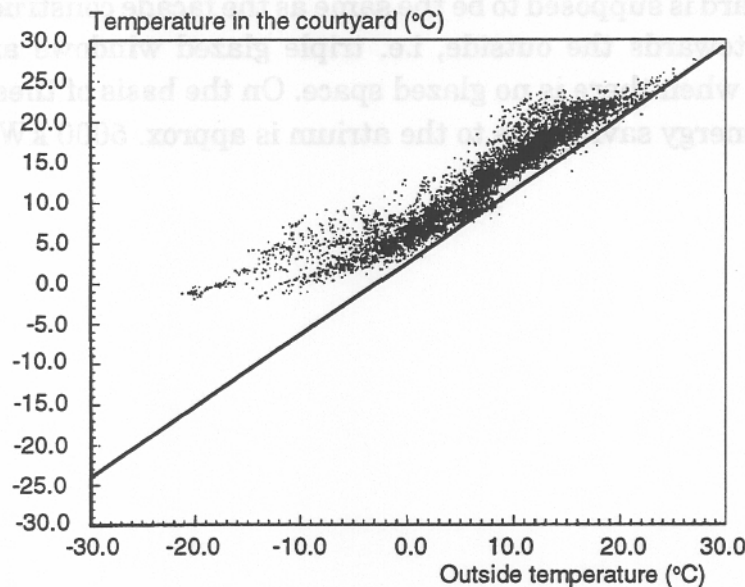


Figure 7.2.4 Temperature in the courtyard measured at a height of 1.4 m during 1987 as a function of outside temperature. The plots represent measured hourly values. The line represents the calculated lowest temperature in the courtyard under passive climatic control conditions, without solar radiation.

The air change rate in the atrium with the vents closed was measured as approx. 0.6 ach. On this occasion, in May, the outside temperature was 20°C and the temperature in the atrium was approx. 25°C. The wind speed was 2 m/s and the global solar radiation was 700–800 W/m². A fan pressurization test showed that at an overpressure at 50 Pa inside the atrium, the leakage flow was equal to 8.8 ach. See section Natural Ventilation and Infiltration.

The effect of the glazed courtyard on energy requirement in the surrounding buildings can be calculated as a reduction of the fabric and ventilation losses from the buildings surrounding the glazed courtyard. Since, generally speaking, the temperature in the courtyard during the heating season is higher than the outside temperature, the fabric losses from the surfaces abutting onto the courtyard decrease. In addition, the supply air temperature is higher in the 7 terrace houses which take their supply air from the courtyard.

From October to April, the temperature in the glazed courtyard is, on average, about 3–5°C higher than the outside temperature when the glazed space is not heated. The temperature difference varies depending on climatic variations in different years.

7.3 Bertolt Brecht Secondary School, Dresden



Atrium function:	Students' common and reading room
Completion of school building:	1970
Completion of atrium:	March 1994
Completion of school building's Energetic retrofitting	Autumn 1995
Heating energy demand of School building:	212 kWh/m ² a (before retrofit) 63 kWh/m ² a (after retrofit)
Heating energy demand of atrium:	not heated

7.3.1 Introduction

In the sixties and seventies, many schools in East Germany were built with open courtyards. These buildings have a very high heating energy demand and also have become too small. The Bertolt Brecht Secondary School in Dresden is an example for all school buildings of this type. It was studied with regard to an appropriate energetic building retrofit. To gain additional usable floor areas and to save heating energy, the courtyards have been roofed over with glass.

average U-value was about $2.1 \text{ W/m}^2\text{K}$, after retrofitting it is about $0.57 \text{ W/m}^2\text{K}$.

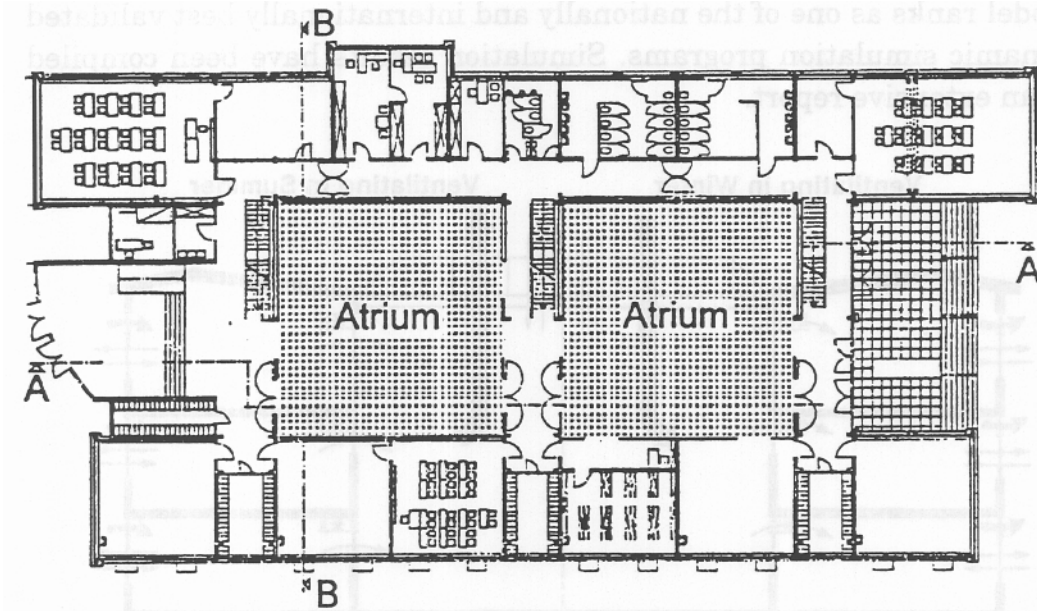


Figure 7.3.1: Ground Level Plan, Bertolt Brecht School

Table 7.3.2: Building Data

Characteristic Dimensions of one Atrium (West)	U-Values [$\text{W/m}^2\text{K}$]	Design Temperatures
length [m] 14.5	- atrium glazing: 1.3	- atrium: not heated
width [m] 14.5	- windows in exterior walls: 1.3	- school: 20°C
height [m] 11	- wall towards atrium: 1.8	
volume [m^3] 2300		

The remaining air change of $2510 \text{ m}^3\text{h}^{-1}$ is supplied directly by the outdoor air. For the other heated, non-classroom spaces of the school building with a volume of 8830 m^3 , a ventilation through the atrium is not planned. The air change assumed for calculation amounts to 0.5 h^{-1} .

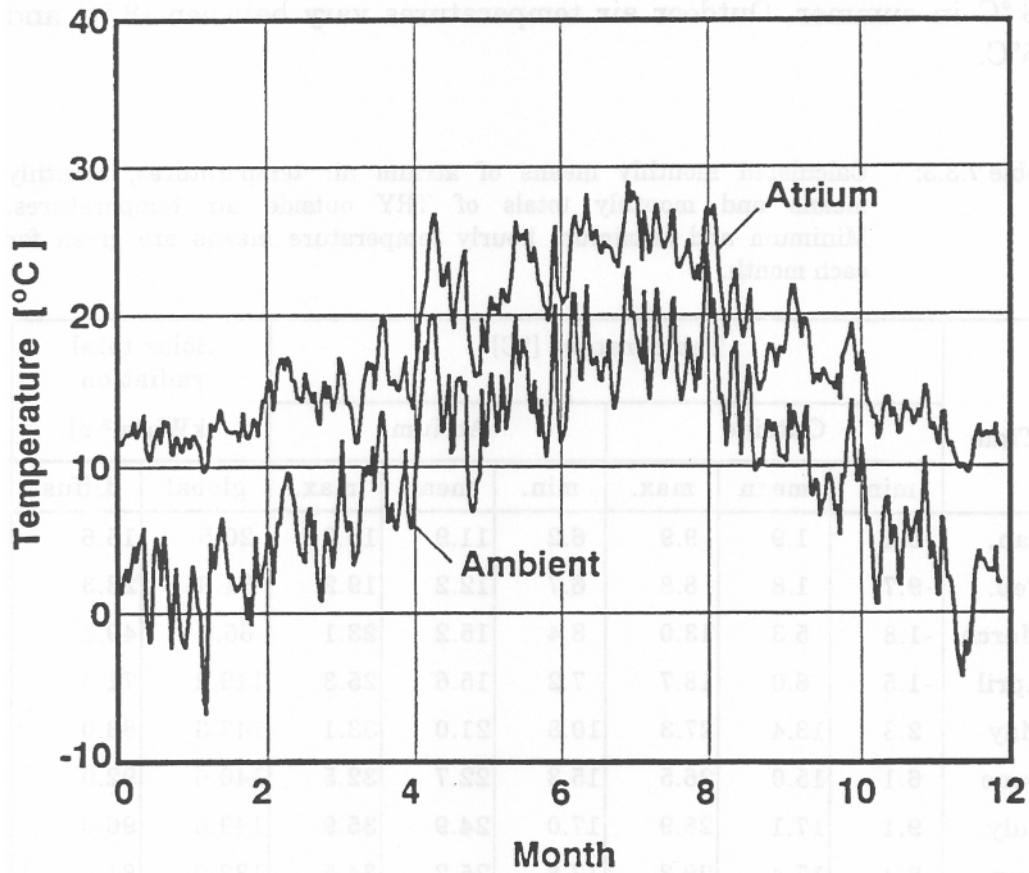


Figure 7.3.3: Calculated daily means of atrium air temperatures and daily means of TRY outside air temperatures.

The air change between atrium and ambience is assumed to come to 0.5 h^{-1} which is corresponding to an air change of $2300 \text{ m}^3\text{h}^{-1}$. In the summer months (May-September) the direction of air supply is reversed. As far as the calculated air temperatures in the atrium, it is assumed that an average outdoor air current of $8800 \text{ m}^3\text{h}^{-1}$ flows through the classrooms into the atrium before leaving the building through the atrium roof windows. The assumed direct air change between atrium and ambience amounts to $2300 \text{ m}^3\text{h}^{-1}$. The air change in the atrium determined for the calculation and related to the atrium volume of 4600 m^3 thus comes to 2.4 h^{-1} related to the total volume of the two atria. The ventilating strategies for winter and for summer are shown in Figure 7.3.2.

The heating energy demand that was calculated with the dynamic simulation program for the school building prior to retrofitting amounts to 212 kWh/m²a. By the energetic retrofitting of the external walls - except the wall adjoining the courtyard - and of the windows and the roof as well, the heating energy demand can be reduced by 99 kWh/m²a to 113 kWh/m²a. The courtyard glass roof, of low-E coated glazing, reduces the heating energy demand to 68 kWh/m²a. With a heated area of 3807 m², this corresponds to a saving of about 171 MWh. This calculation is done on the basis that the classrooms are not ventilated through the atrium. However, if part of the ventilation is done through the atrium, as described above, 5 kWh/m²a of the heating energy demand can be saved in addition.

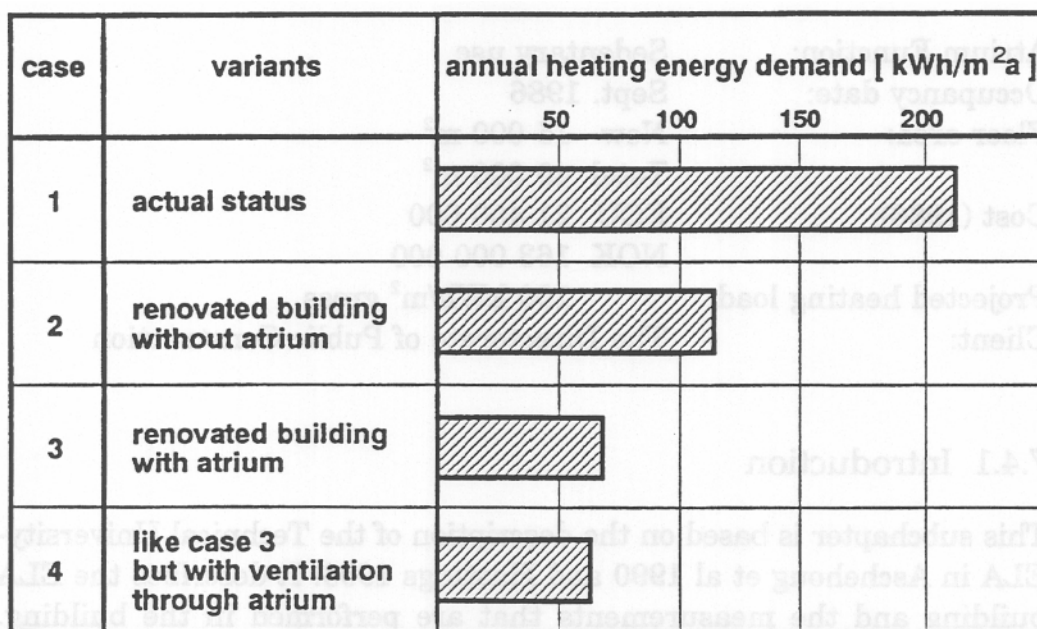


Figure 7.3.4: Annual heating energy demand of the school building prior to retrofitting and for different energy conservation measures.

For a graphical representation of the various calculated options of heating energy demand rates see Figure 7.3.4.

extension project includes offices for faculty and researchers, smaller seminar rooms and exercise labs, light electronics and computer labs, a multi-storey high voltage lab, and a cafeteria. New auditoria were also built, by reconstruction of existing lab facilities.

The extension consists of three new parallel four storey rectangular blocks and four linear shaped atria, filling out the spaces between these and existing buildings.

Table 7.4.1 Climate

October - April:		Annual:	
Degree days: (base 20°C)	4180	Degree days:	5510
Global solar hor.kWh/m ² :	220	Global hor.kWh/m ²	810
Sunshine hours:	470	Sunshine hours:	1350
Relative sunshine:	0.25	Relative sunshine:	0.30
		Average temp.°C:	4.9
		Design temp.°C:	-19

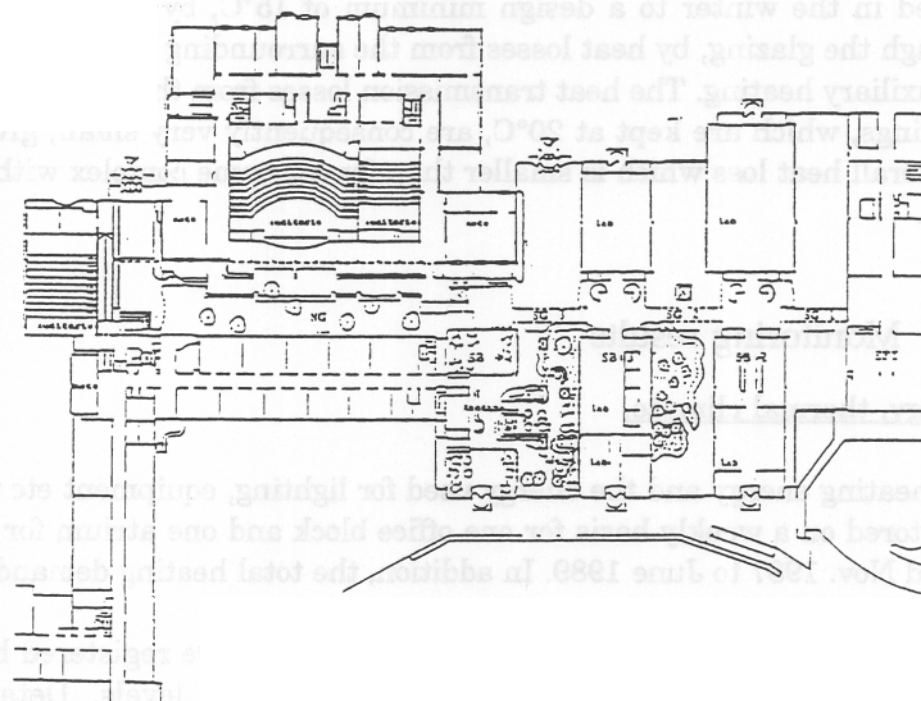


Figure 7.4.1 Ground level plan for the new building complex.

The new buildings are constructed of precast concrete columns, beams, and hollow core slabs, with steel frames as structural support for the atrium glazing. The exterior walls are insulated concrete sandwich panels, with double glazed low-emissivity windows. The intermediate

result of user demands. The atrium spaces were intended to be used for circulation and temporary occupancy only, but because of the general over-crowding of students in the complex, they now use the atria as general study places, which require a higher temperature for thermal comfort. Consequently, the atria heating demand has also risen steadily in the period, while the office heating energy is somewhat reduced, as the transmission losses to the atria now are almost zero.

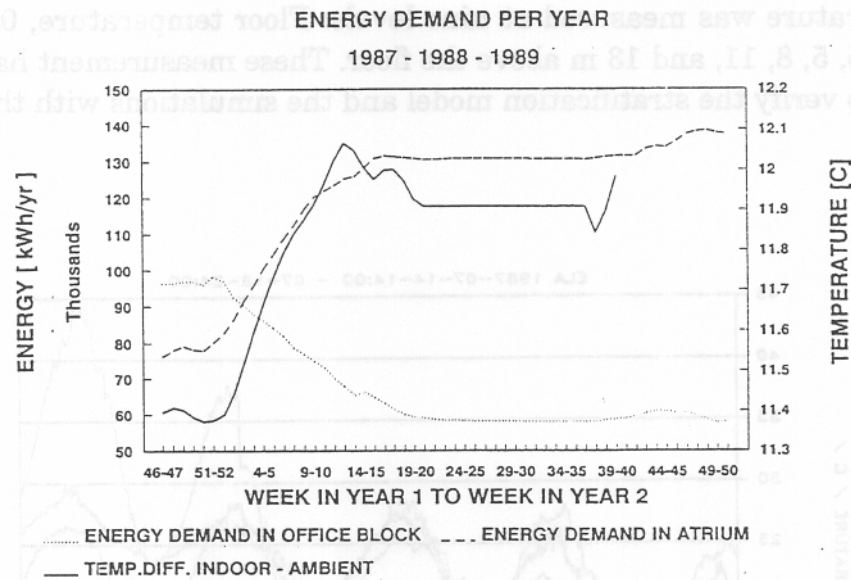


Figure 7.4.2 Trends in the annual heating load in one atrium and one office block.

Table 7.4.3 Energy use in kWh/m²

	Monitored in ELA	Norwegian Universities Average	NS3031 New Office	New laboratory
Office block: - lights, equipm: - heating:	67 41			
Atrium: - heating:	148			
Office block +atrium: - heating: - total:	60 127	270	90-130	150-250

inaccurate, as the mixing fan capacity was inadequate.

Some measurements were also carried out without mixing fans, in order to trace the air flow patterns in the atrium with hatches closed. These showed that the lower part of the atrium had the cleanest air, and that the upper part functioned as an air outlet; an air flow pattern similar to displacement ventilation.

Occupant opinions

The occupants' reactions to thermal comfort, air quality, and daylighting were also obtained in a comprehensive survey. Some major conclusions are:

- There are many complaints about high temperatures and poor air quality in offices facing the atria. Occupants are on the whole satisfied with conditions in the atria themselves. Daylight levels in the offices are considered adequate, but artificial lighting is kept on all year.
- The rating, on linear attribute scales, is quite similar to the rating given the University Center at Dragvold (Subchapter 6.3.13).
- Noise levels in the atria and noise disturbance from the atria to the office spaces also give rise to some complaints.

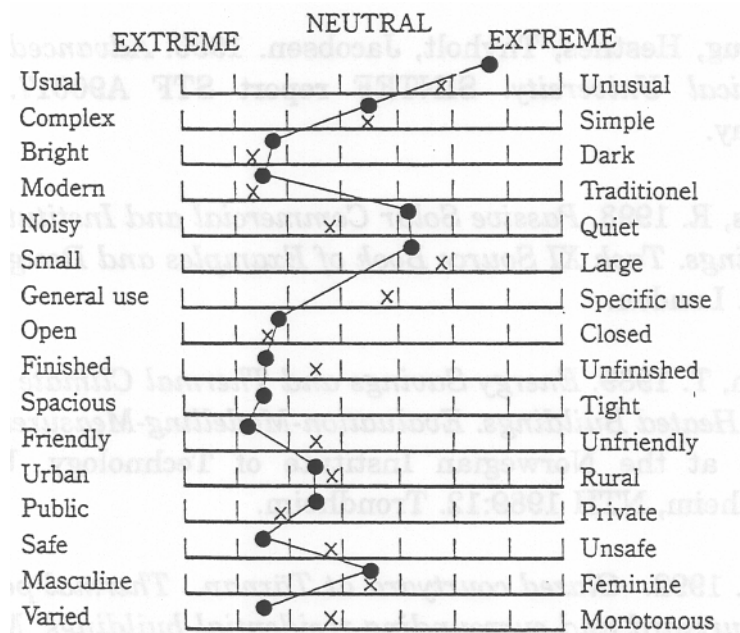


Figure 7.4.4 Occupant rating of the ELA building and the Dragvold University on a seven point scale. ● = Dragvold, X = ELA.

8. The use of CFD in the task XII

8.1 Introduction

Computational fluid dynamics - CFD seems to be a very promising tool in the design process for atria and other large rooms. The continuous development of computer technology and software and the decreasing costs for computing, makes the CFD a must for future design.

CFD-simulations seem to have the most cost-effective use for verification of indoor environment and for trouble shooting. That is for the last stage in the design process before construction. At previous stages in the process, when information is more scarce, experience and simpler tools should be used to keep costs at a low level.

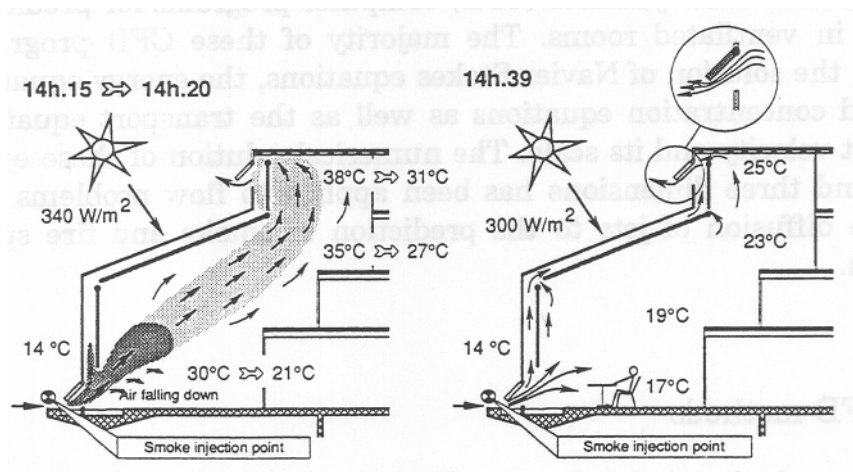
The use of CFD-codes was some years ago limited to experts in fluid dynamics and numerical methods. And those experts mostly computed idealized model-problems to test methods more than to solve engineering problems. Today, user-friendly commercial CFD-programs are offered - there are even special versions for ventilation of rooms. Though, there is still a need for expert knowledge to achieve realistic and accurate solutions from CFD-programs.

The most common CFD-codes include good turbulence models and are capable of giving computational results as good as needed for most engineering purposes. However, realistic results are still dependent on user-knowledge and on computer resources. The user-knowledge needed to simulate indoor climate and energy consumption is a mix of knowledge from HVAC and fluid dynamics with elements from numerical methods and architectural and civil engineering.

The objective of this chapter is on one hand to explain why CFD has been used in the Task 12 and in the other hand to bring attention to and to give guidance to the most essential factors in achieving a realistic and accurate solutions from CFD-simulations of atria.

8.1.2 CFD used in atrium calculations

- The use of CFD is not strictly limited to steady cases, but as it is a time consuming (calculation) simulation tool, so we will use it only in steady condition. This is not too important because normally the atrium structure is light.
- Example of an unsteady case (Nuni); sudden opening of hatches.



Unsteady measurements

- The results of CFD calculation are good in comparison to measurements, if the boundary conditions are sufficiently well defined:

→ 4 The one of the experiment should be known

4 It should be possible to introduce these boundary conditions in the calculations in the right way, this subject will be treated in chapter 3.

- Example of useful informations received from CFD

Temperature field (Comfort, stratification, energy)

Velocity field (Comfort, air exchange rate)

Down draft problems (Comfort)

- Wind influence

The CFD are not a concurrent tool of building dynamic simulation programs but are a complementary, it can be used as an "experiment" to calculate ("mesure") values we need to develop and evaluate simplified models.

Finally, the CFD can also be used for planning measurements with a coarse mesh (or modelling) of the space it is already possible to find the most convenient place to put the sensors.

Momentum (Navier-Stokes) equations :

$$\frac{\partial u_i}{\partial t} + u_j \frac{\partial u_i}{\partial x_j} = (\nu + \nu_t) \frac{\partial^2 u_i}{\partial x_j^2} + g_i (\rho - \rho_0) - \frac{1}{\rho} \frac{\partial p}{\partial x_i} \quad (2)$$

transient convection term diffusion term bouyancy term pressure gradient

Energy equation :

$$\frac{\partial T}{\partial t} + u_j \frac{\partial T}{\partial x_j} = (\alpha + \alpha_t) \frac{\partial^2 T}{\partial x_j^2} + \frac{q'''}{\rho c_p} \quad (3)$$

transient convection term diffusion term source term

$$\frac{\partial k}{\partial t} + u_j \frac{\partial k}{\partial x_j} = \left(\nu + \frac{\nu_t}{\sigma_k} \right) \frac{\partial^2 k}{\partial x_j^2} + \nu_t \left(\frac{\partial u_i}{\partial x_j} + \frac{\partial u_j}{\partial x_i} \right) \frac{\partial u_i}{\partial x_j} - \beta g_j \frac{\nu_t}{\sigma_t} \frac{\partial T}{\partial x_j} - C_D \varepsilon \quad (4)$$

$$\frac{\partial \varepsilon}{\partial t} + u_j \frac{\partial \varepsilon}{\partial x_j} = \left(\nu + \frac{\nu_t}{\sigma_\varepsilon} \right) \frac{\partial^2 \varepsilon}{\partial x_j^2} + \frac{\nu_t C_1 \varepsilon}{k} \left(\frac{\partial u_i}{\partial x_j} + \frac{\partial u_j}{\partial x_i} \right) \frac{\partial u_i}{\partial x_j} - \frac{C_2 \varepsilon^2}{k} \quad (5)$$

u_i represents velocities and x_i represents coordinates in tensor notation while t represents time and p is density of the fluid. T and p represents temperature and pressure, respectively. ν is the kinematic viscosity, α is the thermal diffusivity coefficient C_p specific heat and (β is the volumetric expansion coefficient of the fluid. q''' represents the heating power of a local heat source.

Eq.(3) ensures conservation of energy of each small volume of the flow field. The first term on the left-hand side represents the increase in energy by temperature-increase with time for the fluid in the element. The other three terms account for the net convection of heat into the fluid element. The right-hand terms describes heat conduction and heat sources.

Eq. (4) is a transport equation for turbulent kinetic energy. The terms on the right-hand side represents diffusion, production by velocity gradients and by temperature gradients and dissipation of turbulent kinetic energy.

Eq. (5) is a transport equation for dissipation rate of turbulence.

The equations above can be characterized as a set of coupled non-linear partial differential equations of second order. The equations are of elliptic type. This entails boundary conditions be given for the dependent variables on all parts of a continuous boundary enveloping the flow problem.

During the computation, the dependent variables are solved. Results are expressed as velocity components, turbulent kinetic energy and temperature for each grid or cell in the flow field.

8.2.3 Wall functions

Close to the wall the transport equations do not apply because of the dumping effect of the wall. In that region CFD programs must use algebraic equations called wall function. This approach does not require an ultrafine grid near the surface, so that it also contribute in saving calculation time. This approach will be discussed more in detail in chapter 8.3.

8.2.4 Solution of the transport equation

The general transport equation

The transport equations for momentum, temperature, concentration and the turbulence scales k and c and all have the general form :

$$\frac{\partial}{\partial t} (\rho\phi) + \text{div} (\rho V\phi - \Gamma_{\phi} \text{grad}\phi) = S_{\phi} \quad (8)$$

transient + convection - diffusion = source

where

In order to establish a more relevant parameter, the PPD-index was introduced. The PPD predicts the percentage of dissatisfied persons of a large group. The value for the PPD-index is directly dependent on the value of the PMV-index. It is recommended that the PPD be lower than 10 % to achieve sufficient thermal comfort in indoor environments. That corresponds to $-0.5 \leq \text{PMV} \leq +0.5$.

Mathematical expressions for the PMV- and PPD-indices are given in the ISO 7730.

The activity level of a person is expressed by a value for metabolism, and the thermal insulation of clothing is expressed by a clo-value. These values be set according to planned use of the atrium.

Air temperature and air velocity in every location in the zone of occupancy can be found by performing CFD-simulations for the atrium.

Then there is only one unknown value left to calculate the PMV. That is the value for mean radiant temperature. That value has to be computed by calculating the net exchange of radiation between a person and the surroundings. Generally, a lot of information on geometry and radiation properties for different surfaces have to be specified. A somewhat idealized approach for mean radiant temperature calculation is suggested by Tjelflaat. Calculations are based on the assumption that the atrium is empty except from one person that be placed in any location in the zone of occupancy.

Satisfying general thermal comfort is the most important issue. However, it is also important to evaluate local discomfort for people being in a sedentary position.

Draught is often causing local discomfort and is defined as heat loss by convection from parts of the body to the room air. Air speed and air temperature are the most important factors but it has been found that velocity fluctuations may enhance heat loss considerably. Draft has been considered and discussed by Fanger, and later his co-worker Melikow has given an extensive review of the field and a model for draft risk DR has been developed.

The percentage dissatisfied due to draught is given by:

$$DR = (34 - t_a) (v - 0.05)^{0.62} (0.37v \cdot Tu + 3.143) \quad (9)$$

where v is set equal to 0.05 m/s for $v < 0.05$ m/s and DR is set equal to 100% when DR is calculated to be larger than that.

KAMELEON-II is developed to solve the equations in general orthogonal coordinates. However, only Cartesian, cylindrical and spherical coordinate systems are included with the code. The Cartesian coordinates system is normally used to model ventilated rooms.

Flow boundary conditions at walls can be described as slip or non-slip conditions. Velocities and pressures must be described at inlets while zero-gradient in direction of flow is assumed for the variables at outlets.

The temperature of inlet flows must be given as boundary conditions. At walls, either the temperature or the heat flux must be prescribed.

Within the solution domain, closed or porous obstacles and heat- and contaminant sources and sinks can be modeled to simulate ventilated rooms realistically. An internal fan in the room can also be modeled by using a facility that can lock velocities for small areas within the flow field.

Numerical solution procedure

The finite-difference method is used to discretize the differential equations describing the problem. Three difference schemes are available by selection; the first order upwind-, the hybrid- and the power-law schemes. Normally, problems are first solved by using the upwind method as that is the most economical. The resulting set of algebraic equations is solved on a staggered grid.

To integrate the equations, a pressure correction method based on the simple algorithm is applied to iterate towards a converged solution. The use of 3 alternative improvements of the simple algorithm can be selected. The computational method is basically as described by Patankar (1980).

Three different matrix solvers are available; one for scalar processing computers and two for vector processing computers. One of the solvers for vector computers is for problems where the number of gridpoints is predominant in one direction.

A detailed description of the KAMELEON-II program can be found in Laksa and Vembe (1991).

Pre- and postprocessors

Lizard is a graphical preprocessor used to set up simulation cases for KAMELEON-II. Lizard runs on PCs and workstations. Monitor is a postprocessor used for graphical display of velocity- and temperature fields and for other parameters of interest.

8.2.7 Description of Flovent

Introduction

Flovent is a special-purpose computational fluid dynamic (CFD) program which has been conceived, specified and developed by collaboration between Flomerics Ltd and BSRIA (building serviced research and information association : UK). Flovent is a practical tool meeting the needs of the designers of heating, ventilation (mechanical or natural ventilation) and air-conditioning systems for building. This program is commercially available.

Problem formulation

Flovent is capable of solving the same general flow problems presented in the KAMELEON description. As Flovent is using similar turbulence model and numerical solution procedure as KAMELEON, it is not useful to repeat here this introduction. We will simply point out the principal differences with KAMELEON.

Only cartesian coordinates are available in Flovent

At wall either the temperature, or the temperature and the heat coefficient transfer or the heat flux can be specified.

The thermal effect (inertial) of the wall can be taken into account although it is time consuming (unsteady calculation).

The infra red radiation can be modelled between two different surfaces.

Calculation procedures for thermal environment parameters as comfort have been developed, but not air quality values are available directly from the results (they must be put processed).

•

8.2.8 Limitations

CFD are limited in different directions and need to be improved in the following areas :

The need for a universal turbulence model which is valid near walls and at predominant Reynolds-numbers in the core of the enclosure.

- Need for more accurate prediction of natural and mixed convection at cold or warm surfaces.
- Need for improved modelling of supply jet devices.
- Need for improved computational grid. - Problems with number and size of grid cells and difficulty of achieving grid-independent solutions; especially for large enclosures.
- Need for improved numerical procedure to reach solution of system of finite-difference equations. - It can be difficult or slow to achieve converged solutions, especially for large enclosures with buoyant flow.
- Need for addition of radiation modelling to CFD codes.
- Need for knowledge of the interaction of the airflow with thermal building dynamics.

That said, significant advances in the above areas have been made. Many investigators (Murakami & Kato 1989; Whittle 1991; and others) have argued that common CFD codes are already capable of predicting room air movement with sufficient realism to be of use in design practice, despite their shortcomings.

The second issue is that a high degree of engineering judgement and experience is needed to apply CFD to actual buildings, and achieve realistic solutions. The user must have knowledge from the fields of HVAC and fluid dynamics, with elements from numerical methods as well as architectural and building engineering. There is therefore a need for guidelines for the use of CFD.

•

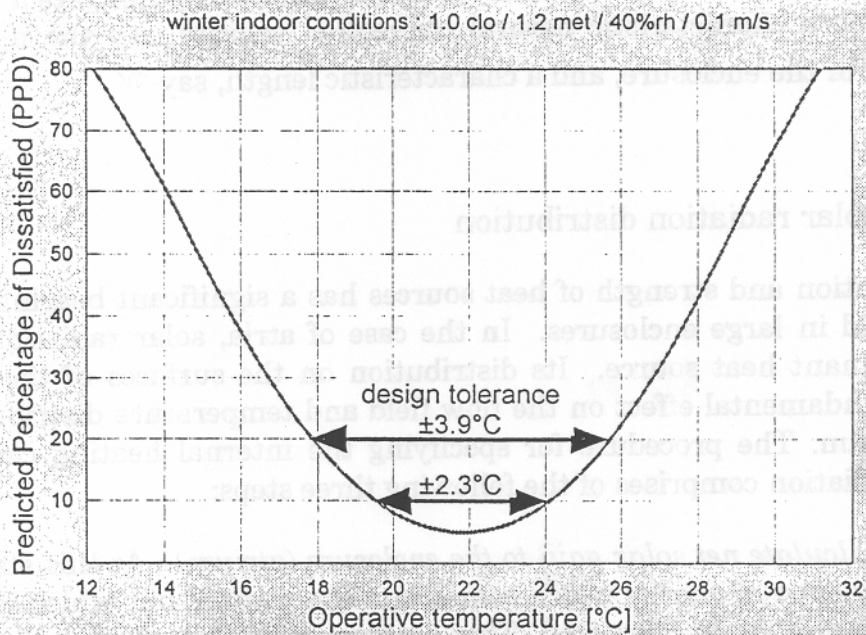


Fig. 1

The accuracy of CFD calculations depends on the integration method, grid size and other parameters. Using a coarse grid causes larger numerical errors. But when modelling atria and other large enclosures, it is computationally costly to use a fine grid throughout the flowfield. Thus for practical applications of CFD, a balance must be struck between computational accuracy and computing cost. The computational accuracy depends not only on the total number of grid points, but also on their distribution over the computational domain. The grid should be most refined in regions of large gradients, in particular near walls, supply jets and outlets.

Borth & Suter (1994) have suggested a dimensionless number G (Equation 11) which can be a guide to determining the required level of grid discretization for 3-dimensional CFD simulation of a room with mixing ventilation.

$$G = \left(\frac{V}{N}\right)^{\frac{2}{3}} \frac{n}{v} \quad (11)$$

In their test case, using a standard k - ϵ turbulence model, a coarse grid of $G > 1$ was found to be sufficient for only qualitative evaluation of the simulation results. The use of a finer grid of $G < 1$, was suggested to be adequate for qualitative purposes. These guidelines can not directly be applied to modelling atria which have predominantly buoyancy-driven flow, though it may be possible to develop relevant guidelines along the

- The last distribution method tried was more rigorous. It takes into account the first specular and two diffuse reflections of the solar radiation. See Figure 2.

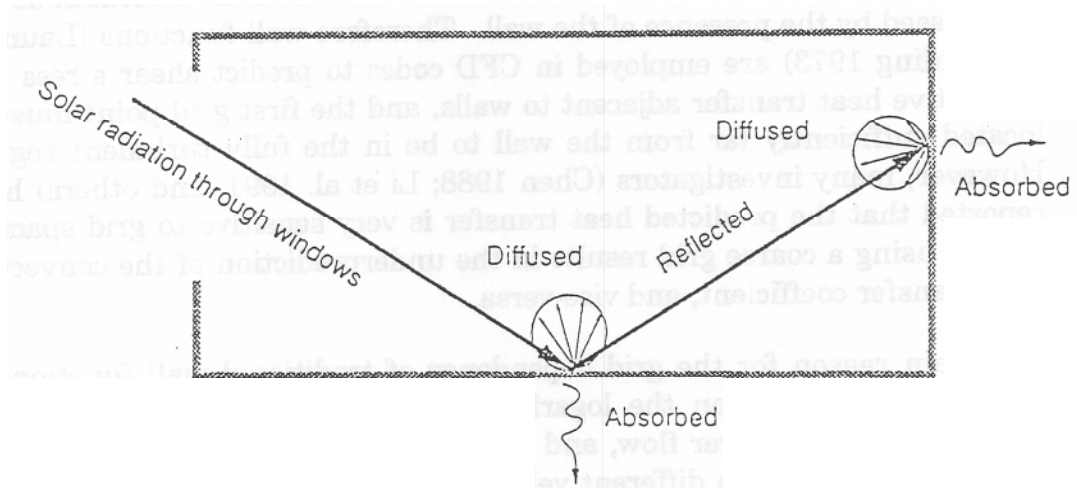


Fig. 2

A heat flux boundary condition was used in all three cases. The results presented and compared with measurements in Figure 3. It is interesting to note that with the distribution based on surface ratio, there was insignificant thermal stratification. Already with the distribution method using only the surface directly heated by the sun, the resulting vertical temperature profile was much closer to that which was measured. The last distribution method was slightly more accurate.

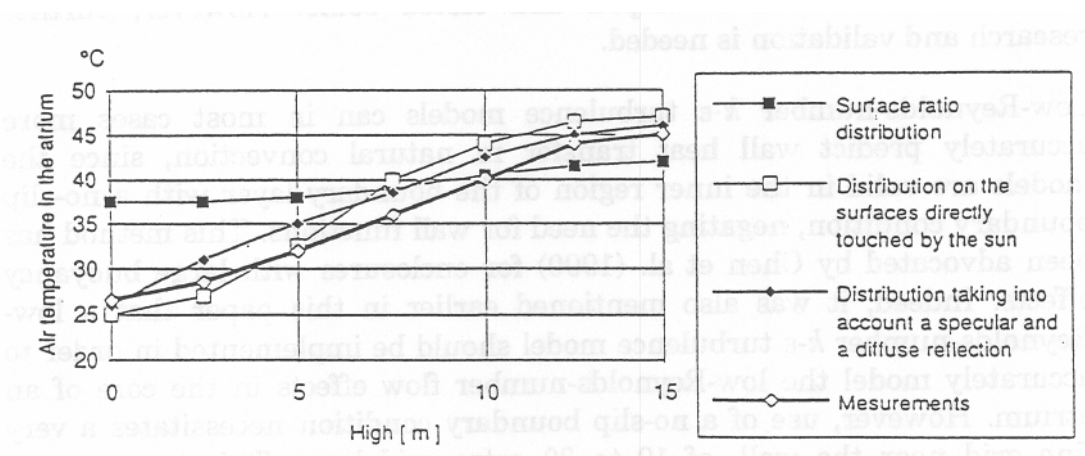


Fig. 3

The current study: The objective of the current study has been to establish the most accurate way of defining natural convection boundary conditions using a k-s model with wall functions, and to quantify the errors involved. A 2-dimensional model of a large atrium (10m high, 10m wide) has been studied with the CFD code Flovent (Figures 4 & 5a). All of the atrium's surfaces are adiabatic except for a high cold wall. The cold wall's U-value ($2 \text{ W/m}^2\text{K}$) and the steady-state outside design air temperature (0°C) are both explicitly known. Air is supplied at low velocity from the roof (20°C , 0.01m/s) and is extracted through a 0.5m wide slot at the foot of the cold wall. The downdraught from the cold wall is therefore 'sucked out' at floor level, such that the air in the core of the atrium is stagnant and thermally stratified. The Rayleigh number for the atrium ($\text{Ra}=7 \times 10^{11}$) is very high, implying predominantly buoyancy-driven airflow. For simplicity, solar radiation was not modelled, and surface-to-surface radiation exchange was only modelled in the last case (Figure 5b). The following topics were investigated:

- Methods of defining boundary conditions
- Grid resolution near the cold wall
- The need for surface-to-surface radiation modelling

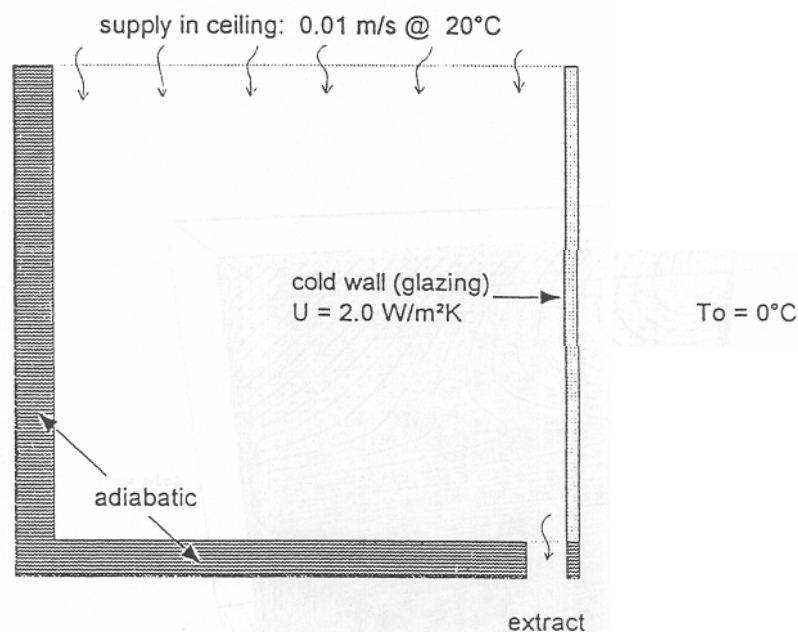


Fig. 4

Study of different boundary condition methods

The following five common methods of prescribing boundary conditions were investigated. For simplicity, each method has been given a shortcode. See also Figure 6.

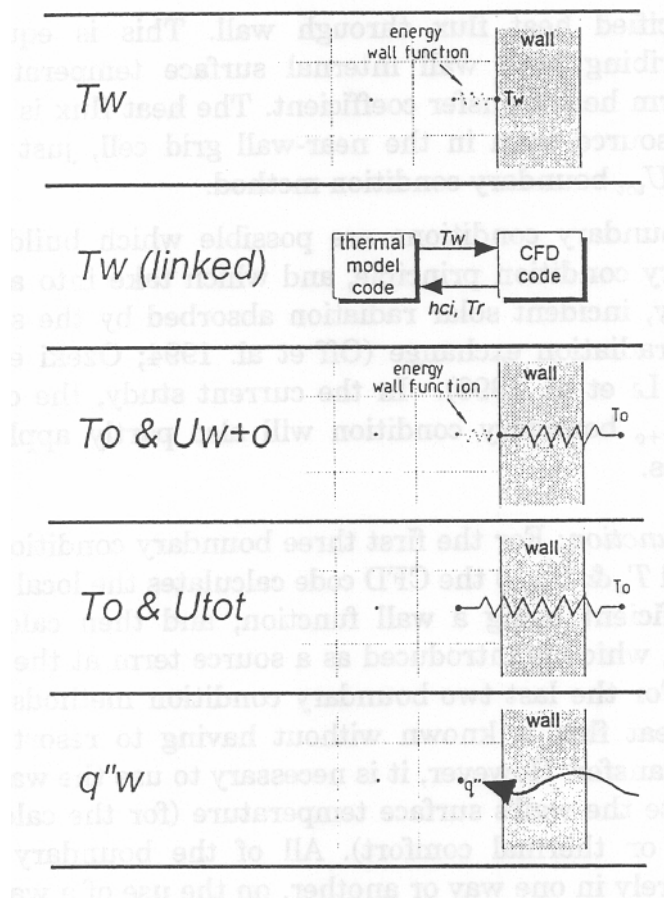


Fig. 6

code	description
T_w	• Specified wall internal-surface temperature.
$T_w(\text{linked})$	• The CFD code using the T_w boundary condition, is iteratively linked to a building thermal modelling code. The thermal model is fed the calculated bulk convective heat transfer coefficient for each surface, and room bulk temperature, from the CFD code, and returns a recalculated value of T_w to the CFD code. In this study the thermal model was set up on a spreadsheet, and the 'linking' was done by hand 7 times at intervals of approximately 500 iterations.

Below is a rendition of how the T_w and q boundary conditions were calculated in the study.

- (1) *Decide the internal & external heat transfer coefficients.* In this case, the values given in Norwegian Standard NS 3031 (1987) were used: $h_{ci}=2.7 \text{ W/m}^2\text{K}$; $h_o=25 \text{ W/m}^2\text{K}$. The choice of internal heat transfer coefficients for real buildings is a matter of debate. A comparison of the natural convection heat transfer coefficient correlations for vertical surfaces (external & in enclosures), collated by Dascalaki et al. (1994), which are valid at the Rayleigh number for the modelled atrium, gave a best fit value of $3.0\pm 0.6 \text{ W/m}^2\text{K}$ which is close to, and understandably slightly higher than the value specified in NS 3031.
- (2) *Decide the bulk air temperature (heat transfer temperature),* which is a function of the inlet/outlet air temperatures in the atrium, and the airflow pattern. In this study it was sensible to assume that $T_r=T_s$ since the cold downdraught mixed little with the room air before being sucked out at floor level. For a general enclosure the relationship is $T_r = x \cdot T_s + (1-x) \cdot T_e$ where x takes a value between 0 and 1.
- (3) *Solve the energy balance for the atrium,* using the assumptions from steps (1) & (2) above, to find q and T_w . The energy balance involves the two equations:
 - $q A_w = c_p (T_s - T_e)$
 - $q = h_{ci} (T_w - T_r)$ where: $T_w = T_r - (T_r - T_o) \cdot U_{tot} / h_{ci}$

In this study, the solution was $q=27.013 \text{ W/m}^2$ and $T_w=9.995^\circ\text{C}$.

A good example of applying the above principles to the design of a real atrium, is given by Kondo & Niwa (1992) who used an advanced multi-zone dynamic thermal model for the calculation of their boundary conditions.

The boundary condition method T_o & U_{tot} relies only on one of the aforementioned assumptions; that of the value of h_{ci} . For the boundary condition methods T_o & U_{w+o} and T_w (linked), no such assumptions had to be made, and so they would not be expected to suffer from errors in this respect.

Additional calculations: The CFD results were imported into a spreadsheet for post-processing. The bulk air temperature (T_r), convective heat transfer coefficient (h_{ci}) at every height along the wall (Equation 12), and nondimensional distance from the wall (y^+) (Equation 13) are some of the post-calculated variables.

$$h_{ci_x} = q_{w_x} (T_r - T_{w_x}) \quad (12)$$

$$y^+ = \frac{y_p u_\tau}{\nu} \quad \text{where } u_\tau = C_\mu^{1/4} k_p^{1/2} \quad (13)$$

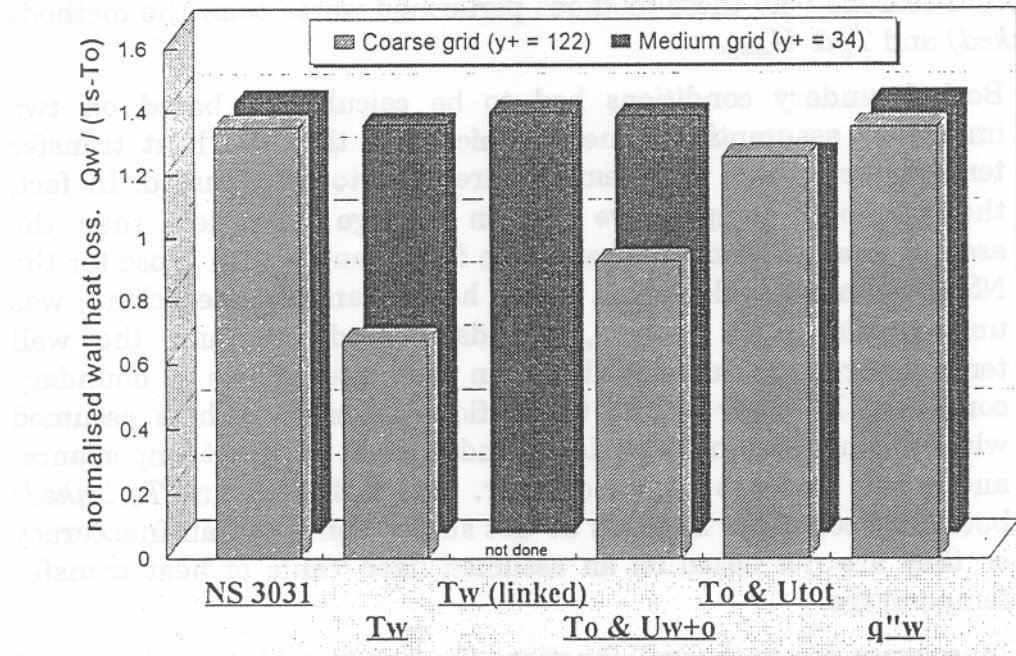


Fig. 8a

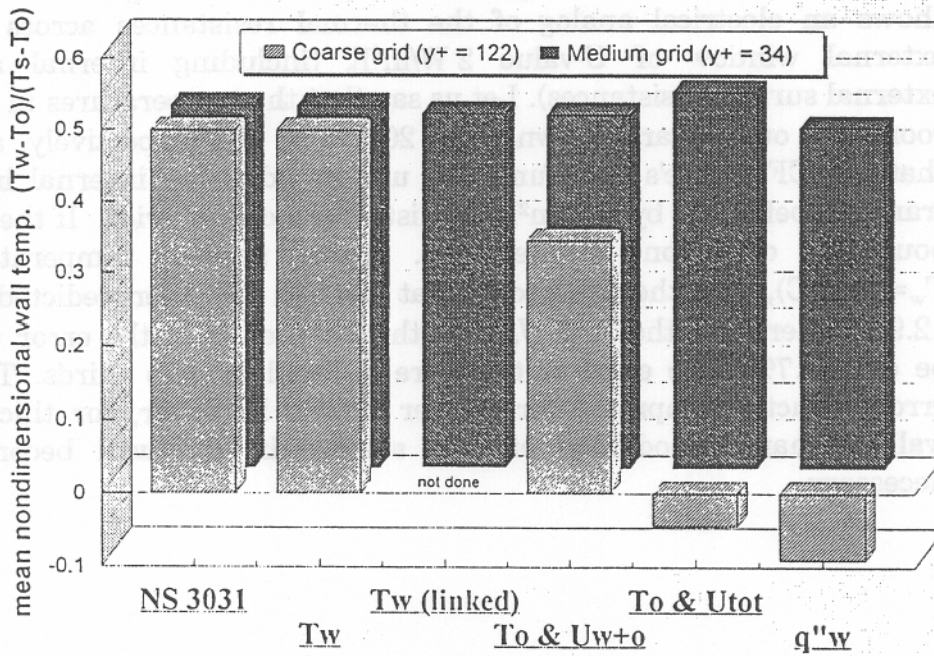


Fig. 8b

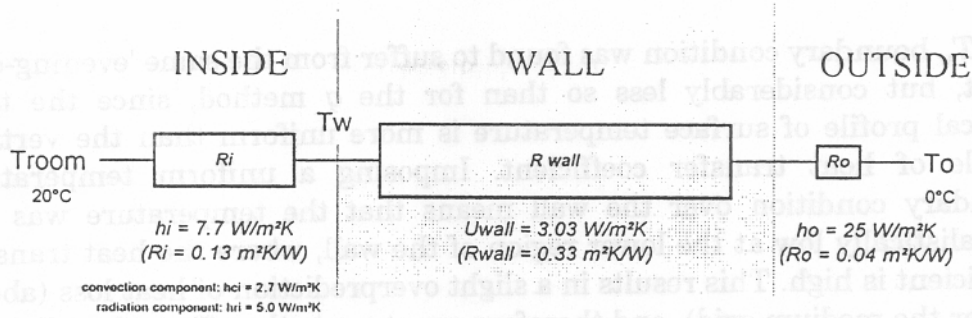


Fig. 9

(3) Enforcing uniform values of T_w , or q along the wall's height is another cause of inaccuracy. For the q boundary condition, this results in an 'evening-out' of wall heat flux, such that the wall heat loss at the top of the cold wall is set unrealistically high and vice versa for the bottom region of the wall. At the top region of the cold wall the convective heat transfer coefficient is low because the cold downdraught is not yet fully developed. The heat transfer coefficient increases with distance down the wall. For the coarse grid, applying the wall functions to calculate the wall surface temperature resulted in large negative temperatures at the top quarter of the wall ($-80^{\circ}C$ at top of wall), which is physically unrealistic. The wall's mean surface temperature was calculated to be $-1.8^{\circ}C$ in the case of the coarse grid calculation; i.e. lower than both the room temperature and outside temperature. This is illustrated in Figure 10 which shows the predicted surface temperature profiles for each boundary condition.

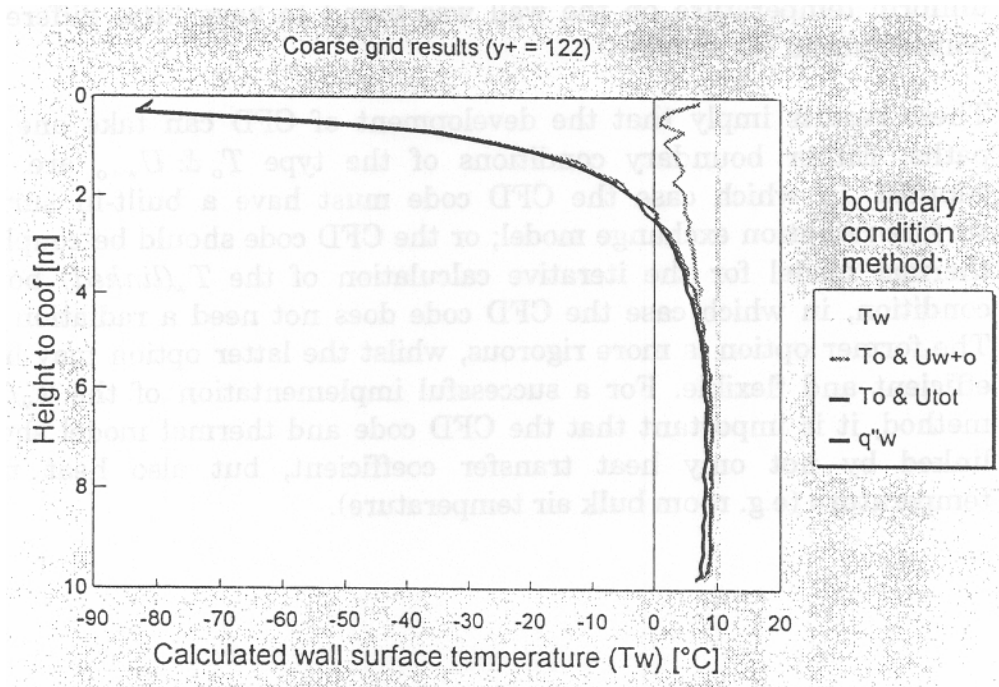


Fig. 10

Further study of grid refinement

A more detailed study was carried out using just the T_o & U_{W+o} boundary condition. Different grades of grid refinement were tested, with the first grid point located in various regions of the draught's boundary layer; from within viscous sublayer ($\Delta y=2.2\text{mm}, y^+=2.4$) to the turbulent outer region ($\Delta y=1000\text{mm}, y^+=207$). Figure 11 shows y^+ versus predicted mean bulk heat transfer coefficient and mean nondimensional wall temperature. It is clear from the chart that the results are highly grid dependent, due mainly to the unsuitability of the wall functions for natural convection boundary layers.

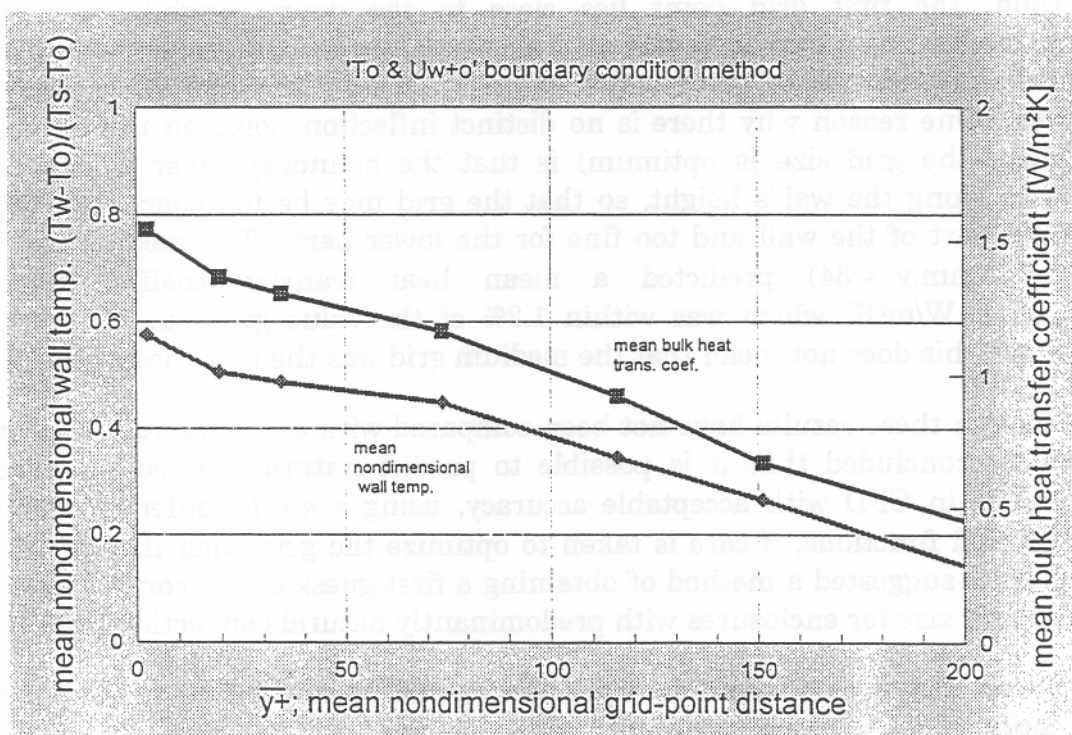


Fig. 11

Combining Equations 14 and 15 gives the following relation for estimating the required near-wall grid element size (Δy) in millimeters:

$$y = 5.35(g\beta\Delta T_f)^{-0.1} H^{0.7} \quad (15)$$

If, after the first CFD simulation, the resulting value of y^+ is unsuitable, then the near-wall grid size should be fine-tuned before performing further simulations. A crude method of fine-tuning the grid is to assume that y is proportional to y^+ (assuming constant wall shear stress through the boundary layer). It is thereby possible to use extrapolation or interpolation to estimate y for $y^+ = 30$.

The need for radiation modelling

For the final part of the study, surface-to-surface long-wave thermal radiation was modelled in the CFD simulation of the model atrium. The radiation fluxes were imposed as plane heat sources/sinks on the internal surfaces of the atrium. A simple radiation model to calculate the radiant fluxes, was set up on a spreadsheet. The radiant fluxes were recalculated and entered into the CFD program 11 times, at intervals of approximately 1700 iterations. Figures 5a and 5b show the resulting temperature and flow fields for the simulations without, and with surface-to-surface radiation. It is clear from these figures that the temperature and flow fields are significantly different. It is therefore vital that CFD simulations of atria should include surface-to-surface radiation exchange.

Models for internal heat sources

The most significant heat source in an atrium is solar gain. Two simple ways of introducing solar gain boundary conditions are:

(1) *Heat flux specification (q):* This is the easiest way, though it is strictly only suitable if the surface is lightweight and well insulated. In this context the q boundary condition does not suffer the same degree of poorly predicted wall temperature, as was observed earlier when the q specification was applied to model heat transfer through a wall of known U-value. Strictly speaking, the value of q should be taken from a dynamic thermal model with surface-to-surface radiation exchange, using the correct distribution of solar gains.

(2) *Surface temperature specification (or $T_w(\text{linked})$):* In this case, a dynamic thermal modelling program is needed to calculate the temperatures of the different surfaces in the atrium, using the correct distribution of solar gains. If the T_w boundary condition is used then the wall heat flux will be erroneous, whereas the $T_w(\text{linked})$ method will more accurately model the wall heat flux.

$$\Delta p = \frac{1}{2} f \rho V^2 \quad (17)$$

V = average velocity through the opening

ρ = density of the air

f = loss coefficient

The effect of the wind on an opening can be taken into account by increasing the relative pressure :

$$P_{\text{stagnation}} = p + \frac{1}{2} C_p \rho W^2 \quad (18)$$

W = wind velocity at the opening level

ρ = density of the outside air

C_p = Pressure distribution coefficient at the opening level

The hydrostatic pressure does not need to be included in the - relative pressure because it is already included in the momentum equation which is solved by the programme. But it is important to define the reference temperature and density. Normally the external air temperature and density are chosen.

The infiltration through leakages of the building envelope can also be defined in the similar way. The problem is to find the location of these leakages, their size and pressure drop coefficient.

Sometimes when the overall air exchange rate has been measured, it is possible to simplify the boundary condition by introducing under the neutral axis the total amount of the outside air in a diffuse way (large opening surface) and by extracting the same amount of air over the neutral axis also in a diffuse way. This method has been used in a winter simulation of the ELA atrium with some success.

Steady-state or transient boundary conditions

The effect of thermal capacity can have a large impact on the environment in an atrium. Ozeki et al. (1994) report that the predicted mean room air temperature in a very large atrium was significantly different when a dynamic simulation was carried out. The swings in temperature were damped (peak temperature was 4°C lower) and delayed significantly (by 3 hours). They conclude that a transient analysis is imperative for such enclosures.

Holmes et al (1990) also report on transient CFD simulation, this time of an office. The CFD code was coupled to a dynamic thermal model to evaluate the performance of the HVAC controls. The computational overhead of coupling a dynamic thermal model was 0.5%, the run time being dominated by the heavy computational requirements of the transient CFD analysis.

8.4 Example of CFD applications in atria

8.4.1 University of Neuchâtel

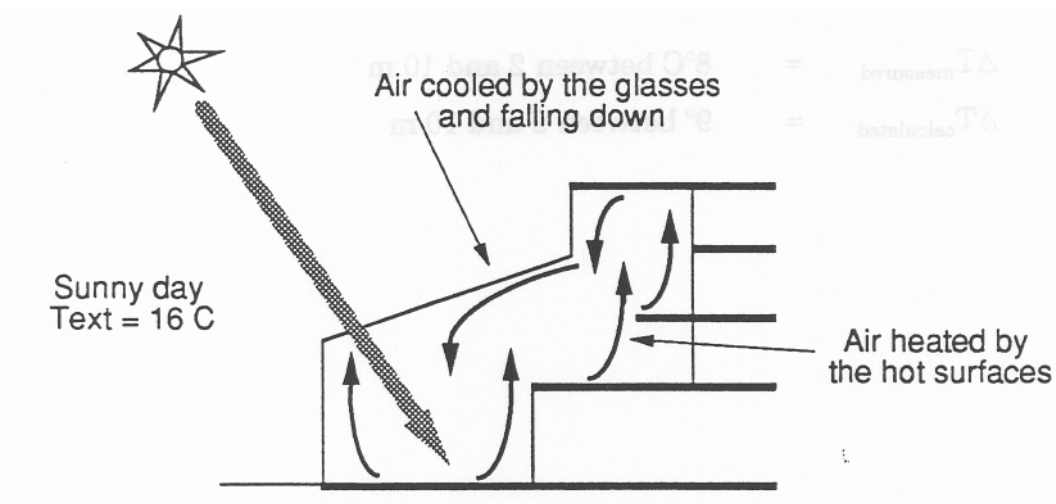
A flow field simulation of some typical cases of the atrium of the university of Neuchatel (CH) has been done during the annex.

This atrium has been presented in chapter 7. 2-D steady calculations have been done for different typical cases :

A) **No solar protections and no passive cooling (no openings)**

No important stratification occurs because the solar gains are directly heating the floor and the wall. The "cold" window surfaces are cooling the air and creating a downdraft flow; the "warm" surfaces as floor and front wall are creating an upwind flow.

These two flows are mixing the air and disturb the stratification of the temperature.



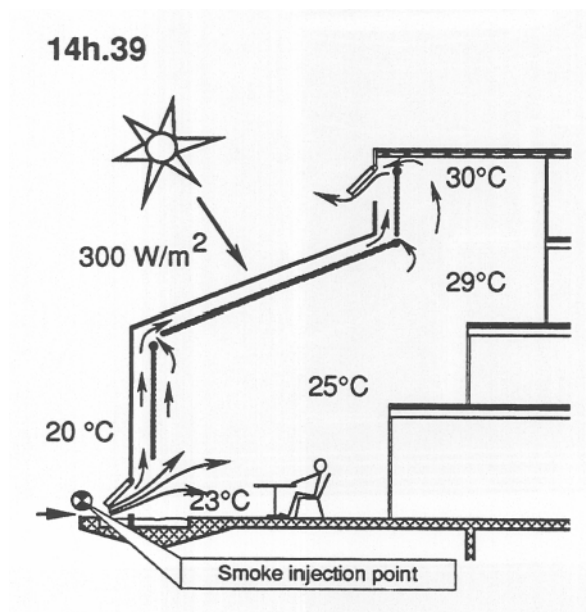
$$\Delta T_{\text{measured}} = 3 \text{ to } 4^{\circ}\text{C between 2 and 10 m}$$

$$\Delta T_{\text{calculated}} = 4^{\circ} \text{ between 2 and 10 m}$$

C) Solar protections with passive cooling

The situation is the same as case B but the lower and upper hatches are opened.

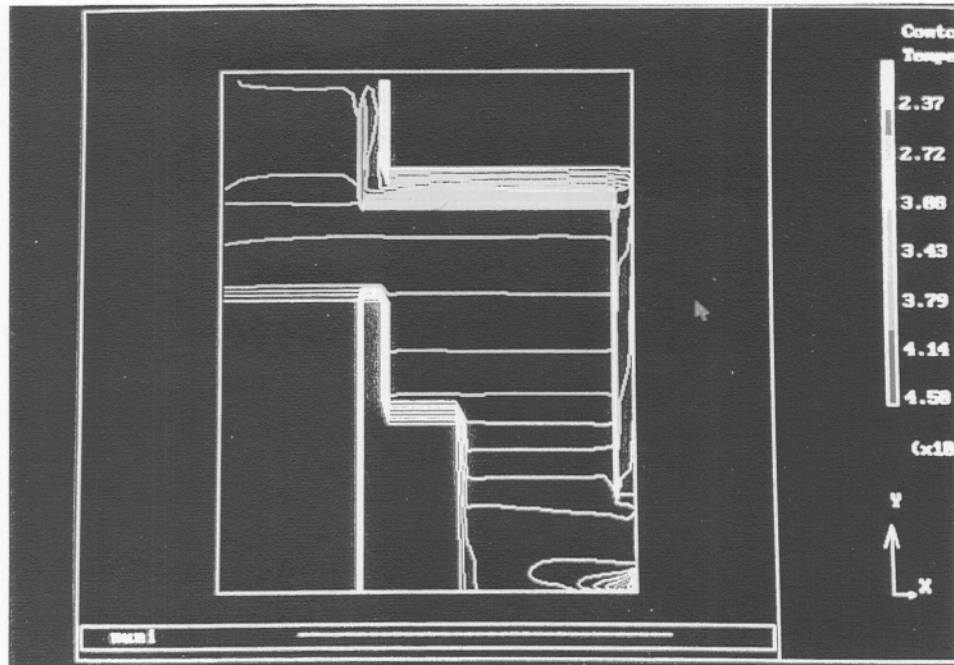
The arrows shown in the next figure are representing the flow direction determined with the aid of smoke flow visualisation.



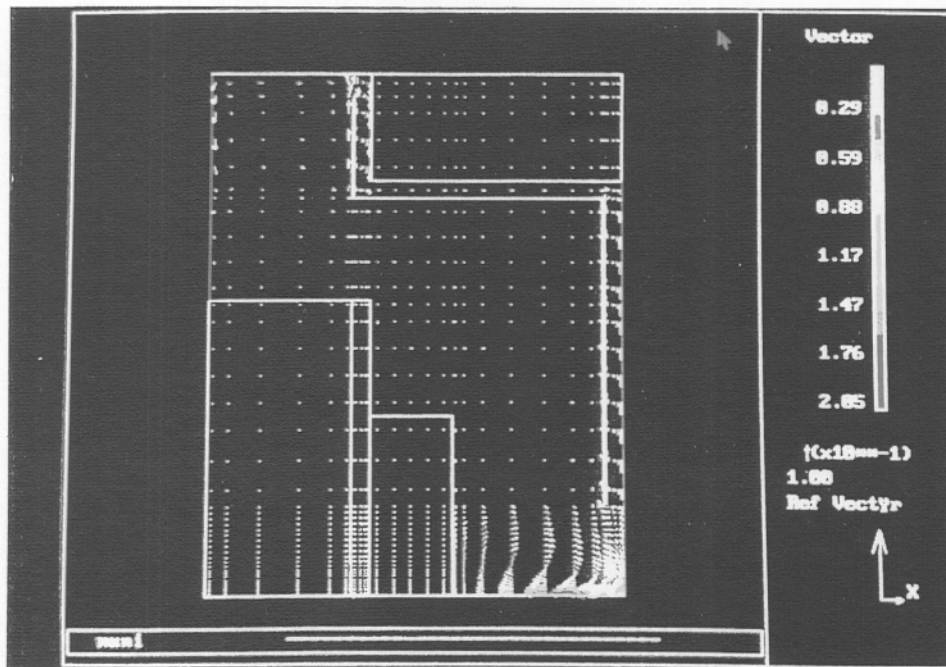
$\Delta T_{\text{measured}} = 5^{\circ}\text{C}$ between 2 and 10 m
 $\Delta T_{\text{calculated}} = 4^{\circ}\text{C}$ between 2 and 10 m

D) Solar protections with only low opening

Here only the low hatches have been opened. The results of the CFD calculation: are shown in the next figures.



$\Delta T_{\text{measured}} = 21^{\circ}\text{C}$ $\Delta T_{\text{calculated}} = 17^{\circ}\text{C}$ between 2 and 10 m



Although a complete quantitative comparison make no sense, because NUNI is a 3-D case and the boundary conditions are complex, one can see that the principal phenomena have been correctly simulated by the program.

8.4.2 Comparison of the measured temperature field in a real atrium with the Flovent and Kameleon calculation

Two typical situations have been calculated with CFD and compared with the measurements :

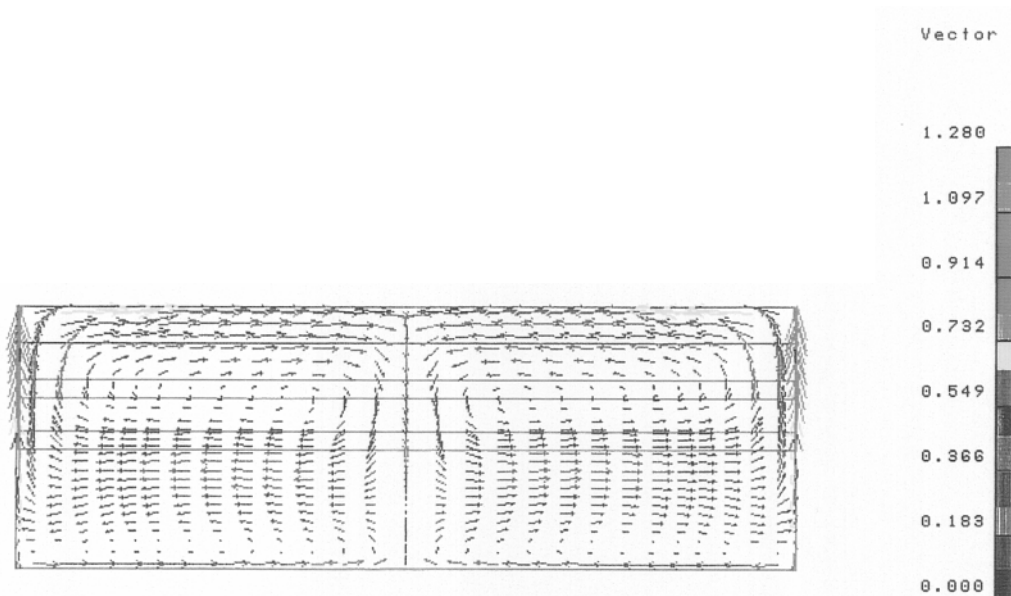
- Winter case with heating convectors (night)
- Summer case with and without opened vents (midday)

The atria used for the comparison is situated in Trondheim (Norway). The data of the building is as follows :

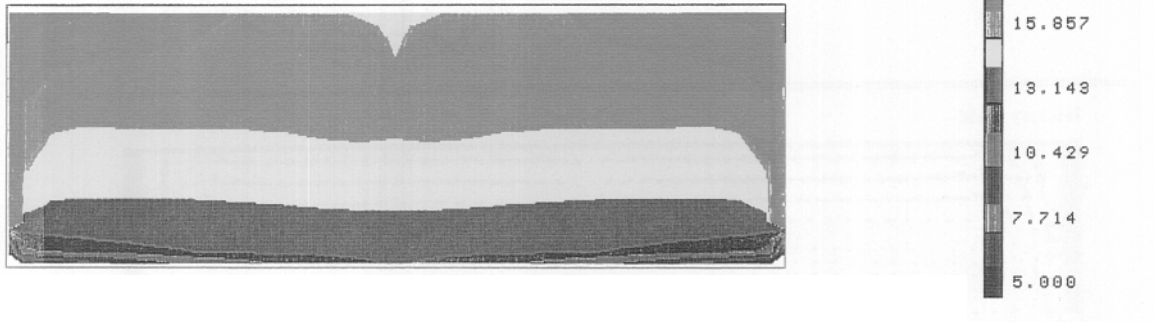
Characteristic measures of one atrium, SG1:	U-values (W/m ² K):	Design temperatures:
Length, m: 46	- Atrium glazing: 2.1	- Atria: 15°C
Width, m: 10	- Windows in exterior walls: 2.1	- Offices: 20°C
Max. Height, m: 16	- Intermediate wall: 3.2	
Volume, m ³ : 7003		

Winter case : night

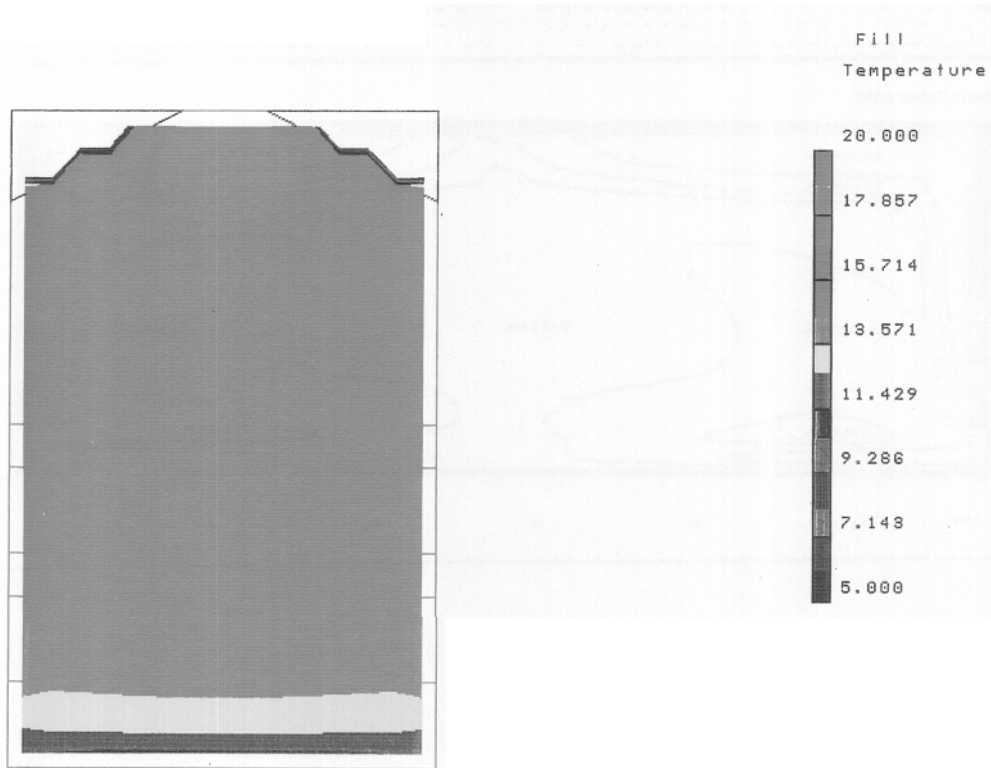
Outside temperature: -19°C Unvalue glasses = 3 W/m²k
 Office temperature: 20°C Unvalue of the walls = 2.1 W/m²k
 heat of convectors situated on the gable 100 kW Infiltration = 0.5 V/h



Calculated flow field in the middle of the atria

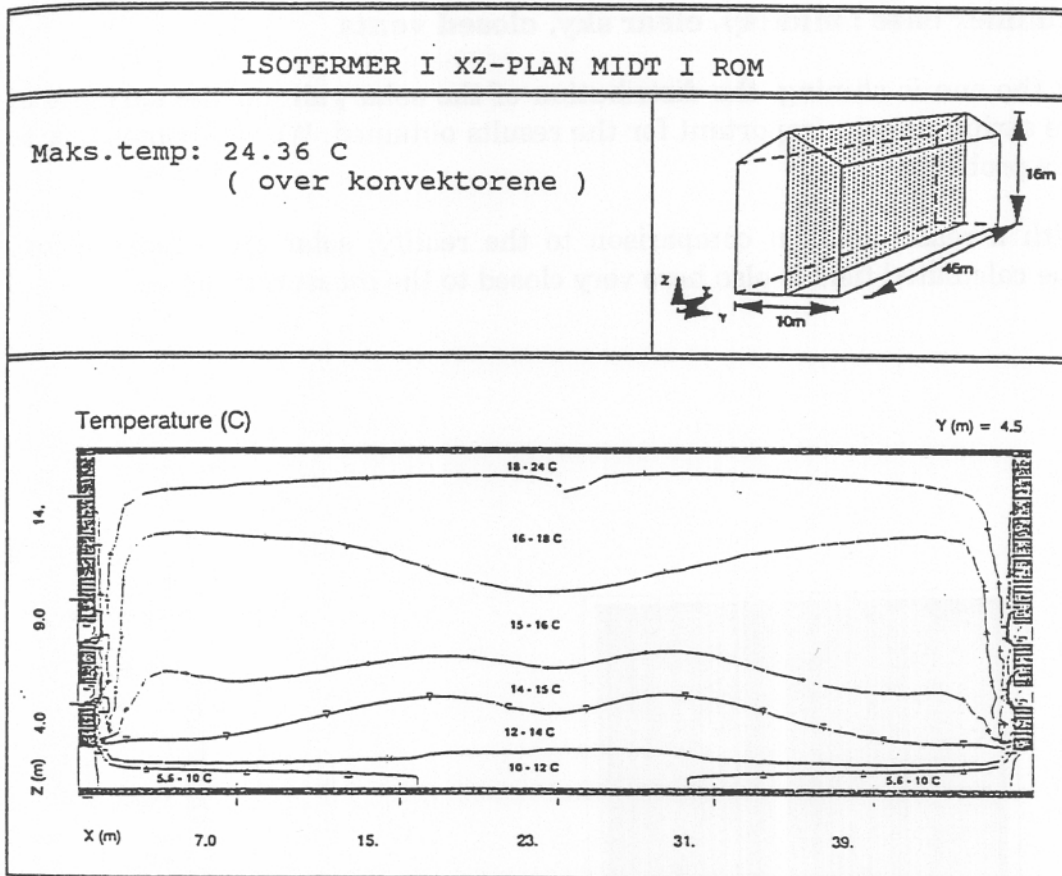


Calculated temperature field in the middle of atria



Calculated and measured temperature field in the section A.

As we can see in the above figure the temperature which has been calculated correspond rather well to the measured values. Similar calculations have been performed with the program Kameleon. The flow and the temperature fields we presented in the next two figures. Also here the comparison is good and shows the ability of CFD if used correctly to predict internal indoors environment.

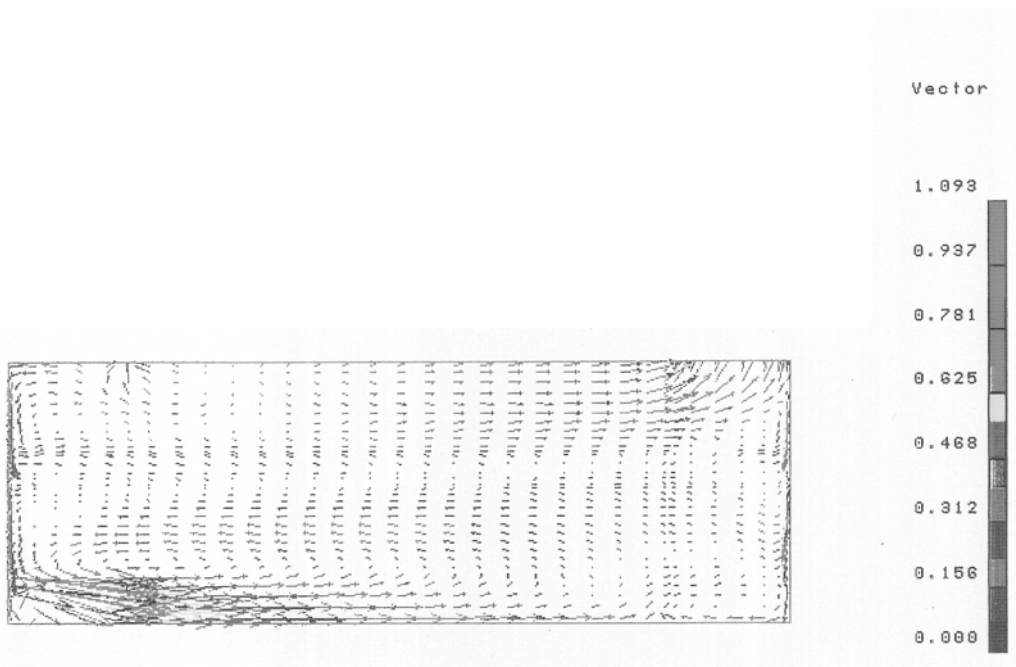


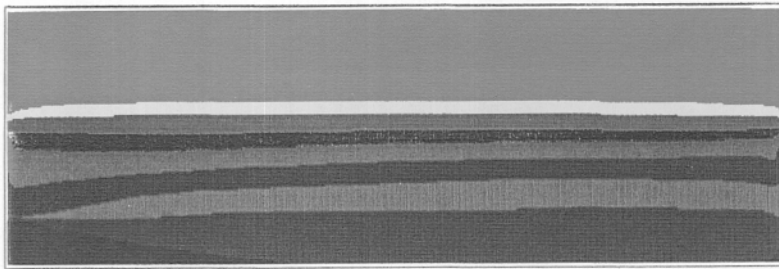
Summer case : Midday, clear sky, opened vents

With opened vents both the temperature stratification and the average temperature level decreases.

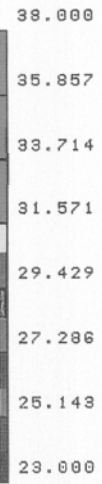
A quantitative comparison is difficult because of some unknown values as the wind velocity, and exact opened surfaces.

The qualitative as effect is predicted correctly by the Flovent calculation, some more complete set of data will be collected in the frame of IEA task 26 and will allow a better comparison. The two following figures illustrate the temperature and flow fields calculated with Flovent with 6 m² opening area, no wind and external air temperature of 23°C.





Fill
Temperature



8.4.3 Validation of simplified model for natural ventilation with CFD calculations

In order to be able to use the atrium also during the summer, it is important to avoid overheating in the atrium. For that two things have to be done :

1. Internal or external shadowing devices
2. Openings -> natural ventilation

The first point will not be discussed here. We will focus the attention on point 2 : cooling by natural ventilation.

Two things are of interest when we try to ventilate an atrium.

- a) Is the necessary cooling load achieved (air exchange rate) ?
- b) Are the velocity in the region of the occupation zone in atrium not too high (comfort problem) and the temperature too low.

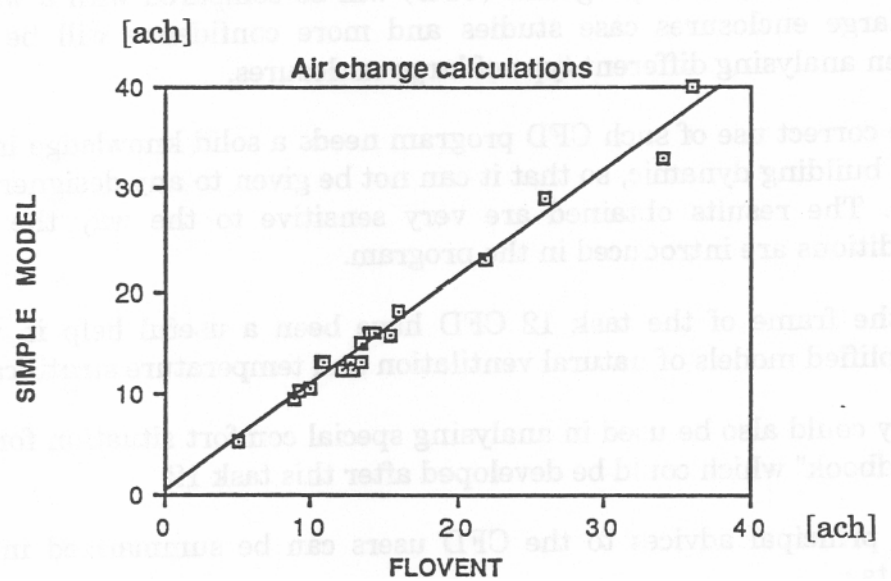
The simplified models should answer to the first question, and allow to determine an air exchange rate of the atrium with the outlet which could be used in the building calculation.

The second question is more difficult to answer with simplified model. Velocity distribution in the occupancy region are given for the moment only by CFD programs. It is for the moment not known if simplified input profiles such as those of wall jets, or displacement ventilation could be applied in this case with some success.

As there is a lack of measurements data in atria, Flovent has been used in order to overcome this problem. The simplified models based on the Bernouille equation have been validated in comparison with the Flovent results in different typical situations.

The figures of the next pages are illustrating some possible situations which could interest the designer.

The next figure shows a global comparison between the results of the simplified models and those obtained with Flovent for different situation and boundary conditions.



These models are really promising in calculating overall air exchange rates when the temperature profile in the atrium is known and well calculated. More detail on these simplified models and their comparison with CFD calculation are given in chapter 6.

- For external walls/floor/roof it is best to use a boundary condition for heat transfer that implicitly depends the outside ambient conditions. Three good ways of doing this have been identified :

One method is to prescribe the outside air temperature and the U-value between the wall's inside surface and the outside air. The CFD code is left to calculate the internal convective heat transfer coefficient. The CFD code must include a radiation exchange model.

A second method is to couple the CFD code with a thermal model. Each iteration, the thermal model is fed the calculated bulk convective heat transfer coefficient for each surface, together with the heat transfer (bulk air temperature), and returns recalculated values of surface temperature to the CFD code. This method gives almost identical results to the method above, although in this case the radiation model should be implemented in the thermal model.

A third method also involves coupling the CFD code with a thermal model. Each iteration, the thermal model is fed the calculated heat transfer temperature from the CFD code, and uses an empirical convective heat transfer coefficient for each surface to recalculate values of wall heat flux that are then fed back to the CFD code. However, the choice of suitable empirical local convective heat transfer coefficients (i.e. between the wall and first row of grid points) is open to debate.

The first two methods are suggested for fine grid analysis. For these two methods it is vital to refine the near-wall grid, as described in the next point. The third method averts the need for a temperature wall function, and so is the best choice for coarse grid analysis.

Conventional wall-functions are inadequate for modelling natural convection boundary layer flow. The results are not independent of near-wall grid resolution, so the user should fine-tune the grid size.

Our study suggest an optimum value for $y^+ = 30$. More research is needed before improved wall-functions for natural/mixed convection can be widely adopted.

- Care should be taken to refine the computational grid in regions of locally steep gradients. Automatic grid generation (adaptive grid methods) makes this easier. Steady-state supply jets should be modelled using either the box method or the prescribed velocity method. This reduces the number of grid points needed to model the atrium.

It is vital to account for heat transfer by surface-to-surface radiation exchange.

- It is important to model the thermal capacity of an atrium's building structure. This is most simply done by carrying out a steady-state CFD simulation of the worst-case (design) condition, using quasi

8.6 Summary

Computational fluid dynamics - CFD seems to be a very promising tool in the design process for atria and other large rooms. The continuous development of computer technology and software and the decreasing costs for computing, makes the CFD a must for future design.

CFD-simulations seem to have the most cost-effective use for verification of indoor environment and for trouble shooting. That is for the last stage in the design process before construction. At previous stages in the process, when information is more scarce, experience and simpler tools should be used to keep costs at a low level.

The objective of this chapter is on one hand to explain why CFD has been used in the Task 12 and in the other hand to bring attention to and to give guidance to the most essential factors in achieving a realistic and accurate solutions from CFD-simulations of atria.

Greek symbols

α	molecular thermal diffusivity ($= k/\rho c_p$) [m^2/s]
α_t	turbulent thermal diffusivity [m^2/s]
β	coefficient of thermal expansion [K^{-1}]
ε	turbulence energy dissipation rate
ν	molecular kinematic viscosity ($= \mu/\rho$) [m^2/s]
ν_t	turbulent kinematic viscosity (eddy kinematic viscosity) [m^2/s]
ρ	fluid density [kg/m^3]
ρ_0	reference fluid density [kg/m^3]
σ_t	turbulent Prandtl number, usually =0.9
$\sigma_{k,\varepsilon}$	empirical coefficients in the k - ε turbulence model

- ISO 7730. Moderate thermal environments - Determination of the PMV and PPD indices and specification of the conditions for thermal comfort. 1990-10-05 (E)
- Jones, P.J. & Whittle, G.E. 1992. Computational fluid dynamics for building air flow prediction : current status and capabilities. Building and Environment, Vol.27, No.3 (July), pp.321-338
- Kondo, Y. & Niwa, H. 1992. Numerical study of an atrium by means of a macroscopic model and k-e turbulence model. Proc. Int. Symp. Room Air Convection and Vent. Effectiveness : Soc. Heat. Air Cond. Sanitary Eng. of Japan, Tokyo, Japan. 22-24 July 1992. pp.109-113
- Lauder, B.E. & Spalding, D.B. 1974. The numerical computation of turbulent flows. Computer methods in applied Mechanics and Engineering, Vol.3, pp.269-289
- Li, Y.; Fuchs, L. & Holmberg, S. 1991. An evaluation of a computer code for predicting indoor airflow and heat transfer. Air Movement and Ventilation Control within Buildings. Proceedings of 12th AIVC Conference. Ottawa, AIC, Vol.3, p.123-136
- Li, Y.; Fuchs, L. & Sandberg, M. 1993. Numerical prediction of airflow and heat-radiation interaction in a room with displacement ventilation. Energy & Buildings, Vol.20, pp.27-43
- Melikow, A.K. 1988. Quantifying draught risk, Br& Kjær Technical Review No.2, Nærum, Denmark.
- Moser, A. 1992. Numerical simulation of room thermal convection - review of IEA Annex 20 results. Proc. Int. Symp. Room Air Convection and Vent. Effectiveness, Tokyo : Soc. Heat. Air Cond. Sanitary Eng. of Japan. 22-24 July. pp.77-86
- Murakami, S. & Kato, S. Numerical and experimental study on room airflow - 3D predictions using the k-e turbulence model. Building and Environment, 1989, vol.24, no.1, p.85-97
- Murakami, S. 1992. Prediction, analysis and design for indoor climate in large enclosures. Roomvent'92. Proceedings of Third International Conference, Aalborg, Denmark : DANVAK. September 1992. Vol.1, pp.1-30
- Nielsen, P.V. 1992. Description of supply openings in numerical models for room air distribution. ASHRAE Transactions, Vol.98, Part.1, pp.963-971
- NS 3031. 1987. Calculation of buildings' energy consumption and demand, for heating and ventilation. (in Norwegian), Norwegian Standards Institution (NSF), 4th ed., May 1987.
- Off, F.; Schälin, A. & Moser, A. 1994. Numerical simulation of air flow and temperature in large enclosures with surface radiation exchange.

9. Building energy simulation programs

9.1 Introduction

This chapter contains a short description of the Building Energy Simulation Programs used in this study. The simulation programs are DEROB (Sweden), Fres (Norway), TRNSYS (developed in USA, used by Switzerland) and *tsbi3* (Denmark).

A building energy simulation model is a simplified description of the building. The simplification has, in this case, been carried out from an energy and indoor climate point of view, so that the model only describes the aspects which are relevant in this connection. This means that it only includes data which form part of the various mathematical formulas and calculation algorithms, which together give an approximate description of the thermal and energy-dependent conditions regarding a building, its systems and operating conditions. As apparent from figure 9.1.1, the building model comprises the following:

- Data for the building's site, including climatic data.
- The building's form, i.e. its division into rooms or zones, delimiting surfaces for these zones, sub-surfaces consisting of windows and doors, as well as the materials used in them.
- Systems and loads in the building, including operating conditions and schedules.
- Data describing patterns of operation and use as well as other conditions for the individual zones.

The heat balance for the air in a zone does not make allowance for the heat capacity of the air which means that the air immediately adjusts itself to alterations in the surroundings. The following influences on the air's thermal condition are differentiated:

9.2 DEROB-LTH

DEROB-LTH which is an acronym for Dynamic Energy Response of Buildings, is a family of 6 modules calculating energy consumption for heating, cooling and ventilation.

DEROB is a flexible simulation tool using an RC (Resistance-Capacitance) network for thermal model design.

DEROB simulates buildings of arbitrary geometries and interprets the presence of shading devices.

The modules were originally developed at the Numerical Simulation Laboratory, School of Architecture, University of Texas, Austin. Since 1985, the DEROB modules are further developed to suit the local needs at the Department of Building Science at Lund Institute of Technology.

Below is a short description of properties of the DEROB modules.

9.2.1 Energy transmission

Walls are made of different materials with different thicknesses and thermal properties. DEROB divides the walls into a suitable number of layers and assigns internal nodes to the wall. A maximum of 7 nodes can be assigned inside each wall. Thermal properties for the walls are assigned by input or by material library. The inner and outer surfaces of the wall are each assigned one thermal node.

Windows are modelled with two surface nodes regardless of the number of panes. Thermal properties are assigned by input or by a windows library. The thermal resistance, including inner and outer film coefficients, is given as input.

Outer surfaces are coupled to other thermal nodes as follows:

- by conduction to the outermost of inner nodes in the wall
- by long wave radiation to the sky and ground
- by convection to the outdoor air

In the heat balance equation, loads from direct, diffuse and ground reflected solar radiation are taken into account.

Inner surfaces are coupled to other thermal nodes as follows:

- by conduction to the innermost of the inner nodes in the wall
- by long wave radiation to the inner surfaces in a volume
- by convection to the indoor air

9.2.4 Infiltration and air movements

Infiltration between a volume and the outdoor air can be modelled. The infiltration is specified by giving values for air change rate according to a time schedule.

If the building has more than one volume, air movements through advection connection between volumes are modelled. The air exchange is driven by the difference in temperature and static pressure.

9.2.5 Ventilation

Ventilation between volumes and to the outdoor air can be modelled. The direction of the forced ventilation can be defined. The sum of all air flows into a volume must be equal to the air flow out from the volume.

9.2.6 Internal gains

Internal loads including people, lighting and appliances can be specified in two ways. The simplest way is to specify a constant value that will be used during all days of the simulation period. The second alternative uses hourly values according to a time schedule. All values can be positive or negative.

9.2.7 Heating and cooling

Heating and cooling can be modelled. Two set points are specified according to an hourly schedule. The equipment used, can be assigned a maximum power. If not defined, the power is supposed to be unlimited, and the temperatures will then always satisfy the given set points.

9.2.8 Other systems

No modelling

9.2.9 Daylight

No modelling

9.2.10 Moisture

No modelling

FRES is developed at SINTEF Division of Applied Thermodynamics, Norway through the years 1988 to 1992. The description below corresponds to the version released in the spring of 1993.

FRES is based on a simplified description where a building is divided into elements. The elements are called thermal nodes as they represent average temperature within the boundary of one element. Several interconnected zones which are connected to a ventilation system can be studied. Equations for conservation of flow, heat and species are formulated for each node. The equations are solved by a finite difference method, hour by hour, for a predefined period. In northern climates it is normally not necessary to consider air stratification when calculating energy consumption (heating requirements and stratification occurs at different times). When the stratification is used as part of the heating strategy, it must be modelled.

A short description of the physical processes modeled is presented.

9.3.1 Energy Transmission

Walls are subdivided into layers to solve one dimensional heat transfer. There is no special modelling of thermal bridges or corner effects. Normally there are four thermal nodes, two at the inner and two at the outer surface. Thermal mass is modelled for the two nodes inside the wall. These nodes are normally 2.5 cm behind the surface. A thermal resistance is defined between the nodes in the wall. The inner surface node is connected to solar radiation from the window, to the other surfaces by long-wave radiation and to the air by convection. The outer surface is connected to the air by both convective and radiative coefficients. No solar radiation or long-wave radiation to other surfaces is modelled at the outer surfaces. All coefficients are constant.

Windows are modelled in a similar way with two thermal nodes. The absorbed part of the solar radiation is absorbed in the inner surface.

The method is acceptable for the design of most walls. With very low U-values, the relative importance of thermal bridges and corners increase, and these effects should be incorporated. The models do not provide the possibility to study movable insulation.

9.3.2 Solar Radiation and Distribution

The model performs hour by hour calculation of direct and diffuse solar radiation. The diffuse part is isotropic. Clouds are modelled with cloud-cover factors. The model works well, but the results seem to give a bit (about 5 %) too high solar radiation. As we get the new climate data

9.3.4 Infiltration, stratification and air movements.

The infiltration is calculated based on air change rate for zone air. It is strongly simplified, as there is no modelling of physical laws. Since no input data exists for better models this is still a good choice. Infiltration is often the largest source of uncertainty in the calculations. The available input data are uncertain.

For cases where stratification may occur, a linear temperature distribution model is provided. Average room temperatures from the stratification model are used when calculating heat transfer through the building elements. The stratification model option is favourable for rooms with large ceiling height.

Air flows may be modelled between zones, between ambience and the zones and as a part of the ventilation system. The flows are defined by their path, flow rate and schedule. The method works well for analysing most common problems. Data are easily available when forced ventilation is studied. For natural ventilation, air flow must be estimated in advance.

9.3.5 Ventilation and air conditioning

Ventilation plants with heat exchanger, heater, cooler, humidifier and fans are modelled. Each component has one thermal node. Both air temperature and humidity is calculated.

The method is good for detailed design when plant dynamics is not very important. It lacks the integrated analysis of the heating system and of a heat pump; Some precalculations and estimates must be performed.

Ventilation through leakages and hatches caused by wind or chimney effect are not modelled. Precalculations must be performed and data given as infiltration with a schedule.

9.3.6 Internal gains

Internal heat gains like lighting, persons and equipment can be defined and scheduled. The user defines radiative and convective part.

9.3.7 Heating and cooling

Heating and cooling can be modelled in each zone locally and in the central air conditioning plant.

9.3.12 Limitations

The program can use up to 120 kb memory for variables and data.

9.3.13 Input and Output

Input is given in a pop down menu system. It provides help and standard data.

Output from the calculations are hourly air and operative temperatures and power consumption. Energy consumption values for heating, cooling, ventilation, humidifiers and equipment in the simulated period are given. Curves showing accumulated temperature values are available.

9.4 TRNSYS Type 56 (version 1.3) : Multi Zone Building

9.4.0 Introduction

This component of the TRNSYS program models the thermal behaviour of a building having up to 25 thermal zones. In each zone, the temperature of the air is assumed fully mixed.

There are two ways to model the equipment for heating, cooling, humidification and dehumidification :

1. Energy rate method
2. Temperature level method

With the energy rate method a simplified model of the air conditioning equipment is implemented within the type 56 component. The user specifies the set temperatures for heating and cooling, set point for humidity control, and maximum cooling and heating rates. These specifications can be different for each zone of the building. If the user desires a more detailed model of the heating and cooling equipment, a temperature level approach is required. In this case separate components are required to model the heating and the cooling equipment. The outputs from the type 56 zone can be used as inputs to the equipment model, which in turn produce heating and cooling inputs to the type 56 zones.

The zone temperature is free floating in the comfort region where the power is zero. If the temperature of a free floating zone is within the heating or cooling region at the end of a timestep, power is applied throughout the timestep so that the first zone temperature just reaches T_{set} . If the power required is greater than the maximum specified, then the maximum power is applied throughout the timestep and the zone temperature is again free floating.

In order to determine either energy demands and floating zone temperatures it is necessary to evaluate the terms of equation 1).

9.4.1 Energy transmission

The walls are modelled according to the transfer function relationship of Mitalas and Arsenault. The wall are subdivided into layers to solve one dimensional heat transfer.

The long-wave radiation exchange between the surfaces within the zone and the convective heat flux from the inside surfaces to the zone air are calculated using a method called "star network" given by Seem - (1987). Area ratios are used to calculate view factors from one surface to the other so that this model is not a geometrical one.

Different types of walls can be defined :

External walls

Internal walls (play a role in solar and internal gains distribution and because of their thermal mass,- but there is no conduction losses associated with the wall because its both surfaces are in the same zone !)

Walls between zones

The temperature of the wall surfaces can be fixed.

A window is considered as a wall with no thermal mass, partially transparent to solar, but opaque to long-wave internal radiation and gains, and is always related with the outdoor conditions.

9.4.2 Solar radiation and distribution

The total solar gains to any zone i are :

For each wall separating zones of floating temperature or having a known boundary condition, it is possible to specify a convective coupling air movement from one zone to the other. This coupling is the mass flow rate that enters the zone across the wall. An equal quantity of air is assumed to leave the zone at zone temperature. Also this mass flow rate can be variable and calculated separately.

9.4.5 Ventilation and air conditioning

The ventilation rates are given in terms of air changes per hour for each zone.

The mass flow rate is the product of the zone air volume, air density, and air change rate. Infiltration occurs from outdoor conditions, while ventilation occurs from a specified (possibly variable as the rates) temperature. Equal amounts of air are assumed to leave the zone at the zone temperature.

The natural ventilation exchanges must be calculated separately and introduced in the zone as variable infiltrations or ventilation rates with ventilation temperature equals to the ambient (external) temperature.

9.4.6 Internal gains

The internal gains are defined as one convective part (in the air) and one radiative (longwave) part. Also these gains can be scheduled as variables. All surfaces are assumed to be black for radiation internal gains. These gains are distributed according to the area ratios.

9.4.7 Heating and cooling

This point has already been treated in the introduction, and we will not come back to it here.

Ratio = Multiplication factor generally in the range of 1 to 10. A moisture balance for any zone results in the following differential equation.

$$M_{eff,i} \cdot \frac{\delta \bar{\omega}_i}{dt} = \dot{m}_{in,f,i}(\bar{\omega}_a - \bar{\omega}_i) + \dot{m}_{v,i}(\bar{\omega}_{v,i} - \bar{\omega}_i) + W_{g,i} + \sum_{walls,i-j} \dot{m}_{cplg,s}(\bar{\omega}_j - \bar{\omega}_i)$$

where

- $\bar{\omega}_a$ = The ambient humidity ratio
- $\bar{\omega}_i$ = The humidity ratio of the zone
- $\bar{\omega}_{v,i}$ = The humidity ratio of the ventilation flowstream
- $\bar{\omega}_{g,i}$ = Internal moisture gains
- $\bar{\omega}_j$ = The humidity ratio of an adjacent zone j

In order to simplify the solution of the simultaneous set of differential equations, the values of at the end of the previous timestep are used in the above expression. If the average humidity ratio of the zone falls below or rises above a setpoint for humidification or dehumidification, then latent energy is added or removed to maintain the humidity ratio at the setpoint. It is assumed that the change in zone humidity ratio occurs instantly so that $\bar{\omega}_i = \bar{\omega}_{i,t}$. In this case

$$\dot{Q}_{lat,i} = h_v [\dot{m}_{in,f,i}(\bar{\omega}_a - \bar{\omega}_{req,i}) + \dot{m}_{v,i}(\bar{\omega}_{v,i} - \bar{\omega}_{req,i}) + W_{g,i} + \sum \dot{m}_{cplg}(\bar{\omega}_{j,t-\Delta t} - \bar{\omega}_{i,t-\Delta t}) - \frac{M_{eff,i}(\bar{\omega}_{req,i} - \bar{\omega}_{i,t-\Delta t})}{\Delta t}]$$

where

- $Q_{lat,i}$ = Latent energy removed (+ dehumidification, - humidification)
- h_v = The heat of vaporization of water
- $\bar{\omega}_{req,i}$ = The setpoint of humidification or dehumidification

Between the two setpoints, the humidity ratio is free floating.

- Gain due to convective coupling with adjacent zones
- Internal convective gains
- Change in internal sensible energy of zone air since beginning of simulation
- Humidity ratio of zone air
- Latent energy demand (-humidification, +dehumidification) (calculated only if heating/cooling defined)
- Net latent energy gains
- Total solar energy entering through windows
- Total radiation absorbed at all inside surfaces within zone, includes solar and gains, but not long-wave exchange with other surfaces
- Total radiation absorbed at all outside surfaces within zone, does not include long-wave from other walls

Other optional outputs are also available:

- Inside surface temperature
- Outside surface temperature
- Description
 - Inside surface temperature
 - Outside surface temperature
 - Energy from the inside surface including convection to the air and long-wave radiation to other surfaces
 - Energy to the outside surface including convection from the air and long-wave radiation
 - Total radiation absorbed at inside surface (except long-wave from other walls)
 - Total radiation absorbed at outside surface (except long-wave from other walls)

9.5.3 Infiltration

Infiltration is uncontrolled air penetrating through leakages in the building envelope. The model for infiltration defines the air-change rate for the current zone in three terms: a basic *air exchange* plus a term which is dependent on the difference between the inside and outside temperature plus a term dependent on the wind speed:

$$n_{\text{venting}} = n_0 + c_t \cdot (t_i - t_u)^p + c_v \cdot v \quad (2)$$

where

n_0 is the basic air change, h^{-1}

t_i, t_o are respectively the indoor and outdoor temperatures, $^{\circ}\text{C}$

p is flow exponent on temperature difference (stack effect), often set to 0.5

c_t is a constant, which is especially dependent on the size of the room and openings as well as the height difference between the openings

c_v is a constant, which is especially dependent on how leaky the building is, the building's geometry as well as the site in comparison with other buildings and the topography/roughness of the land

v is the wind speed, m/s

9.5.4 Solar distribution

The solar radiation transmitted through the windows in the zone, is distributed according to a "key" defined by the User in the following fractions:

- *Lost* is the part of the radiation which is reflected almost immediately back through the window or is in some way "lost" for the current zone.
- *To air* indicates the fraction of the total solar radiation to the zone that is assumed to be transferred to the air by convection. This fraction typically lies between 0.10 and 0.30.
- *To surfaces* is the part of the radiation distributed between the individual constructions in the floor, walls and ceiling. The total solar

much solar radiation can be accepted, but the shading can also be controlled according to the temperature in the zone. There are three possible control strategies for the shading device: *continuous*, *stepwise*, and *on/off* adjustment.

Buildings, trees etc., which at certain times of the year cast shadows on an actual building, can be described as "shadows". A shadow is defined by co-ordinates in connection with a window or a surface. On the basis of a description of the shadow in connection with the calculated solar path, it is possible to define how much the solar radiation through the window will be reduced.

In the connected schedule it is possible to describe variations in the shading coefficient over the day and over the year.

9.5.9 Simulation and results

Using hourly weather data (eg. TRY files) *tsbi3* simulates the multi-zone building and the dynamic interaction of the building fabric and the systems. During simulation day-values and hour-values of user-selected parameters are stored in files for later documentation and statistical analysis.

The recorded day-values are used to set up the complete energy balances for all of the zones and for the whole building. The energy balance can be documented in weeks, in months, or for the whole year.

During simulation *tsbi3* calculates up to several hundred parameters, and therefore the user has to determine which of these data should be recorded.

9.5.10 Documentation of data and results

The calculated hourly values of the *tsbi3* simulation can be documented in simple tables, treated statistically or presented graphically. The user decides which parameters should be presented in the tables or graphs, and he also determines the scaling of the axes.

$I_{t,s}$	=	The solar radiation incident upon the surface
A_s	=	Surface of the window
$M_{eff,i}$	=	Effective moisture capacitance of the zone
$M_{air,i}$	=	The mass of air in the zone
Ratio	=	Multiplication factor generally in the range of 1 to 10. A moisture balance for any zone results in the following differential equation.
$\bar{\omega}_i$	=	The humidity ratio of the zone
$\bar{\omega}_a$	=	The ambient humidity ratio
$\bar{\omega}_{v,i}$	=	The humidity ratio of the ventilation flowstream
$\bar{\omega}_{g,i}$	=	Internal moisture gains
$\bar{\omega}_j$	=	The humidity ratio of an adjacent zone j
$Q_{lat,i}$	=	Latent energy removed (+ dehumidification, -humidification)
h_v	=	The heat of vaporization of water
$\bar{\omega}_{req,i}$	=	The setpoint ofr humidification or dehumidification
n_0	=	the basic air change, h^{-1}
t_i, t_o	=	indoor and outdoor temperatures, respectively, °C
p	=	flow exponent on temperature difference (stack effect), often set to 0.5
c_t	=	a constant, which is especially dependent on the size of the room and openings as well as the height difference between the openings
c_v	=	a constant, which is especially dependent on how leaky the building is, the building's geometry as well as the site in comparison with other buildings and the topography/roughness of the land
v	=	the wind speed, m/s